

Investigations on Dye Sensitized Solar Cells to Optimize its Performance

A Thesis submitted to the University of North Bengal

For the Award of

Doctor of Philosophy

in

Physics

By

Rajat Biswas

Under the guidance of

Prof. Suman Chatterjee



समानो मन्त्रः समितिः समानी

Department of Physics

University of North Bengal

Siliguri- 734 013, West Bengal, India

August 2022

DECLARATION

I hereby declare that the thesis entitled "*Investigations on Dye Sensitized Solar Cells to Optimize its Performance*" has been prepared by me under the guidance of Dr. Suman Chatterjee, Professor, Department of Physics, University of North Bengal. The work is original and no part of this thesis has previously formed the basis for the award of any degree or fellowship.

Rajat Biswas

(Rajat Biswas)

Department of Physics,

University of North Bengal,

Raja Rammohunpur, Siliguri

Darjeeling-734013

West Bengal, India

Date: 10/08/2022

Place: Siliguri

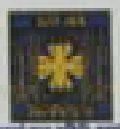
Date: 10/8/2022

Place: Siliguri

DEPARTMENT OF PHYSICS
UNIVERSITY OF NORTH BENGAL

P.O. North Bengal University, Siliguri, Dist. Darjeeling, West Bengal, Pin - 734013, India

Website: www.nbu.ac.in



Phone: +91-(0) 353-276338, Fax: +91-(0) 353-269601

CERTIFICATE FROM THE SUPERVISOR

I certify that Mr. **RAJAT BISWAS** has prepared the thesis entitled, *Investigations on Dye Sensitized Solar Cells to Optimize its Performance* for the award of Ph.D. degree of the University of North Bengal, under my supervision. He has carried out the work at the Department of Physics, University of North Bengal. No part of this thesis has previously formed the basis for the award of any degree or fellowship.

(Dr. Suman Chatterjee)

Professor

Department of Physics,
University of North Bengal,
Raja Rammohunpur, Siliguri
Darjeeling-734013
West Bengal, India

Professor

Department of Physics
University of North Bengal







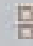

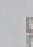
Date: 10/8/2022 .

Place: Siliguri

Document Information

Analyzed document	Rajat Biswas_Thesis_Plag_Check.docx (D141892953)
Submitted	2022-07-09 12:25:00
Submitted by	University of North Bengal
Submitter email	nbupig@nbu.ac.in
Similarity	1%
Analysis address	nbuplg.nbu@analysis.orkund.com

Sources included in the report

W	URL: https://ur.booksc.eu/book/64646431/d9b7da Fetched: 2022-07-09 12:25:37		1
W	URL: https://en.wikipedia.org/wiki/Dye-sensitized_solar_cell Fetched: 2019-09-30 11:53:44		1
W	URL: https://www.sciencedirect.com/topics/chemistry/dye-sensitized-solar-cells Fetched: 2020-10-10 17:29:27		2
W	URL: https://ur.booksc.me/book/3929041/3cc2b3 Fetched: 2022-07-09 12:25:36		1
W	URL: https://www.upo.es/cms1/export/sites/upo/investiga/ccs/documentos/Thesis_JesusIdigoras.pdf Fetched: 2020-05-19 02:45:17		1
W	URL: https://www.nature.com/articles/s41598-020-61363-x Fetched: 2020-07-10 11:35:17		3
W	URL: https://www.science.gov/topicpages/e/efficiency+dye-sensitized+solar Fetched: 2022-04-11 04:45:15		1
W	URL: https://www.hindawi.com/journals/ijp/2013/612095/ Fetched: 2022-05-10 19:46:35		1
W	URL: https://www.science.gov/topicpages/z/zno+nanorod-sno2+nanoparticle Fetched: 2019-12-19 09:25:54		1
W	URL: https://www.sciencedirect.com/science/article/pii/S0030402619320418 Fetched: 2022-01-08 15:30:18		1

Entire Document

Rajat Biswas
10/08/2022Suman Chatterjee
10/8/2022Professor
Department of Physics
University of North BengalHead
Department of Physics
University of North Bengal

*Dedicated to my family,
especially to my mother, wife
and loving daughter
Arohi*

Preface

Photovoltaic technologies represent one of the leading research areas of solar energy. It is one of the most potent renewable alternatives to fossil fuels. Direct conversion of solar radiation into electricity is a renewable, abundant and clean method for producing energy. Though conventional photovoltaic devices (silicon-based solar cells) are promising for the direct conversion of photons into electrons, the prohibitive cost of these cells is uncompetitive with conventional power generating methods. On the contrary, dye-sensitized solar cells (DSSCs) are a non-conventional photovoltaic technology that has attracted significant attention because of their high conversion efficiencies, low cost, non-toxic and recyclable materials and suitability for wide variety of end-user products. This thesis work entitled “*Investigations on Dye Sensitized Solar Cells to Optimize its Performance*” is the outcome of the experimental investigations performed on the fabrication and characterization of DSSCs based on various dyes, photoanode and electrolyte materials.

This thesis focuses on optimizing the different components of a DSSC and studying the influence of various parameters of these component materials on the overall performance of the cell in terms of efficiency and stability. The thesis is broadly divided into seven chapters. **Chapter 1** briefly introduces the world's present energy scenario and an overview of the need for renewable energy sources. This chapter also discusses different generations of photovoltaic technology along with a brief introduction to different components and working principles of dye sensitized solar cells. **Chapter 2** describes the basic theory of the experimental techniques used for characterizing the different components of DSSCs. **Chapter 3** illustrates the charge transfer kinetics and effect of the shape of ZnO nanostructure on the performance of DSSCs based on two natural dyes. **Chapter 4** investigates the impact of surface modification via sol-gel spin coating of ZnO nanoparticles on the performance of WO₃ photoanode-based DSSCs by varying the

concentration of ZnO precursor solution. In **Chapter 5**, the role of chenodeoxycholic acid (CDCA) as dye co-adsorbent and blocking layer in improving the performance of dye sensitized solar cells has been presented. **Chapter 6** deals with investigating the use of gel electrolyte on the stability enhancement of DSSCs. Finally, the critical findings arising from the present work have been summarized in **Chapter 7**.

Rajat Biswas.

Rajat Biswas

Dept. of Physics

University of North Bengal

Date: 10/08/2022

Place: 'Siligumi'

Acknowledgements

There are so many people whose support, encouragement and inspiration are very much necessary to accomplish any significant achievements in life, especially if it involves the elements of fulfilling one's cherished dreams. For me, this thesis is such an important destiny and I am indeed indebted to many people for their wishes and blessings in completing this journey. I take this opportunity to acknowledge and extend my sincere gratitude to all these people who have been involved, directly or indirectly, in making the research work described in this thesis possible.

First, I would like to thank Prof. Suman Chatterjee, my Ph.D. supervisor, for giving me the opportunity to pursue my Ph.D. research with him. It has been a great privilege to work under his able guidance and his dynamic laboratory environment. I greatly appreciate the insights he provided in various studies pursued in my work. His innovative thinking and highly spirited attitude have inspired me to conduct and complete my doctoral research quite efficiently. He has not only grafted my scientific skills and knowledge but also moulded me into a better human being. His guidance always challenged me intellectually and provided a perfect ambience I needed to grow as a materials physicist. I am grateful to him for his critical comments and tremendous efforts in preparing this dissertation. I thank him for their endless support filled with patience and enthusiasm during my whole tenure of Ph.D.

I am deeply grateful to Prof. Pradip Kumar Mandal, Dept. of Physics, University of North Bengal, for his continuous support, fruitful discussion, encouragement and sustained help in performing the research work.

I sincerely thank University of North Bengal for providing me State Fellowship and the Department of Physics for providing infrastructural facilities to pursue the research work.

My heartfelt thank to my seniors and fellow labmates, Dr. Debashis Sinha, Dr. Asim Debnath, Dr. Kartick Chandra Dey, Dr. Debarghya Goswami, Susanta Chakraborty, Aparna Ghosh, Chinmoy Roy, Trinakshi Roy, Joy Sarkar, Pratik Debnath and Avijit Talukdar for stimulating discussions and creating an excellent research environment within the lab.

I would like to extend my thanks to all my friends and well wishers, Arup, Saikat, Bumba, Bubai, Partha, Rajib, Sandip, Sayangam, Somnath, and Prabir for their accompany in the least and the worst time during my research period.

I would like to thank all the faculty members and non-teaching staffs of the Department of Physics, University of North Bengal, for their needful help in the entire period of my research work. I am also grateful to University Science and Instrumentation Centre (USIC) for providing scanning electron microscopy measurement facility.

Last but not the least, I would like take this opportunity to specially acknowledge my wife Tania for her constant support, understanding, unconditional love and care, sacrifices and for being there with me in my ups and downs all throughout the tenure. I want to express my heartfelt gratitude to my adorable daughter Arohi. Her smile and love for me always worked as a stress buster. I would like to take this opportunity to thank my parents, especially Maa, for keeping faith in me. I want to take this opportunity to thank my sister Riya and my brother Arijit also for their invaluable love and support. Words are inadequate for expressing my gratitude towards all of them.

Rajat Biswas

ABSTRACT

Energy, one of the fundamental requirements for society's progress, cannot be created or destroyed; it can only be changed into one form or another. The world's need for energy is growing every day as a result of population growth and ongoing industrialization. Traditionally, fossil fuels like coal, petroleum, and natural gas are used to generate electricity. However, these fuels will eventually run out in addition to devastatingly polluting the environment and posing significant difficulties for earth's living creatures. In order to meet our ever-increasing energy needs, it is necessary to find some unstoppable energy sources that can supplement traditional energy supplies and take their place in the future. The use of renewable energy sources that are free from the issues related to the use of fossil fuels has therefore received attention. Some of the possibilities available to us are solar, wind, tidal waves, geothermal, and biomass.

Although conventional Silicon-based photovoltaic technologies are promising, the expensive cost of these cells makes them uncompetitive with current power generating methods. Contrarily, dye-sensitized solar cells (DSSCs) are a non-traditional photovoltaic technology that has garnered much interest due to its promising conversion efficiencies, low cost, non-toxic, and recyclable components, and adaptability for a wide range of end-user goods. Though many other DSSCs have been studied, the majority of them have not yet gained commercial popularity due to problems with low conversion efficiency, production costs, and lower stability and durability. The main objective of this thesis is to investigate on the different components of DSSC with an aim to optimize its performance in terms of environment-friendly nature, cost-effectiveness, better durability and improved light to electron conversion efficiency. This thesis is broadly organized into seven chapters. The favorable results from this thesis will lead to the following mentioned outcome.

Chapter 1 addresses the world's present energy scenario and an overview of the necessity of renewable energy sources. This chapter also includes a brief discussion about different types of photovoltaic devices available. Furthermore, a basic introduction to DSSC, its construction and role of its different components is also discussed in this chapter. Besides this, the working principle of DSSCs is also described.

Chapter 2 describes the basic theory and detailed description about different experimental techniques viz. X-ray diffraction analysis (XRD), Scanning electron microscopy (SEM), Energy-dispersive X-ray spectroscopy (EDS) study, UV-VIS spectroscopy and Raman spectroscopy used for characterizing the materials of the different components of DSSCs. In addition, the principles of Current-Voltage (I-V) and electrochemical impedance spectroscopy measurement along with the detail description of critical parameters determining the device performance, have also been discussed in this chapter.

Chapter 3 illustrates a comparative evaluation of optical, electrical and electrochemical properties of DSSCs fabricated using vertically aligned ZnO nanorods synthesized using low-cost Sol-Gel spin coating technique on ITO coated glass substrate and ZnO nanopowder and their application in the fabrication of natural dye-based Dye Sensitized Solar Cells. Natural dyes extracted from pomegranate and turmeric are used as sensitizers. Electrochemical impedance spectroscopy (EIS) was employed for a detail investigation of the charge carrier recombination properties and the charge transfer mechanism at different interfaces of the devices.

Chapter 4 contains an investigation on the impact of surface modification via sol-gel spin coating of ZnO nanoparticles on the performance of WO₃ photoanode-based DSSCs by varying the concentration of ZnO precursor solution. The semiconducting material WO₃ was chosen in search of a photoanode material for DSSC alternative to TiO₂. However, the performance

of pure WO_3 based DSSC was found to be extremely poor despite having several advantageous properties. To improve the photovoltaic performance of the cell, the WO_3 surface was coated with varying concentrations of the ZnO precursor solution. It was observed that the concentration of the precursor solution of ZnO highly controls the photovoltaic performance of the DSSC.

Chapter 5 depicts the role of optimum concentration of chenodeoxycholic acid (CDCA) as anti-dye-aggregation material in improving the DSSC performance based on rose bengal dye. Aside from this, the effect of a very thin and compact ZnO blocking layer was also investigated to reduce the charge recombination and hence to improve the performance of dye sensitized solar cells.

Chapter 6 focuses on the use of gel electrolyte in DSSC instead of liquid electrolyte. The leakage problems of liquid electrolyte, electrode corrosion, photo-degradation of attached dyes, and solvent volatility restrict the long-term performance of DSSCs based on liquid electrolyte. To overcome these limitations, gel electrolyte has been used as the volatility of organic solvents can be decreased and leakage can be prevented by gel-type electrolytes. Gel electrolyte-based DSSCs have been fabricated with ethyl cellulose (EC) as gelation material in the conventional liquid electrolyte containing LiI and I_2 as a redox couple in acetonitrile solvent to enhance the stability of the cells. Both TiO_2 and ZnO were used as photoanode materials for different types of DSSCs. Photovoltaic performance, including their stability behavior over a certain period of time were also evaluated.

Chapter 7 summarizes the essential findings and conclusions arising from the present work.

List of Abbreviations

ACN	Acetonitrile
CB	Conduction band
CDCA	Chenodeoxycholic acid
DSSC	Dye sensitized solar cell
EDS	Energy-dispersive X-ray spectroscopy
E_g	Energy band-gap
EIS	Electrochemical Impedance Spectroscopy
FF	Fill Factor
FTO	Fluorine doped Tin oxide
FWHM	Full width at half maximum
HOMO	Highest occupied molecular orbital
I_{max}	Maximum current
I_{sc}	Short-circuit current
ITO	Indium tin oxide
JCPDS	Joint committee on powder diffraction standards
J_{sc}	Short-circuit current density
LUMO	Lowest unoccupied molecular orbital
MEA	Monoethanolamine
MPN	3-methoxypropionitrile
NP	Nanoparticle
NR	Nanorod
PC	Polyvinyl carbonate
PEDOT	[poly(3,4-ethylenedioxythiophene)]
P_{max}	Maximum power
PV	Photovoltaic
Pt	Platinum

RB	Rose Bengal
R_s	Series resistance
R_{sh}	Shunt resistance
SEM	Scanning electron microscopy
TCO	Transparent conducting oxide
V_{max}	Maximum voltage
V_{oc}	Open circuit voltage
XRD	X-ray diffraction
η	Power conversion efficiency
λ_{max}	Maximum absorption wavelength.

Table of contents

Declaration	i
Certificate from the supervisor	iii
Plagiarism report	v
Dedication	vii
Preface	ix
Acknowledgements	xi
Abstract	xiii
List of Abbreviations	xvii
Table of contents	xix
List of tables	xxv
List of figures	xxvii
1. Chapter 1. Introduction to photovoltaic technology and theoretical background of Dye Sensitized Solar Cells	1
1.1. Introduction	3
1.2. Solar Cell Technologies	4
1.2.1. Classical P-N junction silicon solar cells	4
1.2.2. Photovoltaic Generation	7
1.2.2.1. 1st generation: Crystalline Silicon (Poly-silicon or mono-silicon) solar cells	8
1.2.2.2. 2nd generation: Thin film Solar Cell (TFSC)	9
1.2.2.3. 3rd generation Solar Cells	11
1.3. Basic construction and different components of a Dye sensitized solar cell (DSSC)	17
1.3.1. Transparent conducting oxide (TCO) coated glass substrate	18
1.3.2. Photo electrode	19
1.3.3. Dye sensitizer	21

1.3.4. Electrolyte	34
1.3.5. Counter electrode	38
1.4. Basic Operating Principle of DSSC	39
References:	43
2. Chapter 2. Experimental Methods and Characterization	
Techniques for Dye Sensitized Solar Cells	69
2.1. X-Ray Diffraction analysis	71
2.2. Scanning Electron Microscopy (SEM)	72
2.3. UV-VIS spectroscopy	74
2.4. Energy Dispersive X-ray spectroscopy (EDS)	75
2.5. Raman Spectroscopy	76
2.6. Basic parameters to evaluate the performance of DSSCs:	
Solar Cell Terminologies	78
2.6.1. Open circuit voltage (V_{OC})	80
2.6.2. Short circuit current density (J_{SC})	81
2.6.3. Series resistance (R_S)	81
2.6.4. Shunt resistance (R_{sh})	81
2.6.5. Fill Factor (FF)	82
2.6.6. Power Conversion Efficiency (η)	82
2.7. Electrochemical Impedance Spectroscopy (EIS)	83
2.7.1. Theory of Impedance	83
2.7.2. Nyquist and Bode plots	85
2.7.3. Equivalent circuit for impedance measurement of DSSC	87
References	91
3. Chapter 3. Dye Sensitized Solar Cells Based on ZnO Nanostructures and Organic Dyes	95
3.1. Introduction	97
3.2. Experimental Section	99
3.2.1. Structure and Working principle of DSSC	99

3.2.2. Materials used	101
3.2.3. Extraction and Preparation of Organic Dye Sensitizers	101
3.2.4. Preparation of working electrodes	103
3.2.5. DSSC assembling	106
3.2.6. Device Characterization and Measurements	107
3.3. Results and Discussion	108
3.3.1. UV-VIS absorption spectral analysis of the dyes	108
3.3.2. X-ray diffraction analysis of the ZnO film	109
3.3.3. Scanning Electron Microscope Studies	111
3.3.4. Current-Voltage Characteristics study of the cells: Solar cell efficiency measurements	112
3.3.5. Electrochemical impedance spectroscopy study of the cells	117
3.4. Conclusions	120
References	122
4. Chapter 4. Application of WO₃ as alternative photoanode material for Dye Sensitized Solar Cells	127
4.1. Introduction	129
4.2. Materials and Method	131
4.2.1. Preparation of working electrodes	131
4.2.2. Characterization and Measurements	134
4.3. Results and Discussion	134
4.3.1. Structural and phase characterization WO ₃ photoanode	134
4.3.2. Surface Morphology study and energy dispersive spectroscopy of the photoanodes	136
4.3.3. Current-Voltage characterization of the cells	138
4.3.4. Electrochemical impedance spectroscopy	144
4.4. Conclusion	147

References	149
5. Chapter 5. Role of dye co-adsorbent and blocking layer in improving the performance of DSSCs	155
5.1. Introduction	157
5.2. Materials and Methods	162
5.2.1. Materials	162
5.2.2. Preparation of conventional ZnO photoanode	163
5.2.3. Preparation of photoanode with Compact ZnO layer	164
5.2.4. Assembling the devices	164
5.2.5. Characterization and Measurements	165
5.3. Results and Discussion	166
5.3.1. UV-VIS absorption spectral analysis of the dye	166
5.3.2. Structural and phase characterization ZnO compact layer	169
5.3.3. Surface Morphology study and energy dispersive spectroscopy of the photoanodes	171
5.3.4. Photovoltaic characterization of the cells	174
5.3.5. Effect of CDCA	175
5.3.6. Effect of compact ZnO blocking layer	176
5.3.7. Dark current measurement	176
5.3.8. Electrochemical impedance spectroscopy study	179
5.4. Conclusion	184
References	186
6. Chapter 6. Stability Enhancement of Dye-Sensitized Solar Cells Fabricated with Gel Electrolyte	195
6.1. Introduction	197
6.2. Materials and Methods	198
6.2.1. Materials	198

6.2.2.	Preparation of liquid and gel electrolyte	199
6.2.3.	Fabrication of the solar cells	200
6.2.4.	Characterization of the DSSCs	201
6.3.	Results and Discussions	201
6.3.1.	Raman spectroscopy of TiO ₂ and ZnO	201
6.3.2.	Scanning electron microscope (SEM) analysis	202
6.3.3.	Photovoltaic Performance of the DSSCs	203
6.3.4.	Electrochemical behavior analysis of the DSSCs	207
6.3.5.	Stability Study of the Cells	209
6.4.	Conclusion	211
	References	212
7.	Chapter 7. Summary and Conclusions	219
8.	Appendix	225
	Appendix A: Dye sensitized solar cells based on pre-dye treated ZnO nanoparticles	227
	Appendix B: List of Research Journal Publications	243
	Appendix C: List of Conference Presentations	245
9.	Reprint of Selected Papers	247

List of tables

Table 3.1.	Solar Cell parameters of DSSC's fabricated with natural dyes	114
Table 3.2.	Photovoltaic performance of the Rose Bengal sensitized cells.	116
Table 3.3.	Summary of EIS parameters of the DSSCs determined by fitting the experimental data.	119
Table 4.1.	Photovoltaic performance of uncoated and ZnO coated WO ₃ photoanode based DSSC.	140
Table 4.2.	Summary of EIS measurements of the fabricated DSSCs.	146
Table 5.1.	Photovoltaic parameters of DSSCs fabricated with various ZnO photoanodes.	175
Table 5.2	Summary of EIS measurement.	182
Table 6.1.	Summary of photovoltaic parameters of the N719 dye based cells.	204
Table 6.2.	Summary of photovoltaic parameters of the N3 dye based cells.	206
Table 6.3.	EIS measurement results of the Pt-Electrolyte-Pt cells with liquid electrolyte and gel electrolyte having different EC content.	209

List of figures

Figure 1.1	Construction of a p-n junction	5
Figure 1.2	Working of a p-n junction solar cell	6
Figure 1.3	Generation wise classification of solar cells.	7
Figure 1.4	Reported timeline of best Research-Cell conversion efficiencies of different solar cell technologies	15
Figure 1.5	Reported timeline of Solar Module efficiencies of different solar cell technologies	16
Figure 1.6	Basic structure of DSSC.	17
Figure 1.7	Chemical structure of some metal-complex dyes.	24
Figure 1.8	Molecular structure of Coumarine dyes.	25
Figure 1.9	Coumarin dye structures: (a) C343, (b) NKX-2311, (c) NKX-2586, (d) NKX-2753 and (e) NKX-2593.	26
Figure 1.10	Molecular structure of indoline dyes 1-4.	27
Figure 1.11	Classification of plant pigments.	28
Figure 1.12	Chemical structure of Chlorophyll 'a' and chlorophyll 'b'.	29
Figure 1.13	Chemical Structure of comomonly occurring flavonoid.	30
Figure 1.14	Basic chemical structure of anthocyanin pigment. Here 'R' could be replaced with H, OH or OCH ₃ depending on the pigment. The numbers can be substituted with hydroxyl group.	31

Figure 1.15	(a) Basic structure of an Isoprene unit, (b) Chemical structure of Xanthophylls and (c) Chemical structure of Carotene.	32
Figure 1.16	The molecular structures of crocetin and crocin.	32
Figure 1.17	Possible mechanism of the binding between crocetin and TiO ₂ surface .	33
Figure 1.18	Charge transfer and recombination kinetics in DSSC.	35
Figure 1.19	Schematic and basic working mechanism of DSSC.	39
Figure 1.20	Fundamental processes inside dye sensitized solar cell.	41
Figure 2.1	X-ray diffraction at the sample film surface.	71
Figure 2.2	Schematic diagram of Scanning Electron Microscope.	73
Figure 2.3	Experimental setup for SEM and EDS measurement.	74
Figure 2.4	Schematic of UV-VIS spectrophotometer.	74
Figure 2.5	Experimental setup for UV-VIS absorption measurement.	75
Figure 2.6	(a) Stokes Raman Scattering, (b) Anti-Stokes Raman Scattering.	76
Figure 2.7	Schematic diagram of a typical Raman Spectrophotometer.	77
Figure 2.8	One diode equivalent circuit model of a Solar cell.	78
Figure 2.9	Typical I-V characteristics of a solar cell.	78
Figure 2.10	Experimental Setup for I-V measurement.	80

Figure 2.11	Experimental setup for EIS measurement.	83
Figure 2.12	Typical (a) Nyquist and (b) Bode plot.	86
Figure 2.13	(a) Equivalent circuit for a complete solar cell; (b) Simplified circuit for insulating TiO ₂ (potentials around 0 V) as currents are low, Z _d may be skipped and (c) Simplified equivalent circuit of a DSSC when the TiO ₂ is in conducting state (At V _{oc} bias potential)	87
Figure 2.14	Typical Nyquist plot of a DSSC under Open circuit condition.	89
Figure 2.15	Typical Bode plot (Phase) representation of a DSSC.	90
Figure 3.1	Schematic diagram and basic working mechanism of DSSCs based on (a) ZnO nanoparticle (b) ZnO nanorod.	100
Figure 3.2	Chemical structures of Curcumin (a & b) present in turmeric and six major anthocyanins (c- h) present in Pomegranate fruit extracts.	102
Figure 3.3	Chemical structure of Rose Bengal dye.	103
Figure 3.4	Flow chart for preparation of ZnO nanorod layer.	105
Figure 3.5	(a) Spin Coater for seed layer formation (b) vessel for nanorod grow.	105
Figure 3.6	TiO ₂ nanopowder coated ITO (a) during sintering process (b) after sintering.	106
Figure 3.7	(a) Cell Fabricated with Curcumin dye (b) KI + I ₂ Electrolyte.	107
Figure 3.8	Absorption spectra of the curcumin and anthocyanin (pomegranate) sensitizers used to fabricate DSSCs.	108

Figure 3.9	XRD pattern of the ZnO nanorods synthesized by sol-gel spin coating method.	109
Figure 3.10	XRD of TiO ₂ nanopowder.	110
Figure 3.11	XRD of ZnO nanopowder	110
Figure 3.12	SEM image of (a) ZnO nanorods grown on ITO substrate (b) EDX spectra of the nanorod sample showing elemental composition (c) & (d) ZnO nanoparticle deposited sample at lower and higher magnification respectively.	111
Figure 3.13	(a) SEM image of TiO ₂ nanoparticles (b) EDS of TiO ₂ .	112
Figure 3.14	(a) Current density-Voltage characteristics of the cells under illumination (b) Power-Voltage curve to obtain maximum power point.	113
Figure 3.15	The equivalent circuit (single diode model) of a solar cell.	114
Figure 3.16	(a) Dark current measurement (b) I-V characteristics of the cells under illumination fabricated using TiO ₂ and ZnO.	115
Figure 3.17	Power vs. Voltage graph of the cells fabricated with Rose Bnegal	116
Figure 3.18	EIS spectra of DSSCs (a) Nyquist Plot (b) Equivalent circuit for fitting (c) Bode Phase plot and (d) Bode magnitude plot for impedance.	118
Figure 4.1	Energy band positions of several semiconductors.	130
Figure 4.2	(a) N3 dye, (b) Iodolyte AN50 electrolyte, (c) Platisol T used for preparing Pt counter electrode in DSSC fabrication.	133
Figure 4.3	DSSC fabricated with N3 dye and WO ₃ as photoanode material.	133

Figure 4.4	X-ray diffraction pattern of WO ₃ nanoparticles. The peaks correspond to Monoclinic (*) and orthorhombic (▪) phases of WO ₃ respectively.	135
Figure 4.5	Raman spectra of WO ₃ nanoparticle.	136
Figure 4.6	SEM images of (a) Bare WO ₃ photoelectrode; photoelectrodes having WO ₃ coated with (b) 1mM (c) 5mM (d) 10mM (e) 15mM (f) 20mM and (g) 25mM ZnO precursor solution respectively. (h) EDS of Bare WO ₃ and (i) EDS of WO ₃ coated with 5mM ZnO.	137
Figure 4.7	Current-voltage characteristics of different cells under (a) Illumination and (b) Dark.	139
Figure 4.8	Schematic energy level diagram and mechanism of the (a) Conventional DSSC and (b) DSSC with the ZnO barrier.	141
Figure 4.9	Effect of ZnO precursor solution concentration on the values of photovoltaic parameters (a) JSC (b) FF (c) Voc and (d) η.	143
Figure 4.10	Electrochemical Impedance Spectra of the DSSCs (a) Nyquist plot along with equivalent circuit (inset) (b) Bode plot.	140
Figure 5.1	Schematic diagram and working principle of a conventional DSSC.	158
Figure 5.2	Chemical structure of Rose Bengal dye.	160
Figure 5.3	(a) Unfavourable dye-dye interaction in absence of CDCA (b) reduced self-aggregation of dye molecules in presence of CDCA.	161
Figure 5.4	(a) Rose Bengal dye and (b) chenodeoxycholic acid (CDCA).	163

Figure 5.5	Possible transition mechanism in the Rose Bengal molecular system.	167
Figure 5.6	(a) UV-VIS experimental setup (b) absorption spectra of Rose Bengal dye.	168
Figure 5.7	X-ray diffraction pattern of (a) ZnO compact blocking layer (b) ZnO nanoparticles as active layer (c) ZnO blocking/active layer.	170
Figure 5.8	SEM images of ZnO NP active layer (a) at lower magnification (b) at higher magnification.	172
Figure 5.9	SEM images of ZnO blocking layer (a) at lower magnification and (b) at higher magnification.	173
Figure 5.10	EDS and elemental composition of ZnO blocking layer.	174
Figure 5.11	Current-voltage characteristics of different cells under (a) illumination (b) dark.	174
Figure 5.12	Schematic diagram of a DSSC with compact ZnO blocking layer.	176
Figure 5.13	Schematic diagram showing interfacial charge transfer and recombination in case of DSSCs (a) without ZnO BL (b) with compact ZnO BL.	178
Figure 5.14	Effect of CDCA concentration and ZnO blocking layer (BL) on different cell parameters.	179
Figure 5.15	EIS of the DSSCs representing (a) Nyquist plot along with equivalent circuit (inset) and (b) Bode plot.	181
Figure 6.1	Steps of Liquid and Gel electrolyte preparation.	199
Figure 6.2	Raman spectra of (a) TiO ₂ and (b) ZnO nanoparticles.	202

Figure 6.3	Scanning electron microscope (SEM) image of (a) TiO ₂ and (b) ZnO nanoparticles.	203
Figure 6.4	Current-Voltage characteristics of the N719 dye based cells fabricated with TiO ₂ .	204
Figure 6.5	Current-Voltage characteristics of the N3 dye based cells fabricated with (a) TiO ₂ (b) ZnO photoanodes.	205
Figure 6.6	Nyquist plot of the Pt-electrolyte-pt cells with liquid and gel electrolyte with different EC content.	208
Figure 6.5	Stability behaviour of the liquid and gel based DSSCs fabricated with (a)-(d) TiO ₂ and (e)-(h) ZnO as photoanode material.	210

Chapter 1

**Introduction to photovoltaic technology
and theoretical background of Dye
Sensitized Solar Cells**

This Page is intentionally left blank

1.1. Introduction

In this modern technological era, energy has become the most important daily need of our life. With the increasing world population, spreading urbanization and technological advancement, matching the energy supply with the energy demand is the main challenging issue the world is facing these days. The total global energy consumption can be classified into different sources of energy. It is estimated that the primary sources of energy consist of petroleum 36.0%, coal 27.4%, and natural gas 23.0%, amounting to an 86.4% share of fossil fuels in the global primary energy consumption [1]. Burning fossil fuels produces many toxic and greenhouse gases, which affect our environment heavily. Although nuclear power is one feasible option for producing large-scale energy, it has some serious safety and waste management issues. To make it an alternative source of our energy demand, it is required to establish a 1GW nuclear fission power plant every day for the next 50 years on the earth [2]. This is almost impossible. Moreover, the weapon-grade uranium or plutonium fuels might be secretly derived from the nuclear power plants to make nuclear weapons and that could be used for mass destruction. This is another critical concern related to the use of nuclear fuels for power generation.

These environmental consequences related to extensive use of fossil fuels, safety related issues of nuclear power, ever-growing energy demand and depleting stock of fossil fuels have motivated the researchers to search for alternative economically and environmentally sustainable renewable energy sources. Among all the non-polluting and renewable energy sources such as Hydropower, Wind turbines, biomass-derived liquid fuels, biomass-fired electricity generation, solar cells, solar thermal, and geothermal heat, the photovoltaic technology utilizing solar energy has emerged as the most

promising candidate. the annual solar energy that the earth receives is about 3×10^{24} J which is approximately 10^4 times more than the present global energy consumption. So covering 0.1% area of the earth surface with solar cells with an efficiency of 10% would satisfy our present needs. So we are in great need of technologies for efficient conversion, storage, and distribution of this energy [3].

1.2. Solar Cell Technologies

A solar cell is a type of semiconducting device that directly transforms solar energy into electrical energy. Photovoltaic electricity generation employs solar panels consisting of several solar cells. No harmful emission occurs in the process of conversion of solar energy to electricity in the solar cells. Thus it is environmentally sustainable. Aside from the abundance of potentially exploitable solar energy, photovoltaic cells have several other competitive features such as comparatively reduced maintenance, off-grid operation and zero noise pollution, making them ideal for use in remote locations and mobile applications.

Currently, the crystalline silicon modules (including mono-crystalline and large-grain polycrystalline Si) based on bulk wafers dominate the commercial PV module production. These devices are the typical members of a group referred to as the first generation of photovoltaic cells, which accounted for around 85% of the photovoltaic market [4].

1.2.1. Classical P-N junction silicon solar sells

The silicon based solar cell technology is basically rooted on the formation of *p-n* junction as shown in Fig. 1.1. This junction is formed by doping two different regions of the same semiconductor (Si) with trivalent and

pentavalent impurities. An interface between p-type and n-type materials can be created in this manner. As a consequence of accumulation of donor and acceptor ions near the interface, a built in electric field is created in that region. In the so-called depletion layer, this inherent electric field facilitates charge separation.

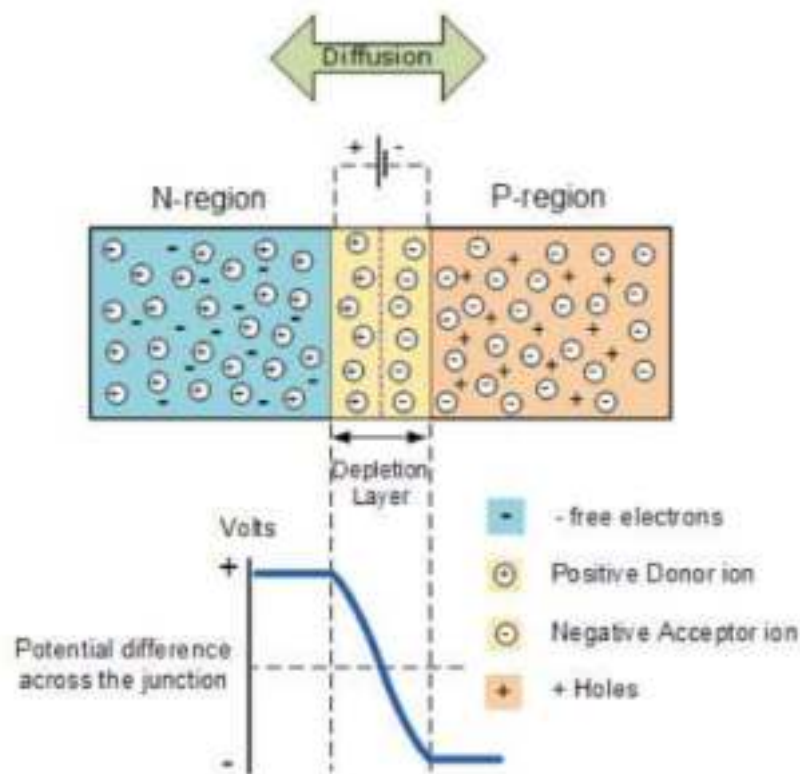


Figure 1.1 Construction of a *p-n* junction [5].

Electron-hole pairs are formed when photons with energies greater than the material's band gap energy incident at the depletion region. The strong built-in electric field existing in the depletion region favours the charge separation, and as a consequence, the electrons move to the *n* region and holes move to the *p* regions, respectively. In presence of an external load, connected across the cell, the accumulated excess electrons and holes pass through the load, creating electricity and ultimately recombining with each other (Fig.1.2).

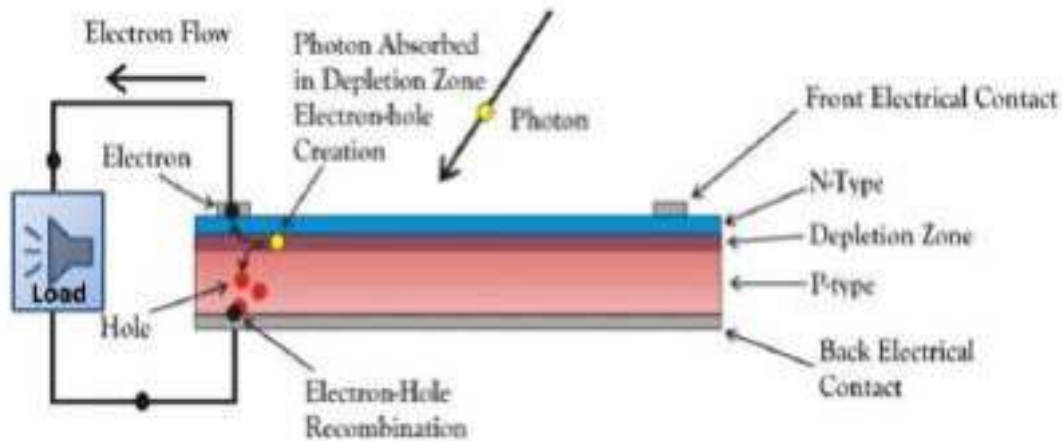


Figure 1.2 Working of a *p-n* junction solar cell [6].

Several theoretical calculations have been performed to estimate the highest power conversion efficiency that can be obtained from a single *p-n* junction Si solar cell. Shockley and Queisser calculated a theoretical upper limit of efficiency to be 33.7 % for a *p-n* junction solar cell based on a semiconductor with band gap energy (E_g) of 1.4 eV [7]. Poor maximum efficiency is caused mainly by two main factors. Firstly, the solar cells do not absorb photons with an energy of $E < E_g$. Secondly, even though the photons with an energy $E > E_g$ get absorbed, they can only transmit the band gap energy to the electric circuit, while the rest ($E - E_g$) amount of energy is lost as thermal dissipation [8]. The following requirements that are to be fulfilled by the solar cells to make it a realistic solution to our present and future energy crisis:

- Broad solar spectrum absorption
- High power conversion efficiency
- Economically cheap

-
-
- Can be fabricated using abundant and environment-friendly raw materials
 - Should have long term stability

1.2.2. Photovoltaic Generation

On the basis of their performance, cost effectiveness and nature of materials used, the solar cell technologies are classified into three major generations (Fig. 1.3).

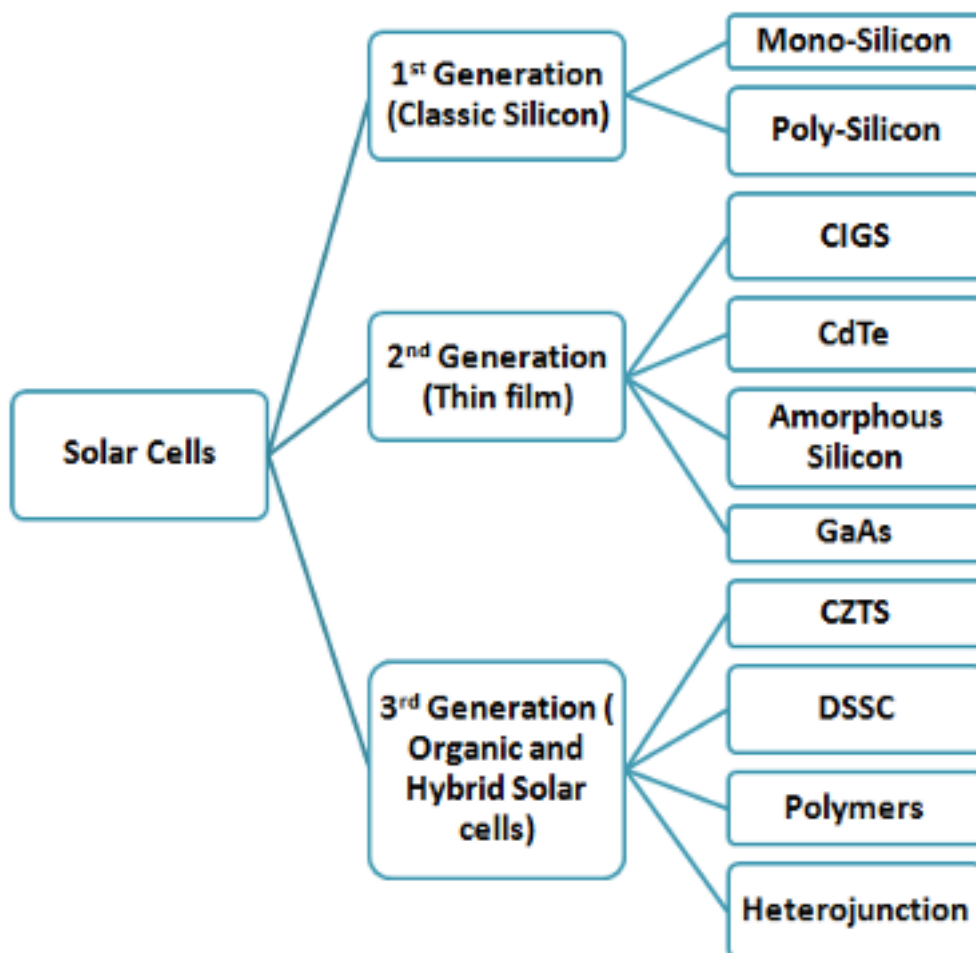


Figure 1.3 Generation wise classification of solar cells.

1.2.2.1. *1st generation: Crystalline Silicon (Poly-silicon or mono-silicon) solar cells*

The first generation contains cells that use high-purity materials with low levels of structural flaws. These solar cells are basically silicon wafer-based and presently the most efficient cells but have high production cost. The working principle of these cells is mainly based on the following steps:

- a. Photo excited generation of electron-hole pair.
- b. Their separation and collection through the P-N junction of a doped semiconductor.

The efficiencies of these cells typically lie in the range of about 25 % [9]. However, despite being the most commonly used and researched material, silicon is not an ideal semiconductor for photovoltaic conversion. It has a low optical absorption coefficient as it is an indirect bandgap semiconductor. Consequently, Silicon substrates of larger thickness are required to effectively absorb the major portion of the incident light. This, combined with the high cost of silicon purification and crystallization, makes silicon solar cell manufacturing prohibitively expensive. As a result, while silicon based first-generation photovoltaics are a reliable and well-established PV technology, their cost-cutting potential appears to be limited. Furthermore, even though there is still opportunity for improvement, silicon solar cell efficiencies are still restricted by the theoretical Shockley-Queisser limit for a single-junction cell [10]. To address the issues with first-generation solar cells, two approaches have been taken: (a) to concentrate on lowering the costs and (b) to boost the energy conversion efficiency and go beyond the Shockley-Queisser limit. The primary focus of the first approach is the development of thin-film solar cells. These devices are commonly known as second generation photovoltaics. On the other hand, third-generation PV technologies are based on approaches

centred on devices that could theoretically overcome the Shockley-Queisser limit.

1.2.2.2. 2nd generation: Thin film Solar Cell (TFSC)

The second generation of solar cells is mainly based on the use of thin film technology. Their constituent material has a thickness of less than 1 μm , which is much thinner than the first generation solar cells. Thin films are deposited on glass, metal or plastic substrate by applying various deposition techniques. The thickness of such films can be varied from a few nanometers to tens of micrometers. This is because thin film materials have a substantially higher absorption coefficient than silicon as they are direct band gap semiconductors. Since these cells use a single p - n junction, they also have a theoretical maximum efficiency restriction similar to first-generation photovoltaics. PV modules made of crystalline silicon must be constructed from individual cells. In contrast, a thin film of the semiconductor materials may be formed on the larger surfaces, which is advantageous for mass production of the devices. Examples of these kinds of materials include amorphous silicon, micro-crystalline silicon, polycrystalline silicon, copper indium selenide, and cadmium telluride.

Among the materials employed, the most established technique is that of amorphous silicon (a-Si), which is frequently utilized in so-called double- or triple-junction cells: these devices are made by assembling several cells with different band gaps, which absorb light in different wavelength regions. This material is used in photovoltaic applications where the power requirement is relatively low. Though these cells have relatively lower efficiency, they are much cheaper to fabricate. The major advantage of these solar cells is that they require only 1% of the silicon for solar cell production. As a result, the

manufacturing cost of these solar cells is dramatically reduced. At the module level, the efficiency of these solar cells ranges between 4 and 8 percent. The low quantum efficiency of amorphous silicon solar cells is the reason behind their low efficiency. These solar cells have low quantum efficiency as a result of the low number of collected charge carriers per incident photon. The efficiency of these amorphous silicon solar cells has been enhanced using tandem and even triple layer devices that feature p-i-n cells stacked one on top of the other [11]. The low efficiency of these cells is due to the existence of many dangling bonds, which resulted as a consequence of the disordered structure of amorphous silicon. Acting like defects, these dangling bonds results in anomalous conductivity in the amorphous silicon material.

Another popular material used for thin-film solar cell fabrication is cadmium telluride (CdTe). It has photovoltaic capabilities very similar to crystalline Si, but with the added benefits of diffuse light absorption and stability to increasing temperature concerns [12]. The only photovoltaic technology based on the thin film which is able to outperform the crystalline silicon PV in terms of cost in the PV market is CdTe. It holds a record with laboratory efficiency as high as 20%, which has been validated at NREL [13]. The key advantage of these solar cells that are appropriate for wide-scale production is the availability of a broad range of manufacturing procedures. The use of rare and toxic materials like cadmium and telluride is the main concern of this technology. Further, Copper indium selenide (CIS) is a material with exceptional long-term stability and potential applications in building-integrated photovoltaics [14]. Another promising material in the field of thin-film solar cell technology is Copper Indium gallium selenide (CIGS). It has a high absorption coefficient and subsequently shows high absorption of light even with much thinner film thickness than other materials. One of the major

advantages of CIGS based cells over other thin film based solar cells is its extended life span without showing any significant decline in its performance. It showed a certified efficiency of 23.35 % in the laboratory scale whereas in module form, it holds a record of efficiency of around 19.64 % [15] [16-18]. Due to low fabrication cost and high efficiency, CIGS cells are regarded as one of the most promising candidate of the thin film solar cell technology. Thin film solar cells also have the advantage of fitting the solar panels on flexible materials like textiles. [19-21].

The development of thin-film technology is still in its early phases, and the efficiencies of small-area laboratory cells do not always convert to large-scale module efficiencies. Aside from this, the usage of toxic compounds like cadmium and rare elements as telluride and indium is one of the major challenges that are encountered by this technology. The employment of toxic materials in a technology that is promoted as environmentally safe is highly controversial.

1.2.2.3. 3rd generation Solar Cells

The third generation encompasses a wide range of technologies and is usually used to describe photovoltaic systems that are not part of the first or second generation solar cells and seek to exceed the Shockley-Queisser limit. This generation of photovoltaic cells relies on a variety of new and low-cost materials such as organic, conductive polymers, small molecules, and organic dye molecules. It uses low-cost fabrication methods that do not require severe temperatures, such as those required for pure silicon-based cells. The primary difference from earlier generations is that the device's basic structure is no longer a *p-n* junction. Now, it possesses a multilayer structure wherein the charge carriers are exchanged. In contrast to their inorganic counterparts, newly

discovered organic and polymeric materials emerged out to be very promising for photovoltaic application for various reasons, including low material consumption, lightweightness, flexibility, and low cost for large-scale manufacture. The areas of research in this field that have attracted the researchers' attention most are extremely thin absorber cells (ETA), organic heterojunction solar cells, hybrid solar cells and dye-sensitized solar cells.

The active layer of an organic heterojunction solar cell is made up of an n-type donor and a p-type acceptor material. Donor materials include polyphenylene vinylene derivatives and poly-alkyl thiophene, whereas some common acceptors include fullerene and its derivatives. The maximum efficiency that has been achieved to date for this class of devices is 5.15 %, check for the recent highest efficiency [22].

Entirely solid inorganic materials are used to fabricate three phase ETA solar cells. A very thin photon absorbing semiconductor material is placed in a sandwich manner in between two highly interpenetrated and transparent semiconductor nanomaterial layers acting as electron and hole transport materials. [23-25]. Semiconductors like TiO_2 and ZnO are generally used as electron conductors, whereas material like CuSCN is used as hole conducting material in these devices.

In contrast, the hybrid solar cells are composed of both the organic and inorganic semiconductor materials. Usually conjugated polymers are the most used organic materials used in these cells to absorb light as well as participate in hole transport. On the other hand, the inorganic material is mainly used as electron conduction material. These materials are mixed together, forming a heterojunction. Efficiencies above 5 % have been recorded for this kind of devices [26].

The breakthrough came in the third generation of solar cells with the discovery of Dye sensitized solar cells in 1991 by O'Regan and Grätzel with a significant energy conversion efficiency of 7.9 % [27]. These cells emerged as one of the leading runners in the race of non silicon based solar cells because of its novel fabrication concept derived from nature's principle (photosynthesis) and easy fabrication procedure using abundant materials and cost effectiveness [28, 29]. Working principle of these cells is often referred as artificial photosynthesis. These cells are usually made up of highly porous film of titanium dioxide nanoparticles photosensitized with dye molecules which absorb sunlight similar to the chlorophyll presents in plant leaves. The porous TiO₂ layer is submerged in a liquid electrolyte solution and a platinum based counter electrode is placed above it. Discovery of these cells opened a new scope in the field of photovoltaic research. Many research groups have been working in this field to improve its performance in terms of efficiency, stability, durability, flexibility and cost-effectiveness. Today, there are various similar solar cell approaches, including solid-state DSSCs [30], quantum dot sensitized solar cells [31, 32], p-type hole conductor-based DSSCs [33], and perovskite solar cells [34-37]. Since their discovery in 2012, perovskite solar cells have become a subject of growing interest among researchers worldwide. Alternatives to the liquid electrolyte in DSSC include gel electrolytes, ionic liquids, and in-situ polymerized hole conductors [38-43]. The outstanding consolidated efforts given by the research community throughout the last 30 years have not only improved the efficiencies of these cells but also uncovered various novel strategies to make rugged and stable DSSCs with satisfactory conversion efficiencies. This includes vigorous work on different semiconductor oxides and their morphologies, different inorganic and organic sensitizers, co-sensitization of different sensitizers, new red-ox electrolyte and counter electrode materials.

The key benefits of the Dye sensitized solar cells are inexpensive large-scale production capability with flexibility. The disadvantages are low efficiency, stability and strength compared to traditional non-organic PV cells. For the most part, organic photovoltaic technology is still in the research and development stages and is not ready for mass commercialization.

The efficiency trend of different generations of solar cells over the years in the form of laboratory research cells and as solar modules are summarized below in Fig. 1.4 and Fig. 1.5, respectively.

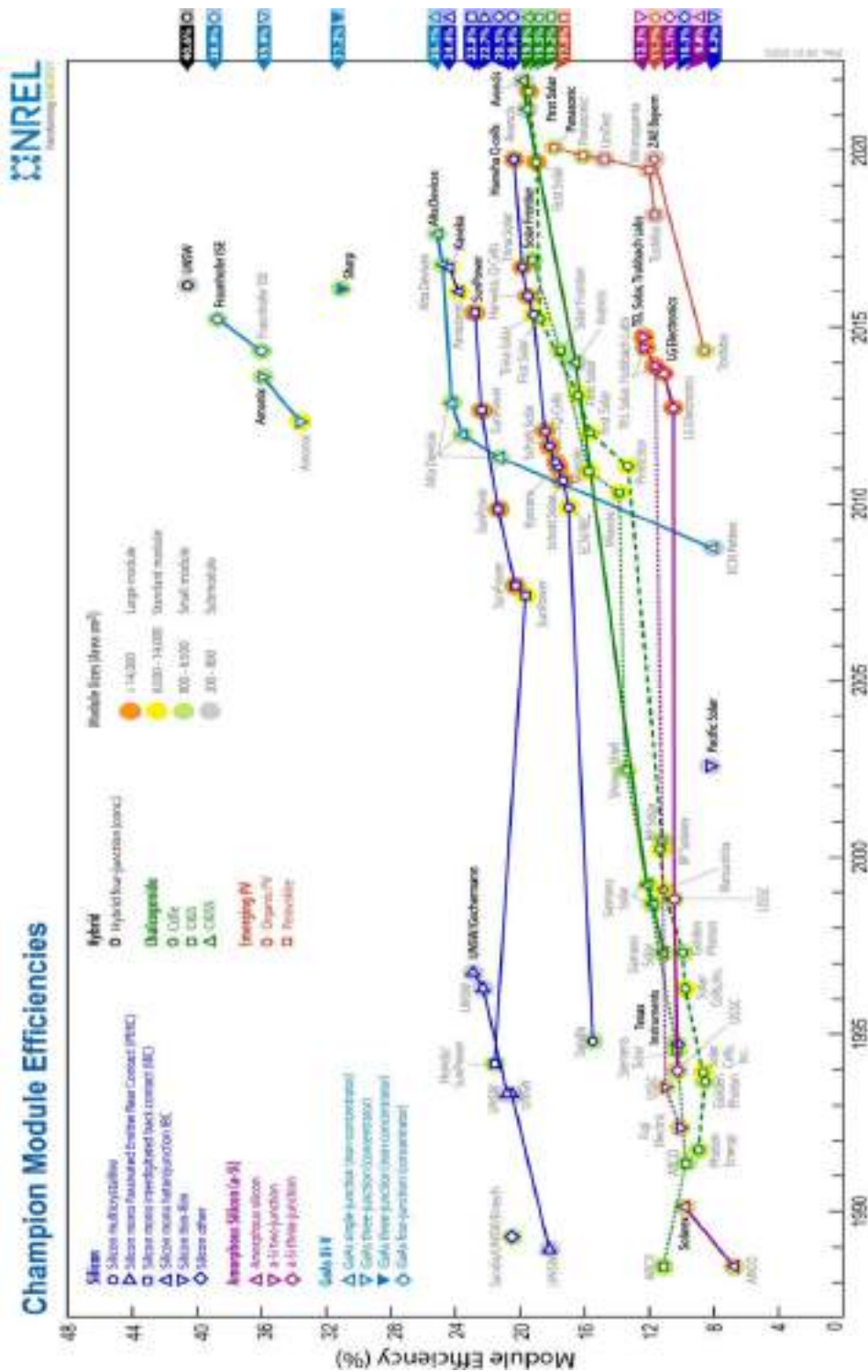


Figure 1.5 Reported timeline of Solar Module efficiencies of different solar cell technologies (National Renewable Energy Laboratory, USA) (<https://www.nrel.gov/pv/module-efficiency.html>)

1.3. Basic construction and different components of a Dye sensitized solar cell

The working of a DSSC is based on the sensitization of wide band gap semiconductors. A typical DSSC consists of five essential elements as follows:

- Transparent conductive oxide coated glass substrate (FTO, ITO etc).
- A photoelectrode with a thin layer of nanostructured wide band-gap semiconductor (usually TiO_2 , ZnO , WO_3 , SnO_2 or Nb_2O_5) attached to the conducting glass substrate.
- A monolayer of dye deposited on the semiconductor's surface to absorb light.
- An electrolyte containing a red-ox couple (typically I⁻/I₃⁻) which acts as a source for electron replacement.
- A counter electrode made of a glass sheet coated with a catalyst to facilitate electron collection (typically platinized FTO, ITO etc).

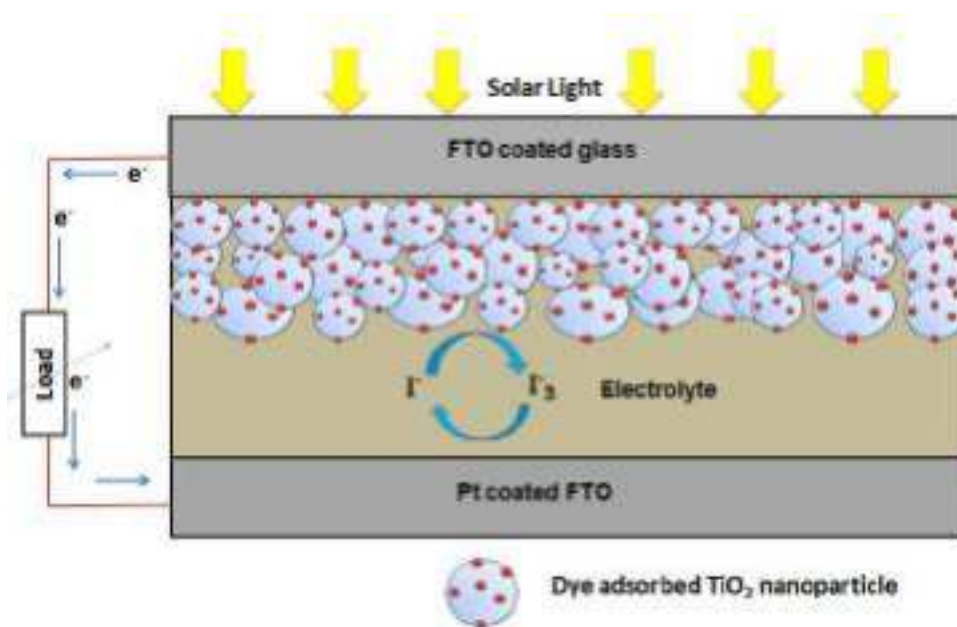


Figure 1.6 Basic structure of DSSC.

1.3.1. Transparent conducting oxide (TCO) coated glass substrate

The electrodes for a conventional DSSC are constructed on the TCO-coated glass substrates [44,45] and the cell is assembled between them. The performance of the DSSC is heavily influenced by the transparent conducting substrate. It serves the role of a current collector as well as a support structure for the semiconductor layer. It has two key characteristics: high optical transparency, which permits natural sunlight to penetrate through to the underlying active material without suffering any undesired solar spectrum absorption, and low electrical resistivity, which promotes electron transport and decreases energy loss.

Both inorganic as well as organic materials have been used to make transparent conducting coatings for photovoltaic usage. Indium tin oxide (ITO), fluorine-doped tin oxide (FTO), and doped zinc oxide [46–48] are examples of transparent conducting oxides (TCO) that are frequently utilized as a layer in inorganic films.. On the other hand, the organic layers have been developed employing graphene and carbon nanotube networks, as well as networks of polymers like PEDOT [poly(3,4-ethylenedioxythiophene)] [49,50] and its derivatives[51-53]. A large variety of TCOs have been designed and researched extensively during the past thirty years. Among them, the most efficient TCO materials frequently utilized in solar applications are ITO and FTO coated glass substrates because of their easy fabrication process along with optimum electrical and optical properties. However, compared to ITO, FTO has better conductivity and better transparency to visible light. Furthermore, the electrical properties of ITO degrade at high temperatures and in the presence of oxygen, whereas FTO remains much more stable in such conditions. Moreover, FTO is cheaper as compared to ITO. Due to these reasons, FTO is mostly preferred over ITO in DSSC fabrications.

1.3.2. Photo electrode

The photoanode comprises of a wide bandgap metal oxide semiconductor coating over a TCO glass substrate, usually deposited via doctor blading, screen printing or dip-coating method. The semiconductors widely used to prepare mesoporous photoanode material are TiO₂ [154-58], ZnO [59-61], SnO₂ [62-64], WO₃ [65-68], Nb₂O₅ [69-71] etc. This layer acts as a dye adsorption surface, accepting electrons from the excited dye and conducting them to the TCO. TiO₂ has been and continues to be the most preferred choice as photoanode material for DSSCs. It has three different crystalline forms: anatase, rutile, and brookite. The brookite form is very difficult to synthesize. So it is not so popularly used to make photoanodes. Rutile (band gap = 3 eV, absorption edge at 413 nm) [72] is the most stable among all the three phases; however, it has a poor electron transfer rate, resulting in low current in DSSC. Moreover, it is not completely transparent in the UV-VIS range of the solar spectrum [73]. As a result, the anatase form of TiO₂ having band gap = 3.2 eV (absorption edge at 388 nm) [74] has been widely used in DSSC fabrication [75].

TiO₂ has certain special features that make it the favoured semiconductor for dye sensitised solar cells. Its conduction band edge is slightly lower than the excited state energy level (LUMO) of many dyes, which is one of the major requirements for the efficient electron injection from dye to semiconductor. Another advantage of TiO₂ is its high dielectric constant (80 for anatase), which allows efficient electrostatic screening of the injected electron from the oxidized dye molecules anchored to the TiO₂ surface, lowering the possibility of recombination before the dye molecule gets reduced by the red-ox electrolyte. As discussed earlier, the larger band gap of anatase

phase of TiO₂ makes it a better choice for dye-sensitized solar cells. It has the ability to absorb only ultraviolet light, leaving the rest of the visible and near-infrared spectrum of the solar light for the dye molecules attached to the surface, depending upon the sensitizers properties. Aside from this, the high refractive index of anatase TiO₂ ($n = 2.5$) enables effective diffuse scattering of the light inside the mesoporous photoanode and hence significantly enhances the light adsorption. As a result, by carefully controlling the TiO₂ surface, one may improve the light absorption and hence the photo anode's light harvesting efficiency.

If we consider a simple planar electrode TiO₂ surface covered with a sensitizer monolayer, only a small percentage of incident light may be absorbed, which is disadvantageous for the device performance. But when a nanocrystalline mesoporous TiO₂ film is used, the effective surface area may be enhanced to 1000 times the area of a planer film. As a result, the dye loading is also enhanced and ultimately increasing the light harvesting efficiency. Usually doctor- blading or screen printing method is to prepare the mesoporous nanostructured film over the TCO substrate. Subsequently, the nanoparticle film is sintered to improve its electronic interconnectivity and charge transfer to the substrate. TiO₂ cells exhibited a highest efficiency of 14.30 % till date [76]. The drawback of mesoporous nanostructured films is the lower charge transfer rate as a result of an extended electron diffusion pathway inside the semiconductor network. To address this significant drawback and provide improved charge transport capabilities, photoanode materials other than nanoparticles, such as 1-D nanostructures like nanotubes, nanorods, and nanowires, are gaining significant attention among researchers [77-83].

Recently, ZnO has emerged as a great potential alternative to TiO₂ due to its fascinating electrical and optical properties along with a simple synthesis

process. ZnO is a wide band gap semiconductor having a direct band gap of 3.37 eV, making it suitable as a photoanode material for DSSC [84, 85]. Moreover, its conduction band edge is placed nearly at same level as that of TiO₂. Apart from this, ZnO is very easy to synthesize, abundant, inexpensive and poses higher electron mobility (200-300 cm²V⁻¹S⁻¹ for bulk material and 1000 cm²V⁻¹S⁻¹ for nanowire) than that of TiO₂ nanoparticles (0.1-4cm²V⁻¹S⁻¹) [86-88]. Furthermore, zinc oxide is popular for its ability to be grown easily with a wide range of nanostructural shapes, such as nanoparticles, nanorods or nanowires, nanotubes, nanoplates, nanosheets etc. Additionally, the 1-D single-crystalline rod-like structure of ZnO nanorods provides a higher surface-to-volume ratio enabling better dye loading [79]. These qualities of ZnO make it a potential alternative to TiO₂ for the fabrication of DSSCs. Currently, the highest efficiency of ZnO photoanode-based DSSCs lies in the range of 8 % [89, 90]. However, the main issue with ZnO is its stability, particularly in aqueous situations. ZnO gets dissolved easily in basic and acidic solutions and has a relatively narrow range of stability. Dissolution of ZnO by anchoring groups like carboxylic acid results in Zn⁺² ions. These Zn⁺² ions subsequently form insoluble complexes with ruthenium dyes like N3 and N719. These insoluble complexes formed in the mesoporous structure disrupt the charge transport process.

1.3.3. Dye sensitizer

The sensitizing dye serves as the heart of a DSSC. By absorbing photons, it generates electrons that are then injected into the conduction band of the metal oxide semiconductor. The characteristics of the dye have a significant impact on the light-harvesting efficiency, thus highly influencing the overall conversion efficiency of the device. A good sensitizer for DSSC must satisfy several criteria in order to achieve high conversion efficiency.

- i. The longer the absorption range of the dye molecule, higher will be the conversion efficiency of the device. So the dye should absorb the sunlight ranging from UV to Infrared region.
- ii. The dye must carry an anchoring group so that it can be anchored firmly to the surface of the metal oxide semiconductor material by forming a chemical bond. The charge transfer from the dye to the semiconductor occurs through this chemical bond. Good adsorption to the semiconductor surface, i.e., Good attachment to semiconductor nanoparticles, ensures rapid electron transfer.
- iii. The excited state (LUMO) of the adsorbed dye molecule should be higher enough than the conduction band edge of the semiconductor oxide so that an energetic driving force can be provided for the electron injection process.
- iv. The sensitizer's highest occupied orbital (HOMO) must be placed low enough so that it can accept electron donation from the electrolyte or a hole conducting material and, consequently, the oxidized could be regenerated.
- v. The adsorbed dye molecule should be thermally and electrochemically stable enough in the working environment to sustain a long operation life under exposure to natural daylight. So it should also have high photostability.
- vi. It should possess high solubility to the solvent used in the dye impregnation.
- vii. The band gap of the dye or HOMO-LUMO gap must be as small as possible while still maintaining a LUMO that is more negative than the conduction band of the semiconductor and HOMO that is more positive than the red-ox species. The HOMO-LUMO gap of the dye sensitizer determines the spectral range of light that it can absorb.

-
-
- viii. Finally, the dye should not suffer aggregation. Dye molecules frequently tend to aggregate on the semiconductor oxide surface, increasing the decay from the excited to the fundamental state and, as a result, lowering electron injection into the semiconductor conduction band. Some additives, such as chenodeoxycholic acid (CDCA), are commonly used as co-adsorbents with the sensitizer in order to reduce the dye aggregation phenomena.

Several photosensitizers for DSSC applications have been studied over the last few decades: they are likely the most researched component of a DSSC device and have been thoroughly evaluated in multiple studies. The typical sensitizers are mainly classified into metal-complex dyes, metal-free organic dyes, and natural dyes [91-95].

Metal complex dye sensitizers, like polypyridyl complexes of Ruthenium (Ru), Osmium (Os), metal porphyrin and phthalocyanine are efficient and reliable dyes for DSSC application. Ruthenium-based metal complexes are the most popular among the metal complex dyes, owing to their excellent photovoltaic characteristics. So far, the most efficient sensitizers in DSSCs have been Ruthenizer 535-bisTBA (known as N719 dye), Ruthenizer 535 (known as N3 dye) and N749 (known as black dye). Their exceptional photovoltaic activity stems from a broad absorption spectrum, well-aligned excited and ground states, and stability in the oxidized state, making them the most suited candidate for DSSC application [96]. However, their poor molar extinction coefficient, inadequate availability of noble metals, high cost, negative environmental impacts and complex synthesis and purification method have compelled researchers to look for metal-free organic dyes and natural dyes [97]. Chemical structures of some popular metal complex dyes are shown in Fig. 1.7.

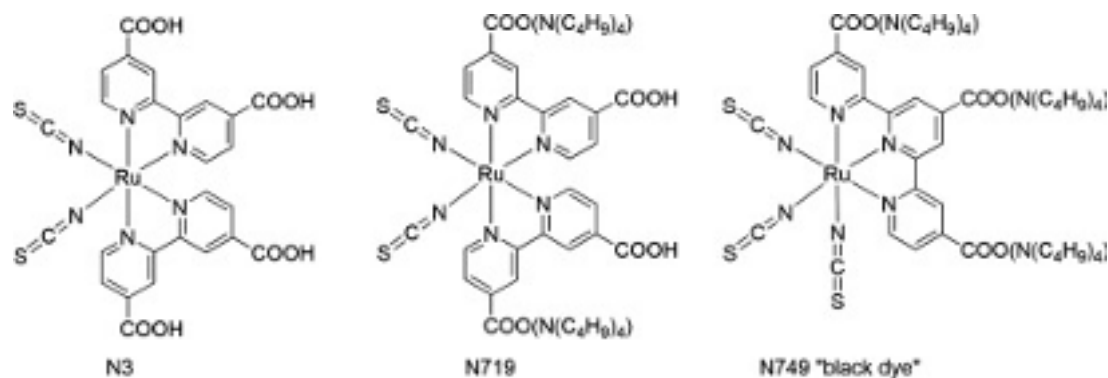


Figure 1.7 Chemical structure of some metal-complex dyes.

Over the last decade, several organic sensitizer families have been presented. Organic dye-based DSSCs have been advancing quite rapidly in recent years, and their conversion efficiencies are comparable to that of polypyridyl ruthenium dye-based cells. In addition, metal-free organic dyes are distinguished by their low cost, high molar extinction coefficients, and diversity of molecular architectures.

Coumarin, indoline, cyanine, merocyanine, hemocyanin, triphenylamine, phenothiazine, tetrahydroquinoline, dialkylaniline, and carbazole are some examples of dyes falling in this category. Fig. 1.8, Fig. 1.9 and Fig 1.10 show molecular structures of some common dyes belonging to this category. Hara et al. presented various coumarin derivatives and achieved an efficiency of 7.4 % [98], which was comparable to the performance of a cell fabricated using N719 dye under similar working conditions. In 2003, Horiuchi and co-workers, for the first time, reported the synthesis and application of indoline dye in DSSC and achieved a conversion efficiency of 6.1 %, which was slightly less than the 6.3 % efficiency obtained with N3 dye under the same experimental conditions [99]. Later in 2004, the same group reported a conversion efficiency of 8 % for a new type of indoline structure [100]. In addition to its high photoconversion

efficiencies, indoline dye was found to be highly stable to photodegradation procedures. Cyanine dyes are well known for having high molar extinction coefficients and have the ability to absorb light in the near-IR region [101, 102]. A novel cyanine dye featuring a triphenylamine as donor, carboxylic acid as acceptor and connected by a low-band-gap benzothiadiazole conjugation fragment had been developed and effectively used to sensitize TiO₂-based DSSC by Tian and his co-workers [103]. It showed an efficiency of 7.62 % under the illumination of 75 mW/cm². Liu et al. developed a novel isophorone sensitizer D-3 based on a donor- π -acceptor system and obtained a remarkable photoconversion efficiency of 7.41 % under 100 mW/cm² illumination.

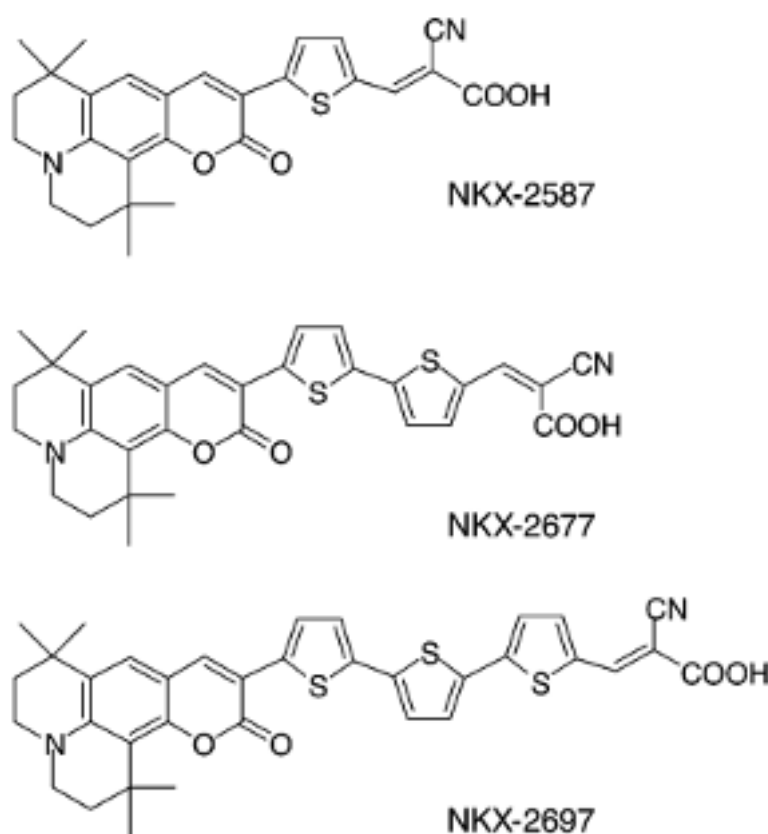


Figure 1.8 Molecular structure of Coumarin dyes.

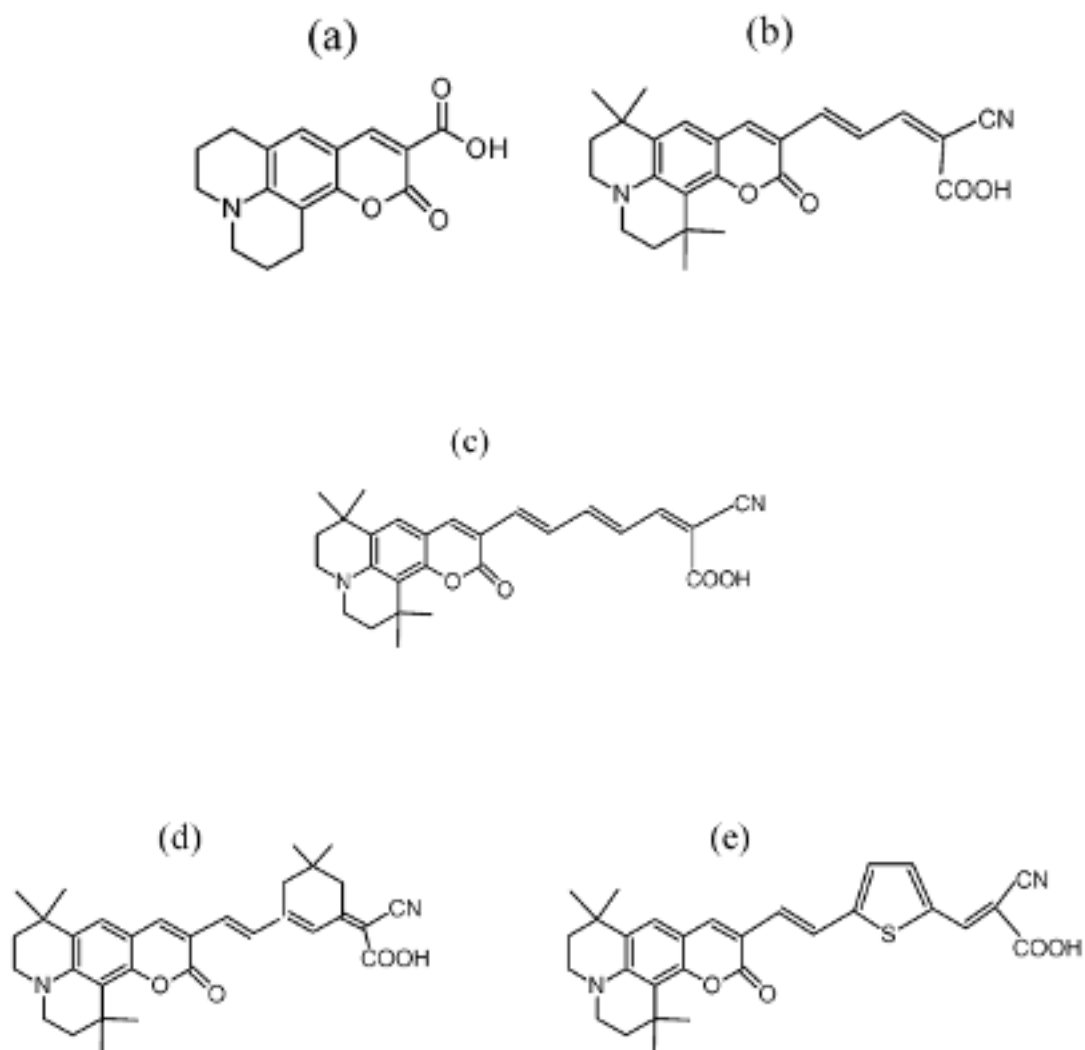


Figure 1.9 Coumarin dye structures: (a) C343, (b) NKX-2311, (c) NKX-2586, (d) NKX-2753 and (e) NKX-2593.

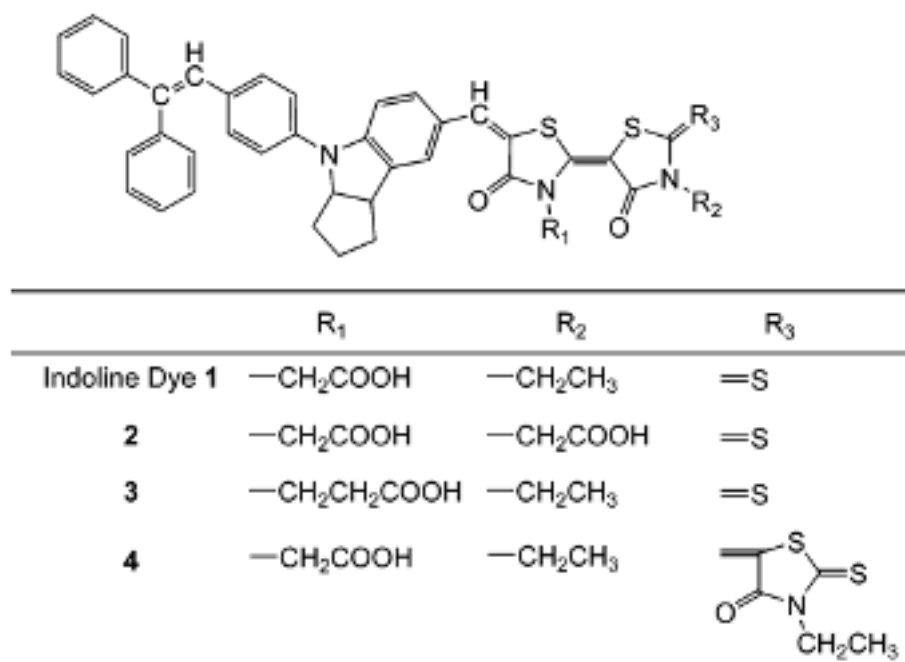


Figure 1.10 Molecular structure of indoline dyes (1-4).

Extensive research has been conducted over the years to determine the feasibility of replacing synthesized dyes with plant-based natural dyes. Various natural fruits, flowers and plant leaves have a variety of colours and contain a variety of pigments that can be extracted and used in DSSCs to harvest solar energy. Natural dyes have several advantages compared to the synthesized dyes. Natural dyes, unlike synthetic dyes, are widely available, simple to prepare, inexpensive, non-toxic, environment friendly, and fully biodegradable [104, 105]. Natural dyes are classified into four major families: chlorophyll, anthocyanin, carotenoids, and flavonoids. Figure 1.11 depicts a flow chart diagram representing the classification of pigments found in plants [106-108].

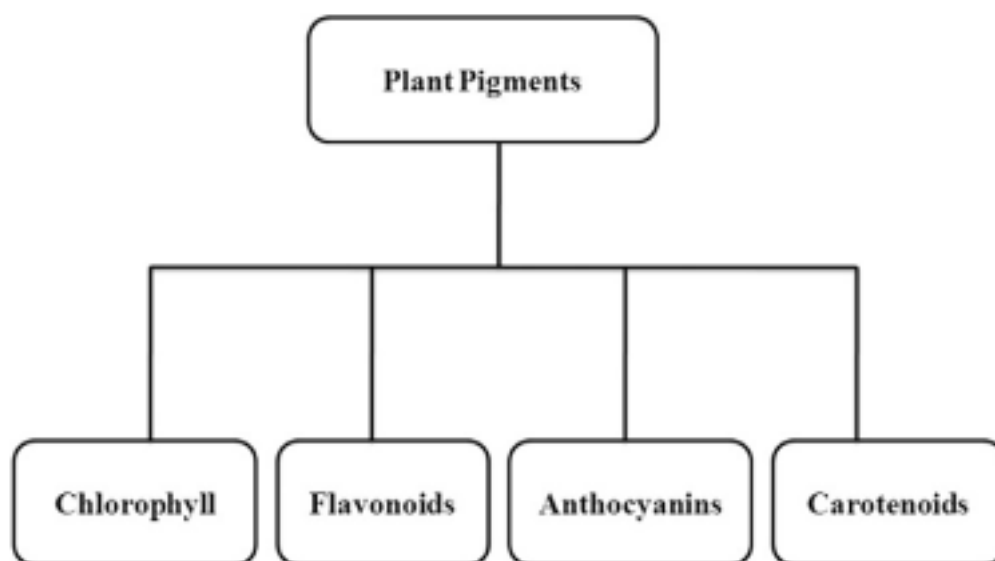


Figure 1.11 Classification of plant pigments.

Chlorophyll is abundant in the leaves of most green plants. It is the natural photosynthetic pigment that gives plants their green colour [109, 110]. The primary functions of chlorophyll are efficient harvesting of light energy and transduction of that energy for photosynthesis, which is primarily accomplished by their spectral properties. Chlorophyll ‘a’ and chlorophyll ‘b’ are the two major types of chlorophylls. Because of their ability to absorb blue and red light, chlorophylls and their derivatives are used as sensitizers in DSSC. The most effective is a chlorophyll a derivative (methyl trans-32-carboxy-pyropheophorbide) [111]. When compared to chlorophyll a, the absorbance spectrum of chlorophyll b has a distinct blue tinge and a red shift. Fig 1.12 depicts the chemical structure of chlorophyll a and chlorophyll b.

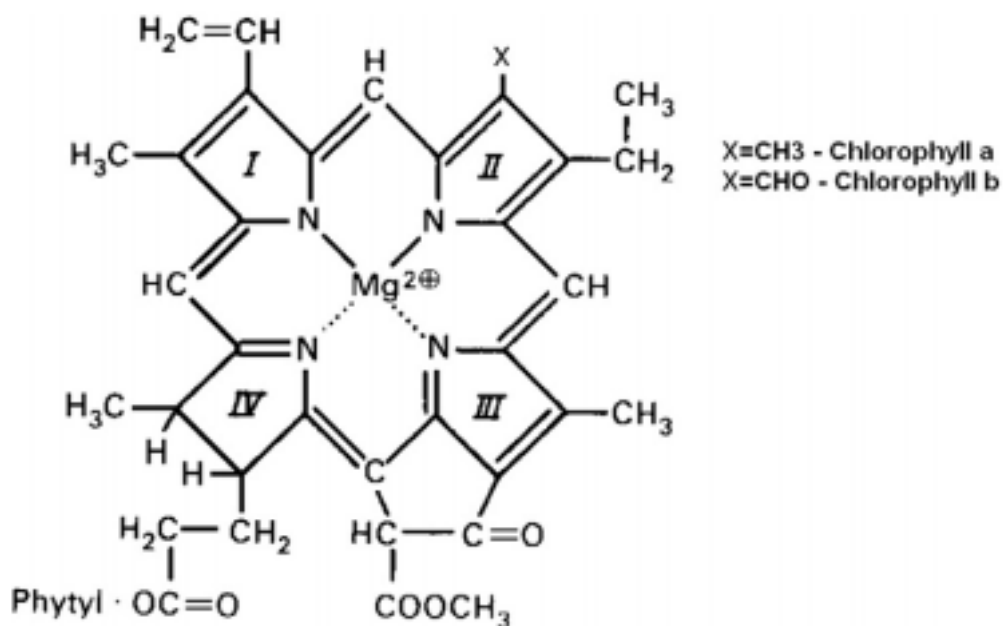


Figure 1.12 Chemical structure of Chlorophyll ‘a’ and chlorophyll ‘b’. [112]

Flavonoids are the most common and biochemically active group of natural constituents that contribute to the colour of flowers [113, 114]. Geissman and Hinreiner coined the term “flavonoid” to describe all compounds whose structure is based on flavones with a basic C₆–C₃–C₆ skeleton [115]. Flavone comprises two benzene rings connected by a ring that distinguishes one flavonoid compound from another. Despite their structural similarities, only a few flavonoids can absorb light in the visible range [111]. The basic chemical structure of a commonly occurring flavonoid is depicted in Fig. 1.13. The number of flavonoid structures found in nature is limited, and they range in oxidation state from flavan-3-ol to flavonols and anthocyanins. Flavonoids are also comprised of flavanones, flavanonols, and flavan-3, 4-diols [116]. Neoflavones or 4-phenyl coumarins, dihydrochalcones or 3-phenylpropiophenones, chalcones or phenyl styryl ketones, isoflavones or 3-phenyl chromones, and auronones or 2-benzylidene-3-coumaranones are also

compounds. The orientation of hydroxy and methoxy groups and their numbers in these two benzene rings distinguish the individual compounds in each class [117]. Fig. 1.13 depicts the structure of commonly occurring flavonoid. [118]

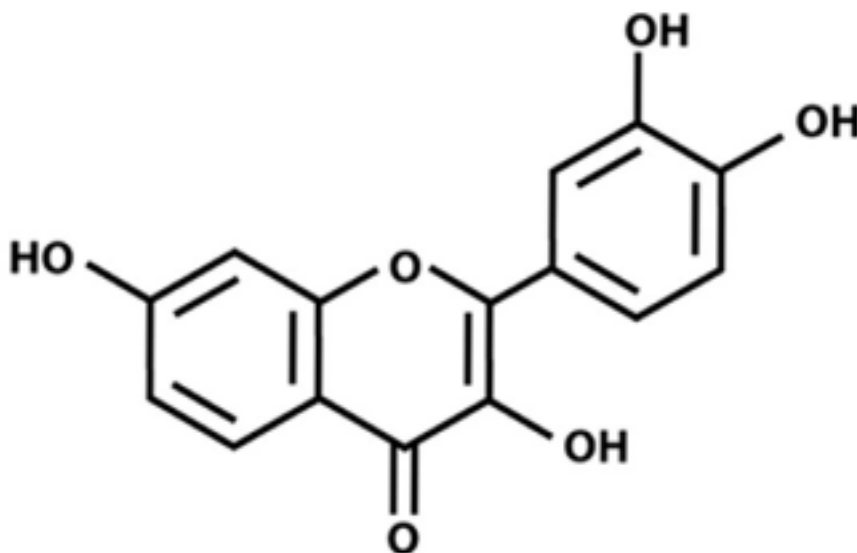


Figure 1.13 Chemical Structure of commonly occurring flavonoid.

Anthocyanins are the second most crucial group of pigments visible to the human eye after chlorophyll [104]. Anthocyanins also influence the amount and quality of light incident on chloroplasts [119]. The anthocyanins found in plants are so diverse that ornamental plants such as dianthus and petunia only have one type of anthocyanin, whereas tulipa, rosa, verbena, for example, has mixture of several. Some fruits, on the other hand, are rich in anthocyanins. Grapes contain a wide range of anthocyanins. Cyanidin is found in apples, cherries, figs, and peaches, while delphinidin is found in eggplant and pomegranate. Cherry sweet and cranberry contain both cyanidin and peonidin. Carbonyl and hydroxyl groups present in anthocyanin molecules from bonding with the TiO₂ molecule, thereby promoting excitation and injection of electrons from the dye molecule to the conduction band of TiO₂. The basic

chemical structure of anthocyanin pigment is shown in Fig. 1.14

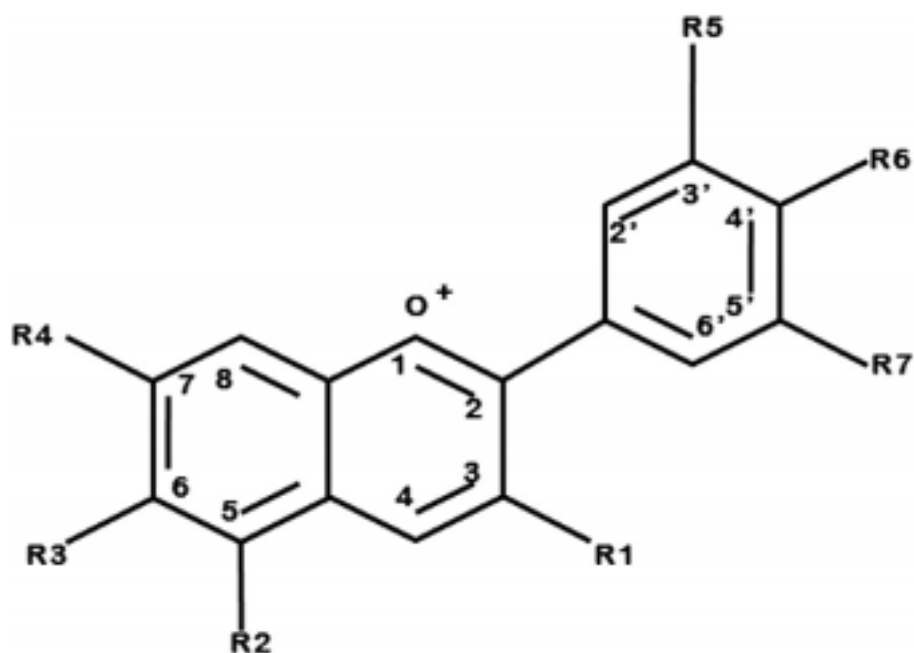


Figure 1.14 Basic chemical structure of anthocyanin pigment. Here ‘R’ could be replaced with H, OH or OCH₃ depending on the pigment. The numbers can be substituted with the hydroxyl group.

Carotenoids are a large family of isoprenoids (with more than 600 members) that give distinguishing red, orange, and yellow colours to many fruits and flowers. The presence of a C₄₀ hydrocarbon backbone distinguishes carotenoids, causing structural and oxygenic changes. Fig. 1.15 shows the chemical structures of some pigments from the carotenoid class [120-122].

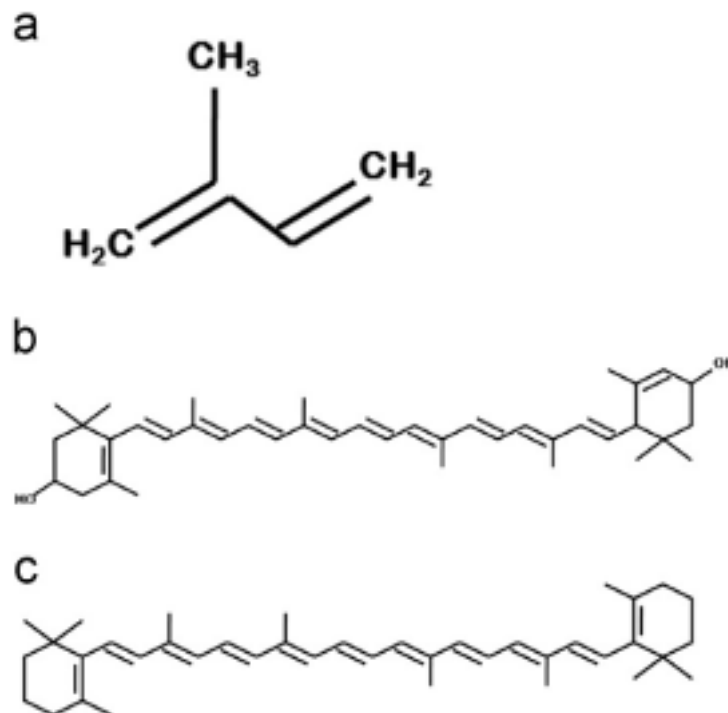


Figure 1.15 (a) Basic structure of an Isoprene unit, (b) Chemical structure of Xanthophylls, and (c) Chemical structure of Carotene.

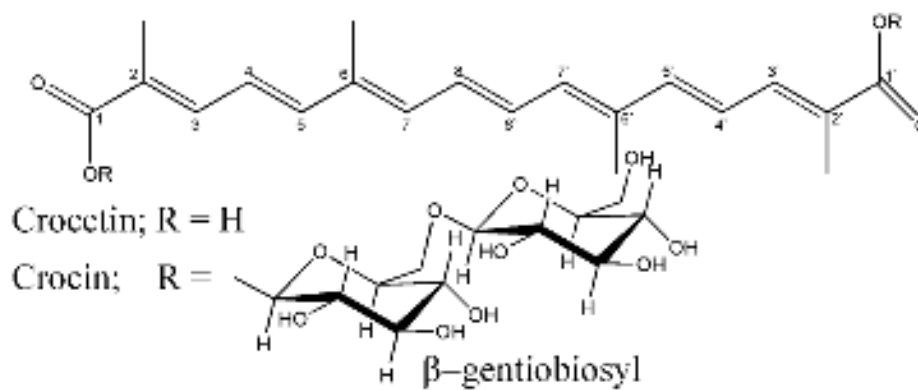


Figure 1.16 The molecular structures of crocetin and crocin.

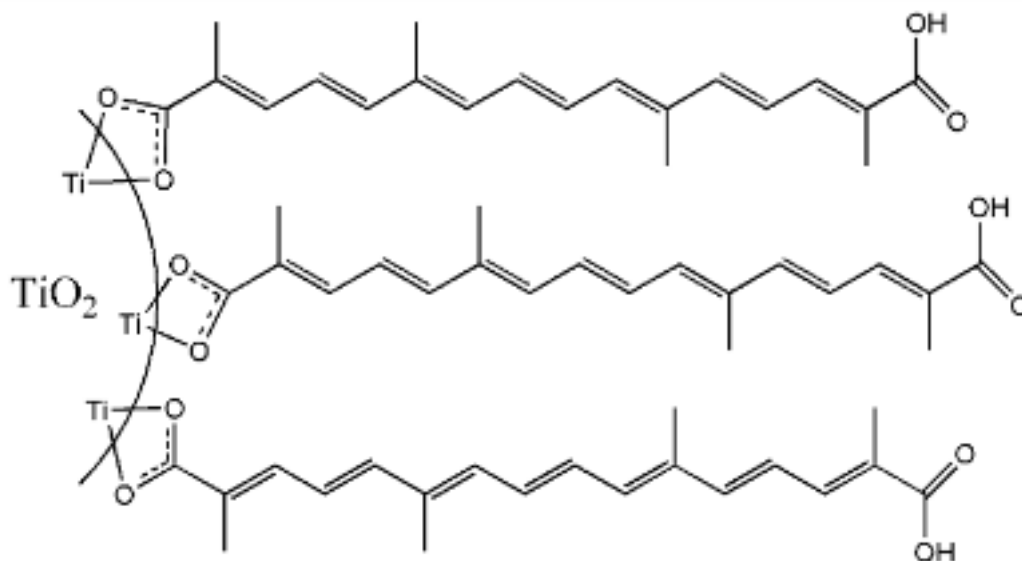


Figure 1.17 Possible mechanism of the binding between crocetin and TiO_2 surface.

Many investigations have been performed to explore all the classes of natural dyes mentioned earlier, such as chlorophyll [123-131], carotenoids [132-134], and flavonoids [135-139]. When compared to DSSCs sensitized with synthetic dyes, the overall cell efficiency of natural dye-based DSSCs is comparatively low. Comparative studies on the performances of DSSCs based on different types of natural dyes have been done by several researchers [105, 140, 141]. To improve the efficiencies of the natural dye based DSSCs further, different dye combinations have been investigated and reported in order to obtain a broader absorption spectrum. Using natural dyes in conjunction with an optimized extraction solvent improves solar light absorption by the dye molecules and allows for more efficient utilization of photon energy. As a result, DSSC sensitized with the dye mixture exhibits higher absorbance and cumulative absorption properties across the entire visible region than DSSC manufactured with single individual dyes [138, 142-147].

1.3.4. Electrolyte

One of the most crucial function in the light-to-electricity conversion process is played by the electrolyte. It acts as an electron transfer mediator, restoring the dye sensitizer molecules from their oxidized state. The following are the requirements for any electrolyte used in a dye-sensitized solar cell:

1. To prevent dye degradation from the oxide surface, the electrolyte must be chemically, thermally, optically, and electrochemically stable over time.
2. The charge carriers must be transported between the working electrode and the counter electrode by the electrolyte. The oxidized dye must be regenerated and restored to its ground state after the electrons are injected into the oxide material's conduction band. As a result, the electrolyte must be selected carefully, taking into account the redox potential and recombination properties of the dye.
3. The electrolyte must allow charge carriers to diffuse quickly into the device and maintain good contact with both the mesoporous nanocrystalline oxide surface and the counter electrode. In case of liquid electrolytes, it is necessary to prevent solution loss due to leakage or evaporation..
4. There should be no significant absorption of visible light by the electrolyte. As I_3^- has its own colour, it reduces visible light absorption by the dye. Additionally, I_3^- ions may react with the injected electrons leading to increased current. That is why the concentration of I^-/I_3^- must be optimized in the electrolytes containing I^-/I_3^- couple.

Depending upon the viscosity, the electrolytes are classified as liquid, quasi-solid, or solid. Electrolytes based on liquid organic solvents are the most common electrolytes used in DSSCs. They are typically made up of a redox

couple dissolved in an organic solvent with a high dielectric constant; additional additives can be added to improve device performance.

Iodide/triiodide (I^-/I_3^-) is the most common redox couple, owing to the slow recombination reaction; these electrolytes are generally prepared by dissolving iodide salts with various cations (K^+ , Li^+ , Na^+ , Mg^+) in a liquid solvent. The kinetics of the (I^-/I_3^-) redox couple with Ruthenium dye (N719) is depicted in Fig.1.18. The injection of photogenerated electrons into the conduction band of TiO_2 takes place on the femtosecond time scale, which is much quicker than the electron recombination process with I_3^- , and the oxidized dye mainly reacts with I^- rather than the injected electrons. I_3^- diffuses to the cathode in the electrolyte to harvest electrons, producing I^- , which then diffuses in the opposite direction towards the TiO_2 electrode and consequently regenerates the dye molecules.

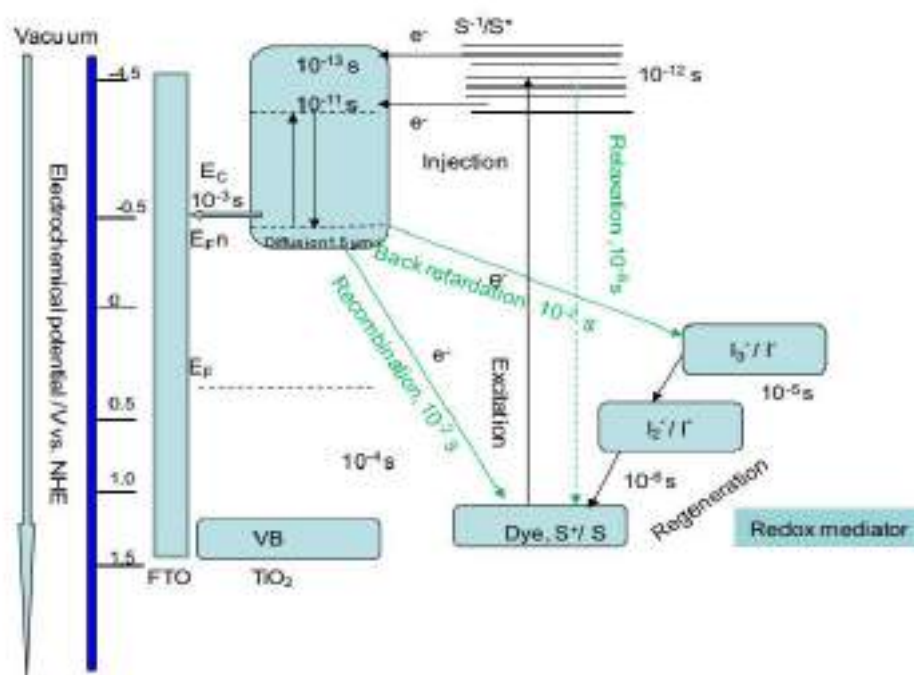


Figure 1.18 Charge transfer and recombination kinetics in DSSC.

(<https://ro.uow.edu.au/theses/3415/>)

However, because of iodine's corrosive properties, researchers have looked into alternative redox couples such as Br-/Br³⁻ [148], SCN⁻/(SCN)³⁻ [149], and SeCN⁻/(SeCN)³⁻ [150], all of which have promising electrochemical and noncorrosive properties but are chemically unstable [151]. Copper and cobalt complexes can also function as redox mediators [152, 153].

Regarding the solvent, it should be chemically stable, have low volatility in the temperature range within which the DSSC is being operated, have a high dielectric constant to facilitate redox couple dissolution faster, low viscosity to promote rapid charge diffusion [151], and should allow for good solubility of the redox mediator and other additives in the electrolyte. It is also essential that the solvent does not cause dye, semiconductor desorption, or dissolve the sealing material into the solvent. Mostly used solvents are polar organic solvents. Acetonitrile (ACN) is the most common and effective solvent used in DSC research because of its excellent performance, stability, low viscosity, and ability to dissolve a wide range of salts and organic molecules. However, unfortunately, the boiling point of acetonitrile is low (78 °C), so 3-methoxypropionitrile (MPN), with a boiling point of 164 °C and low toxicity, is the preferred choice for the long-term stability of DSSCs.

Additives to the electrolyte such as 4-tert-butyl pyridine (4TBP), guanidiumthiocyanate, and methyl benzimidazole (MBI) have been found to be very effective in suppressing the recombination [154-156]. The most likely mechanism behind this reduction in recombination is that when the TiO₂ surface absorbs these additives, they block reduction sites, preventing electron acceptor molecules from coming into contact. A variety of cations and compounds have been added to liquid electrolytes as additives and tested to improve the cell's photovoltaic performance. The most widely used additive is 4-tert-butylpyridine (TBP), which effectively suppresses the dark current and thus increases the fill factor and efficiency values by the introduction of

coordination between N atoms and Ti ions on the TiO₂ surface, thereby limiting electron recombination [157]. When guanidinium thiocyanate (GuSCN) is added in the liquid electrolyte, it increases both the current and voltage due to a positive shift in the conduction band of TiO₂ and leads to a reduction in the charge recombination phenomena [158]. Li cations are another common additive. They can be readily adsorbed on the surface of TiO₂ nanoparticles, resulting in a significant increase in photocurrent density. This effect is caused by the capability of Li ions in lowering the acceptor states of TiO₂, modifying the flat band on the photoanode surface and consequently electron injection process becomes more energetically favourable [159]. When these cations are not present on the surface, the conduction band of the semiconductor shifts downward, lowering the V_{oc} of the cell [160]. These additives can thus enhance the efficiency and stability, even without participating in the fundamental photoelectrochemical processes. However, the concentration of LiI must be kept low because the small Li cations may bind to the TiO₂ matrix and act as recombination centers, reducing device performance [161]. The maximum voltage that can be obtained from the DSSC is theoretically determined by the difference between the quasi-Fermi energy level of TiO₂ and the redox potential of the electrolyte.

The major challenges with using liquid solvent-based electrolytes are their leakage problem, difficulty in sealing and limited long-term stability. These limitations prevent the utilization of the devices with high and consistent efficiency over time. Various alternative solutions have been proposed to address these shortcomings and are currently being researched. Quasi-solid electrolytes and solid electrolytes have attracted special consideration from researchers in this regard. Quasi-solid electrolytes can be derived from organic solvent-based or ionic liquid electrolytes that can be gelled, polymerized, and dispersed in a polymeric material [151, 162-164].

Conductive polymers, hole-conducting molecular solids, and organic p-type conductors, such as poly(3-hexylthiophene) (P3HT) [165] polypyrrole [166], poly(3,4-ethylene dioxythiophene) (PEDOT) [167], polyaniline (PANI) [168] and 2,2',7,7'-tetraakis-(N,N-di-p-methoxyphenyl-amine)9,9'-spirobifluorene (spiro-OMeTAD) [169] are few examples of solid-state electrolytes. However, the photovoltaic performance of DSSCs based on all of these alternative electrolytes is currently lower than those based on liquid solvents, indicating that more research is needed in this field.

1.3.5. Counter electrode

The counter electrode is that important component of a DSSC where the reduction of the redox species occurs. In the case of solid-state DSSCs, the counter electrode collects the holes from the hole transporting material [170]. As the counter electrode, Pt-coated FTO obtained through thermal decomposition [171], sputtering [172] or chemical reduction [173] is typically used. However, due to the high cost and limited resources of Pt, considerable efforts have been made in recent years to replace this Pt catalyst with other low-cost, earth-abundant materials. Due to their excellent catalytic activity, materials such as graphite, carbon black, activated carbon on FTO-glass, and organic-ion doped conducting polymer of poly(3,4-ethylene dioxythiophene)(PEDOT) on both indium tin oxide (ITO) and FTO-glass have also been successfully used as counter electrode materials in DSSCs [174-178]. However, the main issue with the carbon counter electrodes is their adhesion to the substrate surface and their opaque nature.

1.4. Basic Operating Principle of DSSC

A DSSC is the only photovoltaic device with multiple electron transfer processes running in parallel and competition. It utilizes separate mediums for light absorption/carrier generation (dye) and carrier transport (TiO_2 nanoparticles and the electrolyte). In contrast, in a p - n junction semiconductor solar cell, the light absorption, charge separation and transport occur in the same material. Dye molecules play the same role as chlorophyll in leaves: they absorb incident photons and initiate the electron transfer process. The schematic diagram showing the basic working principle of a DSSC is shown in Fig. 1.19.

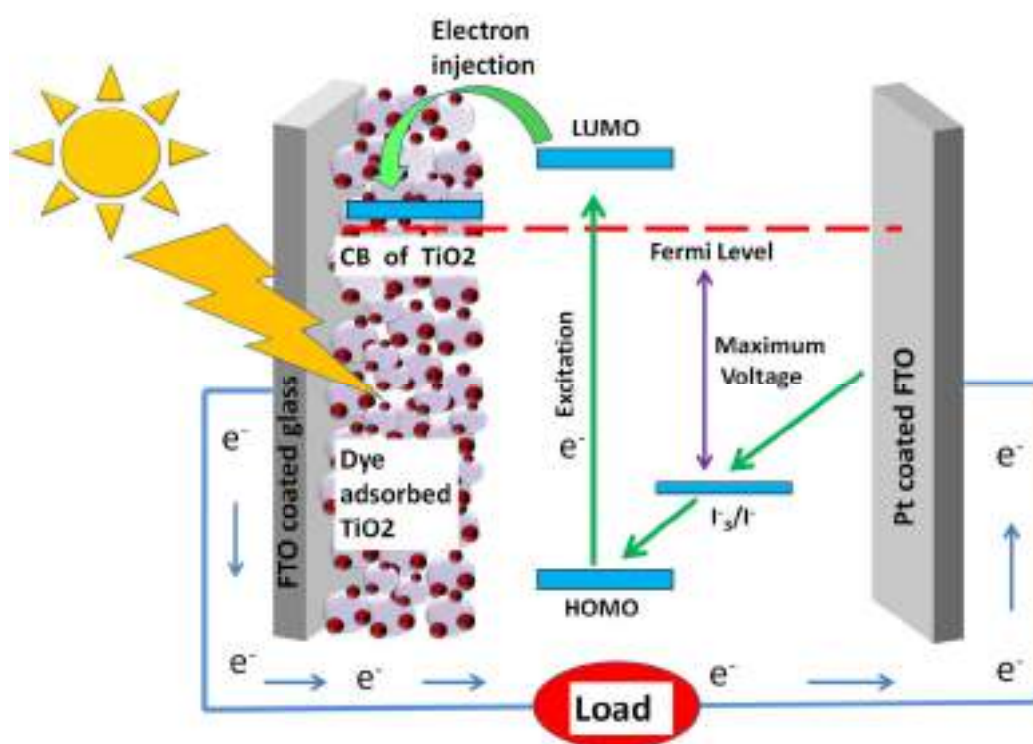


Figure 1.19 Schematic and basic working mechanism of DSSC.

The basic operation steps and electron transfer process occurring inside DSSC are as follows [179-181]:

- a) When exposed to sunlight, photons are absorbed by the dye molecules and the electrons are excited from the HOMO-level to the LUMO-level, instantaneously. This process is known as photo-excitation.
- b) These excited electrons are then injected into the conduction band of TiO_2 , diffuse through it and are utilized at the external load before being collected by the electrolyte at the cathode surface to complete the cycle.
- c) The dye molecule after losing one electron to the TiO_2 gets oxidized. This means it has deficiency one electron. To recover its initial state, the dye molecule must obtain an electron. It obtains this electron from the iodide electrolyte (I^-) and the dye returns to the ground state. This procedure is known as dye regeneration..
- d) This causes the iodide to become oxidized. When the original lost electron reaches the counter electrode, it returns the electron to the electrolyte. I^- ion is regenerated in turn at the counter electrode by the reduction of I_3^- with electrons which have travelled through the external load.

There are also some reverse processes that decrease the overall cell performance. These are given below.

- a) Relaxation of photo excited electron of dye molecule from excited state (LUMO) to ground state (HOMO), both by radiative and non-radiative processes.
- b) Recombination of photo-injected electrons in the TiO_2 to the oxidized species (I_3^-) in the electrolyte.
- c) Recombination of photo-injected electrons in the TiO_2 to the oxidized dye molecule.

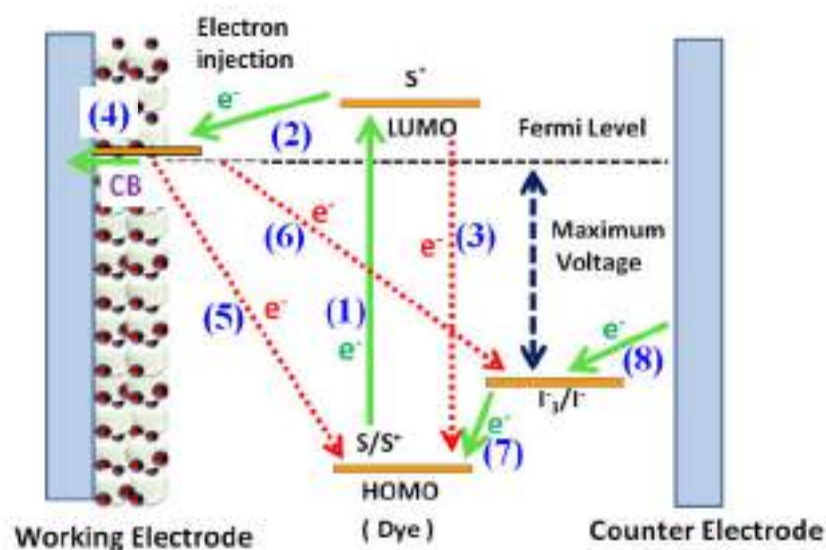


Figure 1.20 Fundamental processes inside dye-sensitized solar cell.

The following are the steps and corresponding equations involved in the cell operation [182,183]:

1. Photo excitation: $S + h\nu$ (Photon) $\rightarrow S^*$ (Excited)
2. Electron injection: S^* (Excited) $\rightarrow e^-_{(CB)}(SC) + S^+$
3. Relaxation: $S^* \rightarrow S + h\nu$ (Photon)
4. Electron transport: $e^-_{(CB)}(SC) \rightarrow e^-$ (TCO)
5. Recombination with the dye: $S^+ + e^-_{(CB)}(SC) \rightarrow S$
6. Recombination: $2 e^-_{(CB)}(SC) + I_3^- \rightarrow 3I^-$
7. Dye regeneration: $2S^+ + 3I^- \rightarrow 2S + I_3^-$
8. Reaction at the counter electrode: $I_3^- + 2e^-(C) \rightarrow 3I^-$

S: Dye sensitizer; S^* : excitation upon irradiation; S^+ : Oxidized dye; SC: Semiconductor; CB: Conduction band; C: Counter electrode.

The above processes are schematically illustrated in Fig. 1.20. The forward processes are depicted with green arrows, whereas red arrows

represent combination and reverse processes. The maximum output voltage is determined by the difference between the Fermi energy level of the semiconductor and the red-ox potential level of the mediator electrolyte [184]. Thus, the device can produce electricity from light without undergoing any permanent physical and chemical change.

References:

- [1] Patel, Nikul K., and Shailesh N. Shah. "Biodiesel from plant oils." In Food, energy, and water, pp. 277-307. Elsevier, 2015.
- [2] European Commission, The Energy Challenge of the 21st Century: The role of Nuclear Energy, <http://europa.eu.int/comm/research/rtdinfo/en.html>
- [3] M. Grätzel, Solar Energy Conversion by Dye-Sensitized Photovoltaic Cells, Inorg. Chem., 2005, 44(20), 6841–6851
- [4] Song, Dengyuan, Jingfeng Xiong, Zhiyan Hu, Gaofei Li, Hongfang Wang, Haijiao An, Bo Yu et al. "Progress in n-type Si solar cell and module technology for high efficiency and low cost." In 2012 38th IEEE Photovoltaic Specialists Conference, pp. 003004-003008. IEEE, 2012.
- [5] https://www.electronics-tutorials.ws/diode/diode_2.html
- [6] Sharma, Divya, Rajesh Mehra, and Balwinder Raj. "Comparative analysis of photovoltaic technologies for high efficiency solar cell design." Superlattices and Microstructures 153 (2021): 106861.
- [7] Shockley, William, and Hans J. Queisser. "Detailed balance limit of efficiency of p-n junction solar cells." Journal of applied physics 32, no. 3 (1961): 510-519.
- [8] Hagfeldt, Anders, Gerrit Boschloo, Licheng Sun, Lars Kloo, and Henrik Pettersson. "Dye-sensitized solar cells." Chemical reviews 110, no. 11 (2010): 6595-6663.
- [9] Battaglia, Corsin, Andres Cuevas, and Stefaan De Wolf. "High-efficiency crystalline silicon solar cells: status and perspectives." Energy & Environmental Science 9, no. 5 (2016): 1552-1576.

-
-
- [10] Avrutin, V., N. Izyumskaya, and H. Morkoç. “Semiconductor solar cells: Recent progress in terrestrial applications.” *Superlattices and Microstructures* 49, no. 4 (2011): 337-364.
- [11] Aberle, Armin G. “Thin-film solar cells.” *Thin solid films* 517, no. 17 (2009): 4706-4710.
- [12] Pagliaro, Mario, Giovanni Palmisano, and Rosaria Ciriminna. *Il nuovo fotovoltaico*. Palermo: Dario Flaccovio Editore, 2008.
- [13] Gloeckler, M., I. Sankin, and Z. Zhao. “CdTe solar cells at the threshold to 20% efficiency.” *IEEE Journal of Photovoltaics* 3, no. 4 (2013): 1389-1393.
- [14] Pagliaro, Mario, Giovanni Palmisano, and Rosaria Ciriminna. *Il nuovo fotovoltaico*. Palermo: Dario Flaccovio Editore, 2008.
- [15] <https://www.pv-magazine.com/2021/03/04/avancis-claims-19-64-efficiency-for-cigs-module/>
- [16] Green, Martin, Ewan Dunlop, Jochen Hohl-Ebinger, Masahiro Yoshita, Nikos Kopidakis, and Xiaojing Hao. “Solar cell efficiency tables (version 57).” *Progress in photovoltaics: research and applications* 29, no. 1 (2021): 3-15.
- [17] Nakamura, Motoshi, Koji Yamaguchi, Yoshinori Kimoto, Yusuke Yasaki, Takuya Kato, and Hiroki Sugimoto. “Cd-free Cu (In, Ga)(Se, S) 2 thin-film solar cell with record efficiency of 23.35%.” *IEEE Journal of Photovoltaics* 9, no. 6 (2019): 1863-1867.
- [18] Jackson, Philip, Roland Wuerz, Dimitrios Hariskos, Erwin Lotter, Wolfram Witte, and Michael Powalla. “Effects of heavy alkali elements in Cu (In, Ga) Se₂ solar cells with efficiencies up to 22.6%.” *physica status solidi (RRL)–Rapid Research Letters* 10, no. 8 (2016): 583-586.
-
-

-
-
- [19] Plentz, Jonathan, Gudrun Andrä, Torsten Pliewischkies, Uwe Brückner, Björn Eisenhauer, and Fritz Falk. "Amorphous silicon thin-film solar cells on glass fiber textiles." *Materials Science and Engineering: B* 204 (2016): 34-37.
- [20] Zhang, Yaokang, Sze-Wing Ng, Xi Lu, and Zijian Zheng. "Solution-processed transparent electrodes for emerging thin-film solar cells." *Chemical Reviews* 120, no. 4 (2020): 2049-2122.
- [21] Arumugam, Sasikumar, Yi Li, Monika Glanc-Gostkiewicz, Russel N. Torah, and Stephen P. Beeby. "Solution processed organic solar cells on textiles." *IEEE Journal of Photovoltaics* 8, no. 6 (2018): 1710-1715.
- [22] GREENY, Martin A., Keith Emery, Yoshihiro Hishikawa, and Wilhelm Warta. "Solar cell efficiency tables (version 37)." *Progress in photovoltaics* 19, no. 1 (2011): 84-92.
- [23] Itzhaik, Yafit, Olivia Niiitsoo, Miles Page, and Gary Hodes. "Sb2S3-sensitized nanoporous TiO2 solar cells." *The Journal of Physical Chemistry C* 113, no. 11 (2009): 4254-4256.
- [24] Lévy-Clément, Claude. "Nanostructured ETA-solar cells." In *Nanostructured Materials for Solar Energy Conversion*, pp. 447-484. Elsevier, 2006.
- [25] Lévy-Clément, Claude, Ramon Tena-Zaera, Margaret A. Ryan, Abou Katty, and Gary Hodes. "CdSe-sensitized p-CuSCN/nanowire n-ZnO heterojunctions." *Advanced Materials* 17, no. 12 (2005): 1512-1515.
- [26] Chandrasekaran, J., D. Nithyaprakash, K. B. Ajjan, S. Maruthamuthu, D. Manoharan, and S. Kumar. "Hybrid solar cell based on blending of organic and inorganic materials—An overview." *Renewable and Sustainable Energy Reviews* 15, no. 2 (2011): 1228-1238.
- [27] Chandrasekaran, J., D. Nithyaprakash, K. B. Ajjan, S. Maruthamuthu, D. Manoharan, and S. Kumar. "Hybrid solar cell based on blending of

- organic and inorganic materials—An overview.” *Renewable and Sustainable Energy Reviews* 15, no. 2 (2011): 1228-1238.
- [28] Gong, Jiawei, Jing Liang, and K. Sumathy. “Review on dye-sensitized solar cells (DSSCs): fundamental concepts and novel materials.” *Renewable and Sustainable Energy Reviews* 16, no. 8 (2012): 5848-5860.
- [29] Upadhyaya, Hari M., S. Senthilarasu, Min-Hung Hsu, and D. Kishore Kumar. “Recent progress and the status of dye-sensitised solar cell (DSSC) technology with state-of-the-art conversion efficiencies.” *Solar Energy Materials and Solar Cells* 119 (2013): 291-295.
- [30] Bach, Udo, Donald Lupo, Pascal Comte, Jacques-E. Moser, F. Weissörtel, J. Salbeck, H. Spreitzer, and Michael Grätzel. “Solid-state dye-sensitized mesoporous TiO₂ solar cells with high photon-to-electron conversion
- [31] Kamat, Prashant V. “Boosting the efficiency of quantum dot sensitized solar cells through modulation of interfacial charge transfer.” *Accounts of chemical research* 45, no. 11 (2012): 1906-1915.
- [32] Kramer, Illan J., and Edward H. Sargent. “The architecture of colloidal quantum dot solar cells: materials to devices.” *Chemical reviews* 114, no. 1 (2014): 863-882.
- [33] Zhang, Xiao Li, Fuzhi Huang, Andrew Nattestad, Kun Wang, Dongchuan Fu, Amaresh Mishra, Peter Bäuerle, Udo Bach, and Yi-Bing Cheng. “Enhanced open-circuit voltage of p-type DSC with highly crystalline NiO nanoparticles.” *Chemical Communications* 47, no. 16 (2011): 4808-4810.
- [34] Kojima, Akihiro, Kenjiro Teshima, Yasuo Shirai, and Tsutomu Miyasaka. “Organometal halide perovskites as visible-light sensitizers

-
-
- for photovoltaic cells.” *Journal of the American Chemical Society* 131, no. 17 (2009): 6050-6051.
- [35] Im, Jeong-Hyeok, Chang-Ryul Lee, Jin-Wook Lee, Sang-Won Park, and Nam-Gyu Park. “6.5% efficient perovskite quantum-dot-sensitized solar cell.” *Nanoscale* 3, no. 10 (2011): 4088-4093.
- [36] Kim, Hui-Seon, Chang-Ryul Lee, Jeong-Hyeok Im, Ki-Beom Lee, Thomas Moehl, Arianna Marchioro, Soo-Jin Moon et al. “Lead iodide perovskite sensitized all-solid-state submicron thin film mesoscopic solar cell with efficiency exceeding 9%.” *Scientific Reports* 2, no. 1 (2012): 1-7.
- [37] Park, Nam-Gyu. “Perovskite solar cells: an emerging photovoltaic technology.” *Materials Today* 18, no. 2 (2015): 65-72.
- [38] Li, Bin, Liduo Wang, Bonan Kang, Peng Wang, and Yong Qiu. “Review of recent progress in solid-state dye-sensitized solar cells.” *Solar Energy Materials and Solar Cells* 90, no. 5 (2006): 549-573.
- [39] Li, Qinghua, Haiyan Chen, Lin Lin, Pinjiang Li, Yuancheng Qin, Mingjun Li, Benlin He, Lei Chu, and Qunwei Tang. “Quasi-solid-state dye-sensitized solar cell from polyaniline integrated poly (hexamethylene diisocyanate tripolymer/polyethylene glycol) gel electrolyte.” *Journal of Materials Chemistry A* 1, no. 17 (2013): 5326-5332.
- [40] Kawano, Ryuji, Hiroshi Matsui, Chizuru Matsuyama, Akihiro Sato, Md Abu Bin Hasan Susan, Nobuo Tanabe, and Masayoshi Watanabe. “High performance dye-sensitized solar cells using ionic liquids as their electrolytes.” *Journal of Photochemistry and Photobiology A: Chemistry* 164, no. 1-3 (2004): 87-92.
- [41] Angaiah, Subramania, Vignesh Murugadoss, Subasri Arunachalam, Pratheep Panneerselvam, and Sarathkumar Krishnan. “Influence of

- various ionic liquids embedded electrospun polymer membrane electrolytes on the photovoltaic performance of DSSC.” *Engineered Science* 4, no. 16 (2018): 44-51.
- [42] Saito, Yasuteru, Norihiro Fukuri, Rohan Senadeera, Takayuki Kitamura, Yuji Wada, and Shozo Yanagida. “Solid state dye sensitized solar cells using in situ polymerized PEDOTs as hole conductor.” *Electrochemistry communications* 6, no. 1 (2004): 71-74.
- [43] Wang, Yanping, Ke Yang, Seong-Cheol Kim, Ramaswamy Nagarajan, Lynne A. Samuelson, and Jayant Kumar. “In situ polymerized carboxylated diacetylene as a hole conductor in solid-state dye-sensitized solar cells.” *Chemistry of materials* 18, no. 18 (2006): 4215-4217.
- [44] Sima, Cornelia, Constantin Grigoriu, and Stefan Antohe. “Comparison of the dye-sensitized solar cells performances based on transparent conductive ITO and FTO.” *Thin Solid Films* 519, no. 2 (2010): 595-597.
- [45] Kawashima, Takuya, Tetsuya Ezure, Kenichi Okada, Hiroshi Matsui, Kenji Goto, and Nobuo Tanabe. “FTO/ITO double-layered transparent conductive oxide for dye-sensitized solar cells.” *Journal of Photochemistry and Photobiology A: Chemistry* 164, no. 1-3 (2004): 199-202.
- [46] Hirahara, N., B. Onwona-Agyeman, and M. Nakao. “Preparation of Al-doped ZnO thin films as transparent conductive substrate in dye-sensitized solar cell.” *Thin Solid Films* 520, no. 6 (2012): 2123-2127.
- [47] Pawar, Bhagwat N., Gangeri Cai, Dukho Ham, Rajaram S. Mane, T. Ganesh, Anil Ghule, Ramphal Sharma, K. D. Jadhava, and Sung-Hwan Han. “Preparation of transparent and conducting boron-doped ZnO

-
-
- electrode for its application in dye-sensitized solar cells.” *Solar Energy Materials and Solar Cells* 93, no. 4 (2009): 524-527.
- [48] Sarker, Subrata, Hyun Woo Seo, Young-Ku Jin, Md Abdul Aziz, and Dong Min Kim. “Transparent conducting oxides and their performance as substrates for counter electrodes of dye-sensitized solar cells.” *Materials Science in Semiconductor Processing* 93 (2019): 28-35.
- [49] Yeon, Changbong, Sun Jin Yun, Jumi Kim, and Jung Wook Lim. “PEDOT: PSS Films with Greatly Enhanced Conductivity via Nitric Acid Treatment at Room Temperature and Their Application as Pt/TCO-Free Counter Electrodes in Dye-Sensitized Solar Cells.” *Advanced Electronic Materials* 1, no. 10 (2015): 1500121.
- [50] Anothumakkool, Bihag, Ishita Agrawal, Siddheshwar N. Bhange, Roby Soni, Onkar Game, Satishchandra B. Ogale, and Sreekumar Kurungot. “Pt-and TCO-free flexible cathode for DSSC from highly conducting and flexible PEDOT paper prepared via in situ interfacial polymerization.” *ACS applied materials & interfaces* 8, no. 1 (2016): 553-562.
- [51] Weerasinghe, Hasitha C., Fuzhi Huang, and Yi-Bing Cheng. “Fabrication of flexible dye sensitized solar cells on plastic substrates.” *Nano Energy* 2, no. 2 (2013): 174-189.
- [52] Yun, Sining, Jilian Nei Freitas, Ana F. Nogueira, Yanmin Wang, Shahzada Ahmad, and Zhong-Sheng Wang. “Dye-sensitized solar cells employing polymers.” *Progress in Polymer Science* 59 (2016): 1-40.
- [53] Toivola, Minna, Janne Halme, Kati Miettunen, Kerttu Aitola, and Peter D. Lund. “Nanostructured dye solar cells on flexible substrates.” *International Journal of Energy Research* 33, no. 13 (2009): 1145-1160.
-
-

-
-
- [54] Sang, Lixia, Yixin Zhao, and Clemens Burda. "TiO₂ nanoparticles as functional building blocks." *Chemical reviews* 114, no. 19 (2014): 9283-9318.
- [55] Gupta, Shipra Mital, and Manoj Tripathi. "A review of TiO₂ nanoparticles." *chinese science bulletin* 56, no. 16 (2011): 1639-1657.
- [56] Hegazy, Aiat, Natacha Kinadjian, Bahareh Sadeghimakki, Siva Sivoththaman, Nageh K. Allam, and Eric Prouzet. "TiO₂ nanoparticles optimized for photoanodes tested in large area Dye-sensitized solar cells (DSSC)." *Solar Energy Materials and Solar Cells* 153 (2016): 108-116.
- [57] Agrawal, Anupam, Shahbaz A. Siddiqui, Amit Soni, Kanupriya Khandelwal, and Ganesh D. Sharma. "Performance analysis of TiO₂ based dye sensitized solar cell prepared by screen printing and doctor blade deposition techniques." *Solar Energy* 226 (2021): 9-19.
- [58] Baek, In Chan, Muga Vithal, Jeong Ah Chang, Jun-Ho Yum, Md K. Nazeeruddin, Michael Grätzel, Yong-Chae Chung, and Sang Il Seok. "Facile preparation of large aspect ratio ellipsoidal anatase TiO₂ nanoparticles and their application to dye-sensitized solar cell." *Electrochemistry Communications* 11, no. 4 (2009): 909-912.
- [59] Meulenkamp, Eric A. "Synthesis and growth of ZnO nanoparticles." *The Journal of Physical Chemistry B* 102, no. 29 (1998): 5566-5572.
- [60] Vittal, R., and Kuo-Chuan Ho. "Zinc oxide based dye-sensitized solar cells: A review." *Renewable and Sustainable energy reviews* 70 (2017): 920-935.
- [61] Lin, Chia-Yu, Yi-Hsuan Lai, Hsin-Wei Chen, Jian-Ging Chen, Chung-Wei Kung, L. R. Vittal, and Kuo-Chuan Ho. "Highly efficient dye-sensitized solar cell with a ZnO nanosheet-based photoanode." *Energy & Environmental Science* 4, no. 9 (2011): 3448-3455.
-
-

-
-
- [62] Gubbala, Suresh, Vidhya Chakrapani, Vivekanand Kumar, and Mahendra K. Sunkara. "Band-edge engineered hybrid structures for dye-sensitized solar cells based on SnO₂ nanowires." *Advanced Functional Materials* 18, no. 16 (2008): 2411-2418.
- [63] Li, Zhengdao, Yong Zhou, Ruzhong Sun, Yan Xiong, Haiquan Xie, and Zhigang Zou. "Nanostructured SnO₂ photoanode-based dye-sensitized solar cells." *Chinese Science Bulletin* 59, no. 18 (2014): 2122-2134.
- [64] Basu, Kaustubh, Daniele Benetti, Haiguang Zhao, Lei Jin, Fiorenzo Vetrone, Alberto Vomiero, and Federico Rosei. "Enhanced photovoltaic properties in dye sensitized solar cells by surface treatment of SnO₂ photoanodes." *Scientific reports* 6, no. 1 (2016): 1-10.
- [65] Zheng, Haidong, Yasuhiro Tachibana, and Kourosch Kalantar-Zadeh. "Dye-sensitized solar cells based on WO₃." *Langmuir* 26, no. 24 (2010): 19148-19152.
- [66] Yong, Seok-Min, Tsvetkov Nikolay, Byung Tae Ahn, and Do Kyung Kim. "One-dimensional WO₃ nanorods as photoelectrodes for dye-sensitized solar cells." *Journal of Alloys and Compounds* 547 (2013): 113-117.
- [67] Rashad, M. M., and A. E. Shalan. "Hydrothermal synthesis of hierarchical WO₃ nanostructures for dye-sensitized solar cells." *Applied Physics A* 116, no. 2 (2014): 781-788.
- [68] Biswas, Rajat, and Suman Chatterjee. "Effect of surface modification via sol-gel spin coating of ZnO nanoparticles on the performance of WO₃ photoanode based dye sensitized solar cells." *Optik* 212 (2020): 164142.
-
-

-
-
- [69] Le Viet, A., R. Jose, M. V. Reddy, B. V. R. Chowdari, and S. Ramakrishna. "Nb₂O₅ photoelectrodes for dye-sensitized solar cells: choice of the polymorph." *The Journal of Physical Chemistry C* 114, no. 49 (2010): 21795-21800.
- [70] Nunes, Barbara N., Leandro A. Faustino, Andressa V. Muller, Andre S. Polo, and Antonio Otavio T. Patrocinio. "Nb₂O₅ dye-sensitized solar cells." *Nanomaterials for solar cell applications* (2019): 287-322.
- [71] Ghosh, Rudresh, M. Kyle Brennaman, Tim Uher, Myoung-Ryul Ok, Edward T. Samulski, L. E. McNeil, Thomas J. Meyer, and Rene Lopez. "Nanoforest Nb₂O₅ photoanodes for dye-sensitized solar cells by pulsed laser deposition." *ACS Applied Materials & Interfaces* 3, no. 10 (2011): 3929-3935.
- [72] Pascual, J., J. Camassel, and H. Mathieu. "Fine structure in the intrinsic absorption edge of TiO₂." *Physical Review B* 18, no. 10 (1978): 5606.
- [73] Pfeifer, Verena, Paul Erhart, Shunyi Li, Karsten Rachut, Jan Morasch, Joachim Brötz, Philip Reckers et al. "Energy band alignment between anatase and rutile TiO₂." *The Journal of Physical Chemistry Letters* 4, no. 23 (2013): 4182-4187.
- [74] Tang, H., H. Berger, P. E. Schmid, F. Levy, and G. Burri. "Photoluminescence in TiO₂ anatase single crystals." *Solid State Communications* 87, no. 9 (1993): 847-850.
- [75] Pfeifer, Verena, Paul Erhart, Shunyi Li, Karsten Rachut, Jan Morasch, Joachim Brötz, Philip Reckers et al. "Energy band alignment between anatase and rutile TiO₂." *The Journal of Physical Chemistry Letters* 4, no. 23 (2013): 4182-4187.
- [76] Kakiage, Kenji, Yohei Aoyama, Toru Yano, Keiji Oya, Jun-ichi Fujisawa, and Minoru Hanaya. "Highly-efficient dye-sensitized solar cells with collaborative sensitization by silyl-anchor and carboxy-

-
-
- anchor dyes.” *Chemical communications* 51, no. 88 (2015): 15894-15897.
- [77] Han, Jingbin, Fengru Fan, Chen Xu, Shisheng Lin, Min Wei, Xue Duan, and Zhong Lin Wang. “ZnO nanotube-based dye-sensitized solar cell and its application in self-powered devices.” *Nanotechnology* 21, no. 40 (2010): 405203.
- [78] Maheswari, D., and P. Venkatachalam. “Enhancing the performance of dye-sensitized solar cells based on organic dye sensitized TiO₂ nanoparticles/nanowires composite photoanodes with ionic liquid electrolyte.” *Measurement* 60 (2015): 146-154.
- [79] Nayeri, Fatemeh Dehghan, Mohammadreza Kolahdouz, Ebrahim Asl-Soleimani, and S. Mohajerzadeh. “Low temperature carving of ZnO nanorods into nanotubes for dye-sensitized solar cell application.” *Journal of Alloys and Compounds* 633 (2015): 359-365.
- [80] Liu, Bin, and Eray S. Aydil. “Growth of oriented single-crystalline rutile TiO₂ nanorods on transparent conducting substrates for dye-sensitized solar cells.” *Journal of the American Chemical Society* 131, no. 11 (2009): 3985-3990.
- [81] Boercker, J. E., E. Enache-Pommer, and E. S. Aydil. “Growth mechanism of titanium dioxide nanowires for dye-sensitized solar cells.” *Nanotechnology* 19, no. 9 (2008): 095604.
- [82] Kandasamy, M., M. Selvaraj, C. Kumarappan, and S. Murugesan. “Plasmonic Ag nanoparticles anchored ethylenediamine modified TiO₂ nanowires@ graphene oxide composites for dye-sensitized solar cell.” *Journal of Alloys and Compounds* 902 (2022): 163743.
- [83] Ko, Seung Hwan, Daeho Lee, Hyun Wook Kang, Koo Hyun Nam, Joon Yeob Yeo, Suk Joon Hong, Costas P. Grigoropoulos, and Hyung Jin Sung. “Nanoforest of hydrothermally grown hierarchical ZnO

- nanowires for a high efficiency dye-sensitized solar cell.” *Nano letters* 11, no. 2 (2011): 666-671.
- [84] Gupta, Ram K., K. Ghosh, R. Patel, S. R. Mishra, and Pawan K. Kahol. “Band gap engineering of ZnO thin films by In₂O₃ incorporation.” *Journal of crystal growth* 310, no. 12 (2008): 3019-3023.
- [85] Tan, Swee Tiam, B. J. Chen, X. W. Sun, W. J. Fan, Hoi Sing Kwok, X. H. Zhang, and S. J. Chua. “Blueshift of optical band gap in ZnO thin films grown by metal-organic chemical-vapor deposition.” *Journal of Applied Physics* 98, no. 1 (2005): 013505.
- [86] Özgür, Ümit, Ya I. Alivov, Chunli Liu, Ali Teke, MAn Reshchikov, S. Doğan, V. C. S. J. Avrutin, S-J. Cho, and and H. Morkoç. “A comprehensive review of ZnO materials and devices.” *Journal of applied physics* 98, no. 4 (2005): 11.
- [87] Bae, H. S., M. H. Yoon, J. H. Kim, and Seongil Im. “Photodetecting properties of ZnO-based thin-film transistors.” *Applied Physics Letters* 83, no. 25 (2003): 5313-5315.
- [88] Zhang, Qifeng, Christopher S. Dandeneau, Xiaoyuan Zhou, and Guozhong Cao. “ZnO nanostructures for dye-sensitized solar cells.” *Advanced materials* 21, no. 41 (2009): 4087-4108.
- [89] He, Yitao, Jing Hu, and Yahong Xie. “High-efficiency dye-sensitized solar cells of up to 8.03% by air plasma treatment of ZnO nanostructures.” *Chemical Communications* 51, no. 90 (2015): 16229-16232.
- [90] Xie, Yahong, Xiaofeng Zhou, Hongyu Mi, Junhong Ma, Jianya Yang, and Jian Cheng. “High efficiency ZnO-based dye-sensitized solar cells with a 1H, 1H, 2H, 2H-perfluorodecyltriethoxysilane chain barrier for cutting on interfacial recombination.” *Applied Surface Science* 434 (2018): 1144-1152.
-
-

-
-
- [91] Mishra, Amaresh, Markus KR Fischer, and Peter Bäuerle. "Metal-free organic dyes for dye-sensitized solar cells: From structure: Property relationships to design rules." *Angewandte Chemie International Edition* 48, no. 14 (2009): 2474-2499.
- [92] Albero, Josep, Pedro Atienzar, Avelino Corma, and Hermenegildo Garcia. "Efficiency Records in Mesoscopic Dye-Sensitized Solar Cells." *The Chemical Record* 15, no. 4 (2015): 803-828.
- [93] Ito, Seigo. "Investigation of dyes for dye-sensitized solar cells: Ruthenium-complex dyes, metal-free dyes, metal-complex porphyrin dyes and natural dyes." *Solar Cells-Dye-Sensitized Devices* (2011): 19-48.
- [94] Shalini, Status, R. Balasundaraprabhu, T. Satish Kumar, N. Prabavathy, S. Senthilarasu, and S. Prasanna. "Status and outlook of sensitizers/dyes used in dye sensitized solar cells (DSSC): a review." *International journal of energy research* 40, no. 10 (2016): 1303-1320.
- [95] Higashino, Tomohiro, and Hiroshi Imahori. "Porphyrins as excellent dyes for dye-sensitized solar cells: recent developments and insights." *Dalton transactions* 44, no. 2 (2015): 448-463.
- [96] Hagfeldt, Anders, Gerrit Boschloo, Licheng Sun, Lars Kloo, and Henrik Pettersson. "Dye-sensitized solar cells." *Chemical reviews* 110, no. 11 (2010): 6595-6663.
- [97] Ito, Seigo. "Investigation of dyes for dye-sensitized solar cells: Ruthenium-complex dyes, metal-free dyes, metal-complex porphyrin dyes and natural dyes." *Solar Cells-Dye-Sensitized Devices* (2011): 19-48.
- [98] Hara, Kohjiro, Zhong-Sheng Wang, Tadatake Sato, Akihiro Furube, Ryuzi Katoh, Hideki Sugihara, Yasufumi Dan-Oh, Chiaki Kasada, Akira Shinpo, and Sadaharu Suga. "Oligothiophene-containing

- coumarin dyes for efficient dye-sensitized solar cells.” *The Journal of Physical Chemistry B* 109, no. 32 (2005): 15476-15482.
- [99] Hara, Kohjiro, Zhong-Sheng Wang, Tadatake Sato, Akihiro Furube, Ryuzi Katoh, Hideki Sugihara, Yasufumi Dan-Oh, Chiaki Kasada, Akira Shinpo, and Sadaharu Suga. “Oligothiophene-containing coumarin dyes for efficient dye-sensitized solar cells.” *The Journal of Physical Chemistry B* 109, no. 32 (2005): 15476-15482.
- [100] Horiuchi, Tamotsu, Hidetoshi Miura, Kouichi Sumioka, and Satoshi Uchida. “High efficiency of dye-sensitized solar cells based on metal-free indoline dyes.” *Journal of the American Chemical Society* 126, no. 39 (2004): 12218-12219.
- [101] Delaey, Els, Frederik van Laar, Dirk De Vos, A. Kamuhabwa, Pierre Jacobs, and Peter de Witte. “A comparative study of the photosensitizing characteristics of some cyanine dyes.” *Journal of Photochemistry and Photobiology B: Biology* 55, no. 1 (2000): 27-36.
- [102] Benson, Richard C., and Henry A. Kues. “Absorption and fluorescence properties of cyanine dyes.” *Journal of Chemical and Engineering Data* 22, no. 4 (1977): 379-383.
- [103] Ma, Xuemei, Jianli Hua, Wenjun Wu, Yinghua Jin, Fanshun Meng, Wenhai Zhan, and He Tian. “A high-efficiency cyanine dye for dye-sensitized solar cells.” *Tetrahedron* 64, no. 2 (2008): 345-350.
- [104] Shalini, S., S. Prasanna, Tapas K. Mallick, and S. Senthilarasu. “Review on natural dye sensitized solar cells: Operation, materials and methods.” *Renewable and Sustainable Energy Reviews* 51 (2015): 1306-1325.
- [105] Richhariya, Geetam, Anil Kumar, Perapong Tekasakul, and Bhupendra Gupta. “Natural dyes for dye sensitized solar cell: A review.” *Renewable and Sustainable Energy Reviews* 69 (2017): 705-718.
-
-

-
-
- [106] Shalini, S., S. Prasanna, Tapas K. Mallick, and S. Senthilarasu. "Review on natural dye sensitized solar cells: Operation, materials and methods." *Renewable and Sustainable Energy Reviews* 51 (2015): 1306-1325.
- [107] Narayan, Monishka Rita. "Dye sensitized solar cells based on natural photosensitizers." *Renewable and sustainable energy reviews* 16, no. 1 (2012): 208-215.
- [108] Kumara, N. T. R. N., Andery Lim, Chee Ming Lim, Mohamad Iskandar Petra, and Piyasiri Ekanayake. "Recent progress and utilization of natural pigments in dye sensitized solar cells: A review." *Renewable and Sustainable Energy Reviews* 78 (2017): 301-317.
- [109] Wang, Xiao-Feng, Junfeng Xiang, Peng Wang, Yasushi Koyama, Shozo Yanagida, Yuji Wada, Kazunori Hamada, Shin-ichi Sasaki, and Hitoshi Tamiaki. "Dye-sensitized solar cells using a chlorophyll a derivative as the sensitizer and carotenoids having different conjugation lengths as redox spacers." *Chemical physics letters* 408, no. 4-6 (2005): 409-414.
- [110] Green, Beverley, William W. Parson, and William W. Parson, eds. *Light-harvesting antennas in photosynthesis*. Vol. 13. Springer Science & Business Media, 2003.
- [111] Lee, David. "Plant pigments and their manipulation. *Annual Plant Reviews* Vol 12. Davies KM, ed. 2004. Oxford/Boca Raton: Blackwell Publishing/CRC Press, Boca Raton. £ 110 (hardback). 352 pp." (2005): 1332-1333.
- [112] Wang, Xiao-Feng, Junfeng Xiang, Peng Wang, Yasushi Koyama, Shozo Yanagida, Yuji Wada, Kazunori Hamada, Shin-ichi Sasaki, and Hitoshi Tamiaki. "Dye-sensitized solar cells using a chlorophyll a derivative as the sensitizer and carotenoids having different

- conjugation lengths as redox spacers.” *Chemical physics letters* 408, no. 4-6 (2005): 409-414.
- [113] Harborne, Jeffrey B. “The flavonoids: advances in research since 1980.” (2013).
- [114] Golden, J. H., R. P. Linstead, and G. H. Whitham. “355. Chlorophyll and related compounds. Part VII. The structure of bacteriochlorophyll.” *Journal of the Chemical Society (Resumed)* (1958): 1725-1732.
- [115] Geissman, T. A., and Elly Hinreiner. “Theories of the biogenesis of flavonoid compounds (Part II).” *The Botanical Review* 18, no. 3 (1952): 165-244.
- [116] Goodwin, Trevor Walworth. “Chemistry and biochemistry of plant pigments.” *Chemistry and biochemistry of plant pigments.* (1965).
- [117] Caula S. A, Villar S. I., Martino V. S., Coussio I. D., Ferraro G. E. (1991) Polyphenols isolated from *Eupatorium buniifolium*. *Rev. Latinoamer. Quim.* 22: 1-3.
- [118] Butt, V. S. "Chemistry and biochemistry of plant pigments: Edited by TW Goodwin Academic Press; London, 1976 Volume 1: xvi+ 870 pages.£ 26.50, \$65.75 Volume 2: xiii+ 373 pages.£ 12.00, \$29.75." (1977): 155.
- [119] Steyn, W. J^H, S. J. E. Wand, D. M. Holcroft, and G. J. N. P. Jacobs. “Anthocyanins in vegetative tissues: a proposed unified function in photoprotection.” *New Phytologist* 155, no. 3 (2002): 349-361.
- [120] Yamazaki, Eiji, Masaki Murayama, Naomi Nishikawa, Noritsugu Hashimoto, Masashi Shoyama, and Osamu Kurita. “Utilization of natural carotenoids as photosensitizers for dye-sensitized solar cells.” *Solar energy* 81, no. 4 (2007): 512-516.
-
-

-
-
- [121] Hug, Hubert, Michael Bader, Peter Mair, and Thilo Glatzel. "Biophotovoltaics: natural pigments in dye-sensitized solar cells." *Applied Energy* 115 (2014): 216-225.
- [122] Hussain, Syed Arshad. "Development of dye sensitized solar cells using Botuje green leaves (*Jathopha Curcas* Linn)." *Science Journal of Physics* 2013 (2013).
- [123] Hao, Sancun, Jihuai Wu, Yunfang Huang, and Jianming Lin. "Natural dyes as photosensitizers for dye-sensitized solar cell." *Solar energy* 80, no. 2 (2006): 209-214.
- [124] Kumara, G. R. A., S. Kaneko, M. Okuya, B. Onwona-Agyeman, A. Konno, and K. Tennakone. "Shiso leaf pigments for dye-sensitized solid-state solar cell." *Solar Energy Materials and Solar Cells* 90, no. 9 (2006): 1220-1226.
- [125] Hernández-Martínez, A. R., S. Vargas, M. Estevez, and R. Rodríguez. "Dye-sensitized solar cells from extracted bracts bougainvillea betalain pigments." In *1st International Congress on Instrumentation and Applied Sciences*, vol. 1, p. 15. 2010.
- [126] Chang, Ho, H. M. Wu, T. L. Chen, K. D. Huang, C. S. Jwo, and Y. J. Lo. "Dye-sensitized solar cell using natural dyes extracted from spinach and ipomoea." *Journal of Alloys and Compounds* 495, no. 2 (2010): 606-610.
- [127] Hao, Sancun, Jihuai Wu, Yunfang Huang, and Jianming Lin. "Natural dyes as photosensitizers for dye-sensitized solar cell." *Solar energy* 80, no. 2 (2006): 209-214.
- [128] Dai, Qing, and Joseph Rabani. "Photosensitization of nanocrystalline TiO₂ films by anthocyanin dyes." *Journal of Photochemistry and Photobiology A: Chemistry* 148, no. 1-3 (2002): 17-24.
-
-

- [129] Dai, Qing, and Joseph Rabani. "Photosensitization of nanocrystalline TiO₂ films by pomegranate pigments with unusually high efficiency in aqueous medium." *Chemical Communications* 20 (2001): 2142-2143.
- [130] Zhou, Huizhi, Liqiong Wu, Yurong Gao, and Tingli Ma. "Dye-sensitized solar cells using 20 natural dyes as sensitizers." *Journal of Photochemistry and Photobiology A: Chemistry* 219, no. 2-3 (2011): 188-194.
- [131] Wongcharee, Khwanchit, Vissanu Meeyoo, and Sumaeth Chavadej. "Dye-sensitized solar cell using natural dyes extracted from rosella and blue pea flowers." *Solar Energy Materials and Solar Cells* 91, no. 7 (2007): 566-571.
- [132] Yamazaki, Eiji, Masaki Murayama, Naomi Nishikawa, Noritsugu Hashimoto, Masashi Shoyama, and Osamu Kurita. "Utilization of natural carotenoids as photosensitizers for dye-sensitized solar cells." *Solar energy* 81, no. 4 (2007): 512-516.
- [133] Hao, Sancun, Jihuai Wu, Yunfang Huang, and Jianming Lin. "Natural dyes as photosensitizers for dye-sensitized solar cell." *Solar energy* 80, no. 2 (2006): 209-214.
- [134] Supriyanto, A., F. Nurosyid, and A. H. Ahliha. "Carotenoid pigment as sensitizers for applications of dye-sensitized solar cell (DSSC)." In *IOP Conference Series: Materials Science and Engineering*, vol. 432, no. 1, p. 012060. IOP Publishing, 2018.
- [135] Ludin, Norasikin A., AM Al-Alwani Mahmoud, Abu Bakar Mohamad, Abd Amir H. Kadhum, Kamaruzzaman Sopian, and Nor Shazlinah Abdul Karim. "Review on the development of natural dye photosensitizer for dye-sensitized solar cells." *Renewable and Sustainable Energy Reviews* 31 (2014): 386-396.

-
-
- [136] Sabagh, Samira, Mohammad Izadyar, and Foroogh Arkan. "Photovoltaic properties of the flavonoid-based photosensitizers: Molecular-scale perspective on the natural dye solar cells." *International Journal of Quantum Chemistry* 120, no. 10 (2020): e26171.
- [137] Omar, Azimah, Mohd Syukri Ali, and Nasrudin Abd Rahim. "Electron transport properties analysis of titanium dioxide dye-sensitized solar cells (TiO₂-DSSCs) based natural dyes using electrochemical impedance spectroscopy concept: A review." *Solar Energy* 207 (2020): 1088-1121.
- [138] Ghann, William, Hyeonggon Kang, Tajbik Sheikh, Sunil Yadav, Tulio Chavez-Gil, Fred Nesbitt, and Jamal Uddin. "Fabrication, optimization and characterization of natural dye sensitized solar cell." *Scientific reports* 7, no. 1 (2017): 1-12.
- [139] Hug, Hubert, Michael Bader, Peter Mair, and Thilo Glatzel. "Biophotovoltaics: natural pigments in dye-sensitized solar cells." *Applied Energy* 115 (2014): 216-225.
- [140] Shalini, S., S. Prasanna, Tapas K. Mallick, and S. Senthilarasu. "Review on natural dye sensitized solar cells: Operation, materials and methods." *Renewable and Sustainable Energy Reviews* 51 (2015): 1306-1325.
- [141] Baby, Ruby, Peter Daniel Nixon, Nallapaneni Manoj Kumar, M. S. P. Subathra, and Nallamuthu Ananthi. "A comprehensive review of dye-sensitized solar cell optimal fabrication conditions, natural dye selection, and application-based future perspectives." *Environmental Science and Pollution Research* (2021): 1-34.
- [142] Kabir, Fahmid, Syed Nazmus Sakib, Sheikh Shehab Uddin, Erteza Tawsif Efaz, and Md Tahmid Farhan Himel. "Enhance cell
-
-

- performance of DSSC by dye mixture, carbon nanotube and post TiCl₄ treatment along with degradation study.” *Sustainable Energy Technologies and Assessments* 35 (2019): 298-307.
- [143] Kabir, F., M. M. H. Bhuiyan, M. S. Manir, M. S. Rahaman, M. A. Khan, and T. Ikegami. “Development of dye-sensitized solar cell based on combination of natural dyes extracted from Malabar spinach and red spinach.” *Results in Physics* 14 (2019): 102474.
- [144] Kabir, Fahmid, Md Mosharraf H. Bhuiyan, Md Robiul Hossain, Humayra Bashar, Md Saifur Rahaman, Md Serajum Manir, Ruhul A. Khan, and Tomoaki Ikegami. “Effect of combination of natural dyes and post-TiCl₄ treatment in improving the photovoltaic performance of dye-sensitized solar cells.” *Comptes Rendus Chimie* 22, no. 9-10 (2019): 659-666.
- [145] Pratiwi, D. D., F. Nurosyid, A. Supriyanto, and R. Suryana. “Performance improvement of dye-sensitized solar cells (DSSC) by using dyes mixture from chlorophyll and anthocyanin.” In *Journal of Physics: Conference Series*, vol. 909, no. 1, p. 012025. IOP Publishing, 2017.
- [146] Bashar, H., M. M. H. Bhuiyan, M. R. Hossain, F. Kabir, M. S. Rahaman, M. S. Manir, and T. Ikegami. “Study on combination of natural red and green dyes to improve the power conversion efficiency of dye sensitized solar cells.” *Optik* 185 (2019): 620-625.
- [147] Kabir, F., M. M. H. Bhuiyan, M. R. Hossain, H. Bashar, M. S. Rahaman, M. S. Manir, S. M. Ullah et al. “Improvement of efficiency of dye sensitized solar cells by optimizing the combination ratio of natural red and yellow dyes.” *Optik* 179 (2019): 252-258.

-
-
- [148] Ferrere, Suzanne, Arie Zaban, and Brian A. Gregg. "Dye sensitization of nanocrystalline tin oxide by perylene derivatives." *The Journal of Physical Chemistry B* 101, no. 23 (1997): 4490-4493.
- [149] Oskam, Gerko, Bryan V. Bergeron, Gerald J. Meyer, and Peter C. Searson. "Pseudohalogen for dye-sensitized TiO₂ photoelectrochemical cells." *The Journal of Physical Chemistry B* 105, no. 29 (2001): 6867-6873.
- [150] Wang, Peng, Shaik M. Zakeeruddin, Jacques-E. Moser, Robin Humphry-Baker, and Michael Grätzel. "A solvent-free, SeCN⁻/(SeCN)³⁻-based ionic liquid electrolyte for high-efficiency dye-sensitized nanocrystalline solar cells." *Journal of the American Chemical Society* 126, no. 23 (2004): 7164-7165.
- [151] Hagfeldt, Anders, Gerrit Boschloo, Licheng Sun, Lars Kloo, and Henrik Pettersson. "Dye-sensitized solar cells." *Chemical reviews* 110, no. 11 (2010): 6595-6663.
- [152] Sapp, Shawn A., C. Michael Elliott, Cristiano Contado, Stefano Caramori, and Carlo A. Bignozzi. "Substituted polypyridine complexes of cobalt (II/III) as efficient electron-transfer mediators in dye-sensitized solar cells." *Journal of the American Chemical Society* 124, no. 37 (2002): 11215-11222.
- [153] Hattori, Shigeki, Yuji Wada, Shozo Yanagida, and Shunichi Fukuzumi. "Blue copper model complexes with distorted tetragonal geometry acting as effective electron-transfer mediators in dye-sensitized solar cells." *Journal of the American Chemical Society* 127, no. 26 (2005): 9648-9654.
- [154] Choi, Hyunbong, Chul Baik, Sang Ook Kang, Jaejung Ko, Moon-Sung Kang, Md K. Nazeeruddin, and Michael Grätzel. "Highly efficient and thermally stable organic sensitizers for solvent-free dye-sensitized

-
-
- solar cells.” *Angewandte Chemie International Edition* 47, no. 2 (2008): 327-330.
- [155] Kopidakis, Nikos, Nathan R. Neale, and Arthur J. Frank. “Effect of an adsorbent on recombination and band-edge movement in dye-sensitized TiO₂ solar cells: evidence for surface passivation.” *The journal of physical chemistry B* 110, no. 25 (2006): 12485-12489.
- [156] Figgemeier, Egbert, and Anders Hagfeldt. “Are dye-sensitized nanostructured solar cells stable? An overview of device testing and component analyses.” *International journal of photoenergy* 6, no. 3 (2004): 127-140.
- [157] Hao, Sancun, Jihuai Wu, Leqing Fan, Yunfang Huang, Jianming Lin, and Yelin Wei. “The influence of acid treatment of TiO₂ porous film electrode on photoelectric performance of dye-sensitized solar cell.” *Solar energy* 76, no. 6 (2004): 745-750.
- [158] Zhang, Changneng, Yang Huang, Zhipeng Huo, Shuanghong Chen, and Songyuan Dai. “Photoelectrochemical effects of guanidinium thiocyanate on dye-sensitized solar cell performance and stability.” *The Journal of Physical Chemistry C* 113, no. 52 (2009): 21779-21783.
- [159] Kelly, Craig A., Fereshteh Farzad, David W. Thompson, Jeremy M. Stipkala, and Gerald J. Meyer. “Cation-controlled interfacial charge injection in sensitized nanocrystalline TiO₂.” *Langmuir* 15, no. 20 (1999): 7047-7054.
- [160] Zakeeruddin, Shaik M., and Michael Grätzel. “Solvent-free ionic liquid electrolytes for mesoscopic dye-sensitized solar cells.” *Advanced Functional Materials* 19, no. 14 (2009): 2187-2202.
- [161] Wang, Peng, Shaik M. Zakeeruddin, Jacques-E. Moser, Robin Humphry-Baker, and Michael Grätzel. “A solvent-free, SeCN⁻/(SeCN)₃-based ionic liquid electrolyte for high-efficiency dye-sensitized
-
-

-
-
- nanocrystalline solar cells.” *Journal of the American Chemical Society* 126, no. 23 (2004): 7164-7165.
- [162] Gunasekaran, Ahalya, Andrea Sorrentino, Abdullah M. Asiri, and Sambandam Anandan. “Guar gum-based polymer gel electrolyte for dye-sensitized solar cell applications.” *Solar Energy* 208 (2020): 160-165.
- [163] Saidi, Norshahirah M., Fatin Saiha Omar, Arshid Numan, David C. Apperley, Mohammed M. Algaradah, Ramesh Kasi, Alyssa-Jennifer Avestro, and Ramesh T. Subramaniam. “Enhancing the efficiency of a dye-sensitized solar cell based on a metal oxide nanocomposite gel polymer electrolyte.” *ACS applied materials & interfaces* 11, no. 33 (2019): 30185-30196.
- [164] Su’ait, Mohd Sukor, Mohd Yusri Abd Rahman, and Azizan Ahmad. “Review on polymer electrolyte in dye-sensitized solar cells (DSSCs).” *Solar Energy* 115 (2015): 452-470.
- [165] Ravirajan, Punniamoorthy, Ana M. Peiró, Mohammad K. Nazeeruddin, Michael Graetzel, Donal DC Bradley, James R. Durrant, and Jenny Nelson. “Hybrid polymer/zinc oxide photovoltaic devices with vertically oriented ZnO nanorods and an amphiphilic molecular interface layer.” *The Journal of Physical Chemistry B* 110, no. 15 (2006): 7635-7639.
- [166] Murakoshi, Kei, Ryuichiro Kogure, Yuji Wada, and Shozo Yanagida. “Solid state dye-sensitized TiO₂ solar cell with polypyrrole as hole transport layer.” *Chemistry letters* 26, no. 5 (1997): 471-472.
- [167] Saito, Yasuteru, Takayuki Kitamura, Yuji Wada, and Shozo Yanagida. “Poly (3, 4-ethylenedioxythiophene) as a hole conductor in solid state dye sensitized solar cells.” *Synthetic Metals* 131, no. 1-3 (2002): 185-187.
-
-

-
-
- [168] Somani, Prakash R., and S. Radhakrishnan. "Solid state electrochemical reaction in photocells made using conducting polyaniline and sensitized with methylene blue." *Journal of Solid State Electrochemistry* 7, no. 3 (2003): 166-170.
- [169] Cai, Ning, Soo-Jin Moon, Lê Cevey-Ha, Thomas Moehl, Robin Humphry-Baker, Peng Wang, Shaik M. Zakeeruddin, and Michael Grätzel. "An organic D- π -A dye for record efficiency solid-state sensitized heterojunction solar cells." *Nano letters* 11, no. 4 (2011): 1452-1456.
- [170] Chung, In, Byunghong Lee, Jiaqing He, Robert PH Chang, and Mercuri G. Kanatzidis. "All-solid-state dye-sensitized solar cells with high efficiency." *Nature* 485, no. 7399 (2012): 486-489.
- [171] Siqian, L. I., Jie HUANG, X. I. E. Jian, Jun ZHANG, Y. E. Cong, and W. A. N. G. Hao. "High Efficient Pt Counter Electrode Prepared by One-step Thermal Decomposition for Dye-sensitized Solar Cell." *Chinese Journal of Materials Research* 29, no. 9 (2015): 656-662.
- [172] Chang, H. C., H. H. Huang, C. Y. Wu, R. Q. Hsu, and C. Y. Hsu. "The photocatalytic activity and compact layer characteristics of TiO₂ films prepared using radio frequency magnetron sputtering." *International Journal of Photoenergy* 2014 (2014).
- [173] Popoola, Idris K., Mohammed A. Gondal, Jwahr M. AlGhamdi, and Talal F. Qahtan. "Photofabrication of highly transparent platinum counter electrodes at ambient temperature for bifacial dye sensitized solar cells." *Scientific reports* 8, no. 1 (2018): 1-12.
- [174] Murakami, Takurou N., Seigo Ito, Qing Wang, Md Khaja Nazeeruddin, Takeru Bessho, Ilkay Cesar, Paul Liska et al. "Highly efficient dye-sensitized solar cells based on carbon black counter

-
-
- electrodes.” *Journal of the Electrochemical Society* 153, no. 12 (2006): A2255.
- [175] Veerappan, Ganapathy, Karunagaran Bojan, and Shi-Woo Rhee. “Sub-micrometer-sized graphite as a conducting and catalytic counter electrode for dye-sensitized solar cells.” *ACS applied materials & interfaces* 3, no. 3 (2011): 857-862.
- [176] Li, Yu-Yan, Chun-Ting Li, Min-Hsin Yeh, Kuan-Chieh Huang, Ping-Wei Chen, R. Vittal, and Kuo-Chuan Ho. “Graphite with different structures as catalysts for counter electrodes in dye-sensitized solar cells.” *Electrochimica Acta* 179 (2015): 211-219.
- [177] Imoto, Kiyooki, Kohshin Takahashi, Takahiro Yamaguchi, Teruhisa Komura, Jun-ichi Nakamura, and Kazuhiko Murata. “High-performance carbon counter electrode for dye-sensitized solar cells.” *Solar Energy Materials and Solar Cells* 79, no. 4 (2003): 459-469.
- [178] Wei, Wei, Hui Wang, and Yun Hang Hu. “A review on PEDOT-based counter electrodes for dye-sensitized solar cells.” *International Journal of Energy Research* 38, no. 9 (2014): 1099-1111.
- [179] Wu, Jihuai, Zhang Lan, Jianming Lin, Miaoliang Huang, Yunfang Huang, Leqing Fan, Genggeng Luo, Yu Lin, Yimin Xie, and Yuelin Wei. “Counter electrodes in dye-sensitized solar cells.” *Chemical Society Reviews* 46, no. 19 (2017): 5975-6023.
- [180] Gregg, Brian A., Francois Pichot, Suzanne Ferrere, and Clark L. Fields. “Interfacial recombination processes in dye-sensitized solar cells and methods to passivate the interfaces.” *The Journal of Physical Chemistry B* 105, no. 7 (2001): 1422-1429.
- [181] Gregg, Brian A. “Interfacial processes in the dye-sensitized solar cell.” *Coordination Chemistry Reviews* 248, no. 13-14 (2004): 1215-1224.
-
-

- [182] Sharma, Khushboo, Vinay Sharma, and S. S. Sharma. "Dye-sensitized solar cells: fundamentals and current status." *Nanoscale research letters* 13, no. 1 (2018): 1-46.
- [183] Nazeeruddin, Md K., Etienne Baranoff, and Michael Grätzel. "Dye-sensitized solar cells: A brief overview." *Solar energy* 85, no. 6 (2011): 1172-1178.
- [184] Baviskar, Prashant K., and Babasaheb R. Sankapal. "Dye-sensitized solar cells." In *Energy Materials*, pp. 179-211. Elsevier, 2021.

Chapter 2

Experimental Methods and Characterization Techniques for Dye Sensitized Solar Cells

This Page is intentionally left blank

2.1 X-Ray Diffraction analysis

X-ray diffraction (XRD) analysis is a technique used to determine the crystal structure of materials in the nanomaterial, thin-film, or bulk material form. In the XRD experiment, a monochromatic X-ray beam is allowed to incident on the sample and the diffraction occurs. Constructive interference is obtained for the glancing angles (θ) corresponding to those (hkl) planes only for which the path difference is equal to the integral multiple (n) of wavelength (λ) of the X-ray used. This condition is given by Bragg's equation

$$2 d \sin\theta = n \lambda \quad (2.1)$$

where d is the interplanar spacing. The schematic diagram of the experimental arrangement is shown in Fig. 2.1. The reflected X-rays make an angle of 2θ with the material surface. A typical XRD pattern consists of these reflection peaks along the y-axis with the diffraction angles 2θ along the x-axis [1, 2].

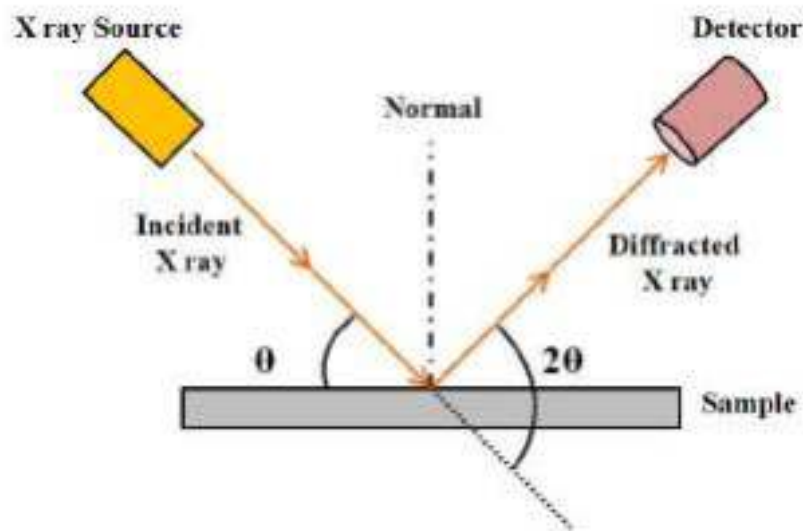


Figure 2.1 X-ray diffraction at the sample film surface.

X-rays are diffracted at specific angles by different crystal planes in nanostructures satisfying Bragg's condition. One can also calculate the interplaner spacing by knowing θ and λ . XRD is usually performed in the θ - 2θ scan mode where a monochromatic X-ray beam is incident on the nanostructure sample surface. X-ray source and detector motion are coupled with each other so that the detector always makes an angle 2θ with the incidence direction. Finally, the output is plotted as a graph between the recorded intensity of the diffracted beam and angle 2θ . The crystalline size (D) of the sample may be calculated using the Scherrer's formula

$$D = \frac{k \lambda}{\beta \cos\theta} \quad (2.2)$$

Where $k \approx 0.9$ and β = Full Width at Half Maximum (FWHM)

In our study, the X-ray diffraction analysis was employed using PAN-analytical X'Pert PRO X-ray diffractometer (CuK α radiation, 30 mA, 40 kV, $\lambda = 1.5406 \text{ \AA}$) to determine the crystalline structure and phase of different nanoparticle samples used in making the photoanode of the DSSCs.

2.2 Scanning Electron Microscopy (SEM)

A scanning electron microscope (SEM) [3-6] is a microscope that creates an image by using electrons rather than light. There are numerous advantages to using a scanning electron microscope over a traditional microscope. The SEM has a large depth of field, allowing for more of a specimen to be in focus at once. As the SEM uses electromagnets instead of optical lenses, the researcher has much more control over the magnification level. Along with that, SEM allows much higher resolution compared to optical microscopes. Because of these advantages, the scanning electron microscope is one of the most helpful research tools available today. An electron gun produces an electron beam at the top of the microscope. The electron beam is focused on the sample with the help of electromagnetic lenses. Electrons and

X-rays are emitted once the incident electron beam interacts with the sample. Detectors present in the instrument collect these scattered electrons, X-rays and covert them into signal.

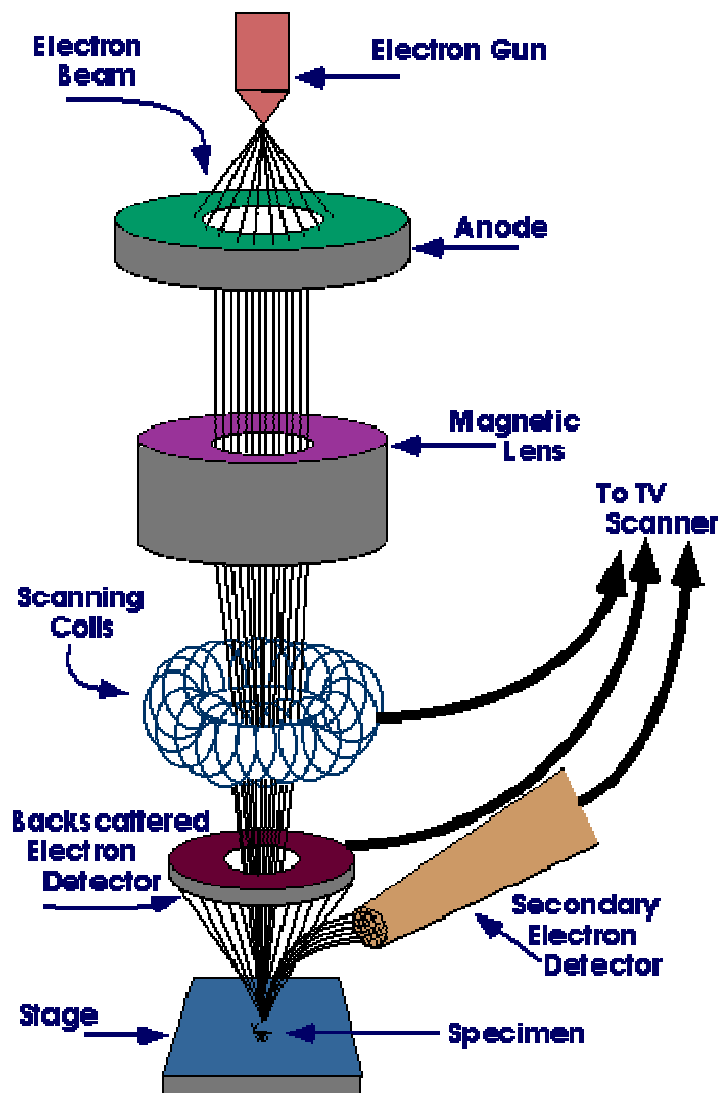


Figure 2.2 Schematic diagram of Scanning Electron Microscope.

(<https://www.purdue.edu/epps/rem/laboratory/equipment%20safety/Research%20Equipment/sem.html>)

The surface morphology of the sample is exposed by producing a visual image corresponding to the signal received, following the same method with which a picture is created on a television screen.



Figure 2.3 Experimental setup for SEM and EDS measurement.

2.3 UV-VIS spectroscopy

In order to study the absorption spectra of the dye solution, UV-VIS spectroscopy was used. In this measurement, the sample is exposed to light within a selected range of wavelengths. Absorption occurs when the incident photon energy surpasses the energy gap between the lower energy orbital (highest occupied molecular orbital-HOMO) and the higher energy unoccupied orbital (lowest unoccupied molecular orbital-LUMO) of the materials, and then the spectrometer records the signal. The block diagram of the UV-VIS spectrophotometer is shown in Fig. 2.4 [7].

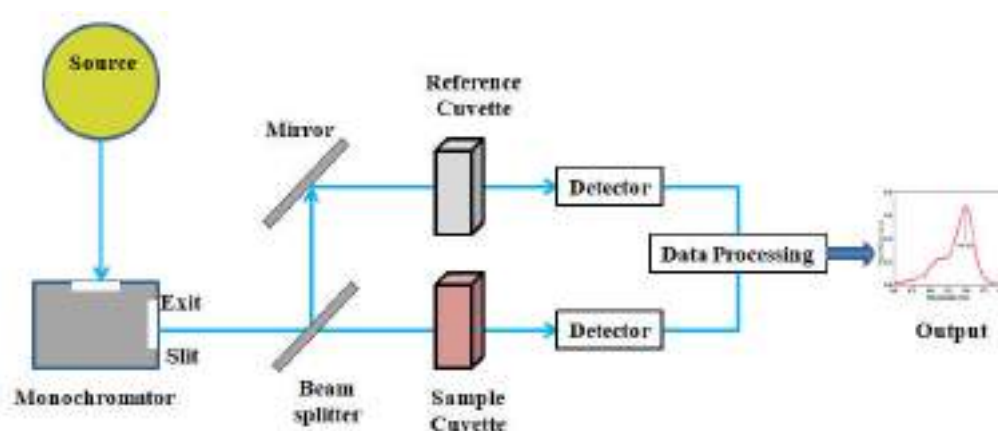


Figure 2.4 Schematic of UV-VIS spectrophotometer.



Figure 2.5 Experimental setup for UV-VIS absorption measurement.

In the present study, the absorbance spectrum measurement of the dye was carried out using a Perkin-Elmer Lambda-35 UV-VIS spectrophotometer.

2.4 Energy Dispersive X-ray spectroscopy (EDS)

Energy Dispersive X-ray Spectroscopy (EDS) study is performed to identify and quantify the elemental composition of the materials [8-10]. The basic working principle of EDS analysis utilizes the interaction of an electron beam with the sample. When primary electrons collide with the sample surface, the inner shell electrons are ejected and X-rays are produced as a result of the transition of the outer shell electrons filling up the vacancy in the inner shell. Due to its unique atomic structure, each element emits a distinct X-ray emission pattern that can be used to perform the atomic compositional analysis of the specimen with an energy dispersive spectrometer. The analysis of these peaks yields both qualitative and semi-quantitative information about the material.

2.5 Raman Spectroscopy

Raman spectroscopy is an analysis technique that measures the vibrational energy modes and provides detailed chemical and structural information about the sample. This information is obtained by detection of the Raman scattering from the sample. When a monochromatic beam of light incident on the sample, most of the scattered light consists frequency same as that of the incident radiation. This is known as Rayleigh scattering. However, a small portion of the scattered light has frequencies above and below the incident frequency which is referred as Raman scattering.

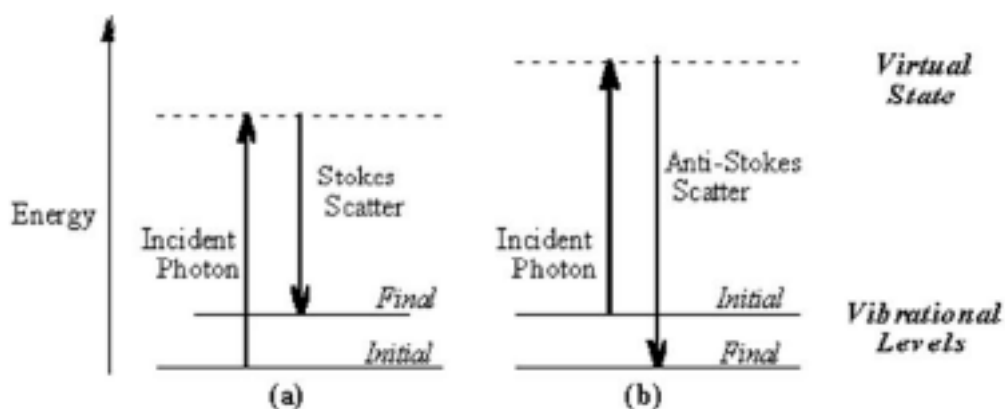


Figure 2.6 (a) Stokes Raman Scattering, (b) Anti-Stokes Raman Scattering.

When a photon beam having energy $h\nu$ suffers an elastic collision with molecules present in the sample, they scatter without suffering any energy exchange with the molecule and thus, the frequency of the scattered light remains unchanged.

However, during the inelastic collision, there will be exchange of energy between the molecule and the photon. Consequently, the scattered light will have a frequency different from the incident frequency. If the molecule absorbs some energy from the incident photon, then it gains some energy and consequently, the scattered photon loses energy. Light scattered with a

frequency lower than the incident frequency is known as Stokes Raman scattering.

On the other hand, when the molecule loses some energy to the scattered photon, the frequency of the scattered light becomes more than the incident light and the corresponding phenomenon is known as Anti-Stokes Raman scattering [11-13].

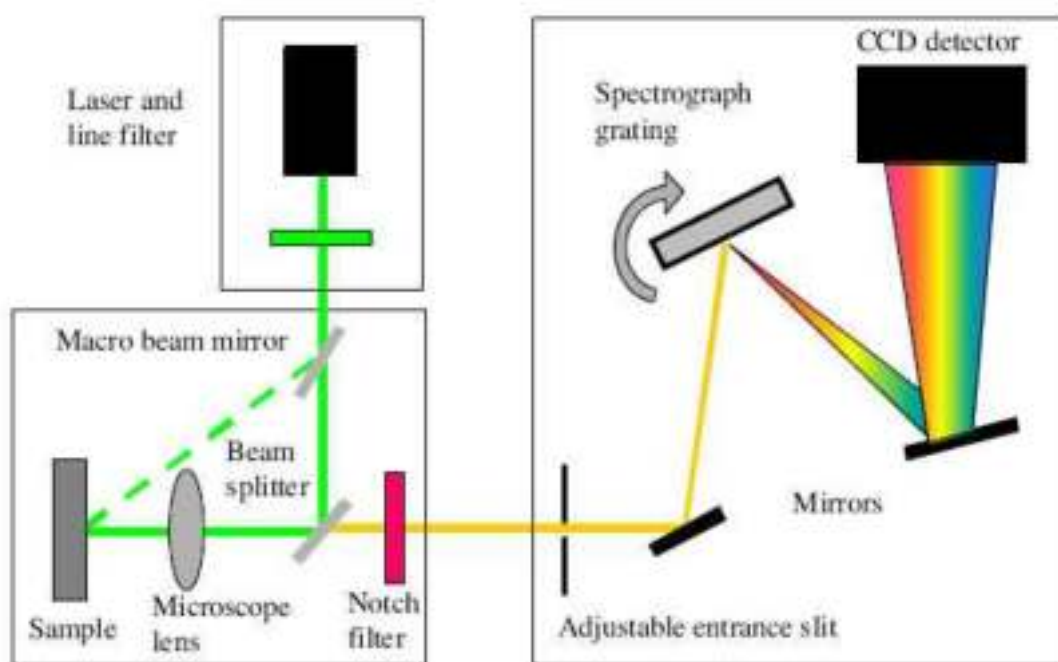


Figure 2.7 Schematic diagram of a typical Raman Spectrophotometer.

(<https://www.sas.upenn.edu/~crulli/TheRamanSpectrophotometer.html>)

In a typical Raman spectrophotometer, a very narrow and monochromatic laser beam (coherent and powerful) is used to excite the target material. Usually, the material is filled inside a narrow quartz or glass tube. The light is scattered by the sample and then collected by a lens. The collected light is passed through a grating Monochromator. Finally, a detector captures the signal and sends it to a computer for decoding.

2.6 Basic parameters to evaluate the performance of DSSCs: Solar Cell Terminologies

Current-voltage measurement is a simple method to evaluate photovoltaic devices under both illumination and dark conditions. Fig. 2.8 represents a simplified equivalent circuit (single diode equivalent model) of a solar cell, including the series (R_s) and parallel resistances (R_{sh}) are added to account for various loss mechanisms a typical I-V curve for a solar cell under illumination and dark.

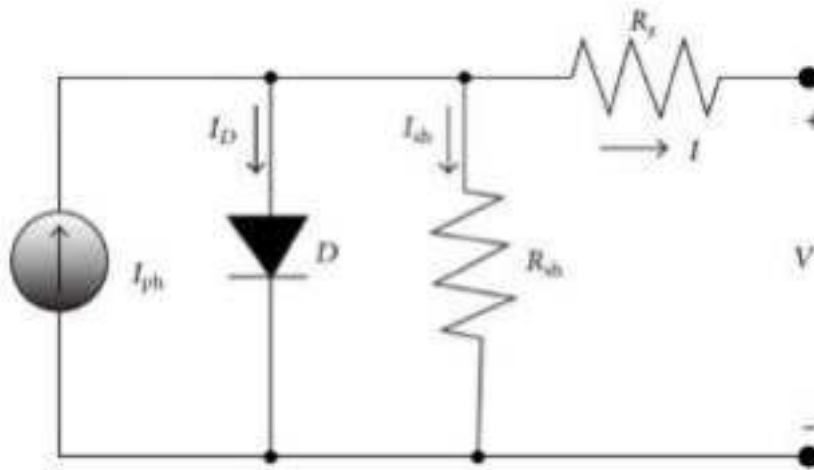


Figure 2.8 One diode equivalent circuit model of a Solar cell [14].

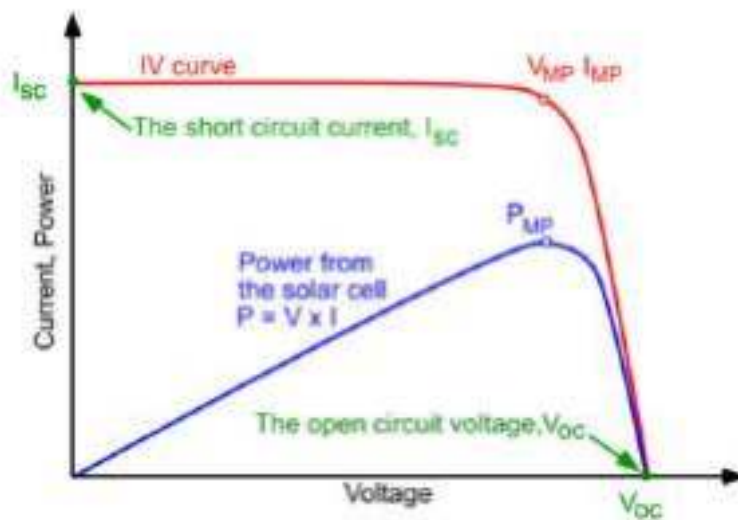


Figure 2.9 Typical I-V characteristics of a solar cell [17].

The current-voltage characteristic of a Solar cell allows us to determine the photovoltaic performance of the cell. The Power-Voltage plot to calculate the maximum power point (P_{MP}), I_{MP} and V_{MP} are represented in Fig. 2.9. Various parameters like photocurrent density (J_{SC}), open-circuit voltage (V_{OC}) and fill factor (FF) can be extracted from the I-V curves. From which the overall photoelectric conversion efficiency (η) can be calculated.

Equivalent circuit modeling is a very important tool required for better understanding and explaining the solar cell performance and analysis of the electrical processes occurring inside the cell. The functioning of a solar cell is generally modeled by a single diode with a constant photo-generated current source, a series (R_s) and shunt resistance (R_{sh}) as shown in Fig. 2.8. The current-voltage relation is given by the equation

$$I = I_{ph} - I_o \left[\exp \left\{ \frac{(q(V + IR_s))}{Ak_B T} \right\} - 1 \right] - \frac{V + IR_s}{R_{sh}} \quad (2.3)$$

where I_{ph} , I_o , R_s , R_{sh} , q , A , k_B and T are the photocurrent, the saturation current of the diode, the series resistance, the shunt resistance, the electron charge, the ideality factor, the Boltzmann constant, and absolute temperature, respectively [16, 17]. The circuit parameters like R_s and R_{sh} are not directly measurable. They are calculated by fitting the experimental J-V curve with equation 2.3 [15].



Figure 2.10 Experimental Setup for I-V measurement.

2.6.1 Open circuit voltage (V_{OC})

Open-circuit voltage is the maximum voltage obtainable from a solar cell and is obtained when a load with infinite resistance is attached to its terminals i.e. the cell current is zero. It is determined by the difference between the redox potential of the electrolyte and the Fermi level of electrons in the semiconductor, namely TiO_2 . For DSSC, V_{oc} is given by:

$$V_{oc} = \frac{E_{CB}}{q} + \frac{kT}{q} \ln\left(\frac{n}{N_{CB}}\right) - \frac{E_{redox}}{q} \quad (volts) \quad (2.4)$$

Where n represents the number of electrons in the TiO_2 conduction band and N_{CB} is the effective density of states [11]. E_{redox} represents the Nernst potential of the redox mediator and first two terms in above equation define the quasi-Fermi level of TiO_2 and.

2.6.2 Short circuit current density (J_{SC})

The short circuit photocurrent (I_{SC}) is the cell photocurrent measured at zero voltage. It is the current obtained from the cell when it is short-circuited or in other words when the load resistance is zero. It largely depends on the photon-generated electrons and the interfacial recombination of the electrons and holes. In general, it is represented in the form of the short circuit current density (J_{SC}) and is defined as $J_{SC}=I_{SC}/A$ (mA/cm^2), Where, A is the effective area of the solar cell. It is a function of the solar illumination, optical properties and charge transfer probability of the cell.

2.6.3 Series Resistance (R_s)

Series resistance, R_s in a solar cell, results from the contact resistance and charge transfer resistance in the semiconductor material. Series resistance reduces the fill factor of the device and thus affects the maximum device power output, while an excessively high value of R_s can also reduce the short-circuit current. The open-circuit voltage is not affected by R_s , since at V_{oc} the total current flow through cell itself is zero and hence the series resistance is zero. An approximate value of the series resistance can be determined from the slope of the I-V curve at the open-circuit voltage point.

2.6.4 Shunt Resistance (R_{sh})

Low shunt resistance provides an alternate path for the photo-generated current causing significant power loss. The effect of low shunt resistance is reduced fill factor and lower open-circuit voltage affecting the maximum power output. The short-circuit current is not affected unless for a very low value since at J_{sc} the total current flows through the outer path and hence through the shunt resistance is low. An approximation of the shunt resistance can be calculated from the slope of the I-V curve at the short circuit current point.

2.6.5 Fill Factor (FF)

The fill factor (FF) is a measure of the maximum power output from a solar cell. It represents the squareness of the I-V curve that is The FF describes how a maximum power rectangle fits under the I-V characteristics and is given by the ratio of the maximum output power to the product of I_{SC} and V_{OC} for the solar cell:

$$FF = \frac{I_{MP}V_{MP}}{I_{SC}V_{OC}} \quad (2.5)$$

Where, V_m and I_m are the voltage and current at the maximum power point. Fill factor, being a ratio of the same physical parameters, has no unit. Fill factor is a function of the series and shunt resistance of the solar cell. For DSSC, it reflects the extent of electrical and electrochemical losses during cell operation. To obtain high FF, R_S should be small, while R_{Sh} needs to be as large as possible.

2.6.6 Power Conversion Efficiency (η)

The power conversion efficiency of a photovoltaic cell is described as the ratio of the maximum electrical energy output of the device to the energy input from the sun. Thus the mathematical definition of efficiency is

$$\eta = \frac{P_{out}}{P_{in}} = \frac{I_{sc}V_{oc}FF}{P_{in}} \quad (2.6)$$

Where P_{in} represents the input power of sunlight. Efficiency is generally expressed in percentage. Besides the solar cell performance, it depends on the incident light spectrum and intensity as well as operating temperature. The internationally recognized standard condition for the efficiency measurement of solar cells is under ‘AM1.5 Global’ solar irradiation and at a temperature of 25°C [18].

2.7 Electrochemical Impedance Spectroscopy (EIS)

The current-voltage measurement of a solar cell is the elementary method to evaluate the overall electro-optical performance of the device. However, it fails to provide detailed information about the limiting factors and resistances offered by the individual components and interfaces of the architecture that inhibit device performance. The electrochemical impedance spectroscopy (EIS) is a very advanced and powerful diagnostic technique that offers simultaneous measurement of various interfacial charge transfer dynamics and recombination mechanisms inside the device. This method is based on analyzing the electrical response of the device to a periodic voltage having variable frequency superimposed on a constant bias potential. These are typically represented by modeling appropriate equivalent circuits in terms of resistors and capacitors [19, 20].



Figure 2.11 Experimental setup for EIS measurement.

2.7.1 Theory of Impedance

The concept of electrical impedance can be realized starting from the theoretical concept of resistance. The electrical resistance of a material

represents the ability of the material to resist the flow of electrical current through it. It is defined by well known Ohm's law as the ratio between voltage (V) and current (I)

$$R = \frac{V}{I} \quad (2.7)$$

But the applicability of this relationship is restricted to a single circuit element, the ideal resistor. However, most of the systems under investigation contain circuit elements with much more complicated behaviour. This implies that the basic idea of resistance should be replaced by a more general parameter: impedance, which incorporates not only the respective amplitudes of voltage and current but also their relative phases. Impedance is also a measure of a circuit's capacity to resist the flow of electrical current in a specific way, but it isn't restricted to the features of a pure resistance. Impedance is a broad term that refers to the collective obstruction to current offered by resistances, capacitances, and inductances present in the device or the circuit. Typically, electrochemical impedance is analyzed by delivering an alternating potential to an electrochemical cell and measuring the current flowing through it. It is generally measured. In order to produce a linear response from the cell, electrochemical impedance is generally measured by applying a small sinusoidal excitation potential and recording the corresponding current response from the device. This current response will also be a sinusoidal wave with the same frequency but a shifted phase. The applied sinusoidal excitation potential can be represented as

$$V = V_o \sin \omega t \quad (2.8)$$

The corresponding current response from the device with a shifted phase may be written as

$$I = I_o (\sin \omega t + \varphi) \quad (2.9)$$

where φ is the phase shift. The impedance of the system may be calculated using a formula similar to Ohm's Law.

$$Z = \frac{V}{I} = \frac{V_o \sin \omega t}{I_o (\sin \omega t + \varphi)} \quad (2.10)$$

It is usually more convenient to represent impedance using complex exponentials. The magnitude and phase of the input and output signals may be represented in a much simpler way using these complex numbers. Furthermore, it provides a more powerful representation for circuit analysis purposes.

The applied potential and current response from the cell can be represented as a complex function having a form like

$$V = V_o \exp(j\omega t) \quad (2.11)$$

and
$$I = I_o \exp j(\omega t - \varphi) \quad (2.12)$$

respectively.

Consequently, the complex impedance may be written as

$$\begin{aligned} Z &= \frac{V}{I} = \frac{V_o}{I_o} \exp(j\varphi) \\ &= Z_o (\cos \varphi + j \sin \varphi) \\ &= Z' + j Z'' \end{aligned} \quad (2.13)$$

where $Z' = Z_o \cos \varphi$ and $Z'' = Z_o \sin \varphi$ are the real and imaginary components of the impedance respectively.

2.7.2 Nyquist and Bode plots

During the impedance measurement, the system is generally kept in a steady condition prior to applying an alternating potential and measuring the corresponding alternating response current through the cell. Globally used impedance measurement setups allow measurement of the complex impedance and phase shift at a particular applied frequency. The impedance of the system as a function of frequency may be easily obtained by varying the frequency of the applied signal in a continuous way. Impedance parameters for specific internal components of the cell can be assigned using proper model equivalent circuits (which might have multiple options dependent on splitting an actual

device into component structures). The recorded data is usually represented in two ways; one is the Nyquist plot depicting the plot between real (Z') and imaginary (Z'') part of the impedance and another is the Bode plot depicting the variation of the magnitude of the impedance ($Z_0 = |Z|$) or phase (φ) with frequency (f) of the applied signal as shown in Fig. 2.12 (a) and fig. 2.12 (b) respectively.

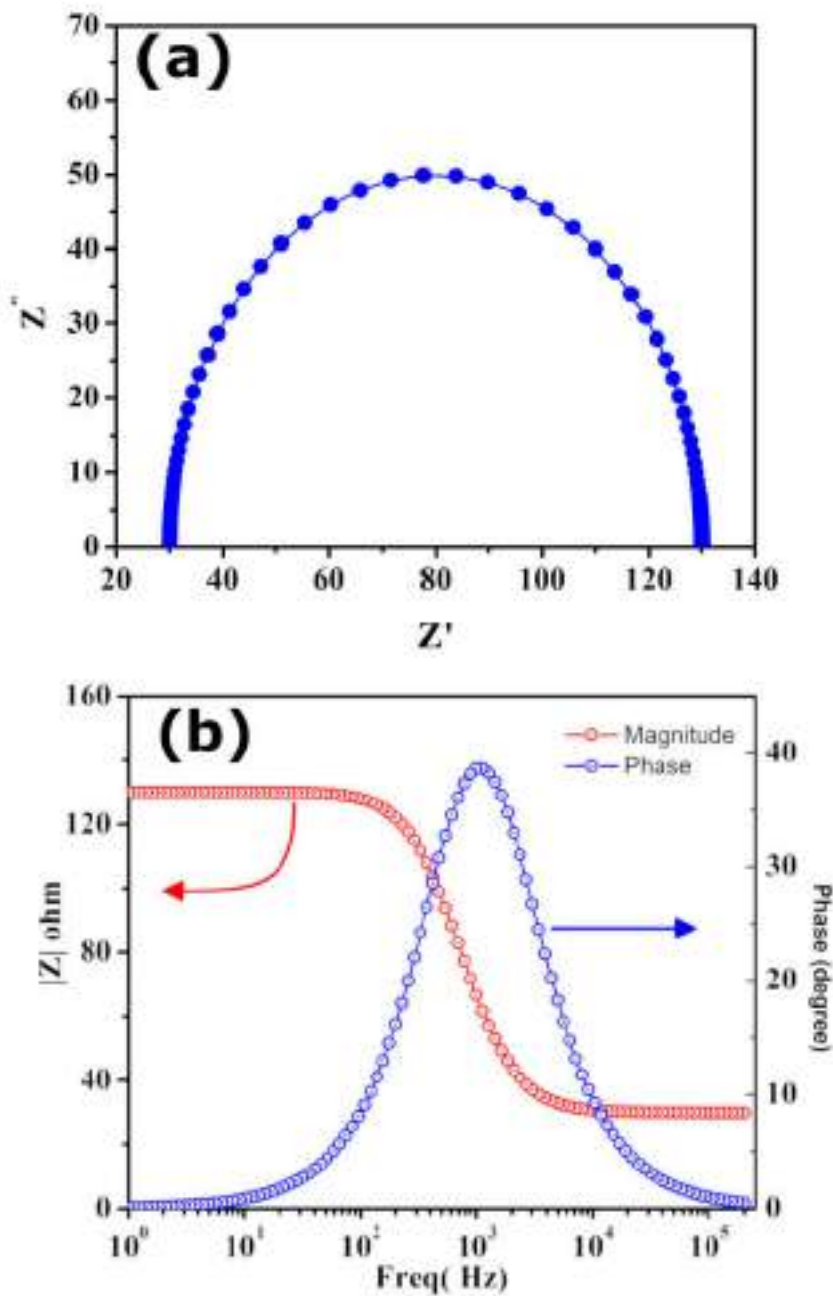


Fig. 2.12 Typical (a) Nyquist and (b) Bode plot.

2.7.3 Equivalent circuit for impedance measurement of DSSC

A dye-sensitized solar cell is a very complex system, and its ultimate impedance response depends on the responses received from various components of the device. The electronic processes that occur within the DSSC are well represented by the transmission line model developed by Bisquet [21]. The transmission line model widely used to represent different charge transfer, recombination and diffusion processes occurring inside DSSC is shown in Fig. 2.13.

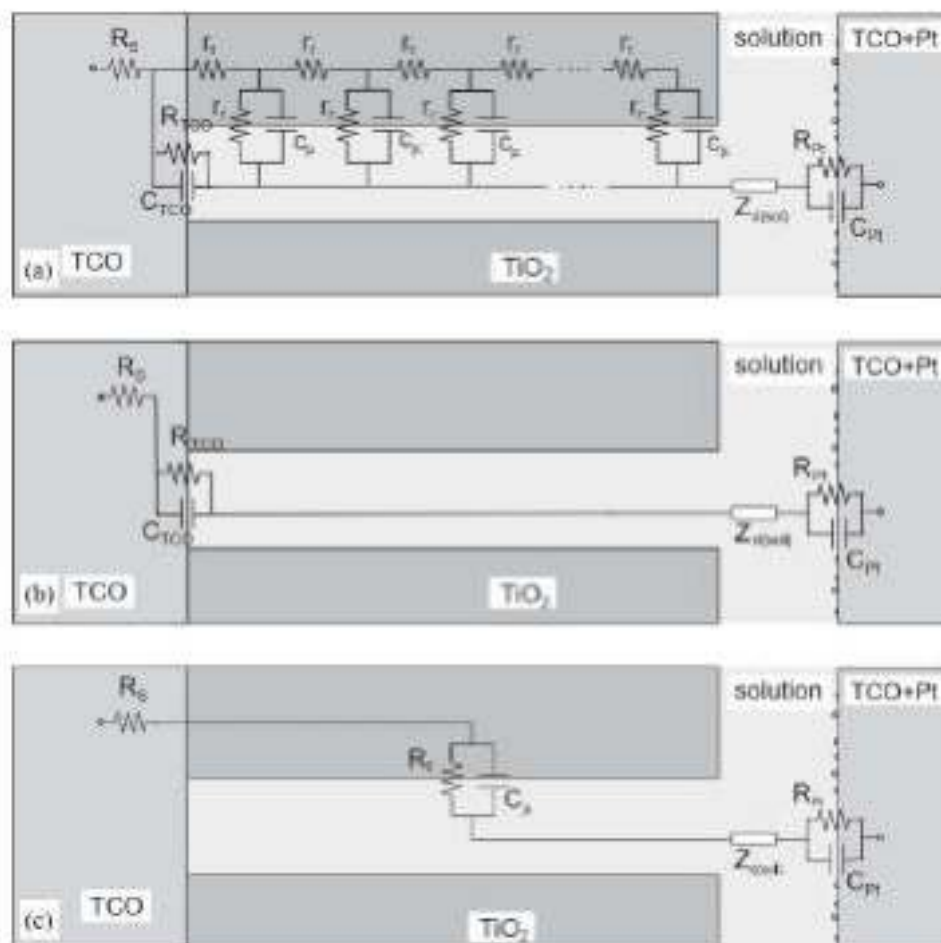


Fig. 2.13 (a) Equivalent circuit for a complete solar cell; (b) Simplified circuit for insulating TiO₂ (potentials around 0 V) as currents are low, Z_d may be skipped and (c) Simplified equivalent circuit of a DSSC when the TiO₂ is in conducting state (At V_{oc} bias potential) [22].

Usually, the EIS measurement is carried out at the potentials near to V_{oc} in order to achieve consistency equivalent to that of a real system. The nanostructured oxide model has been simplified to a columnar model in this illustration, which depicts the mesoporous layer through which the electrolyte solution passes. The different circuit elements are:

- R_s is sheet resistance of the TCO layer and contact resistances.
- $R_t = r_t L$ is the electron transport resistance.
- $R_r = r_r / L$ is the charge transfer resistance related to the recombination of the electrons at the $TiO_2 + dye / electrolyte$ interface.
- R_{TCO} is the charge-transfer resistance for electron recombination from the uncovered layer of the TCO to the electrolyte.
- C_{TCO} is the capacitance at the triple contact TCO/ TiO_2 /electrolyte interface
- C_μ is the capacitance at the $TiO_2 + dye / electrolyte$ interface.
- $Z_d(sol)$ is the impedance of the redox species diffusion into the electrolyte, generally called Nernst impedance Z_N .
- R_{Pt} is the charge transfer resistance at the counter electrode.
- C_{Pt} is the capacitance at the electrolyte/counter electrode interface.

The first three mentioned elements are denoted in lowercase letters in Fig. 2.13(a), meaning the element per unit length for a film of thickness L , because they are distributed in a repetitive arrangement of a transmission line. Physical interpretation of the different electrochemical operations across the interfacial regions of the DSSCs can be made by fitting the EIS spectra with the appropriate equivalent circuit. Generally, a typical Nyquist plot of a DSSC exhibits three semicircles (Fig. 2.14). The first semicircle in the high frequency range (above 100 Hz) describes the charge transfer at the Pt/electrolyte interface (Z_1), the second semicircle at an intermediate frequency range (1-100 Hz) is related to the recombination at the photoanode/electrolyte interface and the charge transport into the semiconductor (Z_2). The third one at low

frequency (below 1 Hz) represents the diffusion in the electrolyte (Z_3) and is attributed to the Nernst contribution. If the voltage is reduced, the two external semicircles are incorporated into the biggest one. Nevertheless, these Nyquist plots have one major limitation: they do not give complete information on the exact frequency used to record one point.

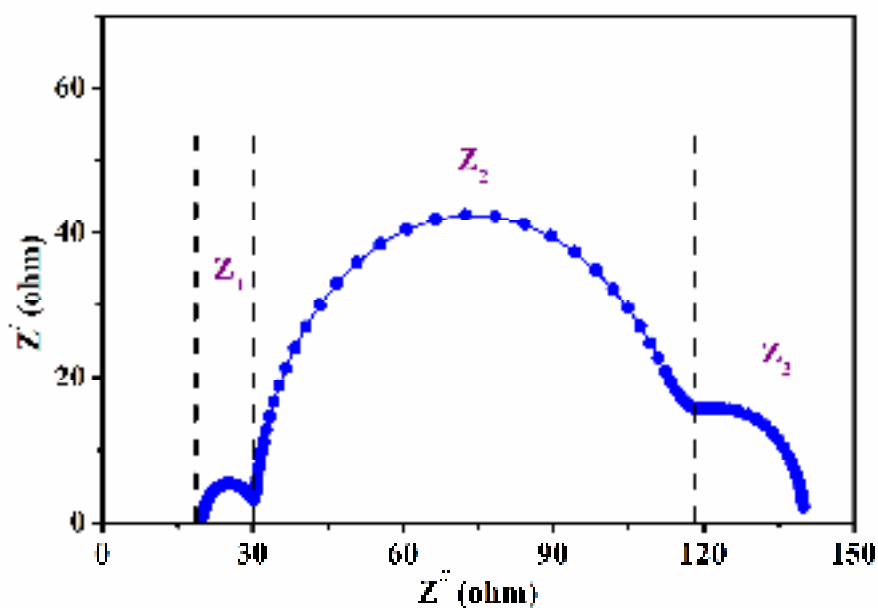


Fig. 2.14 Typical Nyquist plot of a DSSC under Open circuit condition.

Another important representation of the EIS data is Phase bode plot representing Phase ($-\theta$) vs. Frequency (f) curve. Unlike the Nyquist plot, the very important aspect of this plot is that frequency information is not lost.

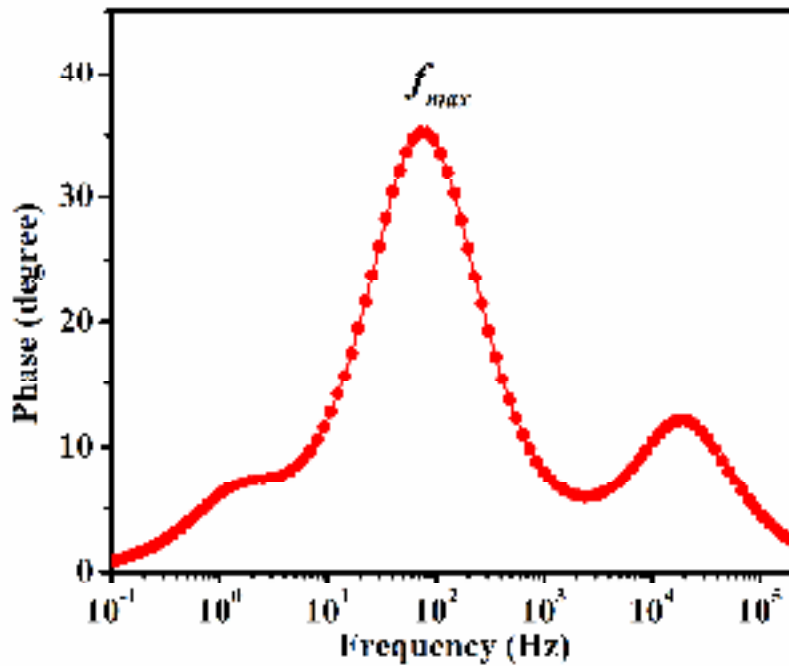


Fig. 2.15 Typical Bode plot (Phase) representation of a DSSC.

The average carrier lifetime can be estimated from phase bode plots (shown in Fig. 2.15) using the formula

$$\tau_e = \frac{1}{2\pi f_{max}}$$

where f_{max} represents peak frequency in the mid-frequency range [23].

References:

- [1] Epp, J.: X-ray diffraction (XRD) techniques for materials characterization. In *Materials characterization using nondestructive evaluation (NDE) methods* (pp. 81-124) (2016). Woodhead Publishing.
- [2] Zhang, L. Z., & Tang, G. Q. :Preparation, characterization and optical properties of nanostructured ZnO thin films. *Optical Materials*, 27(2), 217-220(2004).
- [3] Vernon-Parry, K. D. “Scanning electron microscopy: an introduction.” *III-Vs Review* 13, no. 4 (2000).
- [4] McMullan, D. “Scanning electron microscopy 1928–1965.” *Scanning* 17, no. 3 (1995): 175-185.
- [5] Zhou, Weilie, Robert Apkarian, Zhong Lin Wang, and David Joy. “Fundamentals of scanning electron microscopy (SEM).” In *Scanning microscopy for nanotechnology*, pp. 1-40. Springer, New York, NY, 2006.
- [6] Goldstein, Joseph I., Dale E. Newbury, Joseph R. Michael, Nicholas WM Ritchie, John Henry J. Scott, and David C. Joy. *Scanning electron microscopy and X-ray microanalysis*. Springer, 2017.
- [7] Rocha, F. S., Gomes, A. J., Lunardi, C. N., Kaliaguine, S., & Patience, G. S.: *Experimental methods in chemical engineering: Ultraviolet visible spectroscopy—UV-Vis*. *The Canadian Journal of Chemical Engineering*, 96(12), 2512-2517(2018).
- [8] d’Alfonso, A. J., B. Freitag, D. Klenov, and L. J. Allen. “Atomic-resolution chemical mapping using energy-dispersive x-ray spectroscopy.” *Physical Review B* 81, no. 10 (2010): 100101.
- [9] Allen, Leslie J., Adrian J. D’Alfonso, Bert Freitag, and Dmitri O. Klenov. “Chemical mapping at atomic resolution using energy-dispersive x-ray spectroscopy.” *MRS bulletin* 37, no. 1 (2012): 47-52.

-
-
- [10] Shindo, Daisuke, and Tetsuo Oikawa. "Energy dispersive x-ray spectroscopy." In *Analytical electron microscopy for materials science*, pp. 81-102. Springer, Tokyo, 2002.
- [11] Long, Derek Albert. "Raman spectroscopy." New York 1 (1977).
- [12] Larkin, Peter. *Infrared and Raman spectroscopy: principles and spectral interpretation*. Elsevier, 2017.
- [13] Koningstein, Johannes Arnoldus. *Introduction to the Theory of the Raman Effect*. Springer Science & Business Media, 2012.
- [14] Ma, Jieming, Ka Lok Man, T. O. Ting, Nan Zhang, Sheng-Uei Guan, and Prudence WH Wong. "Approximate single-diode photovoltaic model for efficient IV characteristics estimation." *The Scientific World Journal* 2013 (2013).
- [15] Cotfas, D. T., P. A. Cotfas, and S. Kaplanis. "Methods to determine the dc parameters of solar cells: A critical review." *Renewable and Sustainable Energy Reviews* 28 (2013): 588-596.
- [16] Murayama, Masaki, and Tatsuo Mori. "Equivalent circuit analysis of dye-sensitized solar cell by using one-diode model: effect of carboxylic acid treatment of TiO₂ electrode." *Japanese journal of applied physics* 45, no. 1S (2006): 542.
- [17] Charles, J. P., M. Abdelkrim, Y. H. Muoy, and P. Mialhe. "A practical method of analysis of the current-voltage characteristics of solar cells." *Solar cells* 4, no. 2 (1981): 169-178.
- [18] Smestad, Greg P., Frederik C. Krebs, Carl M. Lampert, Claes G. Granqvist, K. L. Chopra, Xavier Mathew, and Hideyuki Takakura. "Reporting solar cell efficiencies in solar energy materials and solar cells." *Solar Energy Materials and Solar Cells* 92, no. 4 (2008): 371-373.
- [19] Fabregat-Santiago, Francisco, Juan Bisquert, Emilio Palomares, Luis Otero, Daibin Kuang, Shaik M. Zakeeruddin, and Michael Grätzel. "Correlation between photovoltaic performance and impedance
-
-

-
-
- spectroscopy of dye-sensitized solar cells based on ionic liquids.” *The Journal of Physical Chemistry C* 111, no. 17 (2007): 6550-6560.
- [20] Hagfeldt, Anders, Gerrit Boschloo, Licheng Sun, Lars Kloo, and Henrik Pettersson. "Dye-sensitized solar cells." *Chemical reviews* 110, no. 11 (2010): 6595-6663.
- [21] Bisquert, Juan. "Theory of the impedance of electron diffusion and recombination in a thin layer." *The Journal of Physical Chemistry B* 106, no. 2 (2002): 325-333.
- [22] Fabregat-Santiago, Francisco, Juan Bisquert, Germà Garcia-Belmonte, Gerrit Boschloo, and Anders Hagfeldt. "Influence of electrolyte in transport and recombination in dye-sensitized solar cells studied by impedance spectroscopy." *Solar energy materials and solar cells* 87, no. 1-4 (2005): 117-131.
- [23] Bhatt, Parth, Kavita Pandey, Pankaj Yadav, Brijesh Tripathi, and Manoj Kumar. "Impedance spectroscopic investigation of the degraded dye-sensitized solar cell due to ageing." *International Journal of Photoenergy* 2016 (2016).

This Page is intentionally left blank

Chapter 3

**Dye Sensitized Solar Cells Based on
ZnO Nanostructures and Organic Dyes**

This Page is intentionally left blank

3.1. Introduction

With the increasing world population, spreading urbanization and technological advancement, matching the energy supply with the energy demand is the major challenging issue the world is facing these days. The environmental consequences related to extensive use of fossil fuels, safety related issues of nuclear power, ever-growing energy demand and depleting the stock of fossil fuels have motivated the researchers to search for alternative economically and environmentally sustainable renewable energy sources [1]. In such a context of global energy requirements, among all the non-polluting and renewable energy sources, the photovoltaic technology utilizing solar energy has emerged as the most assuring candidate [2]. Though conventional photovoltaic devices (silicon-based solar cells) are promising for the direct conversion of photons into electrons, the prohibitive cost of these cells is non-competitive with conventional power generating methods [3, 4]. On the contrary, dye-sensitized solar cells (DSSCs), invented by O'Regan and Grätzel in 1991, are non-conventional photovoltaic technology based solar cells that have attracted significant attention because of their novel fabrication concept derived from nature's principle (photosynthesis), easy fabrication procedure using abundant materials, cost-effectiveness, suitability for a wide variety of end-user products and can be made flexible. SSC is a device that performs the conversion solar energy into electrical energy based on the principle of sensitization of wide band-gap semiconductors [5]. The photoelectrochemical performance of a DSSC mainly depends on the selected Photoanode material, including its surface morphology and the sensitizing dye used [6-9]. Although a large number of different DSSCs have been investigated, most of them are not commercially popular until now because of their issues with low conversion efficiency, higher production cost, lower stability and durability [10, 11]

Different inorganic, organic and hybrid dyes were employed as sensitizers in DSSCs. But among all of them, the ruthenium complexes are the

most popular sensitizers because of But among all of them, the ruthenium complexes are the most popular sensitizers because of their exceptional charge transfer mechanics and absorption across the complete visible range along with intense metal-to-ligand charge transfer mechanism [12]. But the significant downsides of Ruthenium dyes are its rareness, high cost and complicated synthesis process [13]. Also, ruthenium polypyridyl complexes contain heavy metal, which is harmful to the environment [14]. In order to find out low-cost and environment-friendly alternatives to these expensive ruthenium compounds, researchers are focusing on easily available natural dyes extracted from various natural resources. Many researchers have studied sensitizing effects of several natural dyes derived from various fruits, flowers and leaves [15]. Most of them are used with TiO₂ nanostructures as photoanode [16-20]. However, ZnO has recently emerged as a great potential alternative to TiO₂ due to its fascinating electrical and optical properties. ZnO is a wide band gap semiconductor having a direct band gap of 3.37 eV, making it suitable as a photoanode material for DSSC [21, 22]. Apart from this, ZnO is very easy to synthesis, abundant, inexpensive and poses higher electron mobility (200-300 cm²V⁻¹S⁻¹ for bulk material and 1000 cm²V⁻¹S⁻¹ for nanowire) than that of TiO₂ nanoparticles (0.1-4 cm²V⁻¹S⁻¹) [23-25]. Moreover, the 1-D single-crystalline rod-like structure of ZnO nanorods provides a higher surface-to-volume ratio enabling better dye loading [26]. These qualities of ZnO make it a potential alternative to TiO₂ for the fabrication of DSSCs.

In this study, we aimed to combine natural sensitizers with two types of nanostructured ZnO to get both the advantages of ZnO and also the benefits of natural organic dyes targeting lower fabrication cost, eco-friendly devices along with good cell performance and wanted to find out the best suitable ZnO nanostructure-Natural dye combination. In this regard, we fabricated four DSSCs using two types of natural dyes, anthocyanin extracted from pomegranate (*Punica granatum*) and curcumin extracted from fresh

turmeric(*Curcuma longa*) and their electro-optical responses to investigate their usefulness as natural sensitizers when adsorbed onto ZnO nanorod (NR) and ZnO nanoparticle (NP) films in DSSCs has been studied. Hydroxyl and Carbonyl groups existing the natural sensitizers bound them easily to the surface of the ZnO nanorods, which facilitates very easy electron injection from LUMO of dye molecule to the conduction band of ZnO [27]. Along with that, we have also studied the effect of Rose Bengal as sensitizing dye in TiO₂ and ZnO nanoparticle based DSSCs.

3.2. Experimental Section

3.2.1. *Structure and Working principle of DSSC*

A typical DSSC consists of four elements: a photoanode with a thin layer of mesoporous wide bandgap semiconductor oxide layer (usually TiO₂, ZnO, SnO₂ or Nb₂O₅) over a transparent conducting substrate (ITO or FTO), a monolayer of the sensitizing dye adsorbed on the semiconductor oxide surface to facilitate light absorption, a redox mediator electrolyte solution (typically I⁻ / I₃⁻) in an organic solvent and a counter electrode made up of a catalyst (platinized ITO or FTO) to facilitate charge collection. The schematic of device architecture and working principle of a typical DSSC is shown in Fig. 3.1(a) and Fig. 3.1(b). Upon exposure to the sunlight, dye molecule absorbs photon energy and goes through an electronic state change, the electron jumps from ground state (HOMO) to the excited state (LUMO). As a result, electron injection into the conduction band of the semiconductor oxide (ZnO) film occurs, whereby the dye molecule gets oxidized. This oxidized dye molecule is regenerated by taking an electron from the redox species of the electrolyte (I⁻). Subsequently, I⁻ is regenerated by reduction of I₃⁻ with electrons migrated from photo anode via external load and collected at the counter electrode, completing the cycle [5, 6].

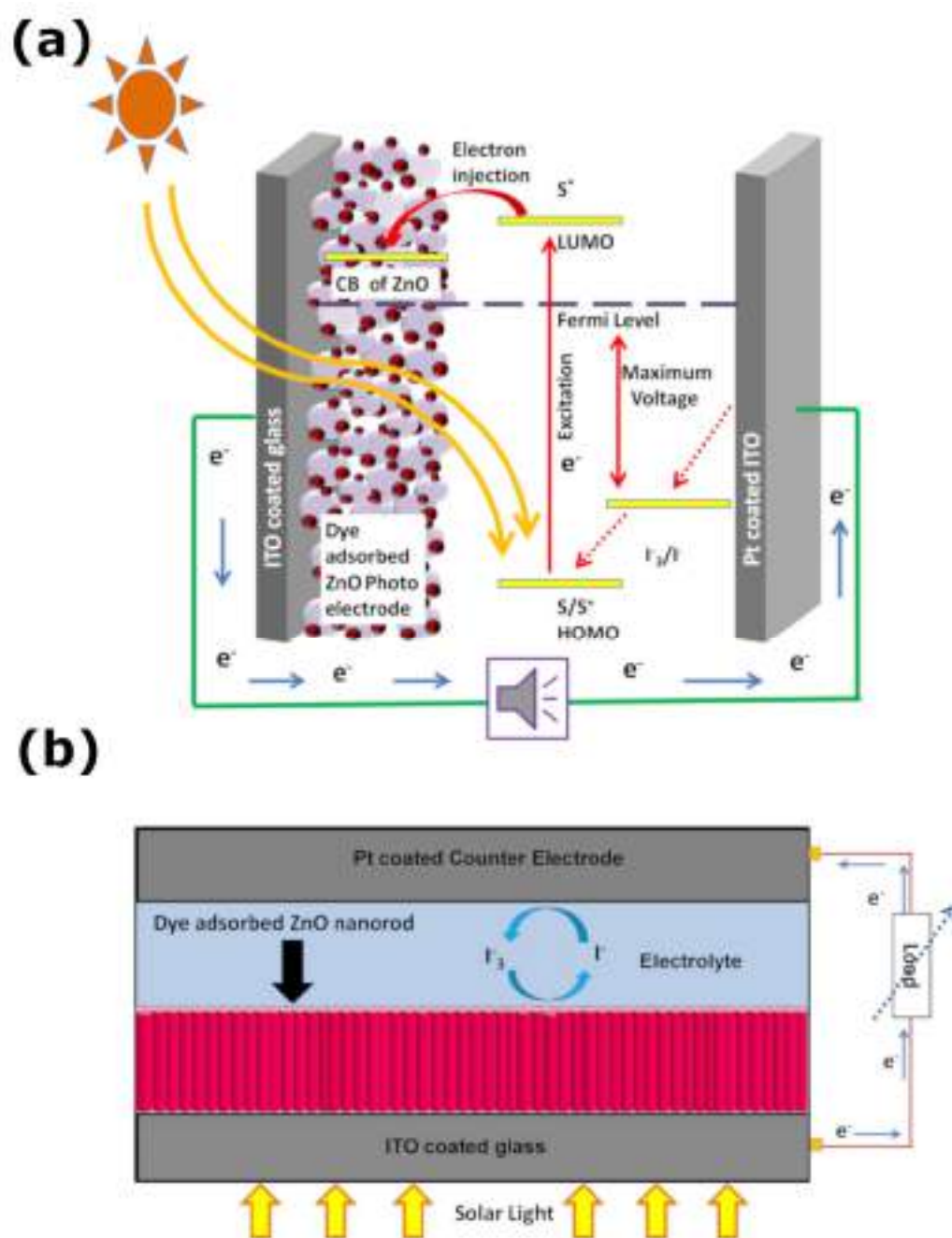


Figure 3.1 Schematic diagram and basic working mechanism of DSSCs based on (a) ZnO nanoparticle (b) ZnO nanorod.

3.2.2. *Materials used*

Transparent ITO coated glass (10 Ω / square) was purchased from Techinstro, India. The liquid platinum paint (Platisol T) purchased from Solaronix, Switzerland, was used to prepare the platinum-coated transparent counter electrode. Commercial ZnO and TiO₂ nanopowder, Zinc acetate dehydrate, Hexamethylenetetramine and Rose Bengal dye, all were purchased from Sigma Aldrich. Ethylene Glycol (Sigma Aldrich) was used as a solvent for the electrolyte preparation using KI (S D Fine-Chemical Ltd., India) and I₂ (RANKEM, India). Meltonix 1170-60(60 μ m) purchased from Solaronix was used as a spacer between the electrodes to avoid short-circuiting between the ITO and electrolyte.

3.2.3. *Extraction and Preparation of Organic Dye Sensitizers*

In the fabrication of Dye Sensitized solar cells, selecting the dyes is a crucial task as it significantly affects the performance and production cost of the cells. By choosing abundant natural dyes instead of expensive synthetic ruthenium dyes we can reduce the production cost by a large amount. In this work, we have chosen Curcumin and pomegranate juice extracts as sensitizers. Curcumin was extracted by grinding turmeric root in an iron mortar and then mixing in 100ml ethanol. After extraction, Solid residues were filtered out to obtain a clear natural dye solution.

For pomegranate extraction of pomegranate juice, afresh pomegranate was squeezed and mixed with 100ml deionized water. This solution is also filtered to obtain pure dye. The dye solutions were properly stored, protecting from direct sunlight for further use. Studies have shown that Curcumin dyes have two forms and they are identified as Keto and Enol [28]. On the contrary, it was found that pomegranate juice mostly contains six types of anthocyanins. These are cyanidin 3-glucoside, cyanidin 3,5-diglucoside, delphinidin 3-glucoside, delphinidin 3,5-diglucoside, pelargonidin 3-glucoside and

pelargonidin 3,5-diglucoside [29]. The chemical structures of these dyes are shown in Fig. 3.2.

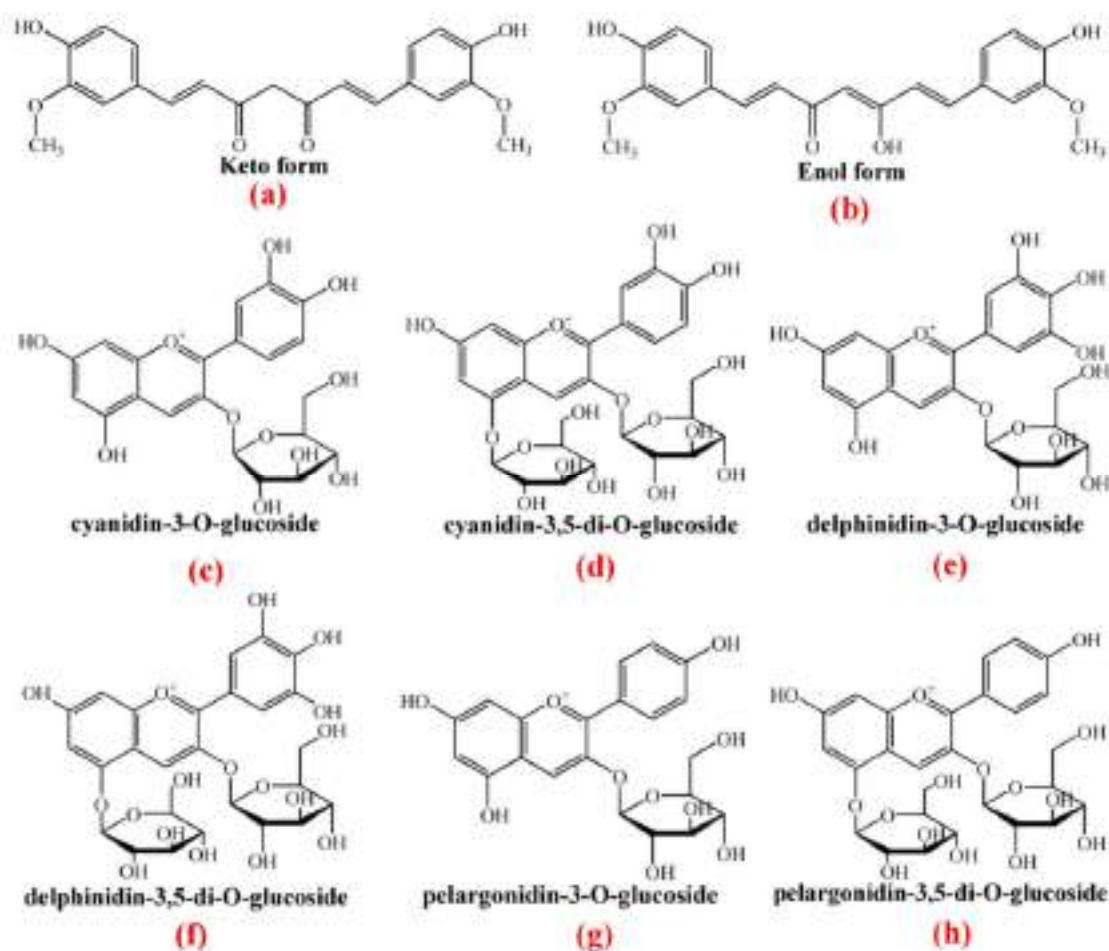


Figure 3.2 Chemical structures of Curcumin (a & b) present in turmeric and six major anthocyanins (c- h) present in Pomegranate fruit extracts.

For Rose Bengal dye sensitization, 0.5 mM ethanolic solution of pure Rose Bengal dye was prepared. Chemical structure of rose bengal dye is shown Fig. 3.3.

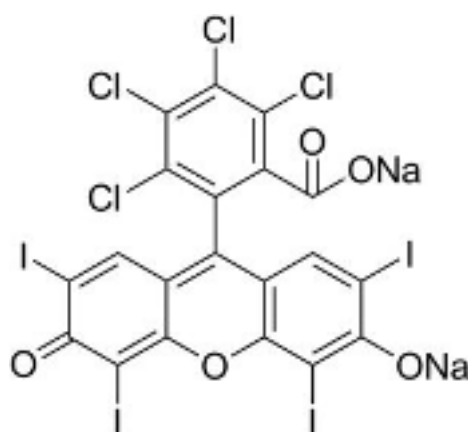


Figure 3.3 Chemical structure of Rose Bengal dye.

3.2.4. Preparation of working electrodes

To prepare the working electrode, first, the ITO coated glass was cut into 2×2cm square shaped pieces. Cleaning of this substrate is very important as it removes any organic or inorganic contaminant present on its surface which can significantly affect the performance of the cells. Furthermore, cleaning enhances the adhesion of the subsequent layers to be deposited over it. The ITO substrates were cleaned using dilute HCl for 15 minutes in an ultrasonic cleaner to remove oxide impurities. Then they were rinsed extensively with deionized water to remove the HCl residues. The substrates were then cleaned in acetone, ethanol and deionized water for 15 minutes each using an ultrasonic bath. Finally, the substrates were dried using a hairdryer. The cleaned substrates were masked using scotch tape on four sides, leaving the central area empty for semiconductor material deposition.

ZnO nanorods were grown on the ITO coated glass substrate following a simple two-step Sol-Gel spin coating protocol followed by hydrothermal growth [30]. In the first step, a thin ZnO seed layer was formed on the ITO glass substrates using 5mM Zinc acetate dehydrate $(\text{CH}_3\text{COO})_2\text{Zn}$, $2\text{H}_2\text{O}$, (98% Merck) in acetone as precursor solution. The solution was mixed well using an ultrasonic bath for 2 hours at room temperature and spun onto cleaned and masked ITO coated glass substrates using a programmable spin coater (Apex Technologies, Model SCU-2008C) at 1000 rpm for 30 seconds. The coated

substrates were then annealed at 350°C temperature for 30 minutes. After evaporation of the solvent, a thin ZnO film was formed whose thickness can be controlled by repeating the above process. In this way, the seed layer is formed. The thickness of the film can also be controlled by varying solution concentrations and the spinning speed of the spin coater [31]. In the second step, vertically aligned ZnO nanorods were grown over the seed layer coated ITO glass substrate by hydrothermal method. In this method, the seed layer coated substrate was immersed in a solution containing an equal proportion of 5mM Zinc acetate dehydrate ($(\text{CH}_3\text{COO})_2\text{Zn}$, $2\text{H}_2\text{O}$ and 5mM Hexamethylenetetramine ($\text{C}_6\text{H}_{12}\text{N}_4$) at 90°C temperature in a Pyrex vessel for 2 hours. This creates an array of vertically aligned ZnO nanorods on the substrate. It was then taken out from the solution and rinsed immediately with ethanol and deionized water to remove any leftover residues from the film surface and allowed to air dry at room temperature. Finally, the ZnO nanorod formation was completed by annealing the film at 450°C for 30min. This ZnO nanorod array coated substrates were then immersed in the dye solutions to allow adsorption of the dye molecules onto the semiconductor nanorod surface for 24 hours. Then the electrodes were taken out from the solutions and rinsed with ethanol and deionized water to remove the excess dye from the photoanode surface of the films and air-dried at room temperature. The counter electrode was prepared by spin coating the platinum precursor solution (platisol T-solaronix) at 1000 rpm for 30 seconds onto a drilled ITO substrate and giving heat treatment at 450°C for 15 minutes. The flow chart representing the whole process of growth of the ZnO nanorods is shown in Fig. 3.4. below.

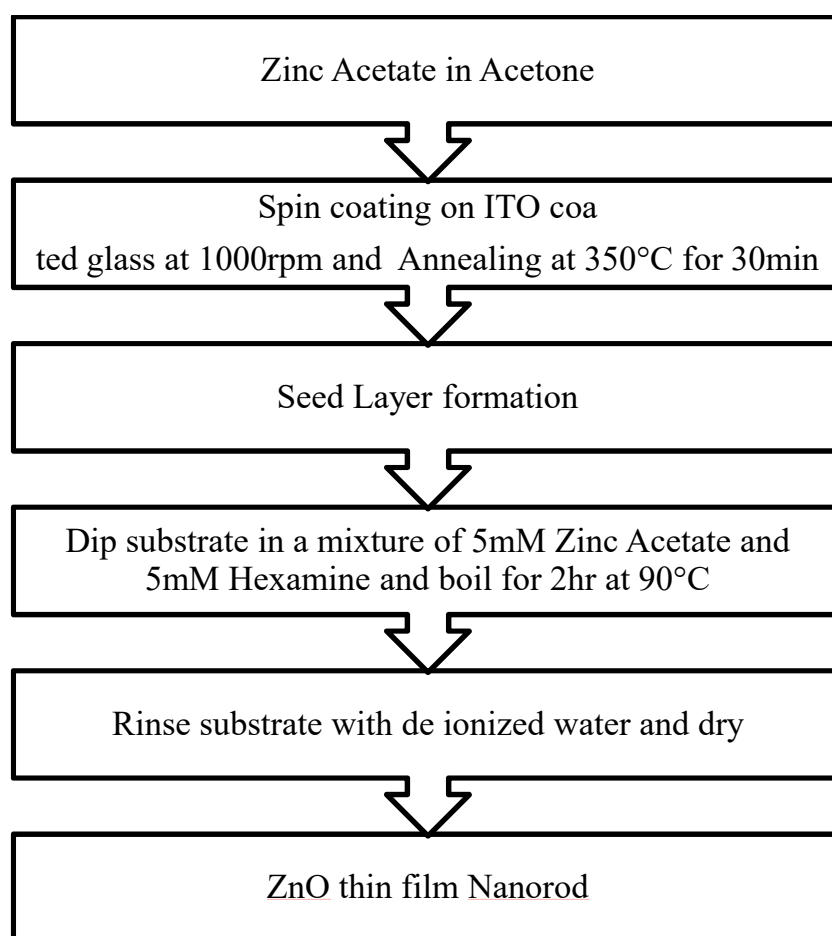


Figure 3.4 Flow chart for preparation of ZnO nanorod layer.

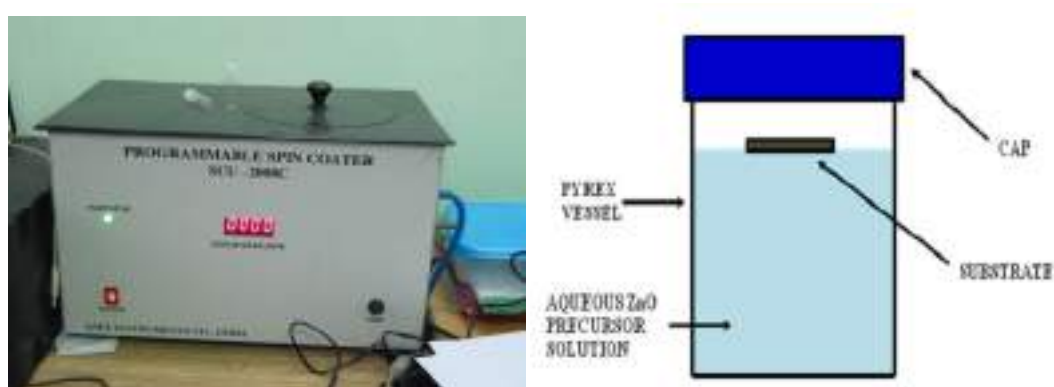


Figure 3.5 (a) Spin Coater for seed layer formation (b) vessel for nanorod grow.

On the other hand, the nanopowder based photoelectrodes were prepared by doctor blade method. At first, 10 gm of the nanopowder was mixed with diluted acetic (1ml in 50 ml deionized water) acid in a mortar and pastel and

added a few drops of Triton X100 (Merck) as surfactant and ground continuously until a homogenous, smooth suspension was obtained. The lump-free slurry was then applied on the conductive side of an ITO-coated glass using the doctor blade method to make a homogeneous layer. To strengthen the bonding between the ITO glass and the semiconductor paste, the nanopowder coated ITO glass plates were sintered in normal atmospheric condition at 450°C for 45 minutes. In the sintering process, after introducing the sample in the furnace, the temperature was raised with a rate of 10°C/5 min until the temperature had reached 350°C and after that, it was increased with a rate of 10°C/10 min until 450°C. When it cooled down to room temperature, the sintered substrates were immersed in the Rose Bengal dye solution for dye adsorption on the surface of the TiO₂ and ZnO nanoparticles for 24 hours. Image of TiO₂ photoanode during sintering process and after sintering is shown in Fig. 3.6.

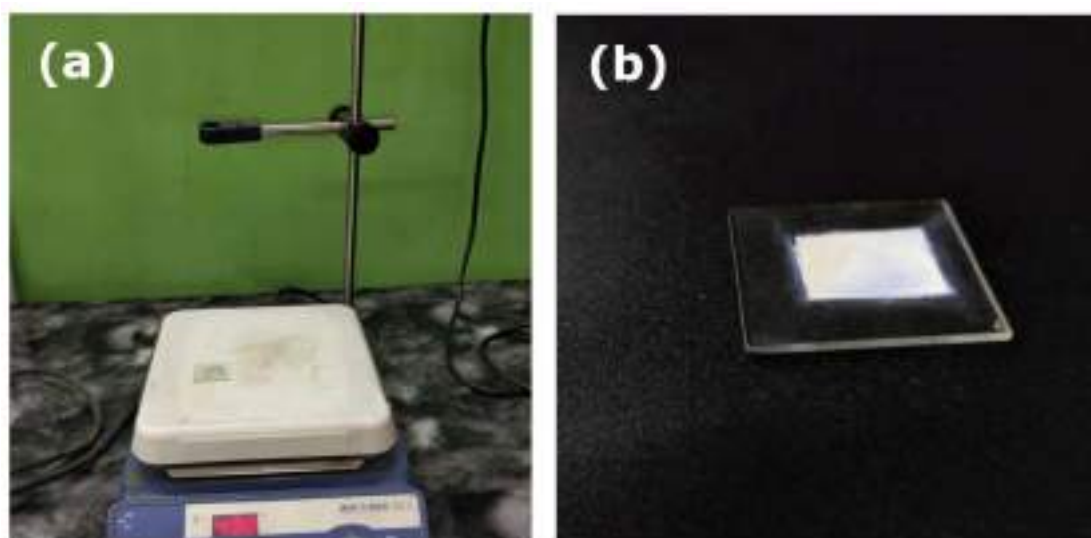


Figure 3.6 TiO₂ nanopowder coated ITO (a) during sintering process (b) after sintering.

3.2.5. DSSC assembling

To assemble the solar cell, the conductive side of the platinum coated counter electrode was placed over the dye adsorbed ZnO nanorod photoanode

so that the platinized side of the counter electrode faces the ZnO film. Surlyn spacer (Meltonix 1170-25 μ m) was placed between them to prevent the uncoated areas of the electrodes from short-circuiting. Two binder clips were used to firmly clamp the two electrodes together in a sandwich manner. The redox electrolyte was prepared by mixing 0.5 M KI and 0.05 M I₂ in Ethylene Glycol (Fig. 3.7 (b)) solvent in a proportionate amount. This electrolyte solution was injected into the cell through the drilled hole on the counter electrode. The hole was then sealed using a hot melt sealant. The effective cell area was 1 cm². Fig. 3.7(a) depicts the picture of a complete cell fabricated using ZnO nanoparticle and curcumin dye.

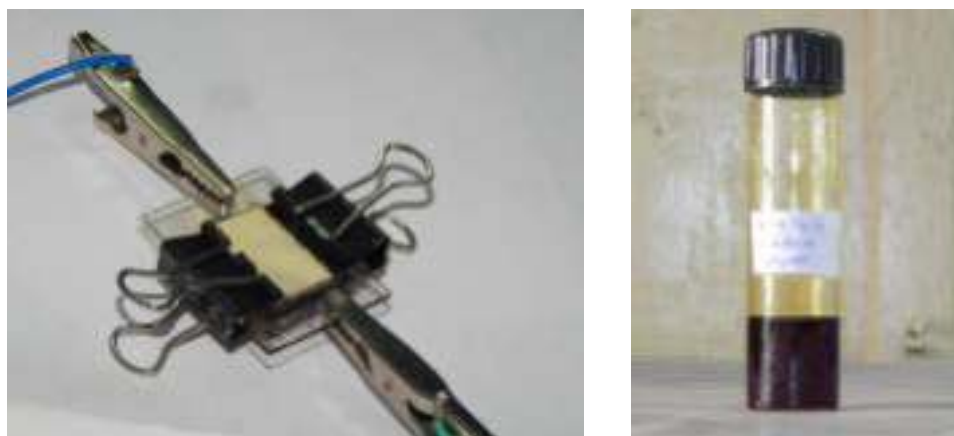


Figure 3.7 (a) Cell Fabricated with Curcumin dye (b) KI + I₂ Electrolyte.

3.2.6. Device Characterization and Measurements

The absorption spectra of the dyes were studied using a Perkin Elmer Lambda-35 UV-VIS spectrophotometer in the wavelength range of 200-600nm range. The crystalline structure of the ZnO films was studied using a PANalytical X'Pert PRO X-ray diffractometer with CuK α (30mA, 40 kV, λ = 1.5406 Å). The surface morphologies of the ZnO films were characterized by using scanning electron microscopy (JEOL). The current-voltage (I-V) characteristics of the fabricated cells under illumination of 100mW/cm² (Oriental Xenon lamp 450W) were recorded by employing a Keithley 2400 source meter connected to a PC.

3.3. Results and Discussion

3.3.1. UV-VIS absorption spectral analysis of the dyes

UV-VIS absorption spectra of the Curcumin, pomegranate and Rose Bengal dye are shown in Fig. 3.8. A clear difference among the absorption peaks of the dyes can be seen. Curcumin exhibits an absorption peak at 422 nm, whereas pomegranate fruit extract solution at 517 nm. The Rose Bengal shows absorption peak at 549 nm. The difference in the absorption peaks is due to the different types of colours and chromophores present in curcumin, pomegranate and Rose Bengal dyes.

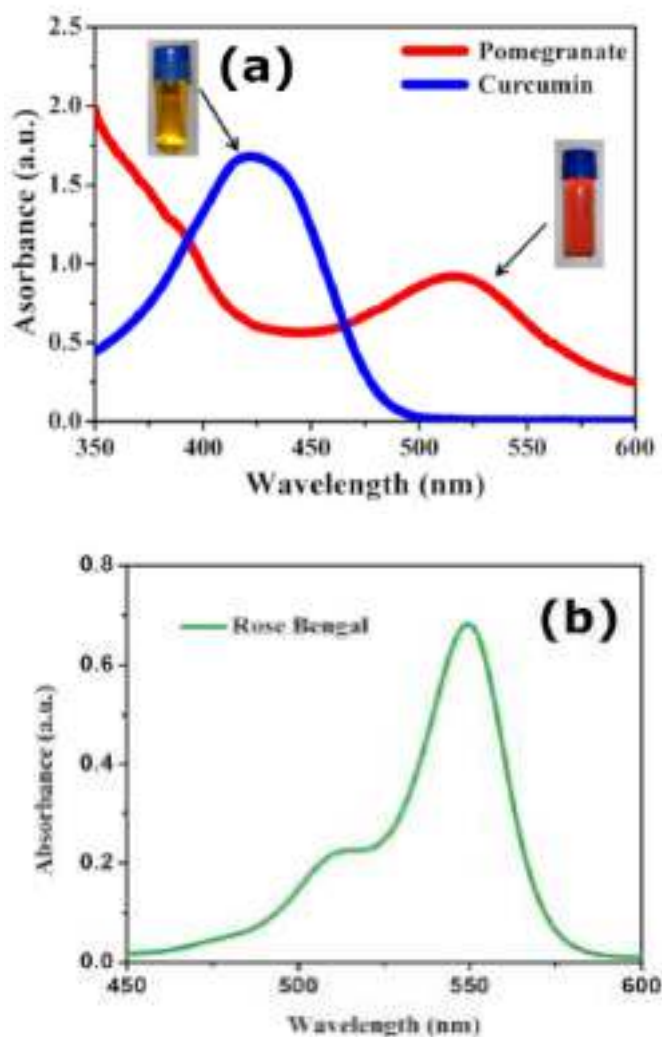


Figure 3.8 Absorption spectra of the (a) curcumin and anthocyanin (pomegranate) (b) Rose Bengal sensitizers used to fabricate DSSCs.

3.3.2. X-ray diffraction analysis of the ZnO film

The structural and crystalline quality information of the synthesized ZnO nanorods, purchased ZnO and TiO₂ nanoparticles were studied using X-Ray diffraction pattern of the samples and shown in Fig. 3.9, Fig. 3.10 and Fig. 3.11 respectively. The consistency of the obtained diffraction peaks of ZnO samples were confirmed by comparing them with the standard JCPDS card no. 36-1451. A remarkably enhanced diffraction peak for the (002) plane at 34.4595 ° can be clearly observed for the ZnO Nanorods. It indicates strong preferential growth of ZnO nanorods along the c-axis and vertical alignment on the ITO substrate and the hexagonal wurtzite structure. XRD of TiO₂ and ZnO nanoparticles are shown in Fig. 3.10 and Fig. 3.11 respectively.

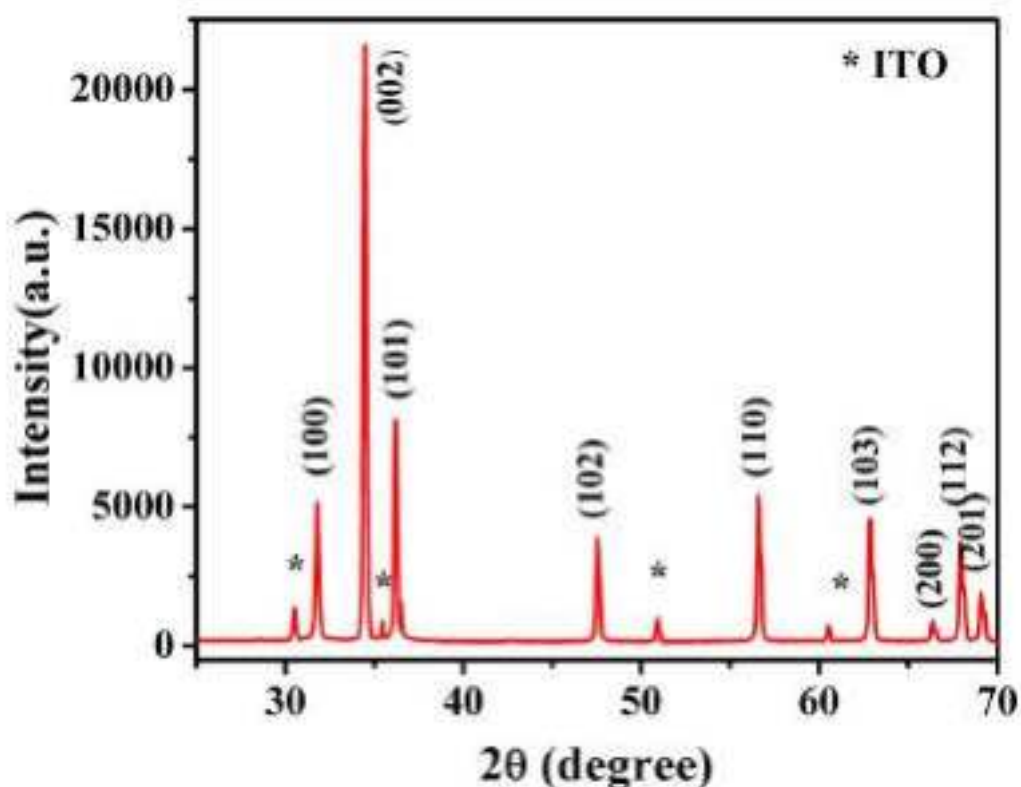


Figure 3.9 XRD pattern of the ZnO nanorods synthesized by a sol-gel spin coating method.

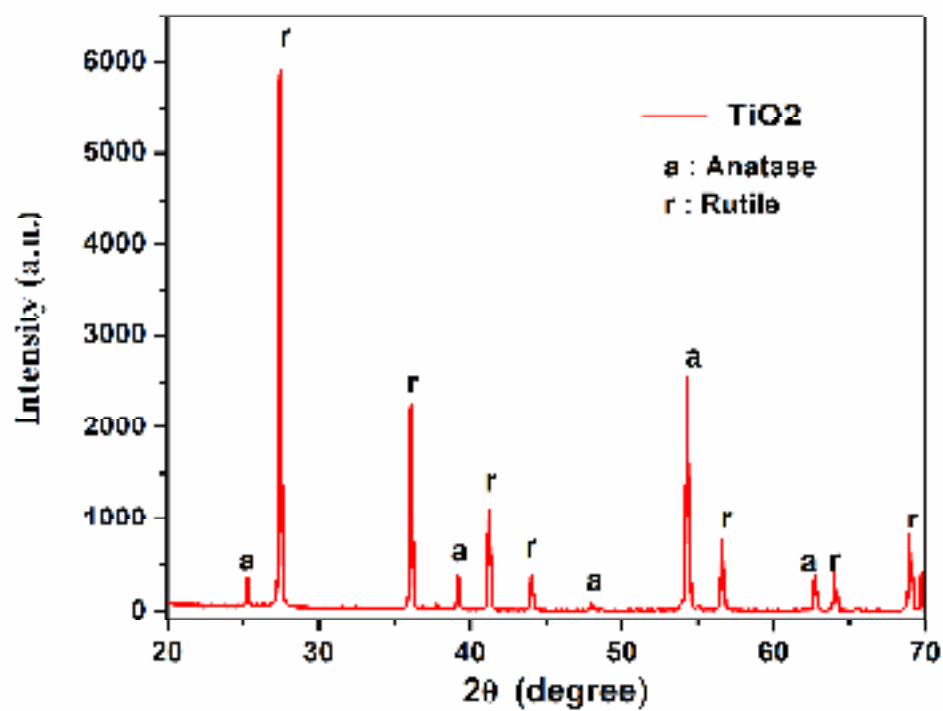


Figure 3.10 XRD of TiO₂ nanopowder.

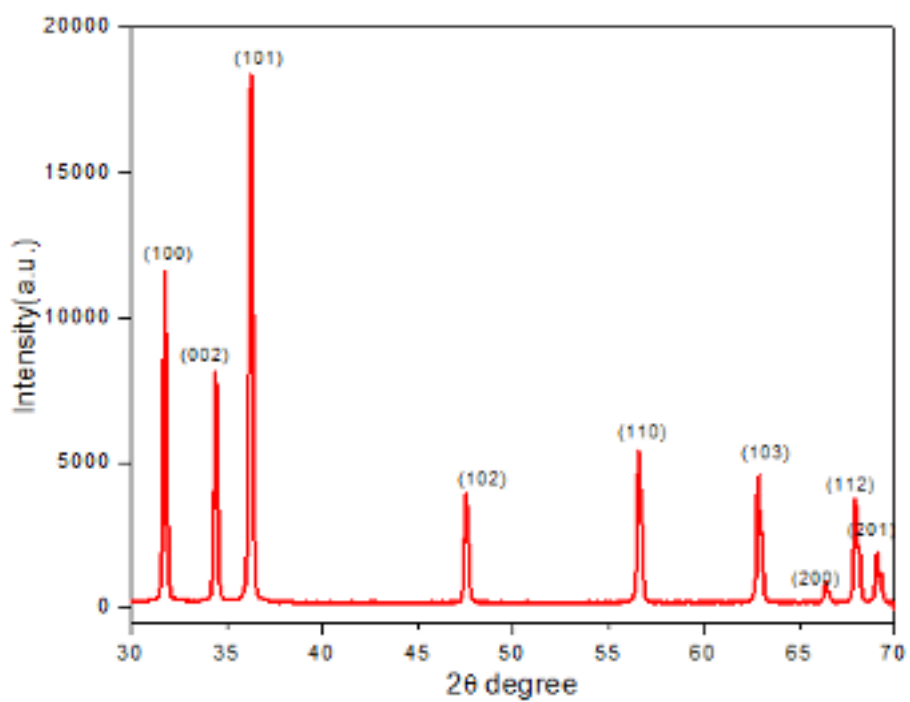


Figure 3.11 XRD of ZnO nanopowder

3.3.3. Scanning Electron Microscope Studies

Scanning electron microscopy (SEM) was carried out to study the morphological properties of the sample film. Fig. 3.12(a) shows the SEM image of the ZnO nanorod arrays on ITO substrate. The SEM observation reveals that most nanorods have grown vertical to the seed layer on the ITO substrate and have a hexagonal wurtzite structure. The nanorods have diameters ranging from 100-200 nm with an average length of 300 to 400 nm and in the case of nanoparticles, the average particle size was around 50nm. EDS analysis was performed to investigate the chemical composition of the nanorods, which is shown in Fig. 3.11(b). It clearly confirms the presence of Zn and O in the photoanode. The unidentified peaks are due to the presence of indium (In) and tin (Sn) in the ITO substrate. The SEM and EDS of TiO₂ nanopartilces are shown in Fig. 3.13.

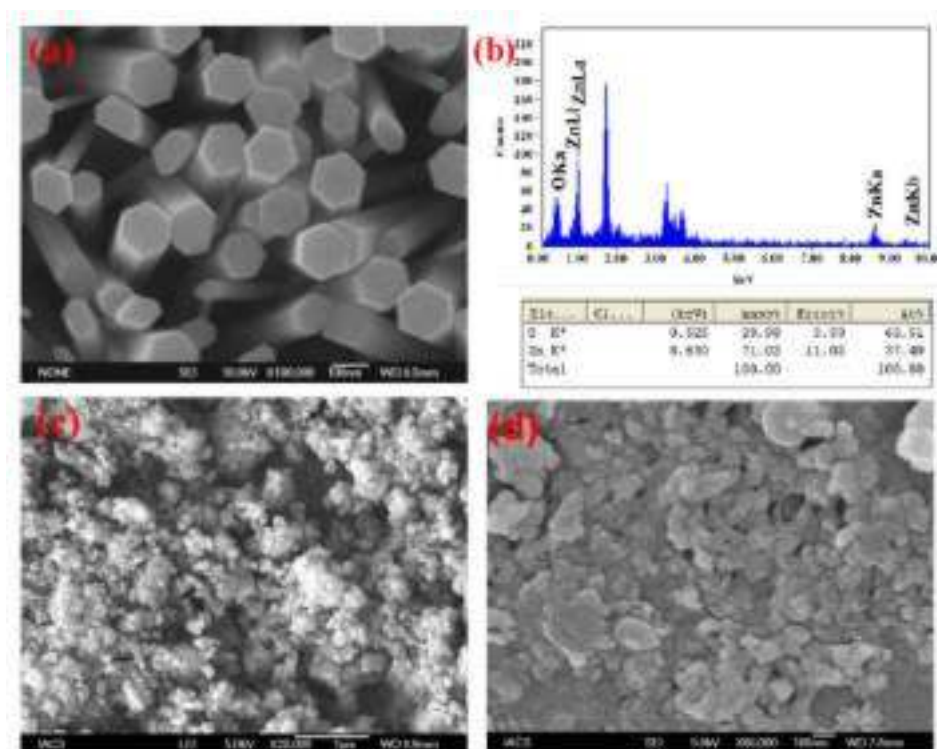


Figure 3.12 SEM image of (a) ZnO nanorods grown on ITO substrate (b) EDS spectra of the nanorod sample showing elemental composition (c) & (d) ZnO nanoparticle deposited sample at lower and higher magnification respectively.

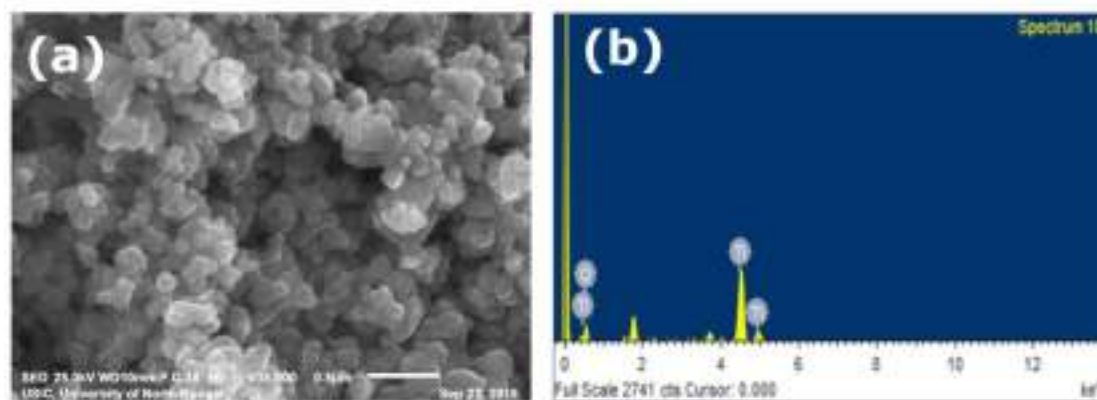


Figure 3.13 (a) SEM image of TiO₂ nanoparticles (b) EDS of TiO₂.

3.3.4. Current-Voltage Characteristics study of the cells: Solar cell efficiency measurements

The current-voltage characteristic of a Solar cell allows us to determine the photovoltaic performance of the cell. The J-V curves of the fabricated cells under the illumination of 100 mW/cm² are shown in Fig. 3.14 (a). The Power-Voltage plot to calculate the maximum power point (P_{\max}), I_{\max} and V_{\max} are represented in Fig.3.14 (b). Table 3.1 shows various parameters extracted from the I-V curves of the ZnO nanorod-based DSSCs fabricated using natural dyes Curcumin and Pomegranate. The solar cell fabricated using Curcumin extract exhibits higher short-circuit photocurrent density (J_{SC}), open-circuit voltage (V_{OC}) and fill factor (FF) compared to the DSSC fabricated using pomegranate extract as a dye. In addition, the Curcumin dye cell shows an improved overall photoelectric conversion efficiency (η) over the anthocyanin dye cell. The efficiency of these natural dye-based cells may be low compared to the synthetic dye-based DSSCs, but these values are comparable to the efficiencies obtained for natural dye-based DSSCs reported by other researchers [33].

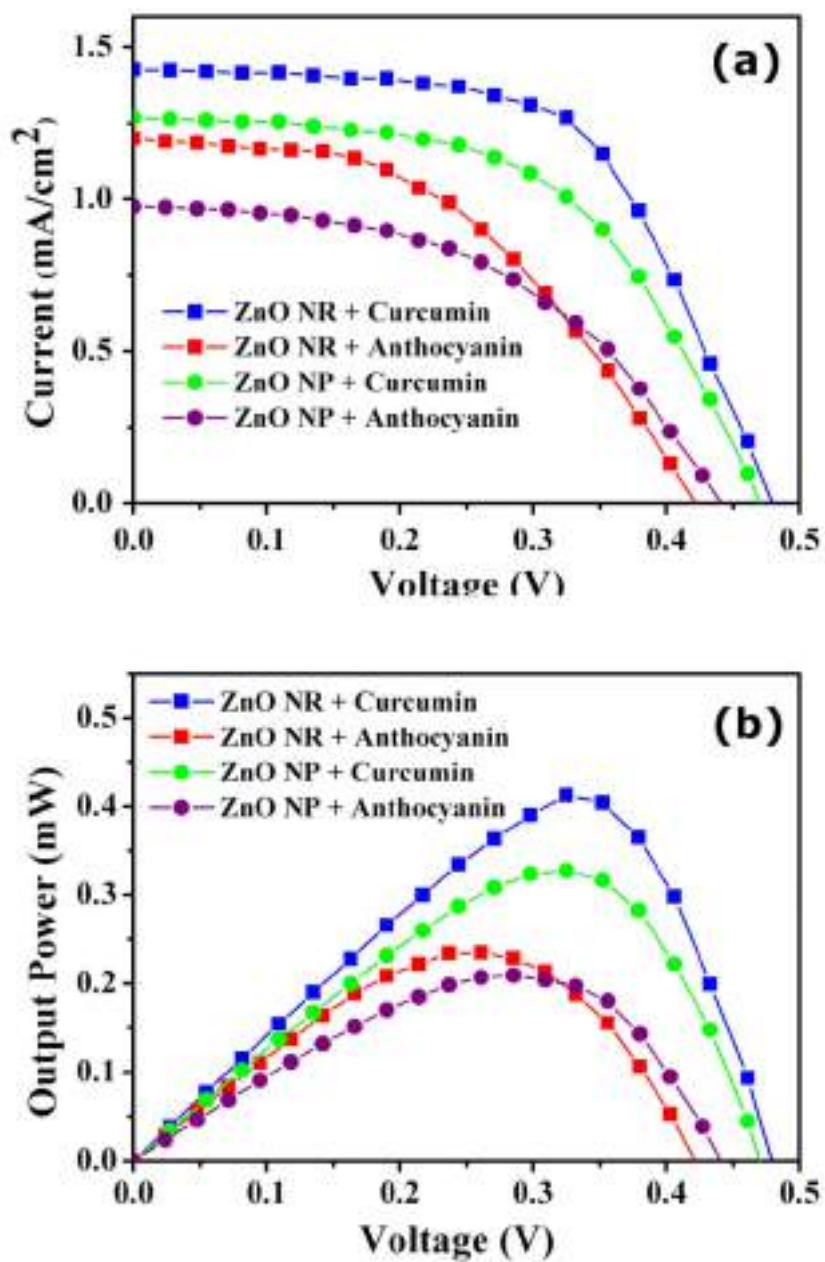


Figure 3.14 (a) Current density-Voltage characteristics of the natural dye based cells under illumination (b) Power-Voltage curve to obtain maximum power point.

Equivalent circuit modeling is a very important tool required for better understanding and explaining the solar cell performance and analysis of the electrical processes occurring inside the cell. The functioning of a solar cell is generally modeled by a single diode with a constant photo-generated current

source, a series (R_s) and shunt resistance (R_{sh}) as shown in Fig.3.15. The current-voltage relation is given by the equation

$$I = I_{ph} - I_o \left[\exp \left\{ \frac{(q(V + IR_s))}{Ak_B T} \right\} - 1 \right] - \frac{V + IR_s}{R_{sh}} \quad (1)$$

where I_{ph} , I_o , R_s , R_{sh} , q , A , k_B and T are the photocurrent, the saturation current of the diode, the series resistance, the shunt resistance, the electron charge, the ideality factor, the Boltzmann constant, and absolute temperature, respectively [34].

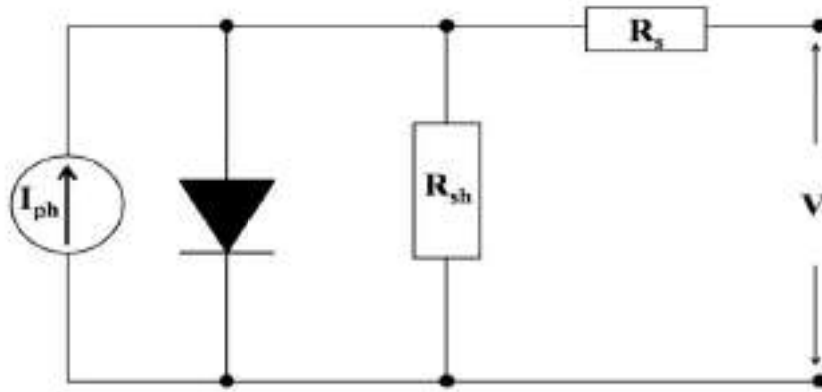


Figure 3.15 The equivalent circuit (single diode model) of a solar cell.

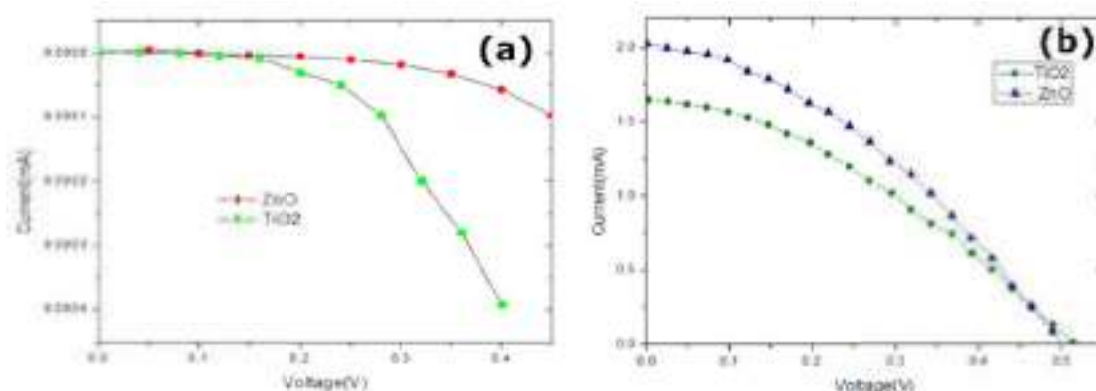
The circuit parameters like R_s and R_{sh} are not directly measurable. Instead, they are calculated by fitting the experimental J-V curve with the equation 1. Values of these parameters obtained for the fabricated cells are also represented in table 3.1.

Table 3.1. Solar Cell parameters of DSSC's fabricated with natural dyes.

Cell Name	Dye used & ZnO nanostructure	J_{sc} (mA/cm ²)	V_{oc} (V)	R_s (Ω cm ²)	R_{sh} (Ω cm ²)	FF	Efficiency (η %)
Cell-1	Curcumin & ZnO NR	1.43	0.49	86.28	7866.28	0.59	0.41
Cell-2	Anthocyanin & ZnO NR	1.20	0.43	116.67	2722.90	0.46	0.24
Cell-3	Curcumin & ZnO NP	1.27	0.46	101.19	6629.31	0.56	0.33
Cell-4	Anthocyanin & ZnO NP	0.98	0.45	146.87	4659.92	0.48	0.21

Cell-1 shows the lowest series resistance (R_s) compared to other cells. This indicates improved electrical contacts, lower junction resistances and better ZnO nanorod morphology in the case of cell-1. Higher series resistance means greater voltage drop inside the cell resulting in lower terminal voltage and sagging of current controlled part of the J-V curve towards the origin, which can be correlated with table 3.1 and Fig. 3.14(a). In addition, from the single diode equivalent circuit of the solar cell (Fig.3.15), it can be clearly seen that R_{sh} provides an alternative path to the photocurrent, which causes power losses in the solar cell. Lower R_{sh} results in partial shorting between the two electrodes of the solar cell giving rise to leakage current. So, the highest value of R_{sh} of cell-1 attributes to the lowest leakage current resulting in improved cell performance. Also, from table 3.1 it can be confirmed that higher shunt resistance results in a higher fill factor and consequently better photoconversion efficiency.

For DSSCs fabricated with Rose Bengal dye, In dark current measurement (Fig. 3.16 (a)) it was observed that TiO_2 cells shows higher dark current than ZnO cells, both sensitized with Rose Bengal dye. The dark current which actually flows in opposite direction to the original current minimizes the cell efficiency. Higher dark current of TiO_2 cell attributes to the lower efficiency.



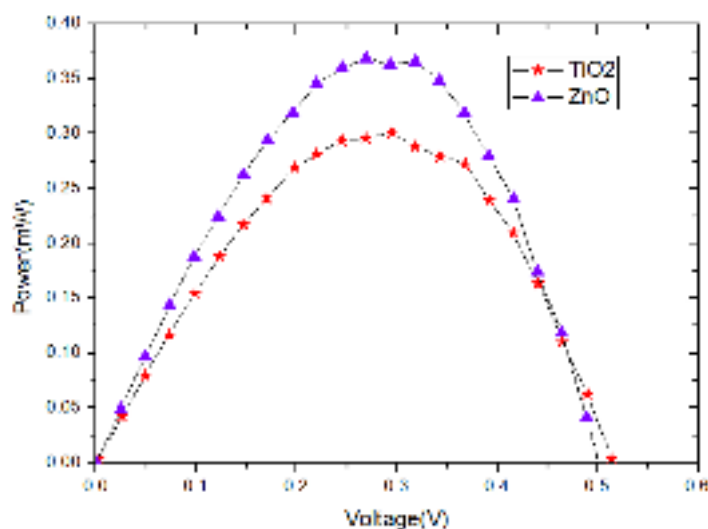


Figure 3.17 Power vs. Voltage graph of the cells fabricated with Rose Bengal.

The I-V characteristic of the cells under illumination is shown in Fig. 3.16 (b). Fig. 3.17 displays the Power-Voltage curve to obtain maximum power points. Table shows comparative performance of the TiO₂ and ZnO cells in terms of open circuit voltage (V_{OC}), Short circuit current (I_{SC}), Fill Factor (FF) and energy conversion efficiency.

Table 3.2 Photovoltaic performance of the Rose Bengal sensitized cells.

Material	I_{SC} (mA/cm ²)	V_{OC} (V)	FF	Efficiency (η %)
TiO ₂	1.65	0.514	0.35	1.18
ZnO	2.03	0.501	0.36	1.47

From table 3.2 we can see that ZnO cells are more efficient than TiO₂ cells when sensitized with Rose Bengal dye. This may be due better adsorption of Rose Bengal dye on ZnO nanoparticle surface than TiO₂ nanoparticle surface. Also the higher dark current of TiO₂ cell (shown in Fig.3.16(a)), which indicates higher recombination of electrons in case of TiO₂ cells than ZnO cells, attributing lower efficiency.

3.3.5. *Electrochemical impedance spectroscopy study of the cells*

The electrochemical impedance spectroscopy is a very useful diagnostic technique that has often been performed to investigate the interfacial charge transfer dynamics and recombination mechanisms occurring inside a DSSC [35]. These are generally modelled using the appropriate equivalent circuit in terms of resistors and capacitors. The EIS measurements were performed using HIOKI Impedance Analyser in the frequency range 0.1 Hz to 190 kHz under dark condition with employing an AC sinusoidal signal having an amplitude of 10mV under the influence of V_{oc} bias voltage. EIS findings as Nyquist plot of the DSSCs are shown in Fig. 3.18(a). Physical interpretation of the different electrochemical operations across the interfacial regions of the DSSCs can be done by fitting the EIS spectra with the equivalent circuit shown in Fig. 3.18(b). Generally a typical Nyquist plot exhibits three semicircles. However, only two semicircles are present in our study due to low-frequency limitation of our instrument. The first smaller semicircle (in the high-frequency range) attributes to the charge transfer resistance at the Pt counter electrode/Electrolyte interface (R_{CE}) and the second semicircle (mid-frequency range) having a higher diameter corresponds to the resistance of charge transfer and recombination process at the ZnO photoelectrode/dye/electrolyte interface (R_{ct}). The intercept of the first semicircle in the high-frequency range on the real axis of the Nyquist plot is associated with the contact resistances and external ohmic series resistance (R_{SER}) of the assembled cell [36]. The experimental Nyquist plot is fitted with the equivalent circuit shown in the inset of Fig. 3.18(a) using MEISP software by Kumho Chemical Laboratories, based on the algorithm developed by Prof. J. R. Macdonald (LEVM v7.0) for non-linear complex least square fitting, and the obtained parameters are represented in table 3.3. The chemical capacitance (C_{μ}) is very useful in illustrating the underlying mechanism through which photoelectrons store free energy and generates current and voltage in the outer circuit [37]. Also, the chemical

capacitance (C_{μ}) reflects charge carrier accumulation on the ZnO film and the density of states in the band-gap region [38]. From table 3.3, it can be seen that Cell-1 exhibits a much higher C_{μ} value than the other cells, which indicates the conversion of a higher amount of photon energy into chemical energy resulting in a higher amount of energy storage by virtue of carrier injection into the conduction band of ZnO. Reduced C_{μ} values for cell-2,3 &4 also suggest poor dye loading [39, 40]. It can also be observed from the Nyquist plot that the recombination resistance (R_{rec}) at the ZnO NR- Dye/ Electrolyte interface is highest for cell-1 compared to the other three cells. This shows that cell-1 has better resistance to the charge recombination between the photo-generated electrons and the electron acceptors in the red-ox electrolyte attributing lower recombination current [41].

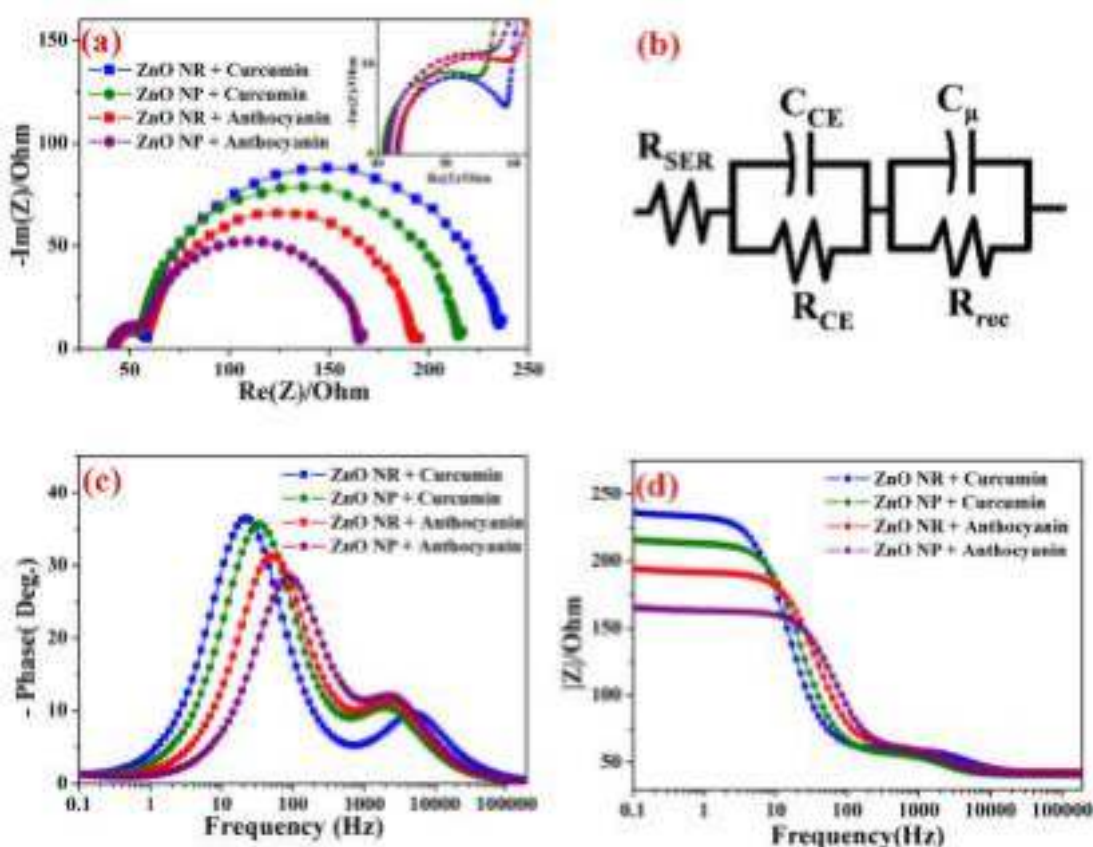


Figure 3.18 EIS spectra of DSSCs (a) Nyquist Plot (b) Equivalent circuit for fitting (c) Bode Phase plot and (d) Bode magnitude plot for impedance.

Table 3.3. Summary of EIS parameters of the DSSCs determined by fitting the experimental data.

Cell Name	Dye used & ZnO microstructure	R _{SER} (Ω)	R _{rec} (Ω)	R _{CE} (Ω)	C _μ (μF)	Peak freq. (Hz)	Electron lifetime (τ _e) (ms)
Cell-1	Curcumin & ZnO NR	42.85	173.21	16.28	83.16	22	7.24
Cell-2	Anthocyanin & ZnO NR	40.93	156.37	15.17	59.41	33.29	4.78
Cell-3	Curcumin & ZnO NP	43.25	129.74	17.56	42.52	51	3.12
Cell-4	Anthocyanin & ZnO NP	41.63	103.56	16.85	29.40	88.48	1.80

As all the cells' counter electrodes were prepared using the same procedure, the values of R_{CE} are almost the same for all four cells. Another important representation of the EIS data is Phase and Magnitude bode plots representing Phase (-θ) vs. Frequency (f) and Magnitude of Impedance (|Z|) vs. Frequency curve. Unlike the Nyquist plot, the very important aspect of this plot is that frequency information is not lost. The average carrier lifetime can be estimated from phase bode plots (shown in EIS Fig. 3.18(b)) using the formula

$$\tau_e = \frac{1}{2\pi f_{max}} \quad (2)$$

where f_{max} represents peak frequency in the mid-frequency range [42]. ZnO NR loaded with Curcumin dye shows the lowest characteristic peak frequency attributing to the highest electron lifetime in the LUMO of the Curcumin dye molecule. It shifts towards higher frequency values for the other cells, which results in decreased electron lifetime (refer to table 3.3). The lowest value of τ_e in ZnO NP cell loaded with anthocyanin (cell-4) extracted from pomegranate juice attributes to the fastest electron recombination leading to degraded overall cell performance.

On the other hand, bode magnitude plots depicted in Fig. 3.18(d) represents the variation of magnitude of impedance with frequency. It may be noted from bode magnitude plot shown in Fig. 3.18.(d) that at low frequencies the magnitude of impedance is high, which indicates higher recombination resistance. But with increase in frequency the impedance starts falling which is due to the faster electron recombination at higher frequencies. In the lower frequency region, the ZnO NR cell sensitized with Curcumin is showing highest magnitude of impedance implying slowest recombination rate, giving rise to highest short circuit current (I_{SC}). In contrary, ZnO NP cell sensitized with anthocyanin extracted from pomegranate fruit shows the lowest impedance in the low frequency region implying fastest recombination process which is reflected in Table 3.3. The possible reason behind these behaviours may be the better adsorption of Curcumin dye molecules over the hexagonal rod shaped ZnO nanostructures in comparison to the other cells. It also can be seen that the value of characteristic frequency shifts towards lower side for increasing value of either R_{rec} or C_{μ} . One more thing can be noted from the impedance plots that the maximum value of phase angle is also decreases with the decrease in value of R_{rec} .

3.4. Conclusions

In this study, hexagonal-shaped ZnO nanorods with preferential growth along (002) plane were successfully grown on ITO substrates using low-cost sol-gel hydrothermal technique. The nanorods have diameters ranging from 100-200nm. XRD study revealed remarkably high crystalline quality of the nanorods. These ZnO nanorod-based substrates were used as photoanodes to prepare DSSCs using natural dyes extracted from pomegranate and turmeric. On the other hand, commercial ZnO nanopowder is also used to fabricate DSSCs using the same natural dyes. Photoelectrochemical performances of all four cells were recorded. From the J-V measurements, a clear enhanced overall cell performance was noticed for the cell constructed using ZnO nanorods and

sensitized using Curcumin dye compared to the other three cells. The probable reason behind this could be the higher amount of Curcumin dye molecule adsorption by the ZnO film due to the better interaction between the carbonyl and hydroxyl groups of Curcumin molecule and the ZnO nanorod film than that of Pomegranate extract. For a deeper understanding of the performances obtained from the cells, the different interfacial mechanisms of the cells were investigated using the EIS technique. It is found that the shape of ZnO nanostructures and different dye molecules present in the extracts affected the electrochemical parameters of the cells. The Best performance of the cell prepared with ZnO nanorod with Curcumin dye is found to be due to highest chemical capacitance (C_{μ}) along with lowest electron recombination rate and fast charge transport along the ZnO nanorod. Therefore, the Curcumin dye should be an alternative to anthocyanin source for natural dye sensitized solar cells. These results also show that the performances of the natural extract based DSSCs can be enhanced significantly by combining suitable natural dye with the appropriate shape of semiconductor nanostructures and they can become a potential alternative to the synthetic sensitizers based DSSCs. In fact, such combination may results in environment-friendly, remarkably low cost and easily manufacturable dye sensitized solar cells. We can also observe that ZnO based cells are more efficient than TiO_2 based cells when sensitized with Rose Bengal dye.

References:

- [1] A. Horvath and E. Rachlew, Nuclear power in the 21st century: Challenges and possibilities, *Ambio* 45 Suppl 1, S38, Jan, (2016).
- [2] S. Chu and A. Majumdar, Opportunities and challenges for a sustainable energy future, *nature* 488, 294, (2012).
- [3] N. L. Chang, Y. Ho-Baillie, A. Wing, P. A. Basore, T. L. Young, R. Evans and R. J. Egan, A manufacturing cost estimation method with uncertainty analysis and its application to perovskite on glass photovoltaic modules, *Progress in Photovoltaics: Research and Applications* 25, 390, (2017).
- [4] A. Kumar, M. Bieri, T. Reindl and A. G. Aberle, Economic Viability Analysis of Silicon Solar Cell Manufacturing: Al-BSF versus PERC, *Energy Procedia* 130, 43, (2017).
- [5] M. Grätzel, Dye-sensitized solar cells, *Journal of Photochemistry and Photobiology C: Photochemistry Reviews* 4, 145, (2003).
- [6] B. O'regan and M. Grätzel, A low-cost, high-efficiency solar cell based on dye-sensitized colloidal TiO₂ films, *nature* 353, 737, (1991).
- [7] Y.-T. Kim, J. Park, S. Kim, D. W. Park and J. Choi, Fabrication of hierarchical ZnO nanostructures for dye-sensitized solar cells, *Electrochimica Acta* 78, 417, (2012).
- [8] C. Jiang, X. Sun, G. Lo, D. Kwong and J. Wang, Improved dye-sensitized solar cells with a ZnO-nanoflower photoanode, *Applied Physics Letters* 90, 263501, (2007).
- [9] J. B. Baxter and E. S. Aydil, Nanowire-based dye-sensitized solar cells, *Applied Physics Letters* 86, 053114, (2005).
- [10] A. Jena, S. P. Mohanty, P. Kumar, J. Naduvath, V. Gondane, P. Lekha, J. Das, H. K. Narula, S. Mallick and P. Bhargava, Dye sensitized solar cells: a review, *Transactions of the Indian Ceramic Society* 71, 1, (2012).

-
-
- [11] J. Gong, J. Liang and K. Sumathy, Review on dye-sensitized solar cells (DSSCs): fundamental concepts and novel materials, *Renewable and Sustainable Energy Reviews* 16, 5848, (2012).
- [12] S. Hao, J. Wu, Y. Huang and J. Lin, Natural dyes as photosensitizers for dye-sensitized solar cell, *Solar energy* 80, 209, (2006).
- [13] H. Zhu, H. Zeng, V. Subramanian, C. Masarapu, K.-H. Hung and B. Wei, Anthocyanin-sensitized solar cells using carbon nanotube films as counter electrodes, *Nanotechnology* 19, 465204, (2008).
- [14] Y. Amao and T. Komori, Bio-photovoltaic conversion device using chlorine-e6 derived from chlorophyll from Spirulina adsorbed on a nanocrystalline TiO₂ film electrode, *Biosensors and Bioelectronics* 19, 843, (2004).
- [15] K.-H. Park, T.-Y. Kim, S. Han, H.-S. Ko, S.-H. Lee, Y.-M. Song, J.-H. Kim and J.-W. Lee, Light harvesting over a wide range of wavelength using natural dyes of gardenia and cochineal for dye-sensitized solar cells, *Spectrochimica Acta Part A: Molecular and Biomolecular Spectroscopy* 128, 868, (2014).
- [16] F. Shao, J. Sun, L. Gao, S. Yang and J. Luo, Growth of various TiO₂ nanostructures for dye-sensitized solar cells, *The Journal of Physical Chemistry C* 115, 1819, (2010).
- [17] X. Mao, R. Zhou, S. Zhang, L. Ding, L. Wan, S. Qin, Z. Chen, J. Xu and S. Miao, High efficiency dye-sensitized solar cells constructed with composites of TiO₂ and the hot-bubbling synthesized ultra-small SnO₂ nanocrystals, *Scientific reports* 6, 19390, (2016).
- [18] D. Maheswari and D. Sreenivasan, Review of TiO₂ nanowires in dye sensitized solar cell, *Applied Solar Energy* 51, 112, (2015).
- [19] B. Roose, S. Pathak and U. Steiner, Doping of TiO₂ for sensitized solar cells, *Chemical Society Reviews* 44, 8326, (2015).
- [20] M. S. Ahmad, A. Pandey and N. A. Rahim, Advancements in the development of TiO₂ photoanodes and its fabrication methods for dye
-
-

-
-
- sensitized solar cell (DSSC) applications. A review, *Renewable and Sustainable Energy Reviews* 77, 89, (2017).
- [21] K. Tennakone, G. Kumara, A. Kumarasinghe, P. Sirimanne and K. Wijayantha, Efficient photosensitization of nanocrystalline TiO₂ films by tannins and related phenolic substances, *Journal of Photochemistry and Photobiology A: Chemistry* 94, 217, (1996).
- [22] J. A. Anta, E. Guillen and R. Tena-Zaera, ZnO-based dye-sensitized solar cells, *The Journal of Physical Chemistry C* 116, 11413, (2012).
- [23] Ü. Özgür, Y. I. Alivov, C. Liu, A. Teke, M. Reshchikov, S. Doğan, V. Avrutin, S.-J. Cho and H. Morkoc, A comprehensive review of ZnO materials and devices, *Journal of applied physics* 98, 11, (2005).
- [24] H. Bae, M. Yoon, J. Kim and S. Im, Photodetecting properties of ZnO-based thin-film transistors, *Applied Physics Letters* 83, 5313, (2003).
- [25] Q. Zhang, C. S. Dandeneau, X. Zhou and G. Cao, ZnO nanostructures for dye-sensitized solar cells, *Advanced Materials* 21, 4087, (2009).
- [26] Y. Zhang, M. K. Ram, E. K. Stefanakos and D. Y. Goswami, Synthesis, characterization, and applications of ZnO nanowires, *Journal of Nanomaterials* 2012, 20, (2012).
- [27] T. Senthil, N. Muthukumarasamy and M. Kang, ZnO nanorods based dye sensitized solar cells sensitized using natural dyes extracted from beetroot, rose and strawberry, *Bulletin of the Korean Chemical Society* 35, 1050, (2014).
- [28] S.-i. Kawano, Y. Inohana, Y. Hashi and J.-M. Lin, Analysis of keto-enol tautomers of curcumin by liquid chromatography/mass spectrometry, *Chinese Chemical Letters* 24, 685, (2013).
- [29] M. Viuda-Martos, J. Fernández-López and J. Pérez-Álvarez, Pomegranate and its many functional components as related to human health: a review, *Comprehensive Reviews in Food Science and Food Safety* 9, 635, (2010).
-
-

-
-
- [30] B. Pradhan, S. K. Batabyal and A. J. Pal, Vertically aligned ZnO nanowire arrays in Rose Bengal-based dye-sensitized solar cells, *Solar Energy Materials and Solar Cells* 91, 769, (2007).
- [31] F. Zhang, C. a. Di, N. Berdunov, Y. Hu, Y. Hu, X. Gao, Q. Meng, H. Sirringhaus and D. Zhu, Ultrathin Film Organic Transistors: Precise Control of Semiconductor Thickness via Spin-Coating, *Advanced Materials* 25, 1401, (2013).
- [32] A. H. Kurda, Y. M. Hassan and N. M. Ahmed, Controlling diameter, length and characterization of zno nanorods by simple hydrothermal method for solar cells, *World Journal of Nano Science and Engineering* 5, 34, (2015).
- [33] H. Zhou, L. Wu, Y. Gao and T. Ma, Dye-sensitized solar cells using 20 natural dyes as sensitizers, *Journal of Photochemistry and Photobiology A: Chemistry* 219, 188, (2011).
- [34] M. Murayama and T. Mori, Equivalent circuit analysis of dye-sensitized solar cell by using one-diode model: effect of carboxylic acid treatment of TiO₂ electrode, *Japanese journal of applied physics* 45, 542, (2006).
- [35] M. Wang, A. M. Anghel, B. Marsan, N.-L. Cevey Ha, N. Postrakulchote, S. M. Zakeeruddin and M. Grätzel, CoS supersedes Pt as efficient electrocatalyst for triiodide reduction in dye-sensitized solar cells, *Journal of the American Chemical Society* 131, 15976, (2009).
- [36] L. Tao, Z. Huo, Y. Ding, Y. Li, S. Dai, L. Wang, J. Zhu, X. Pan, B. Zhang and J. Yao, High-efficiency and stable quasi-solid-state dye-sensitized solar cell based on low molecular mass organogelator electrolyte, *Journal of Materials Chemistry A* 3, 2344, (2015).
- [37] S. S. Negi, Integrated Electronic, Optical, and Structural Features in Pseudo-3D Mesoporous TiO₂-X Delivering Enhanced Dye-Sensitized Solar Cell Performance, *ACS Omega* 3, 1645, (2018).
- [38] G. Di Carlo, A. Orbelli Biroli, M. Pizzotti, F. Tessore, V. Trifiletti, R. Ruffo, A. Abbotto, A. Amat, F. De Angelis and P. R. Mussini, Tetraaryl
-
-

-
-
- ZnII Porphyrinates Substituted at β -Pyrrolic Positions as Sensitizers in Dye-Sensitized Solar Cells: A Comparison with meso-Disubstituted Push–Pull ZnII Porphyrinates, *Chemistry-A European Journal* 19, 10723, (2013).
- [39] J. Bisquert, Chemical capacitance of nanostructured semiconductors: its origin and significance for nanocomposite solar cells, *Physical Chemistry Chemical Physics* 5, 5360, (2003).
- [40] F. Fabregat-Santiago, E. M. Barea, J. Bisquert, G. K. Mor, K. Shankar and C. A. Grimes, High carrier density and capacitance in TiO₂ nanotube arrays induced by electrochemical doping, *Journal of the American Chemical Society* 130, 11312, (2008).
- [41] J. Akilavasan, K. Wijeratne, H. Moutinho, M. Al-Jassim, A. Alamoud, R. Rajapakse and J. Bandara, Hydrothermally synthesized titania nanotubes as a promising electron transport medium in dye sensitized solar cells exhibiting a record efficiency of 7.6% for 1-D based devices, *Journal of Materials Chemistry A* 1, 5377, (2013).
- [42] P. Bhatt, K. Pandey, P. Yadav, B. Tripathi and M. Kumar, Impedance spectroscopic investigation of the degraded dye-sensitized solar cell due to ageing, *International Journal of Photoenergy*, (2016). DOI: 10.1155/2016/8523150

Chapter 4

Application of WO_3 as alternative
photoanode material for Dye Sensitized
Solar Cells

This Page is intentionally left blank

4.1. Introduction

Increasing energy demand and environmental contamination are the two major problems faced by society in recent years. The major energy requirements of the world are fulfilled by fossil fuels (i.e., coal, petroleum and natural gas), which may not be sufficient to overcome the energy crisis in the future due to fast depletion, the rapid development of industrialization and environmental pollution[1-4]. To address these issues, scientists have focused on renewable and environment-friendly energy sources. As Sun represents an immense source of renewable energy, expected to provide an appreciable amount of power in the future, it is the most widespread type of alternative energy source among all the renewable energy sources [5-7]. Dye-sensitized solar cells, an unconventional photoelectrochemical device that directly converts photo-energy into electrical energy, have drawn much more attention than conventional silicon solar cells due to their easy fabrication technique, the low-level requirement of the high-temperature process, cost-effectiveness and environment-friendly nature [8, 9]. But until now, DSSCs are not commercially viable as the reason for their comparatively low conversion efficiency and stability issues compared to the silicon-based solar cells [10]. Photo anode, the heart of a DSSC system plays a key role in enhancing the overall performance of the DSSC by transferring electrons and supporting the Dye molecules [11]. It consists of a nanostructured mesoporous semiconductor film deposited on a conducting glass or a flexible substrate [12, 13]. An ideal photoanode material should have some properties of high charge carrier mobility, significantly high surface areas, environmental friendliness, cost-effectiveness, and comparatively less electron-hole recombination rate. The band edge positions and corresponding band gap values of several commonly used wide bandgap metal oxide semiconductors are shown in Fig. 4.1 [14, 15]. The semiconducting oxide material TiO_2 is mostly used as a photoanode because of

its excellent optical, electrical and chemical properties [16-19]. Although appreciably high

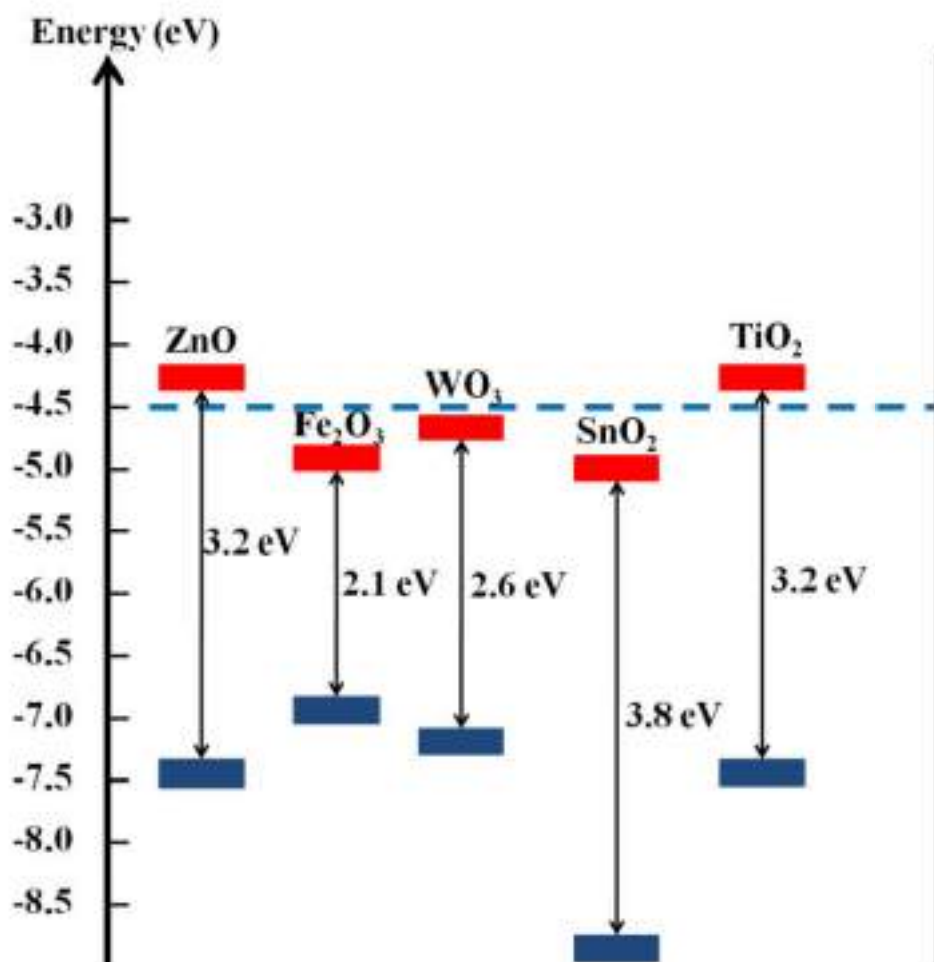


Figure 4.1 Energy band positions of several semiconductors.

conversion efficiency is achieved with TiO₂, its low electron mobility leads many scientists to think about new alternative photoanode materials for better performance of Dye sensitized solar cells [20]. On the other hand, WO₃, a wide bandgap semiconductor having bandgap in the range of 2.6eV-3.1eV has been used extensively in the fabrication of gas sensors, water splitting and photocatalyst [21]. Owing to the favourable bandgap, high electron mobility and extreme stability in harsh environments, it has attracted the attention of researchers as an alternative photoanode material for DSSC fabrication.

Moreover, the nonreactive nature of WO_3 in acidic environments may provide the solution of long-term stability issues in DSSCs with more acidic electrolytes. However, DSSCs based on pure WO_3 photoanode have been proven to be inefficient. On the other hand, DSSCs based on surface modified WO_3 photoanode by ultrathin layer of TiO_2 exhibited significant increase in power conversion efficiency [22]. ZnO can be used as a substitute for TiO_2 due to its agreeable properties in the view of high electron mobility and abundant nanostructure morphologies [23-25]. To the best of our knowledge, however, there are no detailed reports found in which surface modification of WO_3 is done by an ultrathin layer of ZnO in the fabrication of DSSCs. In this work, we have prepared the WO_3 photoanode and a facile sol-gel spin coating technique was utilized to alter the surface property of it by a thin layer of ZnO . Very careful control of the thickness of the ZnO layer is necessary to get the optimum performance out of the solar cell and for this purpose different concentration of ZnO precursor solution was used.

4.2. Materials and Method

4.2.1. *Preparation of working electrodes*

All the reagents used in the fabrication process were of analytical grades. So no further purification was required. To prepare the thin films of the photoanode materials, the ITO coated glass substrates were first cleaned with dilute HCl in an ultrasonic bath for 15 minutes and then thoroughly rinsed with deionized water to remove the HCL residues. Then the substrates were cleaned with acetone and ethanol using an ultrasonic cleaning bath [26].

The working electrode of the DSSC was prepared by following the standard doctor blade method. The WO_3 paste for doctor blading was prepared by mixing WO_3 nanopowder with terpineol as solvent and ethyl cellulose as a binder and stirred continuously in order to obtain a smooth lump-free slurry.

The WO_3 paste was then coated on the conductive side of the cleaned ITO glass substrate and subsequently annealed at 500°C for 2 hr in order to burn out the terpineol and ethyl cellulose contents of the working electrode and strengthens the bonding between the substrate the WO_3 film. In addition to this, the annealing procedure also helps to improve the surface quality of the thin film along with increasing the crystallinity of the sample [22].

The Sol-Gel spin-coating technique was employed to deposit thin layers of ZnO onto the surface of the as-prepared WO_3 photo-anode. Zinc acetate dihydrate $(\text{CH}_3\text{COO})_2\text{Zn} \cdot 2\text{H}_2\text{O}$, (98% Merck) was mixed with acetone at different molar ratios to obtain desired concentrations of ZnO precursor solution. The prepared solutions were then mixed extensively in an ultrasonic bath for 2 hours and then spin-coated on the WO_3 coated substrate using a programmable spin coater (Apex Instruments Co. Pvt. Ltd, Model SpinNXG-P1) at 2000 rpm for 30 seconds. The thickness of the ZnO film can be controlled by varying the precursor solution concentration. In our experiment we have prepared 1 mM, 5 mM, 10 mM, 15 mM, 20 mM, and 25 mM solutions of ZnO precursor and spin-coated them over WO_3 film keeping the number of sol drops unchanged in order to obtain various ZnO film thickness and study the effect on the solar cell performance. The ZnO coated WO_3 electrode was annealed at 450°C for 1 hour. All the electrodes were sensitized by immersing them in a 0.3 mM ethanolic solution of Ruthenium based dye ($\text{C}_{26}\text{H}_{20}\text{O}_{10}\text{N}_6\text{S}_2\text{Ru}$) known as N_3 (Solaronix) for 48 hours. The working electrodes were then removed from the solution and thoroughly rinsed with deionized water and ethanol to remove any excess dye from the semiconductor film surface and air-dried at room temperature.

The counter electrodes of the cells were prepared by spin coating the platinum catalyst precursor solution Platisol-T (Solaronix) on the conducting side of the cleaned ITO coated glasses and heating on a hot plate at 450°C for 15 minutes.

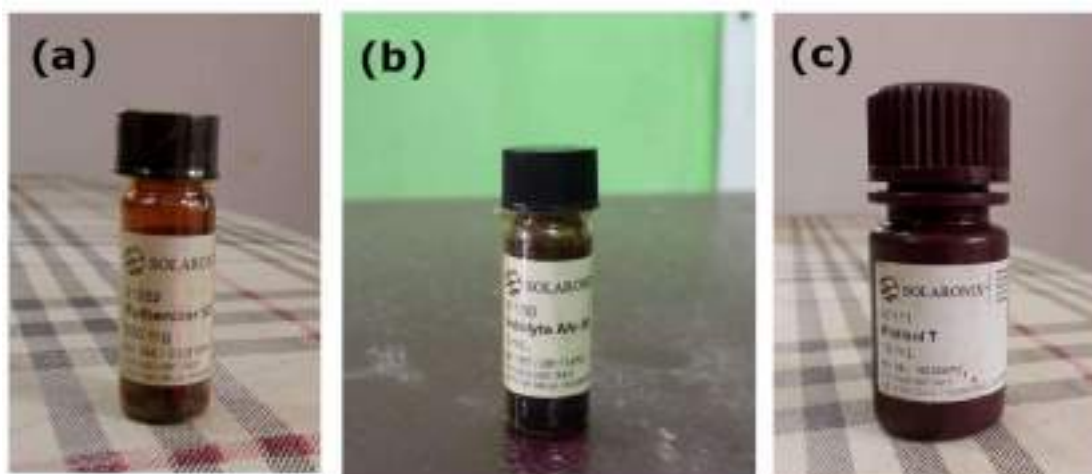


Figure 4.2 (a) N3 dye, (b) Iodolyte AN50 electrolyte, (c) Platisol T used for preparing Pt counter electrode in DSSC fabrication.



Figure 4.3 DSSC fabricated with N3 dye and WO_3 as photoanode material.

The dye adsorbed working electrode and Pt-coated counter electrode was assembled against the coated sides of each other in a sandwich manner using two binder clips with a Surlyn film (Meltonix 1170-25 μm , Solaronix) gasket as a spacer in between them. The liquid electrolyte used in our experiment was a Solaronix high-performance electrolyte (Iodolyte AN50) with iodide/tri-iodide as redox couple, ionic liquid, and lithium salt and pyridine derivative as additives dissolved in acetonitrile solvent. The redox concentration of the electrolyte was 50 mM. The active area of the cells for

illumination was determined by employing a black mask of aperture size 0.25 cm².

4.2.2. Characterization and Measurements

The crystalline structure of the WO₃ and ZnO were analyzed with the help of X-ray diffraction analysis using the PAN-analytical X'Pert PRO X-ray diffractometer (CuK α radiation, 30 mA, 40 kV, λ = 1.5406 Å). Scanning electron microscopy (JEOL) was done to reveal the surface morphology of the prepared thin films. More detailed structural information of the samples was obtained from Raman Spectroscopy. The Photocurrent-Voltage (I-V) characteristics data of the cells were recorded using Keithley 2400 digital source meter with the help of a computer under 100 mW/cm² illumination (Xenon lamp 450W). HIOKI Impedance Analyzer in the frequency range of 0.1Hz to 190 kHz was used to study the electrochemical impedance spectra of the cells.

4.3. Results and Discussion

4.3.1. Structural and phase characterization WO₃ photoanode

Figure 4.3. shows the X-ray diffraction pattern of the as-purchased WO₃ nanopowder. The XRD pattern exhibits the coexistence of both the monoclinic and orthorhombic crystal phases. The peaks corresponding to the monoclinic phase well matches with the standard JCPDS card no. 43-1035 and the orthorhombic phase matches with JCPDS card no. 20-1324. Sharp and strong peaks signify the high crystalline nature of the sample [27, 28].

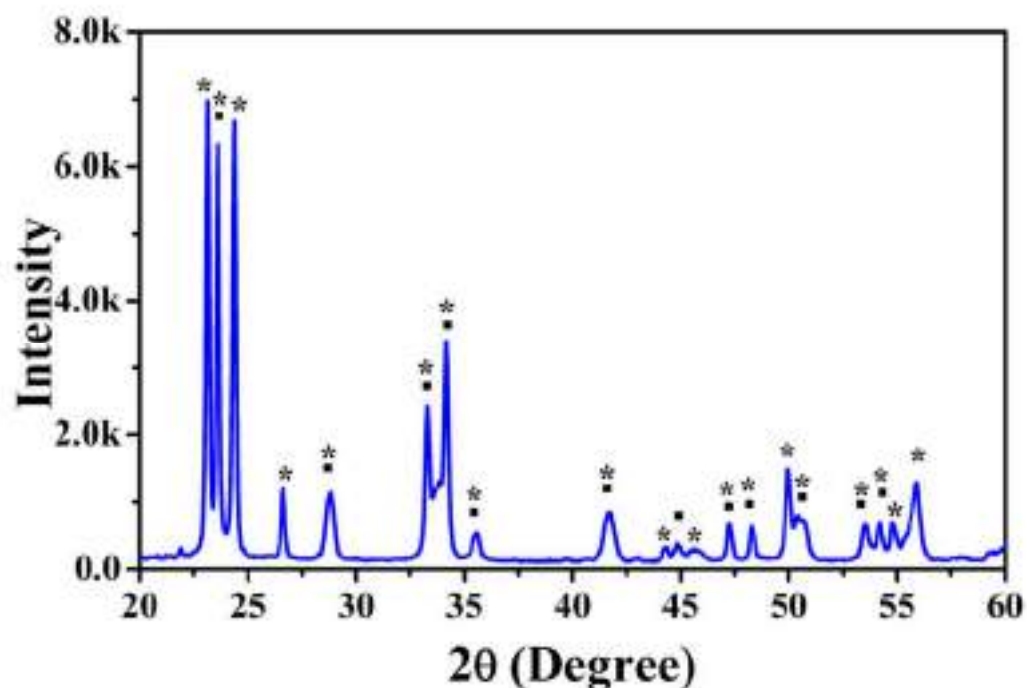


Figure 4.4 X-ray diffraction pattern of WO₃ nanoparticles. The peaks correspond to Monoclinic (*) and orthorhombic (▪) phases of WO₃ respectively.

The crystal phases are further confirmed by Raman spectra of the pure WO₃ powder, which is shown in fig. 4.3 and it consists of well-resolved four sharp Raman peaks at 274, 329, 719 and 807 cm⁻¹. The lower peaks centered at 274 cm⁻¹ and 329 cm⁻¹ attributed to O-W-O bending vibrations and the higher peaks at 719 cm⁻¹ and 807 cm⁻¹ are due to W-O-W stretching mode vibration [29]. Sharp peaks suggest profoundly crystalline nature of the sample. All four Raman peaks attribute to the monoclinic phase [30]. However, the Raman peaks corresponding to the orthorhombic phase lie neighbouring to the peaks mentioned above. Consequently, both phases are believed to be present in the sample. No impurity was found in the Raman spectra of the pure WO₃ sample.

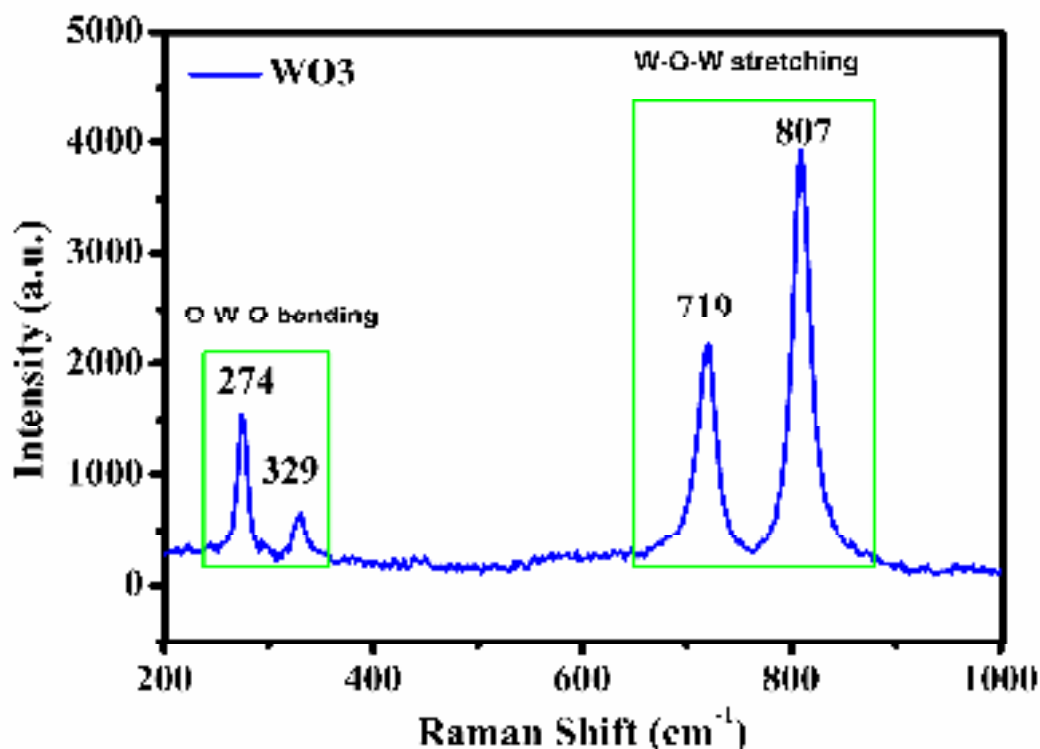


Figure 4.5 Raman spectra of WO_3 nanoparticle.

4.3.2. Surface Morphology study and energy dispersive spectroscopy of the photoanodes

Scanning Electron Microscopy was employed to investigate the surface morphology of the pure and ZnO coated WO_3 photoanodes. Fig. 4.4(a) shows the SEM image of pure WO_3 photoanode on the FTO substrate whereas Fig. 4.4(b-g) show the SEM images of WO_3 photoanodes coated with 1mM, 5mM, 10mM, 15mM, 20mM and 25mM concentrations of ZnO precursor solution concentrations respectively. Highly porous films with nearly spherical shape WO_3 nanoparticle having a diameter in the range of 140nm-150nm can be clearly seen from the SEM images. High porosity the film enhances the surface

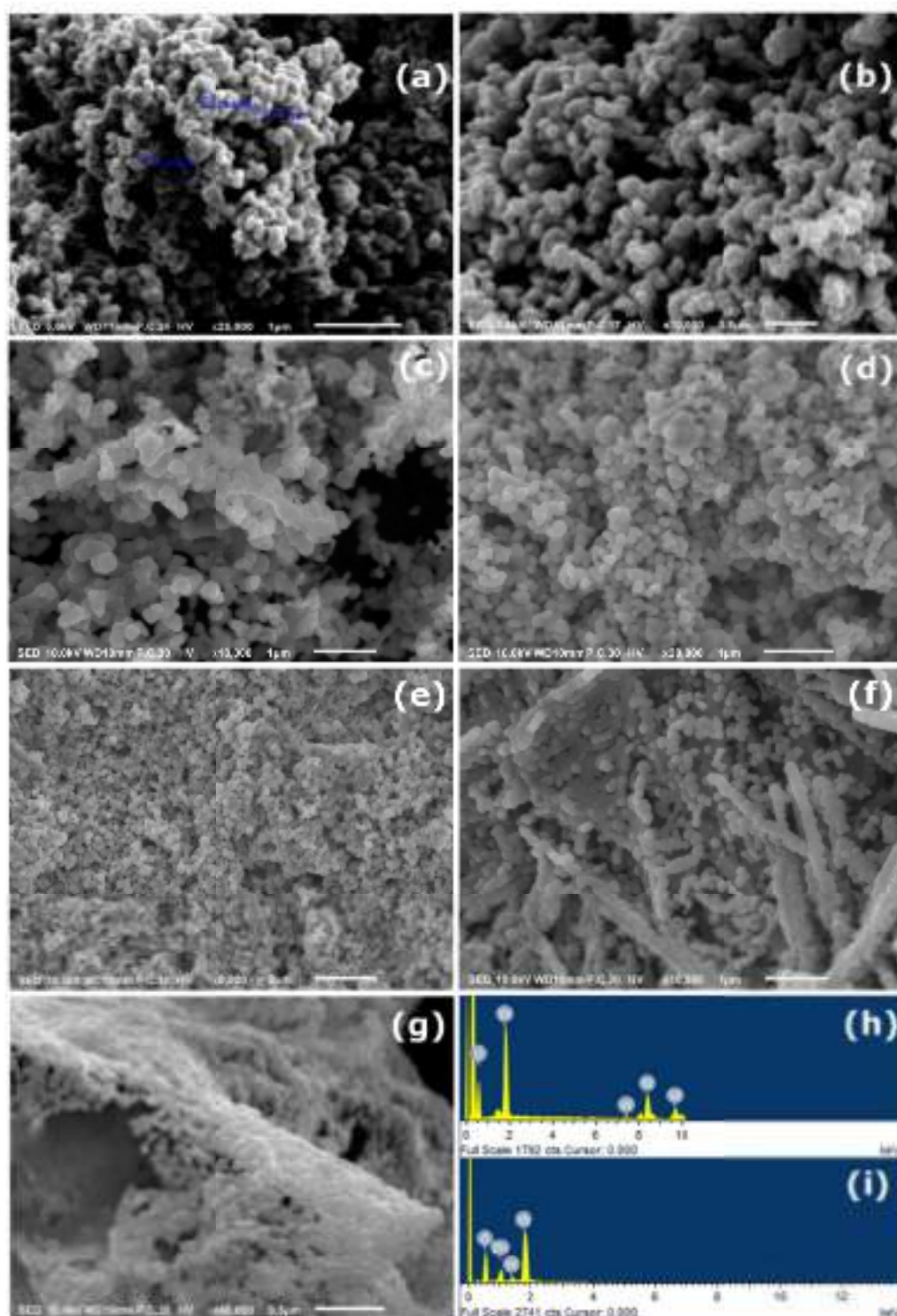


Figure 4.6 SEM images of (a) Bare WO₃ photoelectrode ; photoelectrodes having WO₃ coated with (b) 1mM (c) 5mM (d) 10mM (e) 15mM (f) 20mM and (g) 25mM ZnO precursor solution respectively. (h) EDS of Bare WO₃ and (i) EDS of WO₃ coated with 5mM ZnO.

to volume ratio, consequently increasing the dye loading amount resulting in high photocurrent [31-34]. It can also be observed from the SEM images that the surface morphology of uncoated and ZnO coated WO₃ substrate are not so visually different for low ZnO precursor concentrations, but for higher concentrations like 20 mM and 25 mM, the screening of WO₃ surface by ZnO nanoparticles may be evidently observed in Fig. 4.4(f) and 4.4(g).

The EDS spectrum, which reveals the elementary analysis are shown in fig. 4.4(h) and 4.4(i) for bare WO₃ and the WO₃ surface coated with 5mM ZnO precursor solution concentration respectively. Predominating peaks of W and O₂ in Fig. 4.4(h) unveil that the sample contains only WO₃ whereas in Fig. 4.4 (i) additional strong peak of Zn confirms the presence of ZnO coating over WO₃.

4.3.3. *Current-Voltage characterization of the cells*

The Current-Voltage characteristic is a crucial characterization to investigate the overall photovoltaic performance of a solar cell. Fig. 4.5(a) illustrates the I-V characteristics of the seven DSSCs based on pure and coated WO₃ as photoanodes with different precursor solution concentrations. The overall photoconversion efficiency of the solar cell is given by

$$\eta = \frac{P_{out}}{P_{in}} = \frac{I_{sc}V_{oc}FF}{P_{in}} \quad (1)$$

Where I_{sc} , V_{oc} , FF and P_{in} represent the short circuit current density , open-circuit voltage, Fill factor and incident light power respectively light power respectively. The fill factor is calculated by the formula

$$FF = \frac{I_{max}V_{max}}{I_{sc}V_{oc}} \quad (2)$$

Where V_{\max} and I_{\max} are the voltage and current corresponding to the maximum output power point of the solar cell respectively. All the photovoltaic parameters obtained from the I-V curve are summarized in Table 4.1.

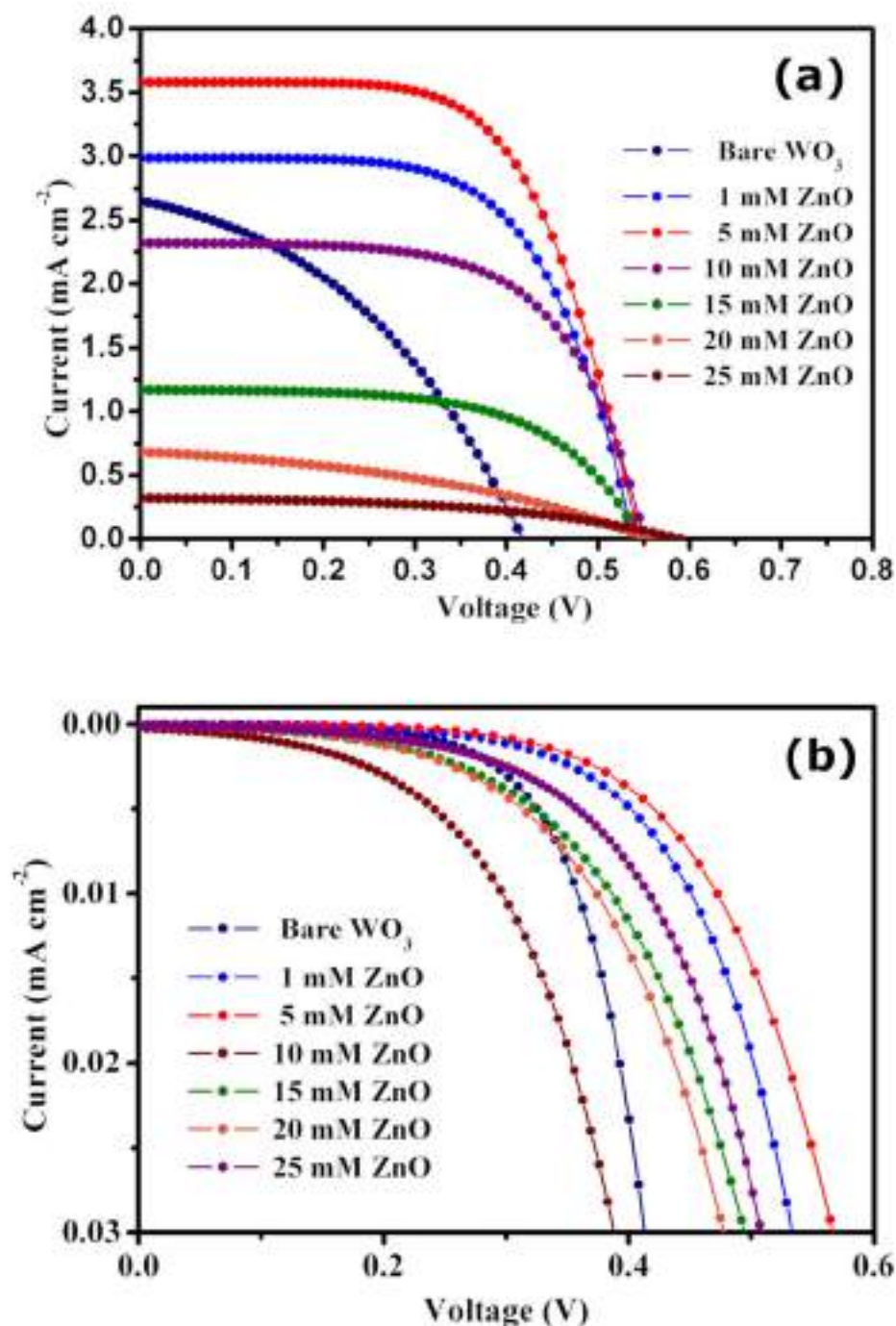


Figure 4.7 Current-voltage characteristics of different cells under (a) Illumination and (b) Dark.

A clear enhancement in the efficiency and fill factor due to the presence of ZnO on the WO₃ surface compared to the bare WO₃ electrode can be observed from Table 4.1. The fill factor, which represents the squareness of the I-V curve [35], is very low for bare WO₃ which in turn decreases cell efficiency. The low fill factor may be attributed to the high recombination rate of electrons for bare WO₃ photoelectrode DSSC. However, a significant improvement in the value of J_{sc} can be noted from table 4.1 upon ZnO coating over the WO₃ surface which demonstrates the positive role of the ZnO layer in reducing the recombination process. The DSSC with 5 mM ZnO precursor solution concentration yielded the highest short circuit photocurrent J_{SC} and efficiency η . But the photocurrent and the efficiency start falling sharply with a further increase in the precursor solution concentration.

Table 4.1. Photovoltaic performance of uncoated and ZnO coated WO₃ photoanode based DSSC.

ZnO precursor solution concentration	J _{sc} (mA/cm ²)	V _{oc} (V)	FF	Efficiency (η %)
Pure WO ₃	2.65	0.42	0.39	0.44
1 mM ZnO	2.98	0.53	0.63	1.07
5 mM ZnO	3.58	0.55	0.62	1.21
10 mM ZnO	2.32	0.56	0.62	0.80
15 mM ZnO	1.67	0.56	0.60	0.38
20 mM ZnO	0.68	0.57	0.38	0.15
25 mM ZnO	0.32	0.58	0.47	0.09

The maximum value of open-circuit voltage is determined by the difference between the Fermi level of the photoanode (metal oxide) material and the red-ox potential of the liquid electrolyte [36]. WO₃ is known to possess a lower conduction band edge (E_{cb}) i.e. more positive E_{cb} thereby reducing the

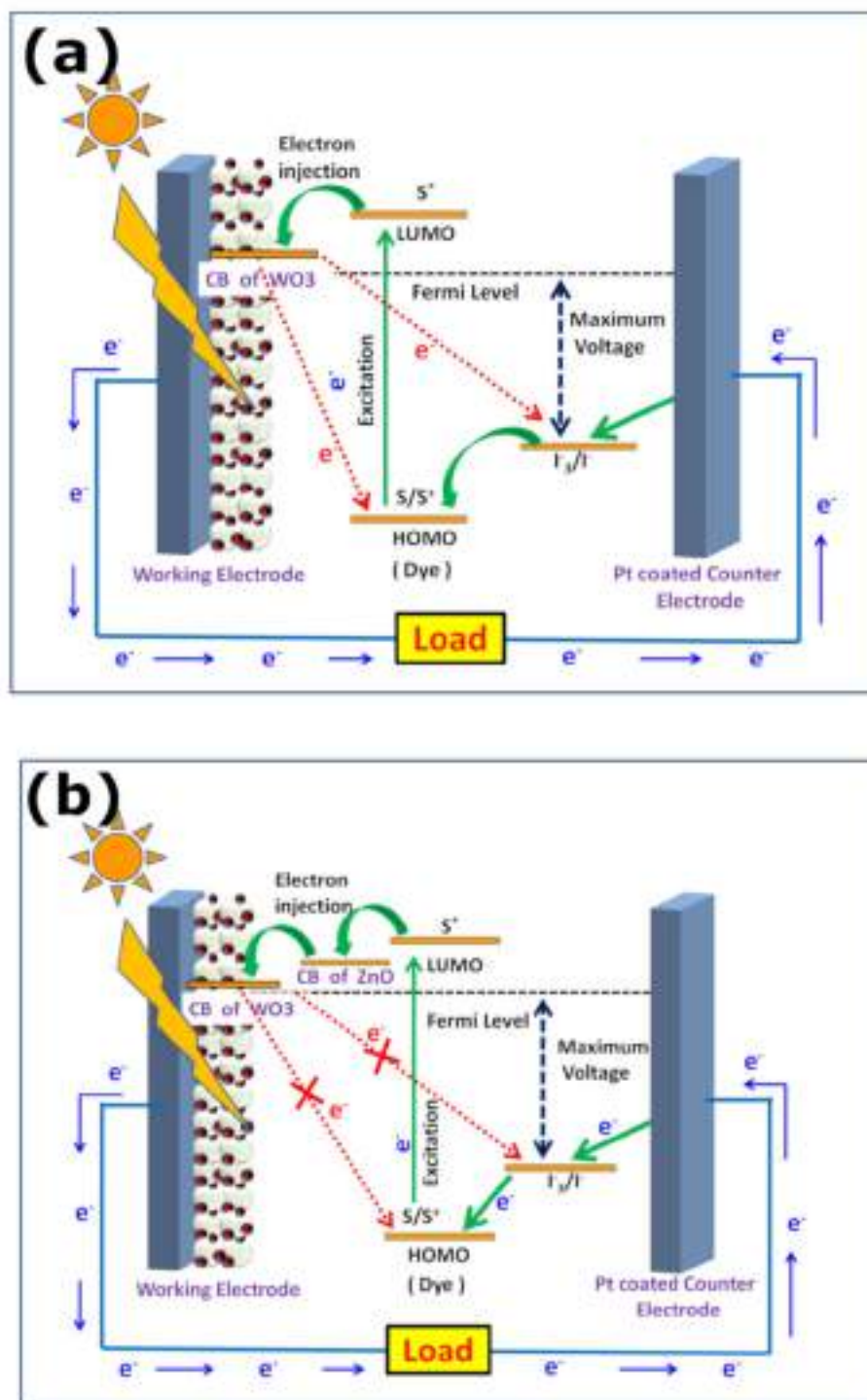


Figure 4.8 Schematic energy level diagram and mechanism of the (a) Conventional DSSC and (b) DSSC with the ZnO barrier.

open-circuit voltage (V_{oc}). However, employing an ultrathin layer of more E_{cb} negative metal oxides like ZnO onto WO_3 surface may increase the value of V_{oc} as the photogenerated electrons from LUMO of dye molecules are now injected to the more negative conduction band of ZnO and then step down to the conduction band of WO_3 which is illustrated in Fig. 4.6 (b).

Furthermore, the energy barrier created due to the incorporation of ZnO onto the WO_3 film surface may prevent the charge carrier recombination and as well as decreasing back transfer of electrons to the HOMO of the dye molecule. Aside from this, the ultrathin layer of ZnO incorporation on the WO_3 surface facilitates the amount of dye adsorption and hence increasing the amount of photon absorption resulting in higher J_{sc} .

The dark current measurement was done in order to interpret the variation of charge recombination reaction of the photogenerated electrons with I_3^- ions at the Pt coated counter electrode/red-ox electrolyte interface. Fig. 4.5(b) shows the dark J-V characteristics of the DSSCs fabricated with uncoated and coated with different concentrations of the ZnO precursor solution. The photoelectron injection from LUMO of dye to the CB of the working electrode is completely absent in the dark condition and hence the dark current is mainly due to the diffusion of electrons from semiconductor to the redox electrolyte [37]. Ultrathin coating of ZnO layer on the WO_3 surface decreases the dark current which can be observed in dark current characteristics in Fig. 4.5(b). On the other hand, the uncoated WO_3 possesses a higher dark current for a particular bias voltage. This may be due to the fact that poor dye loading capacity of WO_3 allows more direct contact between WO_3 surface and liquid electrolyte. This facilitates the back transfer of electrons from WO_3 to electrolyte via reduction of I_3^- into I^- which led to increased dark current [22]. But the coating of ZnO creates an energy barrier that effectively reduces the rate of electron recombination thereby decreasing the dark current, consequently suppressed recombination of charge carriers due to ZnO coating

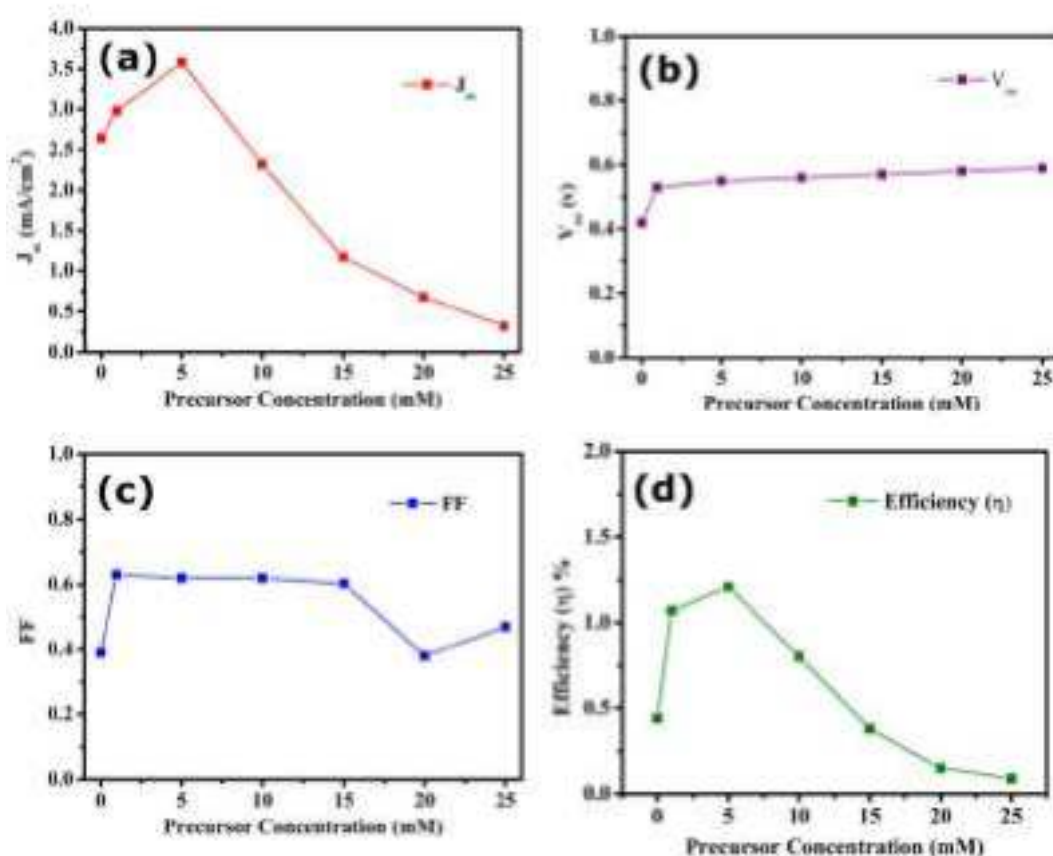


Figure 4.9 Effect of ZnO precursor solution concentration on the values of photovoltaic parameters (a) J_{sc} (b) V_{oc} (c) FF and (d) η .

increases cell FF. In addition to that, a very thin coating of ZnO also improves the dye loading which enables the ZnO treated WO_3 DSSC to harvest more light energy compared to ordinary WO_3 DSSC and significantly enhances current density. However, with the increase in the ZnO precursor concentration of more than 5 mM, the values of FF and J_{sc} start decreasing. This decrease in J_{sc} and FF might be due to the fact that thicker ZnO completely screens WO_3 from dye molecules. Moreover, a higher amount of ZnO content act as recombination sites [38]. Apart from this, an increased amount of ZnO deposition via increasing the ZnO precursor solution concentration promotes aggregation of Zn^{+2} ions and N3 dye which may decrease the photocurrent due

to light loss due to absorption and scattering of light by these aggregates [39-41].

Figure 4.7 shows the variation of the different DSSC performance parameters as a function of ZnO precursor solution concentration. The values of J_{sc} , FF, and η enhanced significantly for the cells with ultrathin ZnO nanoparticles coating as compared to the cell with bare WO_3 nanoparticle thin film. The best performance was obtained with 5 mM ZnO solution concentration with values of cell parameters like J_{sc} , V_{oc} , FF, and η as 3.56 mA/cm², 0.55 V, 0.62 and 1.21 % respectively.

4.3.4. *Electrochemical impedance spectroscopy*

Electrochemical impedance spectroscopy was performed to further explore the interfacial charge transport properties and recombination resistances for a better understanding of the cell parameters. The EIS measurement was carried out at V_{oc} bias voltage and applying an AC voltage of 10mV amplitude to the DSSC under 1 sun illumination in the frequency range 0.1 Hz to 190 kHz. The Nyquist plot of the different DSSCs fabricated using bare WO_3 and with a coating of different concentrations of ZnO onto it are depicted in Fig. 4.8(a). Usually, a typical Nyquist plot consists of three semi-circles. The first semicircle in the high-frequency range is attributed to the charge transport resistance at the Pt counter electrode/ electrolyte interface, while the second semicircle in the mid-frequency range represents the recombination resistance at the semiconductor/dye/electrolyte interface. The third semicircle is associated with Nernst diffusion (Warburg diffusion impedance Z_w) which is the impedance faced by the electrons during diffusion through the electrolyte [39]. However, in our case only two semicircles are present as the third semicircle is usually observed at frequencies below 0.1 Hz [42]. The intersection/intercept of the 1st semicircle on the real axis of the Nyquist plot in the high-frequency range represents the sheet resistance of

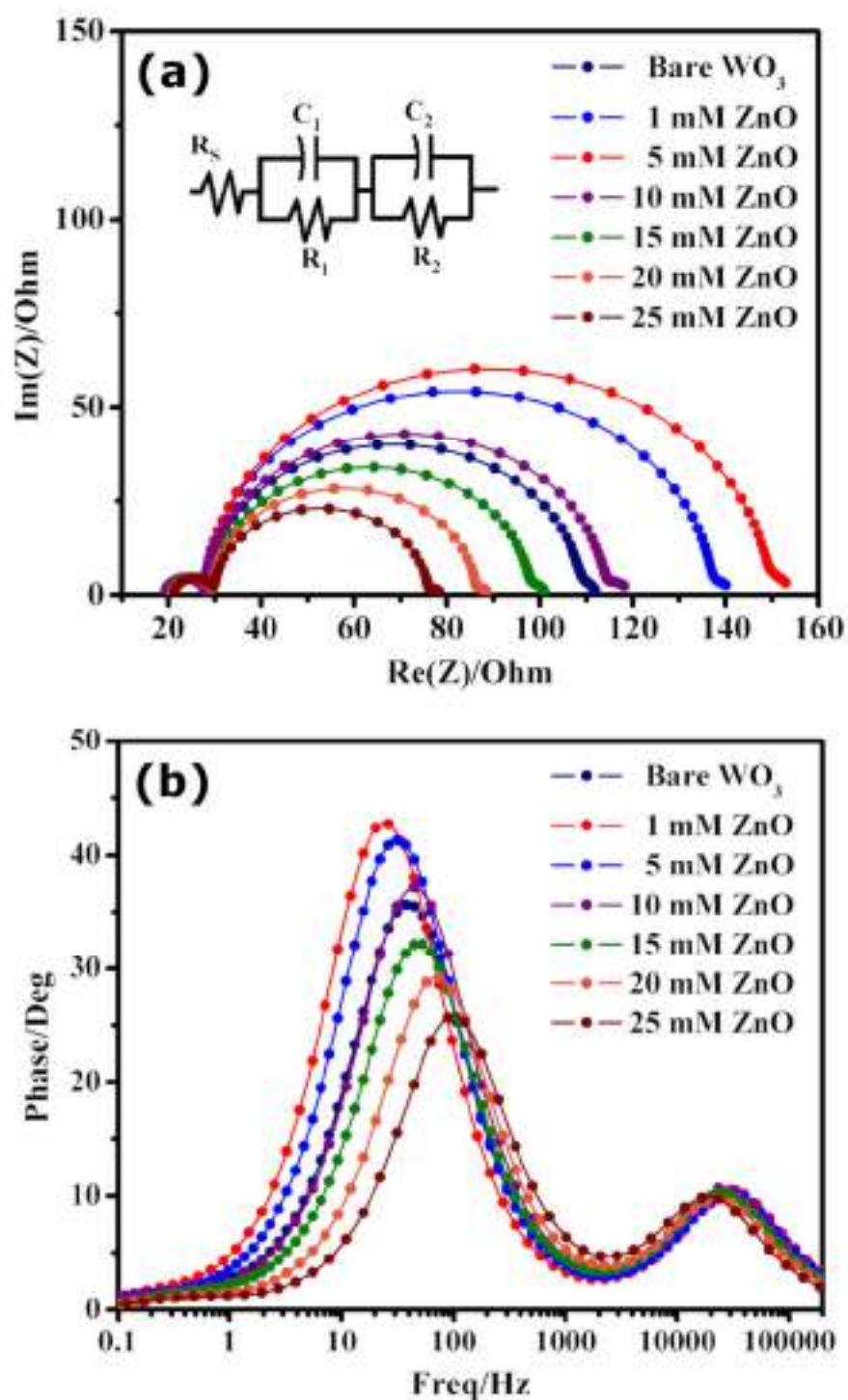


Figure 4.10 Electrochemical Impedance Spectra of the DSSCs (a) Nyquist plot along with equivalent circuit (inset) (b) Bode plot.

FTO and other ohmic contact resistances (R_s) of the assembled cells. The capacitive components C_1 & C_2 in the equivalent circuit are due to the formation of charge double layer between the counter electrode/electrolyte and semiconductor/dye/electrolyte interfaces respectively [43]. The equivalent circuit, shown in the inset of Fig. 4.8(a) is used to fit the experimental Nyquist plot and the obtained EIS parameters are represented in table 4.2. The value of contact resistance (R_s) is almost the same for all the coated cells except the bare WO_3 cell. The increase in the value of R_s in ZnO coated cells may be due to the increase in the number of layers. The value of recombination resistance (R_2) is very low for bare WO_3 . But a gradual increase in R_2 with an increase in ZnO precursor concentration may be observed in Fig. 4.8(a) and table 4.2. The highest value of R_2 is observed for 5 mM ZnO concentration as this much concentration provided the highest amount of dye adsorption without affecting the carrier transport through WO_3 thereby generating the highest number of charge carriers and also reducing the charge carrier recombination at the semiconductor/dye/electrolyte interface.

Table 4.2. Summary of EIS measurements of the fabricated DSSCs.

ZnO precursor solution concentration	R_s (Ω)	R_2 (Ω)	R_1 (Ω)	C_2 (μ F)	Peak freq. f(Hz)	Electron lifetime(τ_e) (ms)
Pure WO_3	19.3	85.2	8.67	84.3	37.18	4.28
1 mM ZnO	19.5	108.3	8.4	103.7	31.36	5.08
5 mM ZnO	19.6	119.7	8.62	125.4	24.15	6.59
10 mM ZnO	20.1	79.57	8.36	98.35	40.72	3.91
15 mM ZnO	20.8	67.57	8.79	87.35	48.47	3.29
20 mM ZnO	21.1	56.23	8.41	68.3	68.67	2.32
25 mM ZnO	21.3	45.76	8.52	55.57	97.29	1.64

Further increase in ZnO concentration starts decreasing R_2 due to poor dye loading on the WO_3 surface. Along with that presence of recombination sites for the free charge carriers in the thick layer of ZnO (38). Thick ZnO layer also makes the thickness of the film such a high that it becomes greater than the diffusion length of the electrons. This decreases the net photocurrent reaching the FTO and lowers the cell performance. The highest value of chemical capacitance C_2 also reflects the transformation of a higher amount of photon energy into chemical energy [44, 45]. To estimate the charge carrier lifetime, the Bode plot representing variation in phase angle (θ) with frequency (f) for varying amounts of ZnO concentration is depicted in Fig. 4.8(b). The electron lifetime is calculated using formula [46-49],

$$\tau_n = \frac{1}{2\pi f_{max}}$$

Where f_{max} represents the characteristic peak frequency of the Bode plot in the mid-frequency range. The lower value of f_{max} is associated with a higher electron lifetime. The DSSC with 5mM ZnO coating has the lowest value of f_{max} leading to the highest lifetime of photogenerated electrons. This enhancement in electron lifetime reduces the recombination process leading to the highest photocurrent among the seven fabricated cells in our study. These results are in accordance with the results obtained from J-V characteristics under illumination and dark.

4.4. Conclusion

In this study, we have fabricated DSSCs based on WO_3 as an alternative photoanode material. The DSSC showed an efficiency of 0.44% with a low FF of 0.39. This was due to very high recombination rates of photoexcited electrons along with poor dye loading due to the highly acidic surface of WO_3 . Apart from that, the lower conduction band edge position of WO_3 limits the open-circuit voltage of the DSSC. In order to improve the performance of WO_3

based DSSC, the effect of inclusion of the ZnO thin layer on the surface of WO_3 was studied. The current densities (J) – voltage (V) characteristics of the prepared cells were compared and a clear enhancement of cell efficiency was recorded upon ZnO coating and the highest efficiency was achieved for 5 mM concentration. Although the incorporation of a thin layer of ZnO onto WO_3 enhances the power conversion efficiency by creating an energy barrier and limiting the electron back-recombination, the thicker layer of ZnO degrades the cell performance by forming an aggregation of Zn^{+2} ions and N_3 dye and reducing the dye adsorption quantity of WO_3 film. This suggests an optimum concentration for ZnO to be deposited over WO_3 film to achieve the highest efficiency. The improvement of the value of V_{oc} due to ZnO coating was attributed to the upward shift in CB of WO_3 . Apart from J-V characteristics, study under illumination and dark, EIS measurement was also performed. It was found that the cell with 5mM of ZnO over WO_3 film has the highest recombination resistance which efficiently retards/suppresses the electron recombination rate and as result, the lifetime of photogenerated electrons is also highest. The decrease in the photoconversion efficiency with further increase in ZnO concentration above optimum value is due to the complete screening of WO_3 film by a thicker layer of ZnO. Therefore, the novel method used here to modify the surface property of the WO_3 photoelectrode of DSSC is found to be promising to enhance the cell performance and thereby develop an efficient WO_3 based Dye sensitized Solar cell.

References:

- [1] Bach W. Global warming: the complete briefing (2nd ed). John Houghton. Cambridge University Press: Cambridge, 1997. Pp. xv + 251. Paperback: ISBN 0521-62932-2, ú12.95; hardback: ISBN 0-321-62089-9, ú35.00. *International Journal of Climatology*. 1998;18(5):579-80.
- [2] Meadows DH, Meadows DL, Randers J, Behrens WW. The limits to growth. New York. 1972;102:27.
- [3] Minger TJ, editor *Greenhouse glasnost: the crisis of global warming: essays*. *Greenhouse/Glasnost: the Sundance Symposium on Global Climate Change,(USA)*, 1989; 1990: Ecco Press.
- [4] Peet J. *Energy and the ecological economics of sustainability*: Island Press; 1992.
- [5] Rose A. A global view of solar energy in rational units. *physica status solidi (a)*. 1979;56(1):11-26.
- [6] Shah A, Torres P, Tscharnner R, Wyrsh N, Keppner H. Photovoltaic technology: the case for thin-film solar cells. *science*. 1999;285(5428):692-8.
- [7] Turner JA. A realizable renewable energy future. *Science*. 1999;285(5428):687-9.
- [8] Gong J, Liang J, Sumathy K. Review on dye-sensitized solar cells (DSSCs): fundamental concepts and novel materials. *Renewable and Sustainable Energy Reviews*. 2012;16(8):5848-60.
- [9] Upadhyaya HM, Senthilarasu S, Hsu M-H, Kumar DK. Recent progress and the status of dye-sensitized solar cell (DSSC) technology with state-of-the-art conversion efficiencies. *Solar Energy Materials and Solar Cells*. 2013;119:291-5.
- [10] Sharma K, Sharma V, Sharma S. Dye-sensitized solar cells: fundamentals and current status. *Nanoscale research letters*. 2018;13(1):381.

-
-
- [11] O'regan B, Grätzel M. A low-cost, high-efficiency solar cell based on dye-sensitized colloidal TiO₂ films. *nature*. 1991;353(6346):737.
- [12] Ito S, Rothenberger G, Liska P, Comte P, Zakeeruddin SM, Péchy P, et al. High-efficiency (7.2%) flexible dye-sensitized solar cells with Ti-metal substrate for nanocrystalline-TiO₂ photoanode. *Chemical Communications*. 2006(38):4004-6.
- [13] Yamaguchi T, Tobe N, Matsumoto D, Nagai T, Arakawa H. Highly efficient plastic-substrate dye-sensitized solar cells with validated conversion efficiency of 7.6%. *Solar Energy Materials and Solar Cells*. 2010;94(5):812-6.
- [14] Cavallo C, Di Pascasio F, Latini A, Bonomo M, Dini D. Nanostructured semiconductor materials for dye-sensitized solar cells. *Journal of Nanomaterials*. 2017;2017.
- [15] Grätzel M. Photoelectrochemical cells. *nature*. 2001;414(6861):338.
- [16] Leung DY, Fu X, Wang C, Ni M, Leung MK, Wang X, et al. Hydrogen production over titania-based photocatalysts. *ChemSusChem*. 2010;3(6):681-94.
- [17] Liu G, Gong J, Kong L, Schaller RD, Hu Q, Liu Z, et al. Isothermal pressure-derived metastable states in 2D hybrid perovskites showing enduring bandgap narrowing. *Proceedings of the National Academy of Sciences*. 2018;115(32):8076-81.
- [18] Liu G, Kong L, Guo P, Stoumpos CC, Hu Q, Liu Z, et al. Two regimes of bandgap red shift and partial ambient retention in pressure-treated two-dimensional perovskites. *ACS Energy Letters*. 2017;2(11):2518-24.
- [19] Wang X, Li Z, Shi J, Yu Y. One-dimensional titanium dioxide nanomaterials: nanowires, nanorods, and nanobelts. *Chemical reviews*. 2014;114(19):9346-84.
- [20] Chandiran AK, Abdi-Jalebi M, Nazeeruddin MK, Grätzel M. Analysis of electron transfer properties of ZnO and TiO₂ photoanodes for dye-sensitized solar cells. *ACS nano*. 2014;8(3):2261-8.
-
-

-
-
- [21] Gillet M, Aguir K, Lemire C, Gillet E, Schierbaum K. The structure and electrical conductivity of vacuum-annealed WO₃ thin films. *Thin Solid Films*. 2004;467(1-2):239-46.
- [22] Zheng H, Tachibana Y, Kalantar-zadeh K. Dye-sensitized solar cells based on WO₃. *Langmuir*. 2010;26(24):19148-52.
- [23] Bae H, Yoon M, Kim J, Im S. Photodetecting properties of ZnO-based thin-film transistors. *Applied Physics Letters*. 2003;83(25):5313-5.
- [24] Özgür Ü, Alivov YI, Liu C, Teke A, Reshchikov M, Doğan S, et al. A comprehensive review of ZnO materials and devices. *Journal of applied physics*. 2005;98(4):11.
- [25] Zhang Q, Dandeneau CS, Zhou X, Cao G. ZnO nanostructures for dye-sensitized solar cells. *Advanced Materials*. 2009;21(41):4087-108.
- [26] Biswas R, Roy T, Chatterjee S. Study of Electro-Optical Performance and Interfacial Charge Transfer Dynamics of Dye Sensitized Solar Cells Based on ZnO Nanostructures and Natural Dyes. *Journal of Nanoelectronics and Optoelectronics*. 2019;14(1):99-108.
- [27] Costantino U, Marmottini F, Nocchetti M, Vivani R. New Synthetic Routes to Hydrotalcite-Like Compounds— Characterisation and Properties of the Obtained Materials. *European Journal of Inorganic Chemistry*. 1998;1998(10):1439-46.
- [28] Oh J-M, Hwang S-H, Choy J-H. The effect of synthetic conditions on tailoring the size of hydrotalcite particles. *Solid State Ionics*. 2002;151(1-4):285-91.
- [29] Daniel M, Desbat B, Lassegues J, Gerand B, Figlarz M. Infrared and Raman study of WO₃ tungsten trioxides and WO₃·xH₂O tungsten trioxide hydrates. *Journal of solid state chemistry*. 1987;67(2):235-47.
- [30] Sadek AZ, Zheng H, Breedon M, Bansal V, Bhargava SK, Latham K, et al. High-temperature anodized WO₃ nanoplatelet films for photosensitive devices. *Langmuir*. 2009;25(16):9545-51.
-
-

-
-
- [31] Hore S, Vetter C, Kern R, Smit H, Hinsch A. Influence of scattering layers on efficiency of dye-sensitized solar cells. *Solar Energy Materials and Solar Cells*. 2006;90(9):1176-88.
- [32] Jin EM, Park K-H, Yun J-J, Hong CK, Hwang M-J, Park B-K, et al. Photovoltaic properties of TiO₂ photoelectrode prepared by using liquid PEG-EEM binder. *Surface Review and Letters*. 2010;17(01):15-20.
- [33] Ko KH, Lee YC, Jung YJ. Enhanced efficiency of dye-sensitized TiO₂ solar cells (DSSC) by doping of metal ions. *Journal of colloid and interface science*. 2005;283(2):482-7.
- [34] Park K-H, Jin EM, Gu HB, Shim SE, Hong CK. Effects of HNO₃ treatment of TiO₂ nanoparticles on the photovoltaic properties of dye-sensitized solar cells. *Materials Letters*. 2009;63(26):2208-11.
- [35] Qi B, Wang J. Fill factor in organic solar cells. *Physical Chemistry Chemical Physics*. 2013;15(23):8972-82.
- [36] Grätzel M. Dye-sensitized solar cells. *Journal of photochemistry and photobiology C: Photochemistry Reviews*. 2003;4(2):145-53.
- [37] Ito S, Liska P, Comte P, Charvet R, Péchy P, Bach U, et al. Control of dark current in photoelectrochemical (TiO₂/I⁻/I₃⁻) and dye-sensitized solar cells. *Chemical Communications*. 2005(34):4351-3.
- [38] Noor S, Sajjad S, Leghari SAK, Shaheen S, Iqbal A. ZnO/TiO₂ nanocomposite photoanode as an effective UV-vis responsive dye sensitized solar cell. *Materials Research Express*. 2018;5(9):095905.
- [39] Adachi M, Sakamoto M, Jiu J, Ogata Y, Isoda S. Determination of parameters of electron transport in dye-sensitized solar cells using electrochemical impedance spectroscopy. *The Journal of Physical Chemistry B*. 2006;110(28):13872-80.
- [40] Al-juaid F, Merazga A, Al-Baradi A, Abdel-wahab F. Effect of sol-gel ZnO spin-coating on the performance of TiO₂-based dye-sensitized solar cell. *Solid-State Electronics*. 2013;87:98-103.
-
-

-
-
- [41] Bedja I, Kamat PV, Hua X, Lappin A, Hotchandani S. Photosensitization of Nanocrystalline ZnO Films by Bis (2, 2 '-bipyridine)(2, 2 '-bipyridine-4, 4 '-dicarboxylic acid) ruthenium (II). *Langmuir*. 1997;13(8):2398-403.
- [42] Sarker S, Ahammad A, Seo HW, Kim DM. Electrochemical impedance spectra of dye-sensitized solar cells: fundamentals and spreadsheet calculation. *International Journal of Photoenergy*. 2014;2014.
- [43] Younas M, Gondal M, Dastageer M, Baig U. Fabrication of cost effective and efficient dye sensitized solar cells with WO₃-TiO₂ nanocomposites as photoanode and MWCNT as Pt-free counter electrode. *Ceramics International*. 2019;45(1):936-47.
- [44] Wang Q, Moser J-E, Grätzel M. Electrochemical impedance spectroscopic analysis of dye-sensitized solar cells. *The Journal of Physical Chemistry B*. 2005;109(31):14945-53.
- [45] Bisquert J. Chemical capacitance of nanostructured semiconductors: its origin and significance for nanocomposite solar cells. *Physical Chemistry Chemical Physics*. 2003;5(24):5360-4.
- [46] Lim SP, Pandikumar A, Huang NM, Lim HN. Silver/titania nanocomposite-modified photoelectrodes for photoelectrocatalytic methanol oxidation. *International Journal of Hydrogen Energy*. 2014;39(27):14720-9.
- [47] Buda S, Shafie S, Rashid SA, Jaafar H, Sharif N. Enhanced visible light absorption and reduced charge recombination in AgNP plasmonic photoelectrochemical cell. *Results in physics*. 2017;7:2311-6.
- [48] Kim SG, Ju MJ, Choi IT, Choi WS, Choi H-J, Baek J-B, et al. Nb-doped TiO₂ nanoparticles for organic dye-sensitized solar cells. *Rsc Advances*. 2013;3(37):16380-6.
- [49] Archana P, Gupta A, Yusoff MM, Jose R. Tungsten doped titanium dioxide nanowires for high efficiency dye-sensitized solar cells. *Physical Chemistry Chemical Physics*. 2014;16(16):7448-54.
-
-

This Page is intentionally left blank

Chapter 5

Role of dye co-adsorbent and blocking layer in
improving the performance of DSSCs

This Page is intentionally left blank

5.1. Introduction

Ever growing global energy requirement and depleting level of fossil fuels have accelerated the demand for efficient power generation from solar photovoltaic (PV) cells in recent years [1-3]. The environmental impact of the use of fossil fuels is another major concern [4]. The current production of photovoltaic (PV) modules is dominated by crystalline silicon modules based on bulk wafers. However, the use of toxic materials and the high production cost of these solar cells have motivated the researchers to find new kinds of less expensive and non silicon-based solar cells to harvest solar energy efficiently [5-8].

Dye-sensitized solar cells (DSSCs) are a non-conventional photovoltaic technology that has attracted significant attention because of their high conversion efficiencies and low cost. O'Regan. B. & Grätzel reported high efficiency cells using nanoporous titanium dioxide (TiO_2) semiconductor electrodes, ruthenium (Ru) metal complex dyes, and iodine electrolyte solutions in the journal of Nature in 1991 [9]. Since then, many studies have been actively carried out on DSSCs and revealed their performance comparable to amorphous silicon thin films [10,11]. These DSSCs have the advantages of low cost, lightweight and easy fabrication, but issues include durability and further improvement of their properties. To respond to these issues, many attempts have been made, such as solidifying electrolytes and improving materials and structures, but there have been no great breakthroughs yet [12,13].

A dye-sensitized solar cell consists of two conducting glass electrodes in a sandwich arrangement. Each layer has a specific role in the cell. The transparent glass electrodes allow the light to pass through the cell. The titanium dioxide serves as a holding place for the dye and participates in electron transfer. The dye molecules collect light and produce excited electrons which cause a current in the cell. The iodide electrolyte layer acts as a source

for electron replacement. The bottom conductive layer is coated with platinum which plays the role of the counter electrode. A schematic structure of a liquid electrolyte DSSC and its working principle is shown in Fig. 5.1. When light passes through the conductive glass electrode, the dye molecules absorb the photons and the electrons in the dye go from the ground state (HOMO) to an empty excited state (LUMO). This is referred to as photoexcitation. The excited electrons jump to the conduction band of the semiconducting dioxide and diffuse across this layer reaching the conductive electrode. Then they travel through the outer circuit and reach the counter electrode. The dye molecules become oxidized after losing an electron to the semiconductor oxide material. The red-ox iodide electrolyte donates electrons to the oxidized dye molecules thereby regenerating them. When the originally lost electron reaches the counter electrode, it gives the electron back to the electrolyte [9,14].

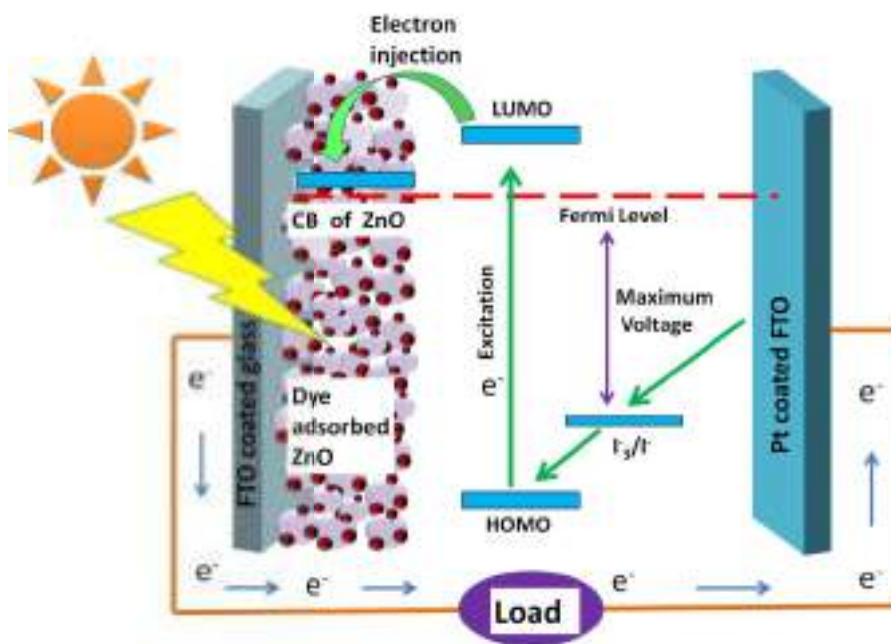


Figure 5.1 Schematic diagram and working principle of a conventional DSSC.

The photovoltaic performance of a DSSC highly depends on all of its components and the fabrication methodology. Therefore, the optimization of every component is extremely crucial to achieve the best performance. Since its

introduction into the science community in 1991, the nanocrystalline photoanode in dye-sensitized solar cells has predominantly been comprised of titanium (TiO_2) nanoparticles as the semiconducting material [9,14,15]. Many researchers became very interested in studying the dye-sensitized solar cell performance fabricated using alternative semiconducting nanomaterials [16,17]. Specifically, Zinc Oxide (ZnO) has been an ideal alternative to TiO_2 because of having a similar conduction band edge that is appropriate for proper electron injection from the excited dyes; moreover, ZnO provides better electron transport due to its higher electronic mobility. Along with that, ZnO is also highly transparent, which allows greater light penetration [18-22].

In this study, ZnO nanoparticles were implemented to fabricate the photoanode of the DSSCs and rose bengal dye was utilized as a sensitizer. To obtain better efficiency, the dye molecules must bind tightly to the mesoporous ZnO photoanode surface with the assistance of their anchoring group to ensure proficient electron injection from the LUMO of the dye molecule to the conduction band (CB) of ZnO .

Ruthenium dyes have long been used as quite efficient sensitizers for the photoanodes of the DSSCs [23-25]. However, these dyes are expensive, difficult to synthesis, requires high production cost, toxic, rare and easily pollute the environment [26]. Owing to these facts, the organic photosensitizer Rose Bengal (RB), emerges as a promising and alternative candidate. It is a xanthenes class photosensitizer having high absorption coefficient and absorbs a wide spectrum of solar radiation. It energetically matches the conduction band edge of ZnO and iodine/iodide redox couple for DSSC application [27,28]. Accordingly, ZnO based DSSC performs specifically well when sensitized with Rose Bengal. Although the efficiency of these type of organic sensitizer based DSSCs is less, production cost per watt will be less compared to the ruthenium based DSSCs even if we achieve moderate efficiency. As the RB dye is an organic dye and does not contain any toxic noble metal such as

ruthenium, there are no environmental pollution related issues with it. It is widely used because of its high absorption coefficient in the visible region of solar spectrum and its molecular structure (Fig. 5.2.) comprises of anchoring groups that can be adsorbed onto the semiconductor oxide surface. For the particular case of ZnO-RB combination, the interaction between the unfilled valance shell of the ZnO and the carboxyl groups present in the dye molecules leads to easy adsorption of the dye molecules on the ZnO surface. Such kind of bonding between the dye molecule and ZnO not only increases adsorptivity of dye but also facilitates electron injection because of the substantial overlap between the electron molecular orbitals of the dye and those of the semiconductor's conduction band [29].

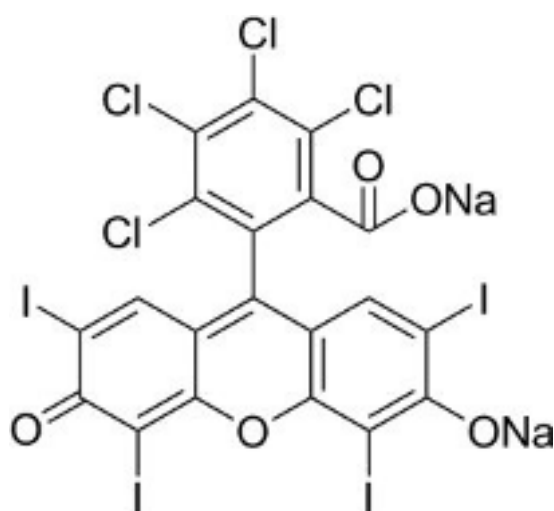


Figure 5.2 Chemical structure of Rose Bengal dye.

However, in case of ZnO photoanode based DSSCs, the dye aggregation on the ZnO surface affects the photoelectron injection by increasing charge recombination and hence limits the overall device performance [30-32]. The use of additives such as Chenodeoxycholic acid (CDCA) is a very useful and widely used strategy in lowering the self-aggregation of dye molecules by suppressing unfavourable dye-dye interactions as shown in Fig. 5.3 and thereby enhances the photoconversion efficiency [33-

35]. However, the strong binding of CDCA molecules to the ZnO surface partially displaces dye molecules and consequently reduces photon harvesting. Therefore, to maximize the positive effect of the co-adsorbent, it is very crucial to carefully optimize the amount of CDCA [36]. Few researchers have studied the role of CDCA as an anti-aggregation agent in ruthenium and organic dye based DSSCs and found it to be very effective in reducing the aggregation of dye molecules over the semiconductor surface [37-40]. But there is no report available related to the application of CDCA on Rose Bengal dye. Herein, we report the investigation on the effect of CDCA as co-adsorbent in the performance of Rose Bengal (RB) dye based DSSCs. Different concentrations of CDCA were studied to identify the optimum value for achieving the best device performance.

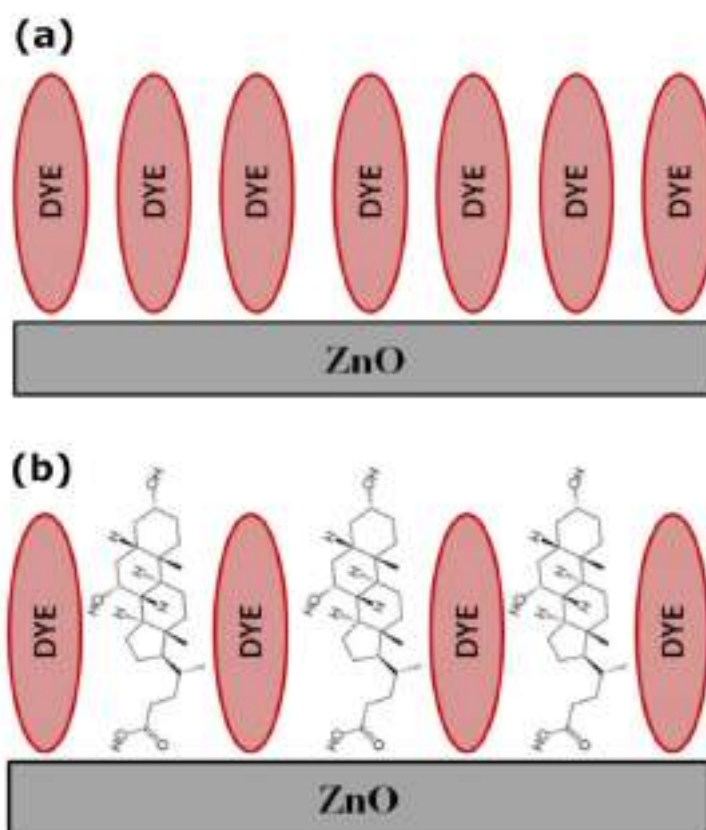


Figure 5.3 (a) Unfavourable dye-dye interaction in absence of CDCA (b) reduced self-aggregation of dye molecules in presence of CDCA.

On the other hand, the mesoporous nature of the ZnO film is very essential to tender high surface area offering more dye loading and thereby generating more photoelectrons. However, small pores present in the nanocrystalline ZnO layer of the photoanode may provide a path for the direct contact between the liquid electrolyte and the FTO substrate. This may allow the electrons of FTO to recombine with the I_3^- ion present in the electrolyte resulting in high recombination current and hence decreased cell performance [41,42]. Therefore, to inhibit the electron back transfer, a promising approach is to modify the FTO/electrolyte interface by adding a compact metal oxide blocking layer. A thin blocking layer (BL) of ZnO was deposited by a facile and cost-effective sol-gel spin coating process before depositing the mesoporous active ZnO layer. In this work, we reported the fabrication and characterization of DSSCs based on ZnO nanoparticles and Rose Bengal dye. The effect of CDCA concentration and the compact ZnO blocking layer in boosting the photovoltaic performance of the device was investigated in terms of photocurrent-voltage (J-V) characteristics and dark current measurement. In addition to that, electrochemical impedance spectroscopy (EIS) analysis was employed to investigate the charge transfer kinetics and electron back reaction of the fabricated cells.

5.2. Materials and Methods

5.2.1. *Materials*

ZnO nanopowder, Zinc acetate dehydrate ($(CH_3COO)_2Zn \cdot 2H_2O$) and Monoethanolamine (MEA) were bought from Sigma Aldrich, India. ethylcellulose and terpineol were bought from TCI Chemicals, India. Transparent FTO coated glass ($10 \Omega/\text{square}$), the high-performance liquid electrolyte (Iodolyte AN50), chenodeoxycholic acid (CDCA) as a dye co-adsorbent and liquid platinum paint (Platisol T) to prepare the platinum-coated counter electrode were purchased from Solaronix, Switzerland. Meltonix 1170-

25 (25 μ m) (Solaronix) was used as a spacer between the working and counter electrode to avoid short-circuiting. All the reagents utilized in the fabrication process were of analytical grades. So no further purification was required.

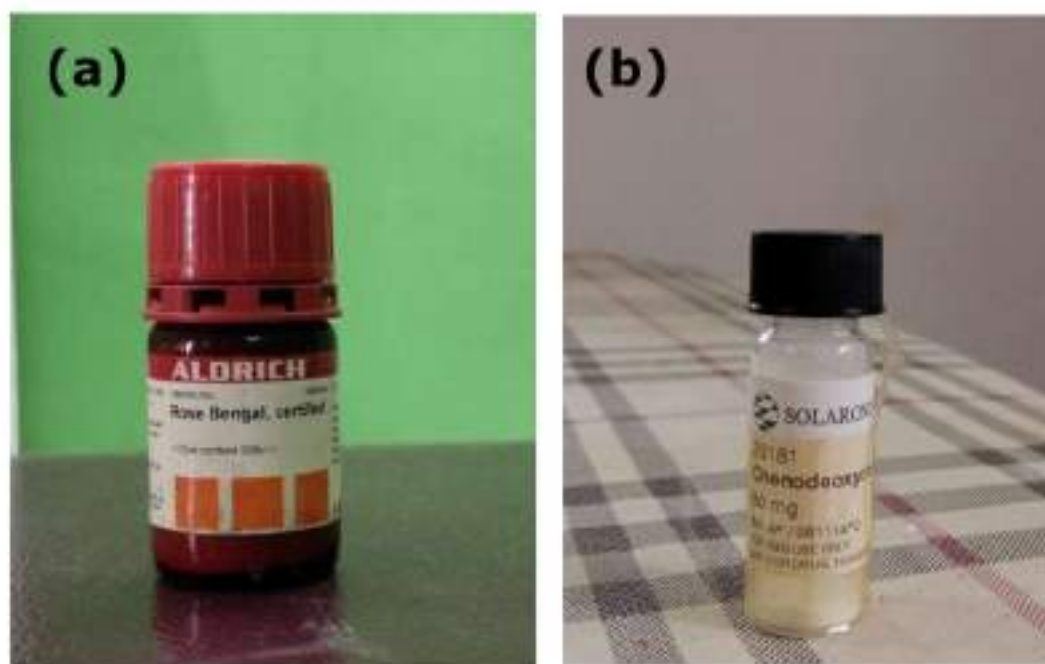


Figure 5.4 (a) Rose Bengal dye and (b) chenodeoxycholic acid (CDCA).

5.2.2. *Preparation of conventional ZnO photoanode*

To prepare the thin films of the photoanode materials, the FTO coated glass substrates were first cleaned with dilute HCl in an ultrasonic bath for 15 minutes and then thoroughly rinsed with deionized water to remove the HCL residues. The substrates were then cleaned with acetone and ethanol using an ultrasonic cleaning bath [17,22]. The mesoporous ZnO photoelectrode of the DSSC was prepared by following the standard doctor blade method. The paste for doctor blading was prepared by mixing 0.5 g of ZnO nanopowder with α -terpineol as a solvent and 0.45 g of ethyl cellulose as a binder [43]. The mixture was stirred continuously to obtain a smooth lump-free slurry. The ZnO paste was then coated on the conductive side of the cleaned FTO glass

substrate and subsequently annealed at 400°C on a hot plate for 30 min to burn out the ethyl cellulose and other organic contents of the working electrode and to strengthening the bonding between the substrate and the ZnO film. In addition to that, the annealing procedure also helps to improve the surface quality of the thin film along with increasing the crystallinity of the sample [44-47].

5.2.3. Preparation of photoanode with Compact ZnO layer

In order to improve the photovoltaic performance of the cells further by preventing the direct contact between FTO and liquid electrolyte, a thin and compact ZnO layer was deposited on FTO coated glass substrate by employing a simple sol-gel spin coating method prior to deposition of mesoporous active ZnO nanoparticle layer. The precursor solution was prepared by mixing Zinc acetate dehydrate ($(\text{CH}_3\text{COO})_2\text{Zn}, 2\text{H}_2\text{O}$) in 50 ml isopropanol as solvent and monoethanolamine (MEA) was used as a stabilizer. The precursor solution concentration was maintained at 0.05 M. The mixture was vigorously stirred at 60° C by a magnetic stirrer for 1 hr. MEA was added dropwise under stirring, yielding a clear homogenous solution. The solution was left for 24 hr at room temperature for aging before it could be used for film deposition. The aged solution was then spin-coated on a cleaned FTO glass substrate with a programmable spin coater (Apex Instruments Co. Pvt. Ltd, Model SpinNXG-P1) at 3000 rpm for 30 s and annealed at 200° C for 20 minutes to form the ZnO blocking layer. Over this compact blocking layer, the mesoporous active layer was coated using the same doctor blade method and then annealed at 400° C as done earlier.

5.2.4. Assembling the devices

One set of ZnO photoanodes were sensitized by immersing them in a 0.5 mM ethanolic solution of pure Rose Bengal dye for 12 hours. Another set of

photoanodes (both with and without ZnO blocking layer) were sensitized with the RB dye solution containing various concentrations (0 mM – 10 mM) of CDCA at room temperature for 12 hours. The working electrodes were then removed from the solution and rinsed thoroughly with deionized water and ethanol to get rid of any excess dye from the thin film surface and left for air drying at room temperature. The platinum catalyst precursor solution (Platisol-T) was spin-coated on the conducting side of the cleaned FTO glasses and heated at 450° C for 15 minutes on a hot plate to prepare the counter electrodes for the cells. The dye adsorbed working electrodes and platinum(Pt)-coated counter electrodes were assembled against the coated sides of each other in a sandwich manner using two binder clips with a Surlyn film (Meltonix 1170-25 μ m, Solaronix) gasket as a spacer in between them. The liquid electrolyte used in the fabrication process was poured inside the cell through fine holes pre-drilled on the counter electrodes. The red-ox concentration of the electrolyte was 50 mM. The active area of the cells for illumination was adjusted to 0.16 cm².

5.2.5. Characterization and Measurements

X-ray diffraction (XRD) analysis is a technique used for the determination of the crystal structure of materials in the nanomaterial, thin-film, or bulk material form. In the XRD experiment, a monochromatic X-ray beam is allowed to incident on the sample and the diffraction occurs. In our study, the X-ray diffraction analysis was employed using PAN-analytical X'Pert PRO X-ray diffractometer (CuK α radiation, 30 mA, 40 kV, λ = 1.5406 Å) to determine the crystalline structure of ZnO nanoparticles used in making the photoanode of the DSSC. Absorbance spectrum measurement of the dye was carried out using a Perkin-Elmer Lambda-35 UV-VIS spectrophotometer. Scanning electron microscopy (JEOL) was used to examine the surface morphology of the prepared ZnO thin films. The current-voltage (J-V)

characterization of the cells was measured under 100 mW/cm² illumination using a Keithley 2400 digital source meter which was controlled by Keithley LabTracer computer software. The overall photoconversion efficiency of the solar cell was calculated using the formula

$$\eta = \frac{P_{\text{out}}}{P_{\text{in}}} = \frac{I_{\text{sc}} V_{\text{oc}} FF}{P_{\text{in}}} \quad (1)$$

Where P_{in} , V_{oc} , I_{sc} and FF denote the incident photon power, open-circuit voltage, the short circuit current density and fill factor respectively. The fill factor was estimated using the following formula:

$$FF = \frac{I_{\text{max}} V_{\text{max}}}{I_{\text{sc}} V_{\text{oc}}} \quad (2)$$

Where I_{max} and V_{max} , respectively, represent values of current and voltage at the maximum output power point of the solar cell. The area of the fabricated cells that was exposed to light was 1 cm². The electrochemical impedance spectroscopy (EIS) of the cells was done in the frequency range of 0.1Hz to 190 kHz under open circuit conditions.

5.3. Results and Discussion

5.3.1. *UV-VIS absorption spectral analysis of the dye*

0.5 mM ethanolic solution of Rose Bengal dye was prepared and its absorption property was studied using Perkin Elmer Lambda-35 UV-VIS spectrophotometer. UV-VIS absorption spectrum of the RB dye is shown in Fig. 5.6 (b). The value of λ_{max} obtained from the absorption spectrum is a very important parameter as it demonstrates the potential of the molecular systems for significant usage as a functional material in DSSC. It can be observed that the Rose Bengal dye absorbs a larger fraction of the solar spectrum in the visible region of 460–600 nm and it shows the highest optical absorption at 549 nm wavelength. The strong absorption peak may be assigned to the intra-molecular

charge transfer (ICT) transitions from the donor to acceptor level within HOMO (Highest Occupied Molecular Orbital)- (Lowest Unoccupied Molecular Orbital)LUMO energy levels as shown in Fig.5.5 [48].



Figure 5.5 Possible transition mechanism in the Rose Bengal molecular system.

The optical energy gap of the dye was calculated to be 2.26 eV from the absorption spectra using equation (3) given below [49] (Ossai et al 2020).

$$E_g = \frac{1240}{\lambda_{max}} \text{ eV} \quad (3)$$

where λ_{max} is the maximum absorption wavelength.

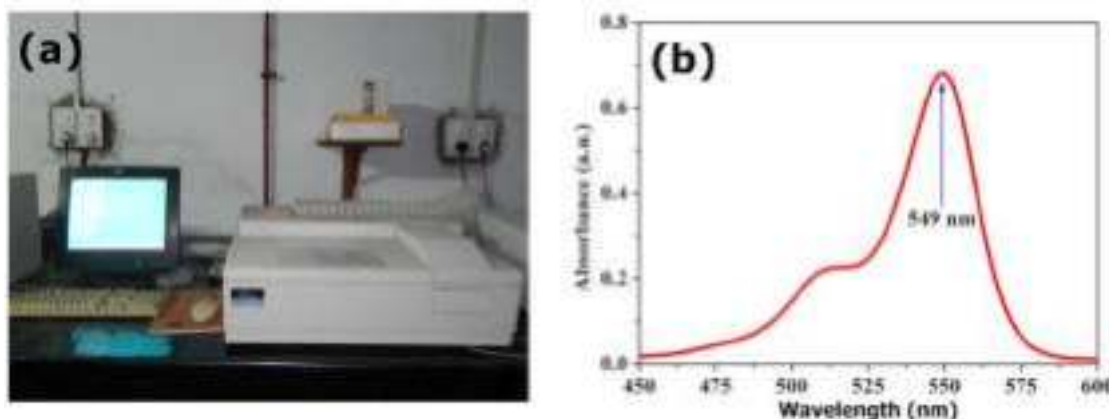


Figure 5.6 (a) UV-VIS experimental setup (b) absorption spectra of Rose Bengal dye.

The dye's HOMO-LUMO energy gap has an impact on how electrons are injected into the ZnO particles' conduction band from the dye's LUMO molecule. It facilitates the vertical electron transition through the dye excitation [50]. On the other hand, indirect transition is a phonon assisted transition where change in momentum must be taken into account. When the photons having energy fairly above the indirect band gap of dye molecule is absorbed by the dye electron, phonons get emitted [51]. As a result the direct band gap is utilized to determine the vertical transition during the course of photosensitization [52,53]. Hence, the lowest electronic transition, which corresponds to the onset of absorption in the UV-visible absorption spectrum, was used to calculate the optical bandgap. It is the energy difference between HOMO and LUMO which is caused by the excitation of electrons from HOMO to LUMO.

5.3.2. *Structural and phase characterization ZnO compact layer*

The X-ray diffraction pattern of the ZnO compact blocking layer, shown in Fig. 5.7 (a), exhibits the hexagonal wurtzite crystal phase of ZnO and the peaks well match with the standard JCPDS card no. 36-1451. The diffraction peaks observed at 2θ values of 31.79° , 34.42° , 36.25° , 47.51° , 56.60° , 62.86° , 67.96° , and 69° corresponds to the reflection from the (100), (002), (101), (110), (103), (112), and (201) lattice planes respectively. Sharp and strong peaks indicate the highly crystalline nature of the material [54,55]. The XRD pattern for the commercial ZnO nanopowder is shown in Fig. 5.7 (b). It can be clearly seen that both the commercial ZnO nanopowder and synthesized ZnO blocking layer showed similar XRD patterns. The XRD pattern of sample with both the blocking and active layer is shown in Fig. 5.7 (c). This is very similar to the XRD pattern of the blocking layer. This is because the blocking layer is more crystalline in nature, which is evident from its XRD pattern with its sharper peaks.

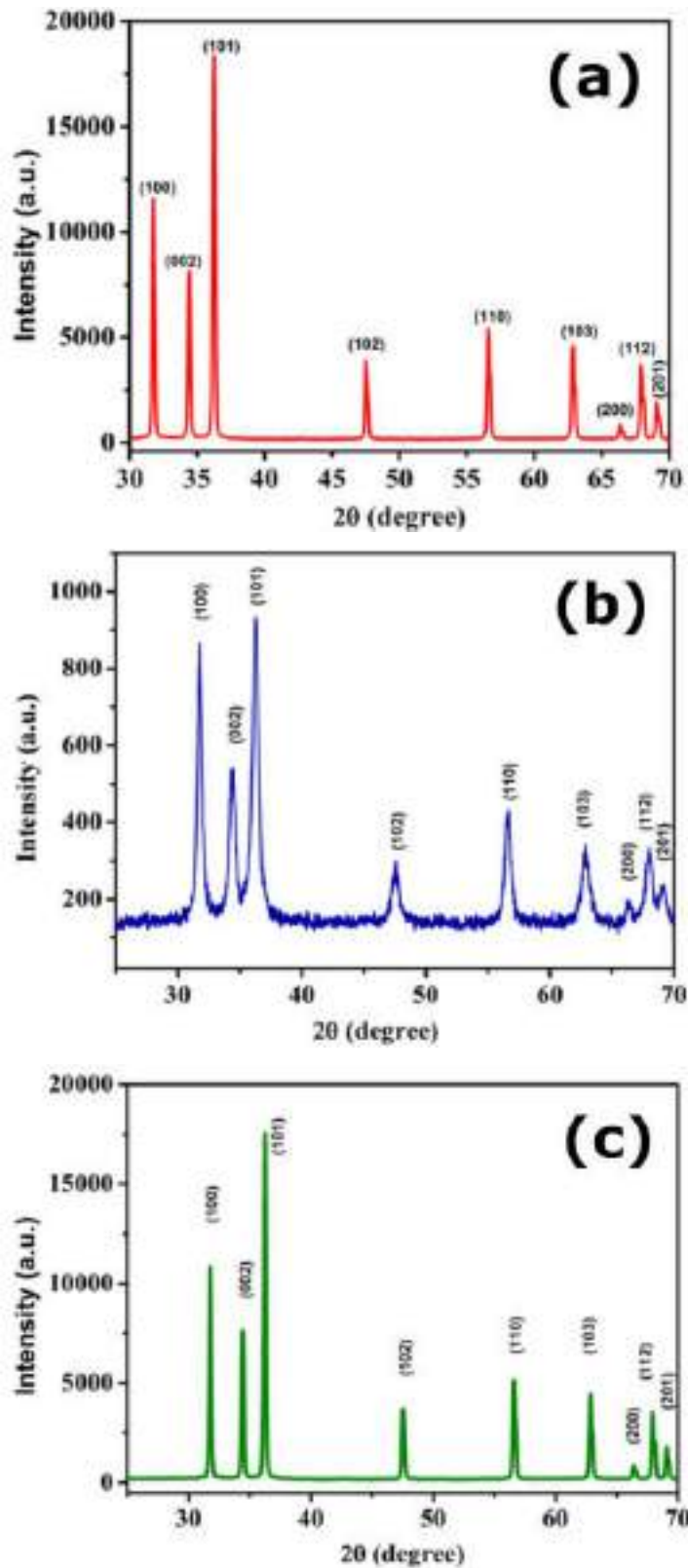


Figure 5.7 X-ray diffraction pattern of (a) ZnO compact blocking layer (b) ZnO nanoparticles as active layer (c) ZnO blocking/active layer.

5.3.3. Surface Morphology study and energy dispersive spectroscopy of the photoanodes

Scanning electron microscopic (SEM) analysis of the ZnO active layer and the compact blocking layer on the FTO substrate was carried out to study the surface morphology and the particle size of the sample. The SEM images of the ZnO active and blocking layers on the FTO substrate are depicted in Fig. 5.8 and Fig. 5.9 respectively. It can be seen from Fig. 5.8 (a) that the ZnO nanoparticles have a hexagonal structure. Fig. 5.9 (a) and 5.8 (b) represent the SEM images of compact blocking layer at low and high magnifications respectively. The diameter of the spin-coated nanoparticles ranges from 150 to 180 nm. Further, the chemical composition and elemental percentage of the compact ZnO film are revealed by the Energy Dispersive X-Ray Spectroscopy (EDS) analysis which is shown in Fig. 5.10. Predominating peaks of Zn and O₂ unveil that the synthesized blocking layer contains pure ZnO.

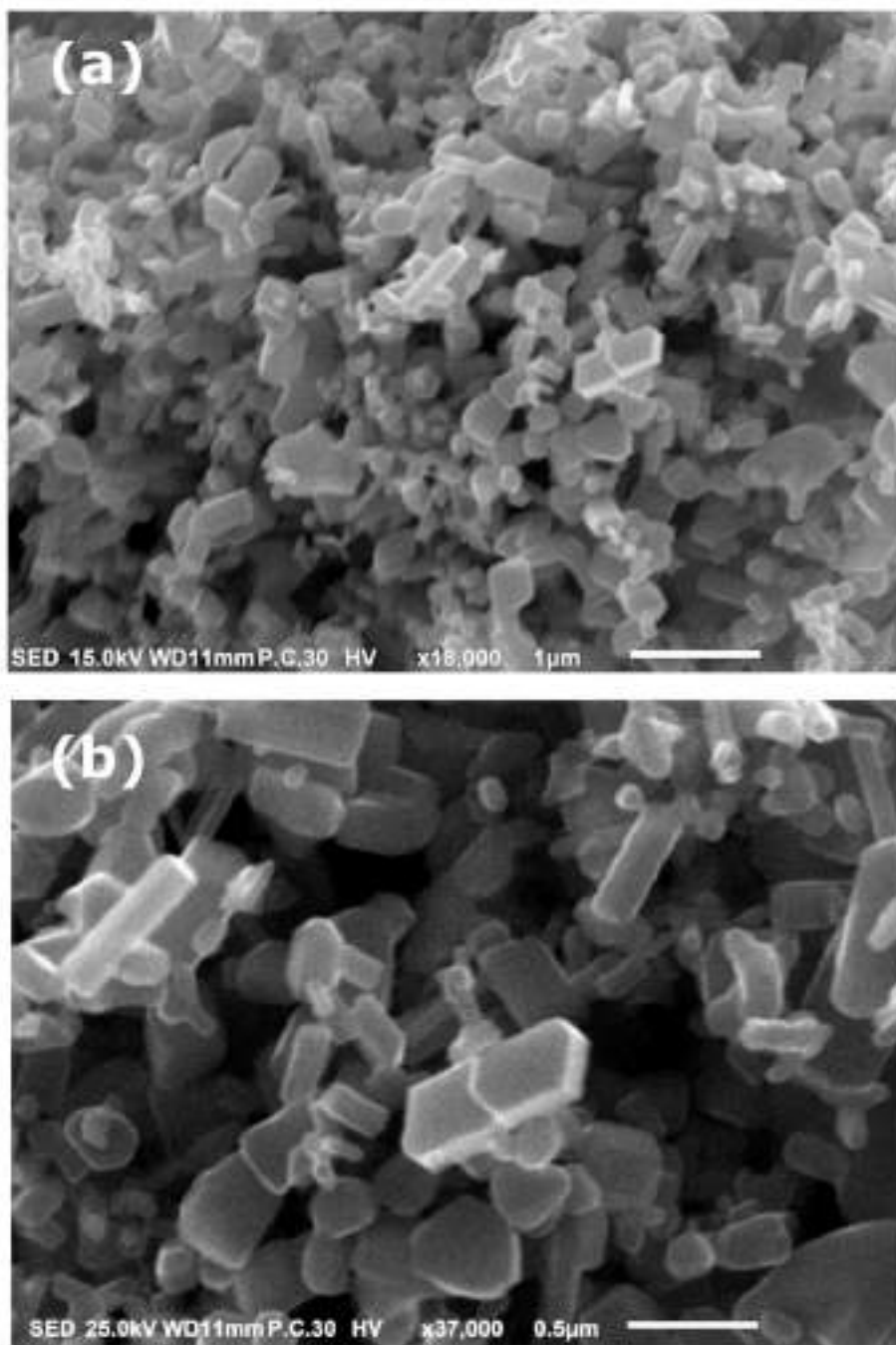


Figure 5.8 SEM images of ZnO NP active layer (a) at lower magnification (b) at higher magnification.

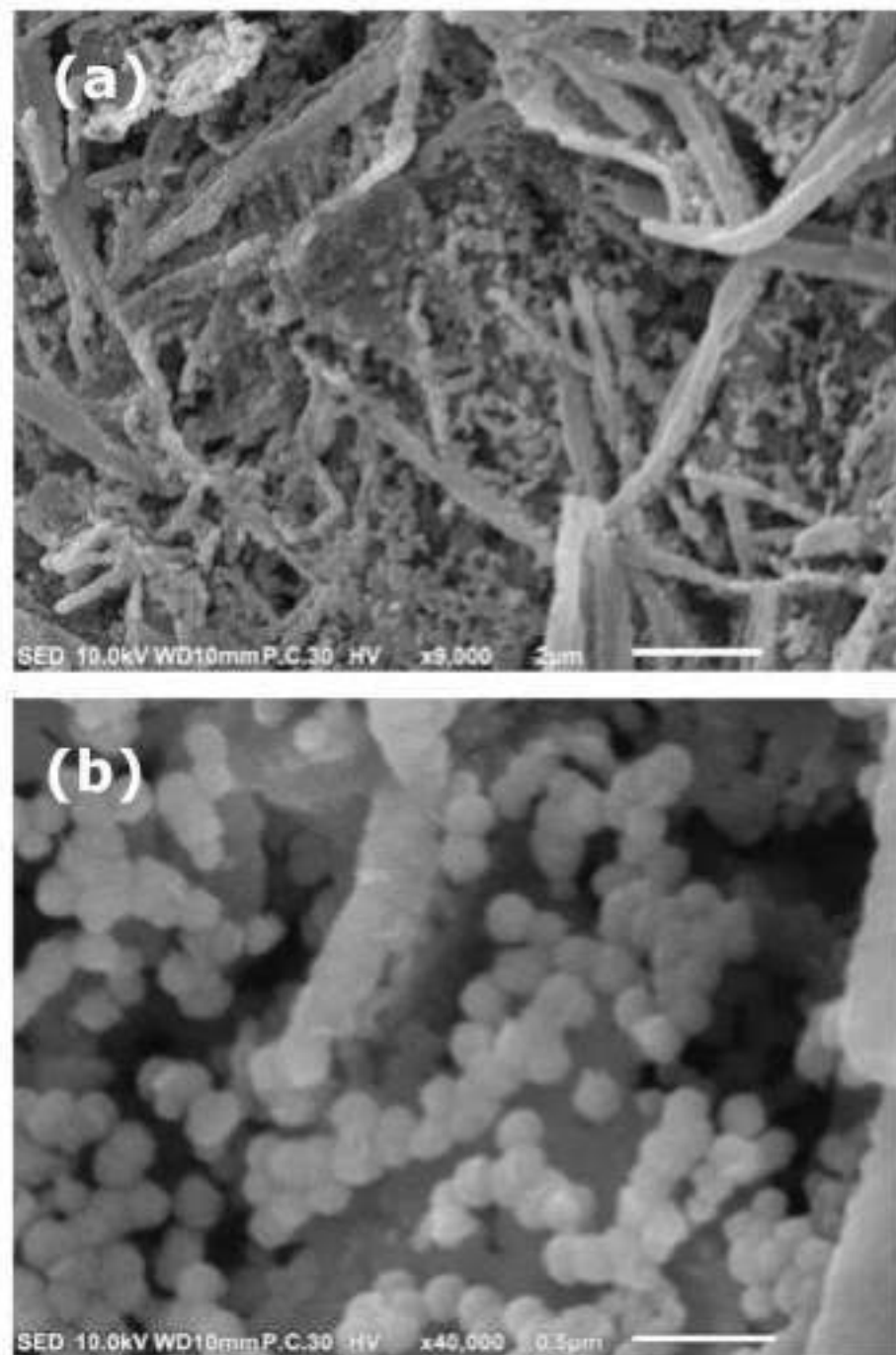


Figure 5.9 SEM images of ZnO blocking layer (a) at lower magnification and (b) at higher magnification.

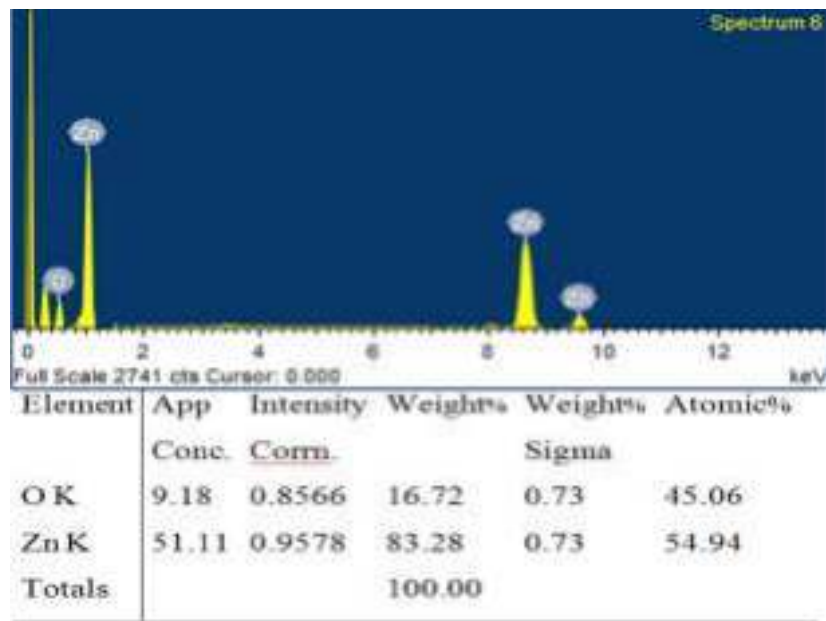


Figure 5.10 EDS and elemental composition of ZnO blocking layer.

5.3.4. Photovoltaic characterization of the cells

The Current-Voltage (J-V) characteristic is a crucial measurement that reveals the value of the overall photovoltaic performance of a solar cell along with the key performance parameters like open circuit voltage and short circuit current density. Fig. 5.11 (a) depicts the J-V characteristics of the DSSCs based on different types of photoanodes under illumination and the obtained photovoltaic parameters for each of the cells are summarized in Table 5.1.

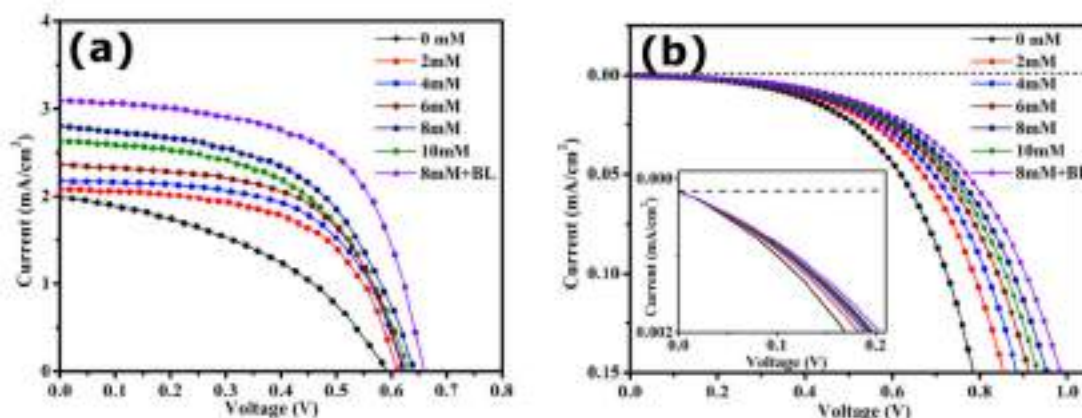


Figure 5.11 Current-voltage characteristics of different cells under (a) illumination (b) dark

Table 5.1.

Photovoltaic parameters of DSSCs fabricated with various ZnO photoanodes

Cell name	CDCA concentration	J_{sc} (mA/cm ²)	V_{oc} (V)	FF	Efficiency (η %)
DSSC1	0 mM	1.98	0.58	0.43	0.49
DSSC2	2 mM	2.08	0.61	0.58	0.74
DSSC3	4 mM	2.18	0.62	0.60	0.81
DSSC4	6 mM	2.36	0.63	0.58	0.86
DSSC5	8 mM	2.80	0.64	0.56	1.00
DSSC6	10 mM	2.63	0.64	0.54	0.91
DSSC7	8 mM + BL	3.09	0.66	0.60	1.22

5.3.5. *Effect of CDCA*

The conventionally prepared DSSC with ZnO nanoparticles and Rose Bengal dye displayed a short circuit current density (J_{sc}) of 1.98 mA/cm², an open circuit voltage (V_{oc}) of 0.58 V, and a fill factor (FF) of 0.43, resulting in a photoconversion efficiency (η) of 0.49 %. However, under the same working conditions, the device performance was found to be highly influenced when CDCA solution was incorporated into the dye solution at various concentrations. From Table 5.1, it can be noted that the value of V_{oc} , as well as J_{sc} , increases with an increase in the concentration of CDCA. Optimum concentration (8mM) provides the finest dye attachment to the ZnO surface. The best device performance was achieved for the optimized CDCA concentration of 8 mM when added with 0.5 mM RB dye solution. This improvement in the performance may be attributed to reduced dye aggregation along with uniform dye adsorption yielding better electron injection into the conduction band of ZnO.

5.3.6. Effect of compact ZnO blocking layer

To avoid the direct contact between the FTO and the liquid electrolyte through the pores present in the nanocrystalline ZnO film in a conventionally prepared DSSC, a thin and compact layer of ZnO was employed as shown in Fig. 5.12. From Table 5.1 it can be observed that the addition of a compact ZnO blocking layer in DSSC7 with 8 mM CDCA additive shows a remarkable enhancement in J_{sc} (3.09 mA/cm^2) and V_{oc} (0.66 V) and consequently the highest value of photoconversion efficiency η (1.22 %) was obtained among all the fabricated cells. Such type of performance enhancement may be accredited to the consolidated effect of improved dye loading due to the addition of CDCA with proper concentration and increased charge collection along with decreased electron recombination at the FTO/ZnO/electrolyte interface hindering the direct contact between FTO and electrolyte by the blocking layer.

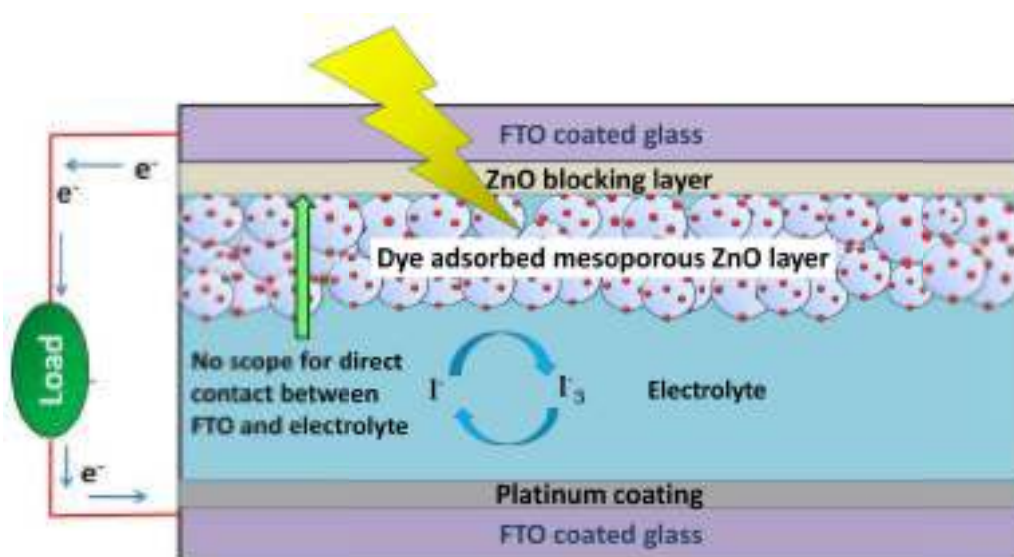


Figure 5.12 Schematic diagram of a DSSC with compact ZnO blocking layer.

5.3.7. Dark current measurement

To explore the effect of CDCA concentration and ZnO blocking layer in the process of electron back transfer, the J-V characteristics were also

measured in the dark which is shown in Fig. 5.11(b). It is regarded as a qualitative method to assess the degree of electron back transfer in DSSCs. The dark current generation is known to be partly due to the presence of exposed FTO sites having direct contact with the liquid electrolyte and the pores left between the ZnO nanoparticles and the FTO surface [41,42]. These exposed FTO sites and the pores of ZnO nanoparticle film would allow the liquid electrolyte to penetrate through ZnO film and directly come in contact with bare FTO sites resulting in recombination losses as shown in the energy band diagram for conventional ZnO NP based DSSC in Fig. 5.13(a). It can be observed from Fig. 5.11(b) that for a particular value of the voltage on the X-axis (i.e. voltage axis) of the dark current characteristics, the corresponding Y-axis value (i.e. value of dark current) is lowest for DSSC7 for that particular voltage. It can also be seen that the dark current has the highest value for conventionally prepared cell (DSSC1) with bare FTO and decreases with an increase in CDCA concentration up to 8 mM. An enlarged plot of the dark current characteristics is provided as an inset in Fig. 5.11(b) so that a clear scenario is observed. For the cell (DSSC7) with compact ZnO BL and 8 mM CDCA solution as dye co-adsorbent, the dark current is reduced significantly for the same bias potential in comparison to all other cells. This demonstrates that the compact ZnO BL reduces the bare FTO site and thereby successfully suppresses the dark current by lowering the electron back transfer. It was also observed that the DSSC7 has the slowest rate of increase of dark current with an increase in bias voltage confirming excellent suppression of electron recombination and consequently reduced current loss.

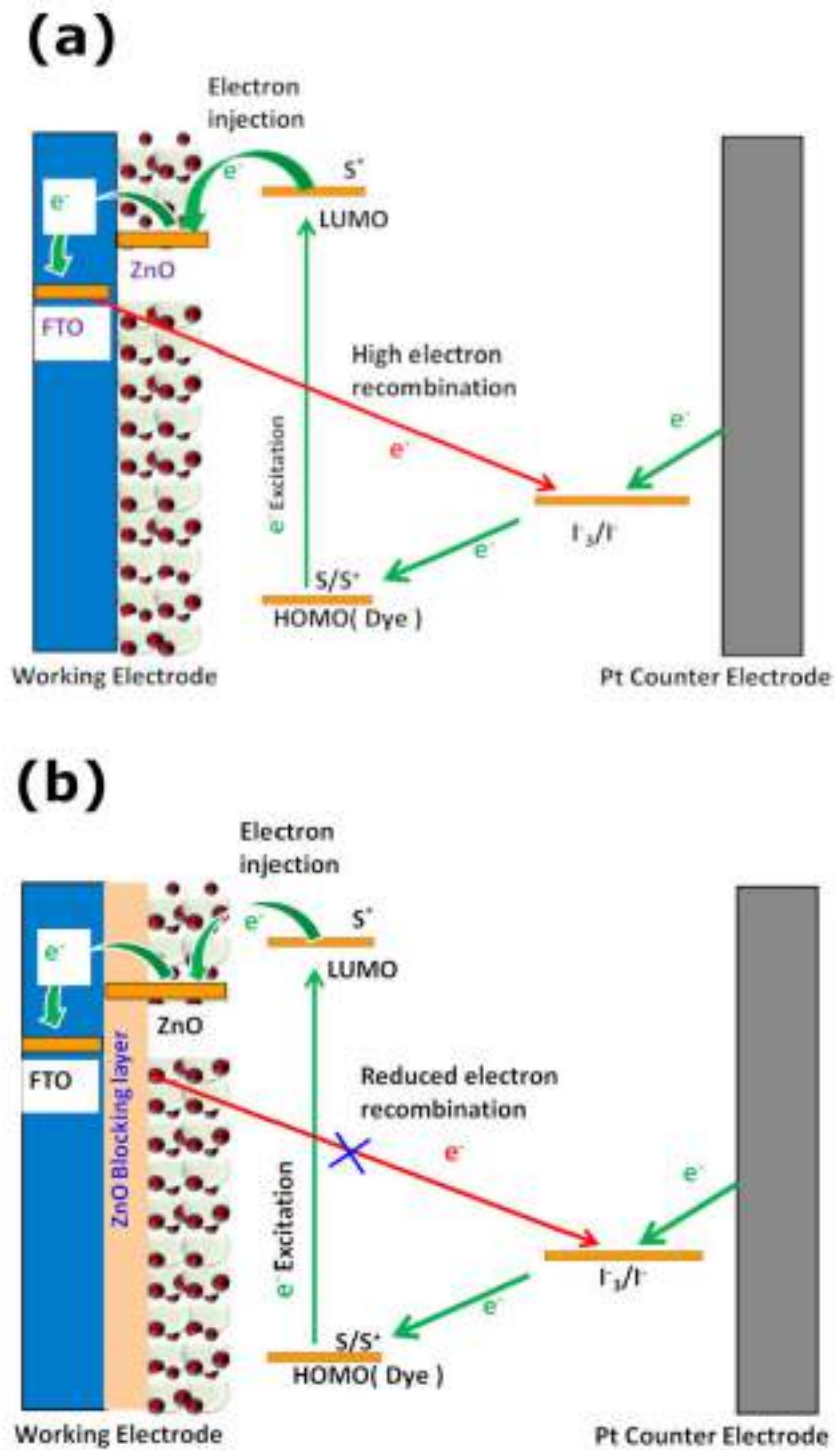


Figure 5.13 Schematic diagram showing interfacial charge transfer and recombination in case of DSSCs (a) without ZnO BL (b) with compact ZnO BL.

The variations of different cell parameters with the concentration of CDCA solution for the fabricated DSSCs are depicted in Fig. 5.14. It can be observed that CDCA concentration highly influences the value of J_{sc} . ZnO BL improves the current further. A small increase in the values of V_{oc} and FF can also be noted from Fig. 5.11 due to these processes. The highest values of cell parameters were obtained for the cell DSSC7.

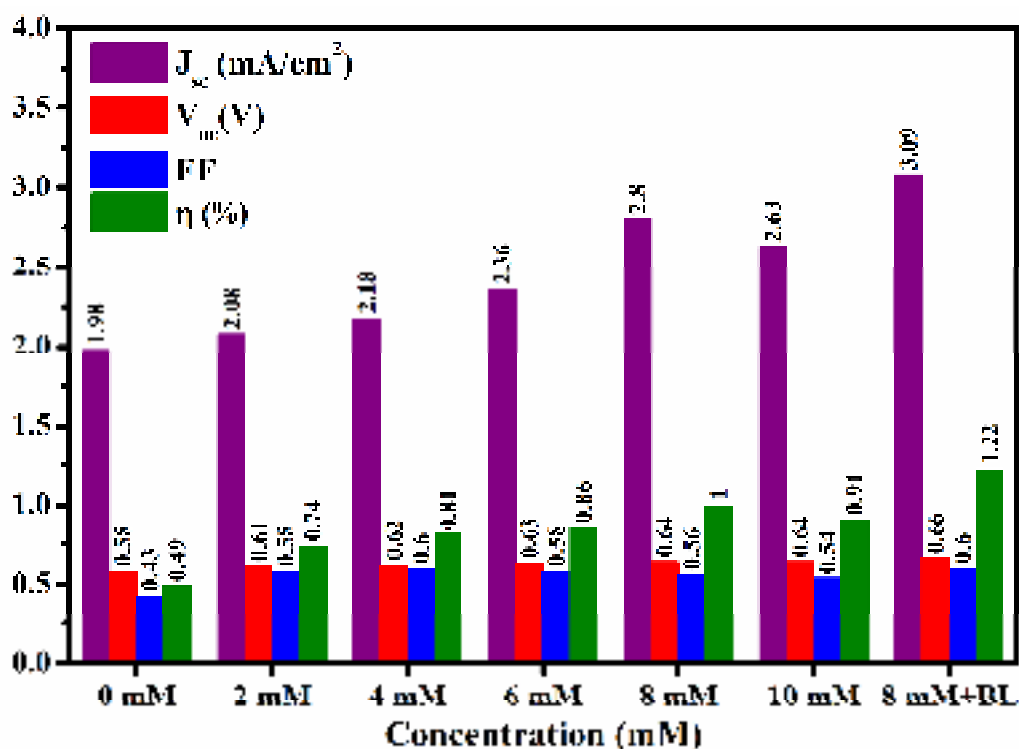


Figure 5.14 Effect of CDCA concentration and ZnO blocking layer (BL) on different cell parameters.

5.3.8. Electrochemical impedance spectroscopy study

To further gain an insight into the influence of CDCA concentration and the coating of compact ZnO blocking layer on the charge transfer and recombination kinetics of the prepared devices, the DSSCs were further investigated by electrochemical impedance spectroscopic (EIS) measurement in dark under V_{oc} bias voltage with 10 mV AC perturbation amplitude. This

gives a more precise understanding of the limiting factors for the cell performance parameters. In the EIS measurement done under the dark condition and with an applied bias voltage, electrons from FTO are injected into the conduction band of ZnO and then transported through the ZnO network. Some of the injected electrons recombine with the I_3^- ion present in the electrolyte giving rise to the recombination phenomenon [56]. Fig. 5.14(a) shows the Nyquist plot of all the prepared cells exhibiting two obvious semicircles. The curves are fitted using the equivalent circuit shown in the inset of Fig. 5.15(a) and the EIS measurement results obtained in terms of resistances and capacitances are summarized in Table 5.2. The charge transfer resistance (R_{pt}) and double layer capacitance (C_{pt}) at the Pt counter electrode/electrolyte interface is responsible for the first semicircle in the high-frequency range, while the second semicircle in the mid-frequency range may be assigned to the charge transfer and recombination resistance (R_{rec}) and chemical capacitance (C) at the ZnO/dye/electrolyte interface [36,57,58]. The intercept at the real axis of the Nyquist plot represents the series resistance (R_s) of FTO and other ohmic contacts like connecting cables, clamps and clips used to connect the cells for measurement. [59,60].

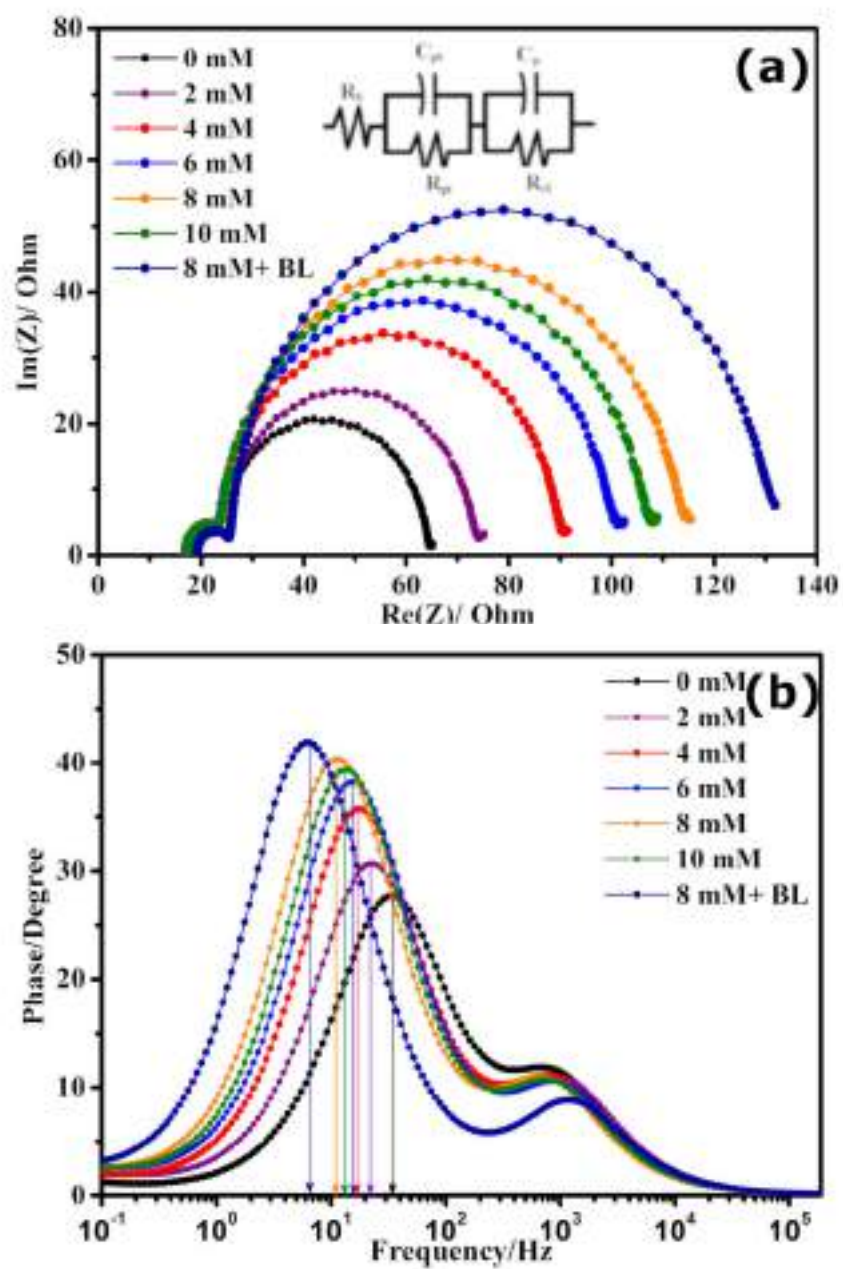


Figure 5.15 EIS of the DSSCs representing (a) Nyquist plot along with equivalent circuit (inset) and (b) Bode plot.

Table 5.2 Summary of EIS measurement.

Cell name	CDCA concentration	R_s (Ω)	R_{pt} (Ω)	R_{rec} (Ω)	Peak freq. f(Hz)	Electron lifetime (τ_e) (ms)
DSSC1	0 mM	17.15	6.51	40.2	34.21	4.65
DSSC2	2 mM	17.23	6.55	48.8	22.13	7.19
DSSC3	4 mM	17.05	6.46	65.4	17.05	9.34
DSSC4	6 mM	17.12	6.23	75.2	15.62	10.94
DSSC5	8 mM	17.36	6.65	87.6	11.03	14.45
DSSC6	10 mM	17.29	6.37	81.4	13.13	12.13
DSSC7	8 mM + BL	19.23	6.39	102.7	6.54	24.35

The small semicircles in the high-frequency range are almost identical indicating nearly similar values of R_{pt} for all four kinds of cells as all of them have similar Pt counter electrodes and the same electrolyte. On the contrary, a substantial dissimilarity can be observed in large semicircles in the mid-frequency range. This indicates that the charge transport and recombination behaviour at the ZnO/dye/electrolyte interface was extensively affected due to working electrode modification by the addition of CDCA and incorporation of the blocking layer. The middle arc of the Nyquist plot for the conventionally prepared DSSC has the lowest diameter indicating the lowest recombination resistance (R_{rec}) and thus representing the highest recombination process among all the cells. The diameter is evidently larger for the CDCA treated cells indicating its positive role in increasing the recombination resistance and hence lowering the recombination phenomena. It can be observed from Table 5.2 that the recombination resistance increases in the order of DSSC1 < DSSC2 <

DSSC3 < DSSC4 < DSSC6 < DSSC5 < DSSC7 indicating that the recombination resistance increases with an increase in CDCA concentration from 0 to 8 mM and decreases at 10 mM concentration. The larger R_{rec} value indicates it is more difficult to transfer the injected electrons from the ZnO back to the electrolyte, and thus the back recombination can be suppressed in the cell, thus giving a higher J_{sc} and V_{oc} . The highest value of recombination resistance is obtained when the optimum CDCA concentration (8 mM) is combined with the ZnO blocking layer in DSSC7 leading to the highest J_{sc} and V_{oc} of 3.09 mA/cm² and 0.66 V respectively and consequently best device performance. The highest recombination resistance is obtained for the cell with the blocking layer as the blocking layer prevents the injected electrons to come in direct contact with the electrolyte and consequently reduces the direct capture of electrons by the I_3^- ions of the electrolyte. Furthermore, the CDCA addition with optimum concentration and blocking layer increases the number of electrons accumulated in the conduction band of ZnO which led to increased electron density. This creates a small shift of Fermi level for the electrons present in the ZnO. This rise in Fermi level slightly improves V_{oc} which can also be observed from Table 5.1 [36,61].

Apart from recombination resistance, the second semicircle also provides information about the electron lifetime in the conduction band of ZnO which gives the measure of the rate at which the recombination reaction occurs. This lifetime is inversely proportional to the oscillation frequency at which the peak on the second arc is obtained. But, since, the frequency information is missing in the Nyquist plot; the electron lifetime can be calculated from the phase bode plot using the formula

$$\tau_e = \frac{1}{2\pi f_{peak}} \quad (4)$$

where f_{peak} represents the peak frequency of phase Bode plot in the mid-frequency range as shown in Fig. 5.15(b). A shift in the peaks may be observed in the Bode plots of the DSSCs prepared following different procedures. Shifting of peak frequency towards lower frequency represents longer electron lifetime (τ_e) and slower recombination process. The calculated electron lifetimes for all the cells are summarised in Table 5.2. The highest electron lifetime of 24.35 ms is obtained for the cell fabricated with 8 mM CDCA concentration along with ZnO compact blocking layer (DSSC 7). The increased electron lifetime due to CDCA and blocking layer effectively enhances the photoconversion efficiency (PCE) which is in good agreement with the results obtained from J-V measurement. The reduced dye aggregation in presence of CDCA and inhibition of electron recombination by the blocking layer may be accounted for this.

5.4. Conclusion

Effects of co-adsorption of CDCA and ZnO blocking layer were investigated in Rose Bengal dye based DSSCs. The surface, photovoltaic and electrochemical properties of all the cells were extensively studied. The strong binding of CDCA molecules to the ZnO surface partially displaces dye molecules and consequently reduces photon harvesting. Excessive CDCA concentration implies significantly reduced dye attachment to the ZnO surface leading to decreased amount of light energy absorption. Therefore, to maximize the positive effect of the co-adsorbent, it is very crucial to carefully optimize the amount of CDCA. The amount of CDCA has been optimized by adjusting its concentration in the dye solution and found that the best device performance was obtained for 8 mM concentration. At optimized co-adsorbent concentration, the reduced dye loading due to the presence of CDCA and consequently decreased light-harvesting was compensated by the increased electron injection efficiency leading to maximum device efficiency of 1 %. The performance was further increased from 1.00 % to 1.22 % when a compact

ZnO blocking layer was added to the FTO before depositing the mesoporous ZnO active layer. This was due to the suppression of electron back transfer from the FTO to the liquid electrolyte. These results indicate that the addition of CDCA as a dye co-adsorbent and the introduction of ZnO blocking layer is an effective way to boost the performance of Rose Bengal dye based DSSCs. The efficiency of the fabricated cells is low as the dye used in this study is rose bengal. Though the efficiency is low here compared to the ruthenium based cells, it lies in the range of efficiency of rose bengal dye based DSSCs obtained by other researchers. Higher efficiencies can be obtained by using high performance ruthenium dye.

References:

- [1] Bach, W.: Global warming: the complete briefing (2nd ed). John Houghton. Cambridge University Press: Cambridge, 1997. Pp. xv + 251. Paperback: ISBN 0521-62932-2, ??12.95; hardback: ISBN 0-321-62089-9, ??35.00. Int. J. Climatol. (1998). [https://doi.org/10.1002/\(sici\)1097-0088\(199804\)18:5<579::aid-joc278>3.3.co;2-0](https://doi.org/10.1002/(sici)1097-0088(199804)18:5<579::aid-joc278>3.3.co;2-0)
- [2] Meadows, D.H., Meadows, D.L., Randers, J., Behrens, W.: The Limits to Growth - Club of Rome. (1972). <http://www.donellameadows.org/wp-content/userfiles/Limits-to-Growth-digital-scan-version.pdf>
- [3] Hosenuzzaman, M., Rahim, N.A., Selvaraj, J., Hasanuzzaman, M., Malek, A.B.M.A., Nahar, A.: Global prospects, progress, policies, and environmental impact of solar photovoltaic power generation, 41, 284-297 (2015). <https://doi.org/10.1016/j.rser.2014.08.046>
- [4] Barbir, F., Veziroğlu, T.N., Plass, H.J.: Environmental damage due to fossil fuels use. Int. J. Hydrogen Energy. 15(10), 739-749 (1990). [https://doi.org/10.1016/0360-3199\(90\)90005-J](https://doi.org/10.1016/0360-3199(90)90005-J)
- [5] Goetzberger, A., Hebling, C., Schock, H.W.: Photovoltaic materials, history, status and outlook. Materials Science and Engineering: R: Reports. 40(1), 1-46 (2003). [https://doi.org/10.1016/S0927-796X\(02\)00092-X](https://doi.org/10.1016/S0927-796X(02)00092-X).
- [6] Alharbi, F., Bass, J.D., Salhi, A., Alyamani, A., Kim, H.C., Miller, R.D.: Abundant non-toxic materials for thin film solar cells: Alternative to conventional materials. Renew. Energy. 36, 2753–2758 (2011).
- [7] Lee, T.D., Ebong, A.U.: A review of thin film solar cell technologies and challenges, 70, 1286–1297 (2017). <https://doi.org/10.1016/j.rser.2016.12.028>
- [8] Yamamoto, K., Yoshimi, M., Tawada, Y., Okamoto, Y., Nakajima, A.: Cost effective and high-performance thin film Si solar cell towards the 21st century. Sol. Energy Mater. Sol. Cells. 66, 117–125 (2001).

-
-
- [https://doi.org/10.1016/S0927-0248\(00\)00164-1](https://doi.org/10.1016/S0927-0248(00)00164-1)
- [9] O'Regan, B., Grätzel, M.: A low-cost, high-efficiency solar cell based on dye-sensitized colloidal TiO₂ films. *Nature*. 353(6346), 737-740 (1991). <https://doi.org/10.1038/353737a0>
- [10] Chiba, Y., Islam, A., Komiya, R., Koide, N., Han, L.: Conversion efficiency of 10.8% by a dye-sensitized solar cell using a TiO₂ electrode with high haze. *Appl. Phys. Lett.* 88, 223505 (2006). <https://doi.org/10.1063/1.2208920>
- [11] Grätzel, M.: Solar energy conversion by dye-sensitized photovoltaic cells. *Inorg. Chem.* 44(20), 6841-6851 (2005). <https://doi.org/10.1021/ic0508371>
- [12] Chung, I., Lee, B., He, J., Chang, R.P.H., Kanatzidis, M.G.: All-solid-state dye-sensitized solar cells with high efficiency. *Nature*. 485(7399), 486-489 (2012). <https://doi.org/10.1038/nature11067>
- [13] Cai, N., Moon, S.J., Cevcey-Ha, L., Moehl, T., Humphry-Baker, R., Wang, P., Zakeeruddin, S.M., Grätzel, M.: An organic D- π -A dye for record efficiency solid-state sensitized heterojunction solar cells. *Nano Lett.* 11(4), 1452-1456 (2011). <https://doi.org/10.1021/nl104034e>
- [14] Grätzel, M.: Dye-sensitized solar cells, *J. Photochem. Photobiol. C Photochem. Rev.* 4(2), 145-153 (2003). [https://doi.org/10.1016/S1389-5567\(03\)00026-1](https://doi.org/10.1016/S1389-5567(03)00026-1).
- [15] Shao, F., Sun, J., Gao, L., Yang, S., Luo, J.: Growth of various TiO₂ nanostructures for dye-sensitized solar cells. *J. Phys. Chem. C.* 115(5), 1819-1823 (2011). <https://doi.org/10.1021/jp110743m>
- [16] Tiwana, P., Docampo, P., Johnston, M.B., Snaith, H.J., Herz, L.M.: Electron mobility and injection dynamics in mesoporous ZnO, SnO₂, and TiO₂ films used in dye-sensitized solar cells. *ACS Nano*. 5(6), 5158-5166 (2011). <https://doi.org/10.1021/nn201243y>
- [17] Biswas, R., Chatterjee, S.: Effect of surface modification via sol-gel
-
-

-
-
- spin coating of ZnO nanoparticles on the performance of WO₃ photoanode based dye sensitized solar cells. *Optik (Stuttg)*. 212, 164142 (2020). <https://doi.org/10.1016/j.ijleo.2019.164142>
- [18] Zhang, Q., Dandeneau, C.S., Zhou, X., Cao, C.: ZnO nanostructures for dye-sensitized solar cells, 21(41), 4087-4108 (2009). <https://doi.org/10.1002/adma.200803827>
- [19] Guillén, E., Peter, L.M., Anta, J.A.: Electron transport and recombination in ZnO-based dye-sensitized solar cells. *J. Phys. Chem. C*. 115(45), 22622-22632 (2011). <https://doi.org/10.1021/jp206698t>
- [20] Quintana, M., Edvinsson, T., Hagfeldt, A., Boschloo, G.: Comparison of dye-sensitized ZnO and TiO₂ solar cells: Studies of charge transport and carrier lifetime. *J. Phys. Chem. C*. 111(2), 1035-1041. (2007). <https://doi.org/10.1021/jp065948f>
- [21] Vittal, R., Ho, K.C.: Zinc oxide based dye-sensitized solar cells: A review. *Renew. Sustain. Energy Rev.* 70, 920-935 (2017). <https://doi.org/10.1016/j.rser.2016.11.273>
- [22] Biswas, R., Roy, T., Chatterjee, S.: Study of Electro-Optical Performance and Interfacial Charge Transfer Dynamics of Dye Sensitized Solar Cells Based on ZnO Nanostructures and Natural Dyes. *J. Nanoelectron. Optoelectron.* 14(1), 99-108 (2019). <https://doi.org/10.1166/jno.2019.2445>
- [23] Ito, S., Nazeeruddin, M.K., Liska, P., Comte, P., Charvet, R., Péchy, P., Jirousek, M., Kay, A., Zakeeruddin, S.M. and Grätzel, M.: Photovoltaic characterization of dye-sensitized solar cells: effect of device masking on conversion efficiency. *Progress in photovoltaics: research and applications*, 14(7), pp.589-601 (2006). <https://doi.org/10.1002/pip.683>
- [24] Aghazada, S. and Nazeeruddin, M.K.: Ruthenium complexes as sensitizers in dye-sensitized solar cells. *Inorganics*, 6(2), p.52 (2018). <https://doi.org/10.3390/inorganics6020052>
-
-

-
-
- [25] Nazeeruddin, M.K., Baranoff, E. and Grätzel, M.: Dye-sensitized solar cells: a brief overview. *Solar energy*, 85(6), pp.1172-1178 (2011).
<https://doi.org/10.1016/j.solener.2011.01.018>
- [26] Sayyed, S.A., Beedri, N.I., Kadam, V.S. and Pathan, H.M.: Rose Bengal sensitized bilayered photoanode of nano-crystalline TiO₂-CeO₂ for dye-sensitized solar cell application. *Applied Nanoscience*, 6(6), pp.875-881 (2016). <https://doi.org/10.1007/s13204-015-0495-6>
- [27] Pradhan, B., Batabyal, S.K. and Pal, A.J.: Vertically aligned ZnO nanowire arrays in Rose Bengal-based dye-sensitized solar cells. *Solar energy materials and solar cells*, 91(9), pp.769-773 (2007).
<https://doi.org/10.1016/j.solmat.2007.01.006>
- [28] Duffy, N.W., Peter, L.M., Rajapakse, R.M.G. and Wijayantha, K.G.U.: Investigation of the kinetics of the back reaction of electrons with triiodide in dye-sensitized nanocrystalline photovoltaic cells. *The Journal of Physical Chemistry B*, 104(38), pp.8916-8919 (2000).
<https://doi.org/10.1021/jp001185z>
- [29] Rani, S., Shishodia, P.K. and Mehra, R.M.: Enhancement of photovoltaic performance of quasi-solid state dye sensitized solar cell with dispersion of a hole conducting agent. *Materials Science-Poland*, 28(1), p.281 (2010).
- [30] Kim, H., Veerappan, G., & Park, J. H.: Conducting polymer coated non-woven graphite fiber film for dye-sensitized solar cells: superior Pt-and FTO-free counter electrodes. *Electrochimica Acta*, 137, 164-168(2014).
<https://doi.org/10.1016/j.electacta.2014.06.012>
- [31] Patwari, J., Sardar, S., Liu, B., Lemmens, P., & Pal, S. K.: Three-in-one approach towards efficient organic dye-sensitized solar cells: aggregation suppression, panchromatic absorption and resonance energy transfer. *Beilstein journal of nanotechnology*, 8(1), 1705-1713(2017).
<https://doi.org/10.3762/bjnano.8.171>
-
-

-
-
- [32] Zhang, L., Cole, J.M.: Dye aggregation in dye-sensitized solar cells. *J. Mater. Chem. A*. 5(37), 19541-19559 (2017). <https://doi.org/10.1039/c7ta05632j>
- [33] Buene, A.F., Almenningen, D.M., Hagfeldt, A., Gautun, O.R., Hoff, B.H.: First Report of Chenodeoxycholic Acid-Substituted Dyes Improving the Dye Monolayer Quality in Dye-Sensitized Solar Cells. *Sol. RRL*. 4(4), 1900569 (2020). <https://doi.org/10.1002/solr.201900569>
- [34] Kumar, V., Gupta, R., Bansal, A.: Role of chenodeoxycholic acid as co-additive in improving the efficiency of DSSCs. *Sol. Energy*. 196, 589-596 (2020). <https://doi.org/10.1016/j.solener.2019.12.034>
- [35] Ismail, M., Ahmad Ludin, N., Hisham Hamid, N., Adib Ibrahim, M., Sopian, K.: The Effect of Chenodeoxycholic Acid (CDCA) in Mangosteen (*Garcinia mangostana*) Pericarps Sensitizer for Dye-Sensitized Solar Cell (DSSC). In: *Journal of Physics: Conference Series*. Vol. 1083, No. 1, p. 012018 (2018). doi :10.1088/1742-6596/1083/1/012018
- [36] Li, J., Wu, W., Yang, J., Tang, J., Long, Y., Hua, J.: Effect of chenodeoxycholic acid (CDCA) additive on phenothiazine dyes sensitized photovoltaic performance. *Sci. China Chem.* 54(4), 699-706 (2011). <https://doi.org/10.1007/s11426-011-4227-9>
- [37] Inoue, T., Pandey, S. S., Fujikawa, N., Yamaguchi, Y., & Hayase, S.: Synthesis and characterization of squaric acid based NIR dyes for their application towards dye-sensitized solar cells. *Journal of Photochemistry and Photobiology A: Chemistry*, 213(1), 23-29(2010). <https://doi.org/10.1016/j.jphotochem.2010.04.015>
- [38] Lee, K. M., Suryanarayanan, V., Ho, K. C., Thomas, K. J., & Lin, J. T.: Effects of co-adsorbate and additive on the performance of dye-sensitized solar cells: A photophysical study. *Solar energy materials and*
-
-

-
-
- solar cells, 91(15-16), 1426-1431(2007).
<https://doi.org/10.1016/j.solmat.2007.03.009>
- [39] Yum, J. H., Jang, S. R., Humphry-Baker, R., Grätzel, M., Cid, J. J., Torres, T., & Nazeeruddin, M. K.: Effect of coadsorbent on the photovoltaic performance of zinc phthalocyanine-sensitized solar cells. *Langmuir*, 24(10), 5636-5640(2008). <https://doi.org/10.1021/la800087q>
- [40] Lu, H. P., Tsai, C. Y., Yen, W. N., Hsieh, C. P., Lee, C. W., Yeh, C. Y., & Diau, E. W. G.: Control of dye aggregation and electron injection for highly efficient porphyrin sensitizers adsorbed on semiconductor films with varying ratios of coadsorbate. *The Journal of Physical Chemistry C*, 113(49), 20990-20997(2009). <https://doi.org/10.1021/jp908100v>
- [41] Yang, Y., Peng, X., Chen, S., Lin, L., Zhang, B., Feng, Y.: Performance improvement of dye-sensitized solar cells by introducing a hierarchical compact layer involving ZnO and TiO₂ blocking films. *Ceram. Int.* 40(9), 15199-15206 (2014).
<https://doi.org/10.1016/j.ceramint.2014.07.001>
- [42] Yeoh, M.E., Chan, K.Y.: Efficiency Enhancement in Dye-Sensitized Solar Cells with ZnO and TiO₂ Blocking Layers. *J. Electron. Mater.* 48(7), 4342-4350 (2019). <https://doi.org/10.1007/s11664-019-07207-5>
- [43] Wong, K.K., Ng, A., Chen, X.Y., Ng, Y.H., Leung, Y.H., Ho, K.H., Djurišić, A.B., Ng, A.M.C., Chan, W.K., Yu, L., Phillips, D.L.: Effect of ZnO nanoparticle properties on dye-sensitized solar cell performance. *ACS Appl. Mater. Interfaces.* 4(3), 1254-1261 (2012).
<https://doi.org/10.1021/am201424d>
- [44] Elilarassi, R., Chandrasekaran, G.: Effect of annealing on structural and optical properties of zinc oxide films. *Mater. Chem. Phys.* 121(1-2), 378-384 (2010). <https://doi.org/10.1016/j.matchemphys.2010.01.053>
- [45] Shivaraj, B.W., Murthy, H.N.N., Krishna, M., Satyanarayana, B.S.: Effect of Annealing Temperature on Structural and Optical Properties of
-
-

-
-
- Dip and Spin coated ZnO Thin Films. *Procedia Mater. Sci.* 10, 292-300 (2015). <https://doi.org/10.1016/j.mspro.2015.06.053>
- [46] Al-Kahlout, A.: Thermal treatment optimization of ZnO nanoparticles-photoelectrodes for high photovoltaic performance of dye-sensitized solar cells. *J. Assoc. Arab Univ. Basic Appl. Sci.* 17(1), 66-72. (2015). <https://doi.org/10.1016/j.jaubas.2014.02.004>
- [47] Pandey, P., Parra, M.R., Haque, F.Z., Kurchania, R.: Effects of annealing temperature optimization on the efficiency of ZnO nanoparticles photoanode based dye sensitized solar cells. *J. Mater. Sci. Mater. Electron.* 28(2), 1537-1545 (2017). <https://doi.org/10.1007/s10854-016-5693-9>
- [48] AR SAYYED, S.A., Beedri, N.I., Kadam, V.S. and Pathan, H.M.: Rose bengal-sensitized nanocrystalline ceria photoanode for dye-sensitized solar cell application. *Bulletin of Materials Science*, 39(6), pp.1381-1387(2016). <https://doi.org/10.1007/s12034-016-1279-7>
- [49] Ossai, A. N., Alabi, A. B., Ezike, S. C., & Aina, A. O. :Zinc oxide-based dye-sensitized solar cells using natural and synthetic sensitizers. *Current Research in Green and Sustainable Chemistry*, 3, 100043(2020). <https://doi.org/10.1016/j.crgsc.2020.100043>
- [50] Henson, Z.B., Zhang, Y., Nguyen, T.Q., Seo, J.H. and Bazan, G.C.: Synthesis and properties of two cationic narrow band gap conjugated polyelectrolytes. *Journal of the American Chemical Society*, 135(11), pp.4163-4166 (2013). <https://doi.org/10.1021/ja400140d>
- [51] Seo, D.K. and Hoffmann, R.: Direct and indirect band gap types in one-dimensional conjugated or stacked organic materials. *Theoretical Chemistry Accounts*, 102(1), pp.23-32 (1999). <https://doi.org/10.1007/s002140050469>
- [52] Nguyen, W.H., Bailie, C.D., Burschka, J., Moehl, T., Grätzel, M., McGehee, M.D. and Sellinger, A.: Molecular engineering of organic
-
-

-
-
- dyes for improved recombination lifetime in solid-state dye-sensitized solar cells. *Chemistry of Materials*, 25(9), pp.1519-1525 (2013).
<https://doi.org/10.1021/cm3036357>
- [53] Prima, E.C., Al Qibtiya, M., Yulianto, B. and Dipojono, H.K.: Influence of anthocyanin co-pigment on electron transport and performance in black rice dye-sensitized solar cell. *Ionics*, 22(9), pp.1687-1697 (2016).
<https://doi.org/10.1007/s11581-016-1673-6>
- [54] Costantino, U., Marmottini, F., Nocchetti, M., Vivani, R.: New synthetic routes to hydrotalcite-like compounds - Characterisation and properties of the obtained materials. *Eur. J. Inorg. Chem.* 1998(10), 1439-1446 (1998).
[https://doi.org/10.1002/\(sici\)1099-0682\(199810\)1998:10<1439::aid-ejic1439>3.0.co;2-1](https://doi.org/10.1002/(sici)1099-0682(199810)1998:10<1439::aid-ejic1439>3.0.co;2-1)
- [55] Oh, J.M., Hwang, S.H., Choy, J.H.: The effect of synthetic conditions on tailoring the size of hydrotalcite particles. In: *Solid State Ionics* (2002)
- [56] Liu, X., Zhang, Q., Li, J., Valanoor, N., Tang, X., Cao, G.: Increase of power conversion efficiency in dye-sensitized solar cells through ferroelectric substrate induced charge transport enhancement. *Sci. Rep.* 8(1), 1-8 (2018). <https://doi.org/10.1038/s41598-018-35764-y>
- [57] Mazloum-Ardakani, M., & Arazi, R.: Improving the effective photovoltaic performance in dye-sensitized solar cells using an azobenzenecarboxylic acid-based system. *Heliyon*, 5(3), e01444(2019).
<https://doi.org/10.1016/j.heliyon.2019.e01444>
- [58] Zhao, Y., Lu, F., Zhang, J., Dong, Y., Zhang, B., & Feng, Y.: Stepwise co-sensitization of two metal-based sensitizers: probing their competitive adsorption for improving the photovoltaic performance of dye-sensitized solar cells. *RSC advances*, 7(17), 10494-10502(2017).
<https://doi.org/10.1039/C6RA28473F>
-
-

- [59] Ondersma, J.W., Hamann, T.W.: Impedance investigation of dye-sensitized solar cells employing outer-sphere redox shuttles. *J. Phys. Chem. C*. 114(1), 638-645 (2010). <https://doi.org/10.1021/jp908442p>
- [60] Chou, J.C., Lu, C.C., Liao, Y.H., Lai, C.H., Nien, Y.H., Kuo, C.H., Ko, C.C.: Fabrication and Electrochemical Impedance Analysis of Dye-Sensitized Solar Cells with Titanium Dioxide Compact Layer and Graphene Oxide Dye Absorption Layer. *IEEE Trans. Nanotechnol.* 18, 461-466 (2019). <https://doi.org/10.1109/TNANO.2019.2913537>
- [61] Wei, L., Yang, Y., Zhu, Z., Fan, R., Wang, P., Dong, Y., Chen, S.: Effect of different donor groups in bis(6-methoxypyridin-2-yl) substituted co-sensitizer on the performance of N719 sensitized solar cells. *RSC Adv.* 5(117), 96934-96944 (2015). <https://doi.org/10.1039/c5ra19417b>

Chapter 6

**Stability Enhancement of Dye-
Sensitized Solar Cells Fabricated with
Gel Electrolyte**

This page is intentionally left blank

6.1. Introduction

Due to continuously increasing energy demand, the polluting environment, and the rising price of fossil fuels, scientists are constantly thinking of new ways to find pollution-free renewable energy sources [1]. The natural resources that can renew themselves over time are called renewable energy sources [2]. It is believed that solar energy would be the main source of alternative energy [3]. Conventional Crystalline and polycrystalline silicon solar cells have attained energy conversion efficiency of over 20%, but due to their complicated and difficult fabrication process and high cost [4], people have started to think about its alternative. Grätzel and co-workers first reported DSSCs as a useful substitute for conventional solar cells [1], and subsequently, a considerable interest has been developed in DSSCs because of their easy fabrication technique and low cost [5].

Photo anode of a DSSC performs a vital role in determining the overall performance of the DSSC by transporting electrons and supporting the Dye molecules [7, 8]. The semiconducting oxide material TiO_2 is mostly used as a photoanode because of its excellent optical, electrical, and chemical properties [9-12]. Although appreciably high conversion efficiency is achieved with TiO_2 , its low electron mobility results in low electron mobility have led to renewed investigations into new alternative wide-bandgap photoanode materials like ZnO , WO_3 , and SnO_2 for better performance of Dye-sensitized solar cells [13-15]. Researchers are also using natural dyes extracted from different fruits, vegetables, and flowers in search of low-cost DSSC fabricated with environment-friendly and non-toxic material [16-20].

But the electrolyte has a close interaction with all the components of DSSC and it determines the time stability of the cell. Due to this, scientists have been paying more attention to electrolytes these days [21, 22]. Though the theoretically estimated maximum photoelectric conversion efficiency of a DSSC is 29 % [23] has been recorded with liquid electrolytes, the actual

efficiency of 14.3% could be achieved. This is due to leakage problems of liquid electrolytes, electrode corrosion, photo-degradation of attached dyes, and solvent volatility restricts the long-term performance of DSSCs [24]. To overcome these limitations, gel electrolytes have been used instead of liquid electrolytes as the volatility of organic solvents can be decreased and leakage can be prevented by gel-type electrolytes [25]. Gel electrolytes are usually prepared by adding materials of high molecular weights with organic solvents and iodides. Polyvinyl carbonate (PC), Acetonitrile (ACN), and ethylene carbonate (EC) are an example of some of the popularly used solvents and Lithium iodide (LiI), potassium iodide (KI), Sodium iodide are some of the commonly utilized iodides with iodine (I_2). For gelation of liquid electrolytes, many materials are used, namely polyethylene glycol, polyvinylidene fluoride-co-hexafluoropropylene (PVDF-HFP), polyethylene oxide, etc. [26].

In this study, we prepared gel electrolytes using ethyl cellulose (EC) as a gelator in the liquid electrolyte and fabricated DSSCs with both liquid and gel electrolytes to study to study their overall photovoltaic performance, including their performance stability over a certain period. We used both TiO_2 and ZnO as working electrode material. The effect of EC concentration on the performance of DSSCs was also examined. A detailed comparison of photoelectric properties of all the cells is presented in the investigation.

6.2. Materials and Methods

6.2.1 Materials

All the chemicals used in this study were purchased from commercial sources and used as received. Fluorine-doped tin oxide (FTO) glass slides (10 Ω /square; thickness 2.2 mm), ruthenium dye (N3 and N719), Surlyn spacer, and Platinum Precursors solution (Plastisol T) for counter electrode preparation, all were purchased from Solaronix, Switzerland. Titanium dioxide nanopowder (TiO_2), ZnO nanopowder, Lithium Iodide (LiI), and Iodine (I_2)

were purchased from Sigma-Aldrich, India. The chemicals, used in gel preparation are Acetonitrile (Merck, India), 4-tert-butylpyridine (TCI CHEMICALS, Japan), Tetrabutylammonium iodide (Merck), Ethyl Cellulose (Sigma-Aldrich, India), acetone (C_3H_6O), ethanol (C_2H_5OH), and acetic acid (CH_3CO_2H) (Sigma-Aldrich, India). All the reagents purchased were of analytical grade and were used without further purification.

6.2.2 Preparation of liquid and gel electrolyte

The liquid electrolyte, used in this study, was prepared by mixing LiI (0.5M) and I_2 (0.05M) in 10 ml acetonitrile solvent. To prepare the gel electrolyte, ethyl-cellulose powder mixed with ethanol was added to the prepared liquid electrolyte at different amounts to yield gel electrolyte of concentrations of 2, 4, 6, 8 and 10 wt%. Fig.6.1 represents different steps of electrolyte preparation.

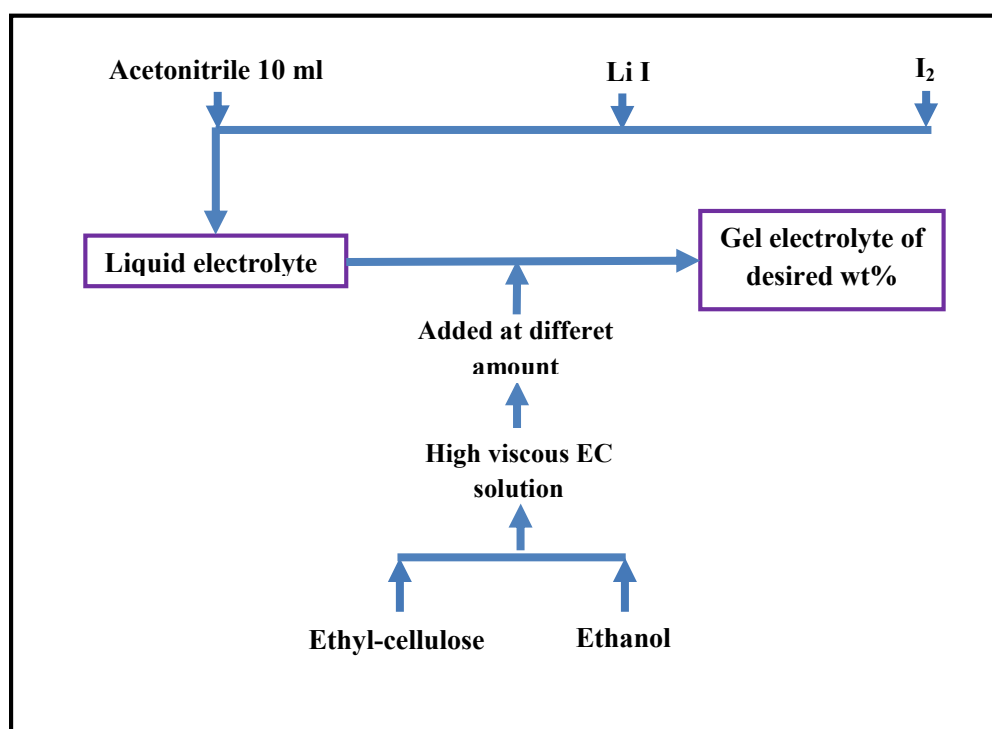


Figure 6.1 Steps of Liquid and Gel electrolyte preparation.

6.2.3 Fabrication of the solar cells

The TiO₂ and ZnO working electrodes of the DSSC were prepared by following the standard procedure [27]. At first, 10 gm of the nanopowder was mixed with diluted acetic (1ml in 50 ml deionized water) acid in a mortar and pestle and added a few drops of Triton X100 (Merck) as surfactant and ground continuously until a homogenous, smooth suspension was obtained. The lump-free slurry was then applied on the conductive side of an FTO-coated glass using the doctor blade method to make a homogeneous layer. To strengthen the bonding between the FTO glass and the semiconductor paste, the nanopowder coated FTO glass plates were sintered in normal atmospheric condition at 450°C for 45 minutes. In the sintering process, after introducing the sample in the furnace, the temperature was raised with a rate of 10°C/5 min until the temperature had reached 350°C and after that, it was increased with a rate of 10°C/10 min until 450°C. When it cooled down to room temperature, the sintered substrates were immersed in the ruthenium dye (N3) solution for dye adsorption on the surface of the TiO₂ and ZnO nanoparticles for 24 hours. FTO glass coated with a platinum catalyst (Plastisol-T) and heated at 400°C was used as a counter electrode and a sealed sandwich-type cell was fabricated by assembling dye adsorbed working electrode and the platinum (Pt) coated counter electrode with Surlyn film as a spacer between them. The electrolyte was introduced into the assembled cell through a pre-drilled hole on the counter with a syringe. Gel electrolyte having different EC concentration was used in different cells for the investigation. A small piece of Surlyn spacer and glass glue was used to seal the hole and finally, the cells were connected to the external circuit with the help of alligator clips. Different electrolyte concentrations were used to fill the cells.

6.2.4 Characterization of the DSSCs

After completing the fabrication of two different cells with liquid and gel type electrolytes, the cells were placed under artificial solar illumination of $100\text{mW}/\text{cm}^2$ and connected with the J-V measurement system to calculate the photoelectric conversion efficiencies [28]. The photocurrent voltage (J-V) characteristics were recorded using a Keithley 2400 source meter. Simulated sunlight was supplied using a xenon lamp (450W). The photovoltaic performances were recorded at a 24 hr interval to investigate the long-term stability of the DSSCs. The ethyl cellulose as gelator was selected for its easy availability and low cost. Symmetrical cells having Pt-electrolyte-Pt structure were configured to perform the EIS measurement of the electrolyte system. Pt electrodes were prepared by coating the FTO substrate using the same Pt catalyst solution as used in conventional DSSCs.

6.3 Results and Discussions

6.3.1 Raman spectroscopy of TiO_2 and ZnO

Fig. 6.2 shows the Raman spectra of TiO_2 and ZnO nanopowders. The Raman shifts of Fig. 6.2 (a) at 235, 447, and 612 cm^{-1} are attributed to the combination of two-phonon scattering modes, E_g and A_{1g} modes of the rutile phase, respectively[29, 30]. According to the literature values, all the observed spectroscopic peaks listed in Fig. 6.2 (b) can be assigned to a wurzite ZnO structure. Among these Raman peaks, the E_2 mode centred at 437 cm^{-1} has a stronger intensity and narrower line-width, which indicates that the as-grown products are composed of ZnO with a hexagonal wurtzite structure and good crystal quality [31].

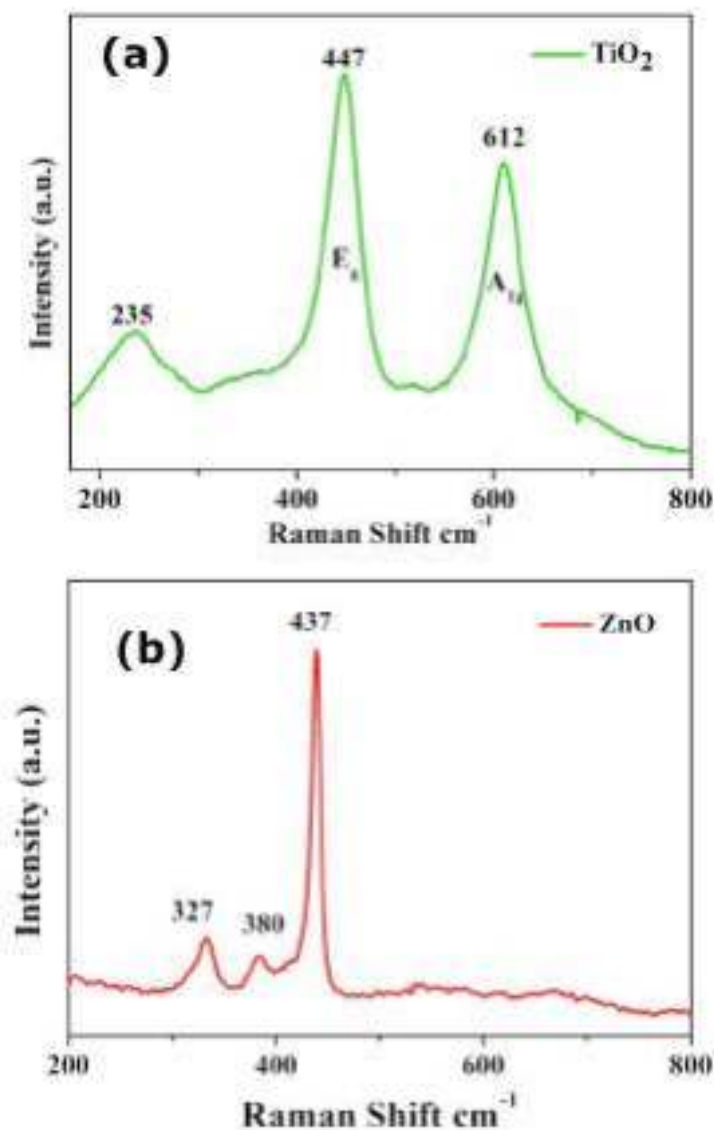


Figure 6.2 Raman spectra of (a) TiO₂ and (b) ZnO nanoparticles.

6.3.2 Scanning electron microscope (SEM) analysis

The scanning electron microscope (SEM) was used to examine the surface morphology of the photoanode films over the FTO glass substrate [29]. The highly porous morphology of the TiO₂ and ZnO nanostructure films deposited on the FTO glass substrate can be observed from the SEM images shown in Fig. 6.3(a) and Fig. 6.3(b) respectively.

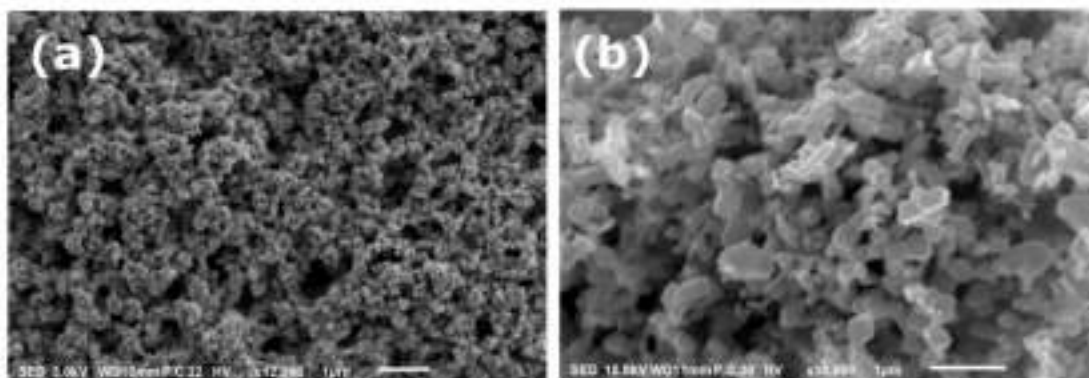


Figure 6.3 Scanning electron microscope (SEM) image of (a) TiO₂ and (b) ZnO nanoparticles.

The average particle size of the TiO₂ nanoparticles was about 20 nm while that was in a range of 40-300 nm for ZnO. The highly porous structure of the semiconductor thin film resulted in greater dye molecule adsorption on the surface of the TiO₂ and ZnO nanoparticles. Also, the smaller particle size of the TiO₂ nanoparticles compared to ZnO provides a higher overall surface area for dye molecule attachment for a particular volume of the photoanode. More dye adsorption causes more electron excitation from HOMO to LUMO of dye molecules after photon absorption [32].

6.3.3 Photovoltaic Performance of the DSSCs

The Current-Voltage (I-V) characteristics of the N719 dye and TiO₂ photoanode based DSSCs fabricated using liquid and gel-based electrolytes are shown in Fig. 6.4.

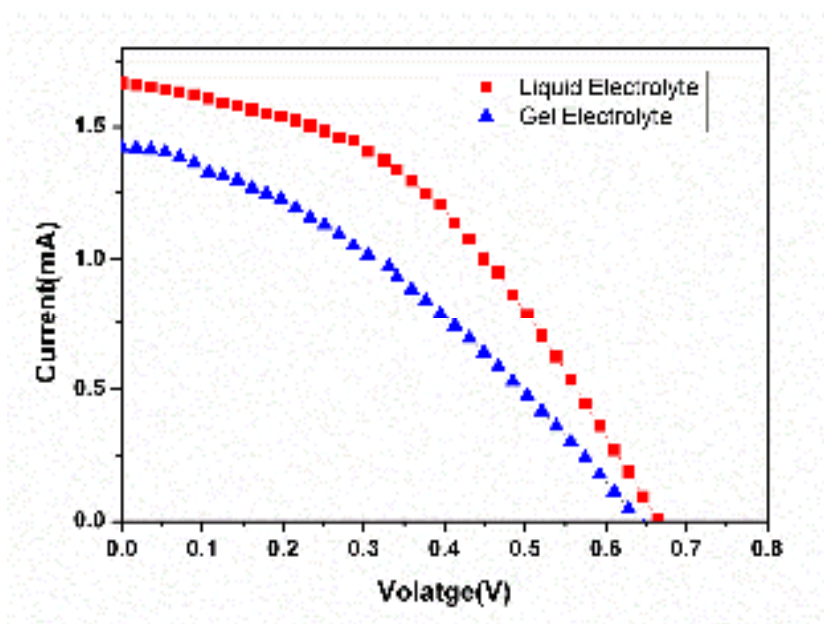


Figure 6.4 Current-Voltage characteristics of the N719 dye based cells fabricated with TiO_2 .

The different electrical parameters of the cells obtained from the I-V characteristics are listed in Table 6.1 below.

Table 6.1. Summary of photovoltaic parameters of the N719 dye based cells.

Electrolyte used	J_{sc} (mA/cm^2)	V_{oc} (V)	FF	Efficiency (η %)
Liquid	1.67	0.662	0.43	1.90
Gel	1.42	0.646	0.35	1.29

The energy conversion efficiency of gel electrolyte based DSSC was lower than liquid electrolyte based DSSC. The photovoltaic efficiency of DSSCs using liquid and gel type electrolytes is 1.90% and 1.29% respectively. Table 6.1 represents the various photovoltaic parameters extracted from the I-V curves of the cells with liquid and gel electrolytes. The solar cell fabricated using liquid electrolyte exhibits higher short-circuit photocurrent density (J_{sc}),

open-circuit voltage (V_{OC}), and fill factor (FF) compared to the DSSC fabricated using gel electrolyte as a dye.

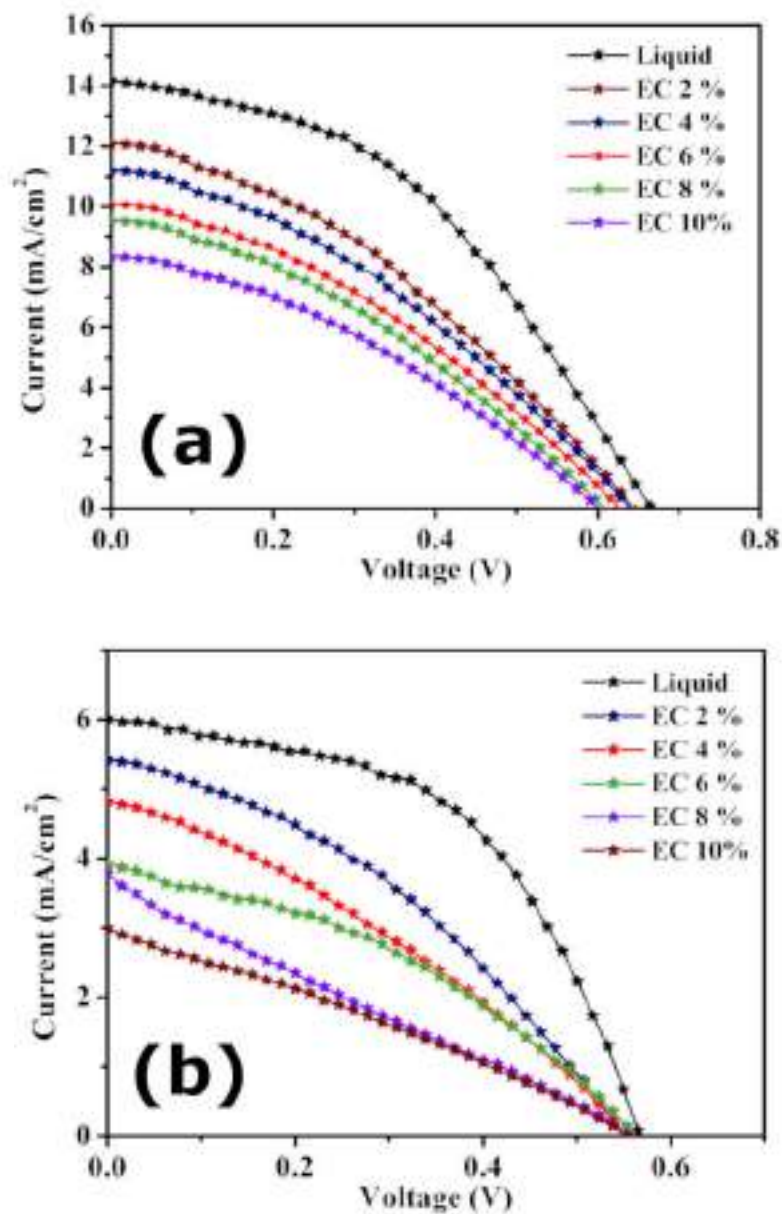


Figure 6.5 Current-Voltage characteristics of the N3 dye based cells fabricated with (a) TiO₂ (b) ZnO photoanodes.

The Current-Voltage (I-V) characteristics of the DSSCs fabricated using liquid and gel-based electrolytes are shown in Fig. 6.5. The different electrical parameters of the cells obtained from the I-V characteristics are listed in Table 6.2 below.

Table 6.2. Summary of photovoltaic parameters of the N3 dye based cells.

Cell	wt% of EC	J_{sc} (mA/cm ²)	V_{oc} (V)	FF	Efficiency (η %)
TiO ₂	0	14.16	0.66	0.43	4.01
	2	12.0	0.64	0.37	2.84
	4	11.18	0.64	0.35	2.50
	6	10.06	0.63	0.34	2.15
	8	9.51	0.61	0.34	1.97
	10	8.33	0.60	0.34	1.70
ZnO	0	6.01	0.56	0.51	1.71
	2	5.41	0.55	0.36	1.07
	4	4.82	0.55	0.32	0.85
	6	3.91	0.56	0.36	0.79
	8	3.79	0.55	0.24	0.50
	10	2.99	0.55	0.28	0.46

It can be seen from Fig. 6.5(a) and 6.5(b) that for both TiO₂ and ZnO photoanode based DSSCs, there is a loss of device performance with an increase in EC content. This is due to increased electrolyte viscosity and decreased ionic diffusion coefficient with an increase in EC amount. The energy conversion efficiency of gel electrolyte based DSSCs was much lower than the liquid electrolyte based DSSCs in both TiO₂ and ZnO photoanode based cells. The photovoltaic efficiency of DSSCs using liquid and gel type electrolytes is 4.01 % and 2.84 % respectively for TiO₂ based cells, and

for ZnO based cells, these values are 1.71 % and 1.10 % respectively. Table 6.2 represents the various photovoltaic parameters extracted from the I-V curves of the cells with liquid and gel electrolytes. The efficiency of the gel-based DSSC for both the N719 and N3 dye may be low compared to the liquid electrolyte based DSSC, but the values of cell parameters obtained are found to be comparable to the efficiencies obtained for gel electrolyte based DSSCs [32]. For both TiO₂ and ZnO photoanodes, we had the highest efficiency in gel-based cells for 2 wt% EC concentration. The TiO₂ based devices showed better performance as compared to ZnO based devices which were quite expected.

6.3.4 Electrochemical behavior analysis of the DSSCs

Electrochemical Impedance Spectroscopy (EIS) is a very useful technique for interpreting the kinetics of charge transport processes in different layers of DSSCs [33]. To quantify the effect of EC content on the diffusion property of the electrolyte, EIS measurement was employed in Pt-electrolyte-Pt cells with an electrolyte having various content of EC in the liquid electrolyte and the obtained Nyquist plot is shown in Fig. 6.6. Generally the Nyquist plot of a Pt-electrolyte-Pt cell consists of two semicircles. First semicircle corresponding to high-frequency range represents the charge transfer resistance in the Pt-electrolyte interface, and the second semicircle in the low-frequency range represents Warburg diffusion element due to diffusion of iodide / triiodide ion in the electrolyte. An equivalent circuit shown in the inset of Fig. 6.4 is incorporated to analyze the EIS data. R_s corresponds to the series resistance of the electrical contacts and the FTO substrate present in the cell, R_{Pt} represents the resistance in the Pt counter electrode/electrolyte interface and C_{Pt} represents corresponding capacitance. W represents impedance (corresponding resistance is R_w) due to the Warburg diffusion process of I^-/I_3^- in the electrolyte [22, 33-36].

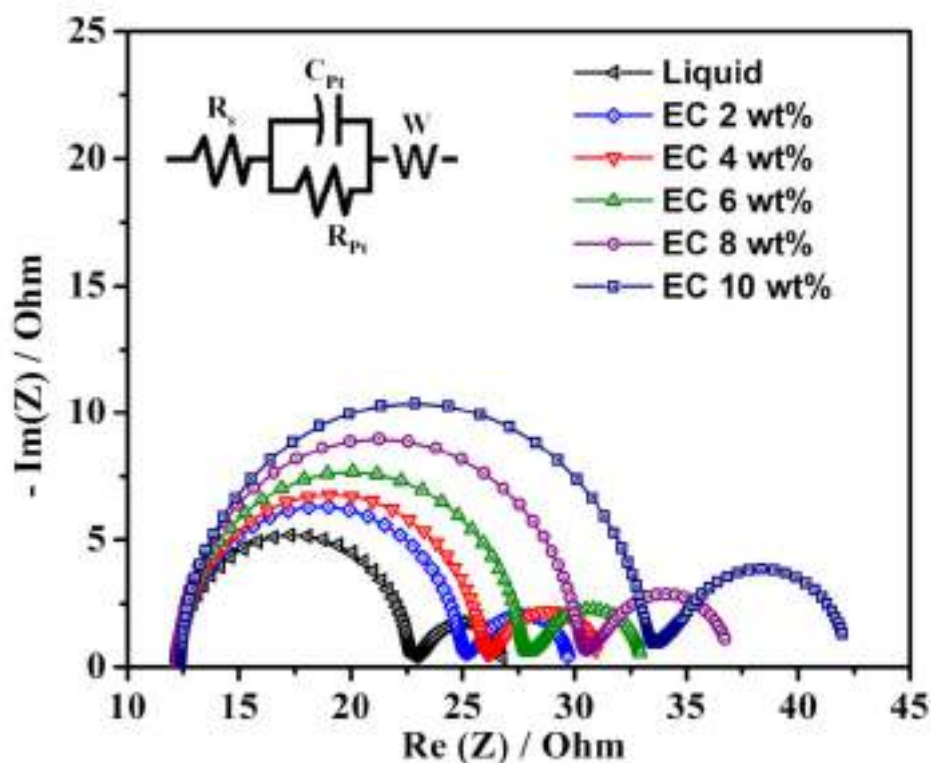


Figure 6.6 Nyquist plot of the Pt-electrolyte-potential cells with liquid and gel electrolyte with different EC content.

Different parameters extracted from Fig. 6.6 by fitting with the equivalent circuit are summarised in Table 6.3. The variations in R_{pt} and R_w are caused by the differences in conductivities in the relevant electrolytes. It can be seen that both R_{pt} and R_w is the lowest for liquid electrolyte, indicating the highest conductivity of the electrolyte [37]. Increased values of R_{pt} and R_w with increase in EC content indicates decreased conductivity and hence decreased cell performance which is in well agreement with the current-voltage measurement of both TiO_2 and ZnO cells given in Table 6.2. Increased values of diffusion resistance (R_w) with increased EC content implies decreased diffusion rate of I^- and I_3^- ions in the electrolyte and thereby slightly lowering the J_{sc} and η with an expected increase in device stability by preventing leakage of electrolyte. It also suggests that the more viscous gel electrolyte does not

affect the charge transfer process very much for EC concentration of 2 Wt% in the photoanode/electrolyte interface of the cell as compared to the liquid electrolyte.

Table 6.3. EIS measurement results of the Pt-Electrolyte-Pt cells with liquid electrolyte and gel electrolyte having different EC content.

EC Concentration	$R_s(\Omega)$	$R_{Pt}(\Omega)$	$R_w(\Omega)$
0 Wt% (Liquid)	12.25	10.30	4.25
2 Wt%	12.30	12.52	4.93
4 Wt%	12.32	13.46	5.27
6 Wt%	12.28	15.25	5.48
8 Wt%	12.25	17.83	6.85
10 Wt%	12.41	20.58	9.23

6.3.5 Stability Study of the Cells

To explore the effect of electrolytes on long-term stability, the DSSCs were characterized by performing photovoltaic measurement over time. The sealed cells were placed under 1 sun illumination and J-V measurements were recorded every day over fifteen days. The stability check was performed for both TiO_2 and ZnO DSSCs fabricated with liquid and gel electrolytes. The gel electrolyte with EC content of 2 wt% was only chosen for stability measurements and the cells with gel electrolytes having EC content of more than 2 wt% showed significantly decreased efficiency. Figure 6.7 depicts J_{sc} , V_{oc} , FF, and η over time for liquid DSSCs and gel DSSCs fabricated with both TiO_2 and ZnO as photoanode material.

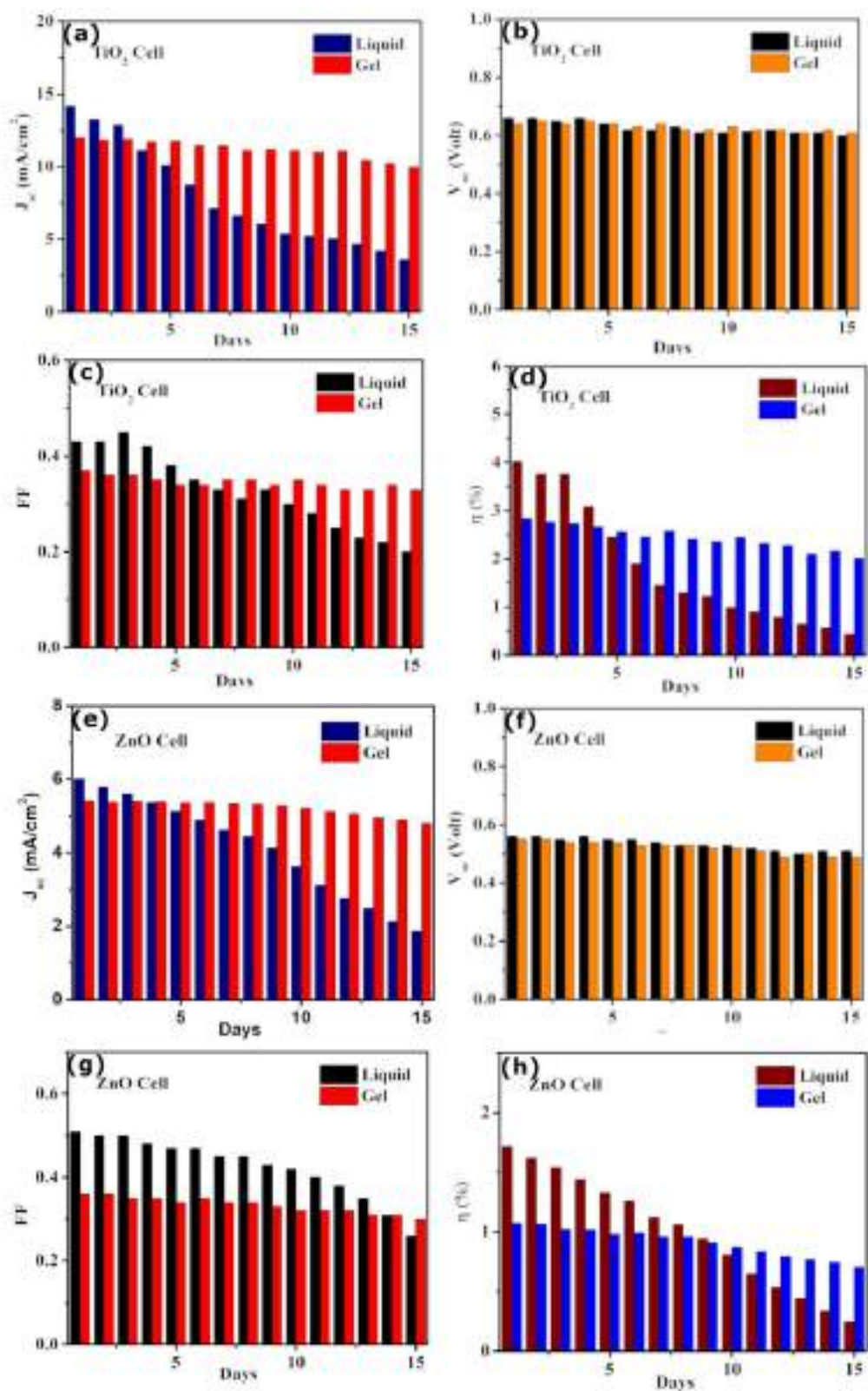


Figure 6.7 Stability behaviour of the liquid and gel based DSSCs fabricated with (a)-(d) TiO_2 and (e)-(h) ZnO as photoanode material.

It is clearly evident from Fig.6.75 that incorporating EC into the DSSC electrolyte improves device stability significantly for both types of DSSCs. V_{oc} remains almost unchanged for both liquid and gel electrolytes, whereas FF and J_{sc} decrease rapidly for liquid electrolyte-based DSSCs, but this decline is much slower for Gel electrolyte cells. Consequently, the efficiency of the gel electrolyte-based cells is well stable compared to the efficiency of liquid electrolyte-based cells, which decreases rapidly over time. It is clear that even though there is a slight decrease in the efficiency of the gel electrolytes, the cell developed with gel electrolytes shows better stability than that with liquid electrolyte. The improvement in long-term stability is probably due to the higher viscosity of gel, inhibiting the ionic migration to stabilize the system over a longer time and also by controlling the evaporation of liquid electrolytes [38]. Also, the higher stability of the gel electrolyte gives it better cost-effectiveness than the liquid electrolyte.

6.4 CONCLUSION

DSSCs were fabricated with pure TiO_2 and ZnO photoanodes with liquid and gel-type electrolyte, and cell performances were recorded. The liquid electrolyte cells exhibited higher short-circuit photocurrent density, open-circuit voltage, fill factor, and efficiency compared to the gel electrolyte based DSSCs. Though the efficiency of the gel-based DSSC is lower than the liquid electrolyte DSSC, the cell parameters obtained were comparable to the parameters obtained for gel electrolyte DSSCs by other researchers. Comparing these two types of DSSCs, it is clear that though the photovoltaic performance of gel electrolyte DSSC is slightly lower than liquid electrolyte DSSC, the performance of gel-based DSSC remains noticeably stable while for the liquid electrolyte the stability decreases remarkably over time. It is also found that the EC based gel electrolyte with proper EC wt% can be used to increase the stability of both TiO_2 and ZnO photoanode based DSSCs.

References:

- [1] Grätzel, M., “Dye-sensitized solar cells”, *Journal of photochemistry and photobiology C: Photochemistry Reviews*, vol. 4, no. 2, pp. 145-153, 2003.
[https://doi.org/10.1016/S1389-5567\(03\)00026-1](https://doi.org/10.1016/S1389-5567(03)00026-1)
- [2] Elliott, D., “Renewable energy and sustainable futures”, *Futures*, vol. 32, no. 3-4, pp.261-274., 2000.
[https://doi.org/10.1016/S0016-3287\(99\)00096-8](https://doi.org/10.1016/S0016-3287(99)00096-8)
- [3] Gong, J., Liang, J., Sumathy, K., “Review on dye-sensitized solar cells (DSSCs): fundamental concepts and novel materials”, *Renewable and Sustainable Energy Reviews*, vol. 16, no. 8, pp. 5848-5860, 2012.
<https://doi.org/10.1016/j.rser.2012.04.044>
- [4] Blakers, A., Zin, N., McIntosh, K. R., Fong, K., “High-efficiency silicon solar cells”, *Energy Procedia*, vol. 33, pp. 1-10, 2013.
<https://doi.org/10.1016/j.egypro.2013.05.033>
- [5] McConnell RD., “Assessment of the dye-sensitized solar cell. *Renewable and Sustainable Energy Reviews*”, vol. 6, no. 3, pp. 271-93, 2002.
[https://doi.org/10.1016/S1364-0321\(01\)00012-0](https://doi.org/10.1016/S1364-0321(01)00012-0)
- [6] Sharma K, Sharma V, Sharma SS, “Dye-sensitized solar cells: fundamentals and current status”, *Nanoscale research letters*, vol. 13, no. 1, pp. 381, 2018.
<https://doi.org/10.1186/s11671-018-2760-6>
- [7] Al-Alwani MA, Mohamad AB, Ludin NA, Kadhum AA, Sopian K., “Dye-sensitised solar cells: development, structure, operation principles, electron kinetics, characterization, synthesis materials & natural photosensitizers”, *Renewable & Sustainable Energy Reviews*, vol. 65, no. 1, pp. 183-213, 2016.
<https://doi.org/10.1016/j.rser.2016.06.045>
-
-

-
-
- [8] O'regan B, Grätzel M. A, “low-cost, high-efficiency solar cell based on dye-sensitized colloidal TiO₂ films”, *Nature*, vol. 353, no. 6346, pp. 737-740, 1991.
<https://doi.org/10.1038/353737a0>
- [9] Leung DY, Fu X, Wang C, Ni M, Leung MK, Wang X, et al. “Hydrogen production over titania-based photocatalysts”, *ChemSusChem*, vol. 3, no. 6, pp. 681-694, 2010.
<https://doi.org/10.1002/cssc.201000014>
- [10] Liu G, Gong J, Kong L, Schaller RD, Hu Q, Liu Z, et al., “Isothermal pressure-derived metastable states in 2D hybrid perovskites showing enduring bandgap narrowing”, *Proceedings of the National Academy of Sciences*, vol. 115, no. 32, pp. 8076-8081, 2018.
<https://doi.org/10.1073/pnas.1809167115>
- [11] Liu G, Kong L, Guo P, Stoumpos CC, Hu Q, Liu Z, et al., “Two regimes of bandgap redshift and partial ambient retention in pressure-treated two-dimensional perovskites”, *ACS Energy Letters*, vol. 2, no. 11, pp. 2518-2524, 2017.
<https://doi.org/10.1021/acseenergylett.7b00807>
- [12] Wang X, Li Z, Shi J, Yu Y, “One-dimensional titanium dioxide nanomaterials: nanowires, nanorods, and nanobelts”, *Chemical Reviews*, vol. 114, no. 19, pp. 9346-9384, 2014.
<https://doi.org/10.1016/j.ijleo.2019.164142>
- [13] Biswas R, Chatterjee S, “Effect of surface modification via sol-gel spin coating of ZnO nanoparticles on the performance of WO₃ photoanode-based Dye-Sensitized Solar Cells”, *Optik*, 2019 Dec 28:164142.
<https://doi.org/10.1016/j.ijleo.2019.164142>
-
-

-
-
- [14] Lee JH, Park NG, Shin YJ, “Nano-grain SnO₂ electrodes for high conversion efficiency SnO₂-DSSC”, *Solar energy materials and solar cell*, vol. 95, no. 1, pp. 179-183, 2011.
<https://doi.org/10.1016/j.solmat.2010.04.027>
- [15] Zheng H, Tachibana Y, Kalantar-Zadeh K, “Dye-sensitized solar cells based on WO₃”, *Langmuir*, vol. 26, no. 24, pp. 19148-19152, 2010.
<https://doi.org/10.1021/la103692y>
- [16] Karki IB, Nakarmi JJ, Mandal PK, Chatterjee S, “Effect of organic dyes on the performance of ZnO based dye-sensitized solar cells”, *Applied Solar Energy*, vol. 49, no. 1, pp. 40-45, 2013.
<https://doi.org/10.3103/S0003701X13010052>
- [17] Ayalew WA, Ayele DW, “Dye-sensitized solar cells using natural dye as light-harvesting materials extracted from *Acanthus sennii* chiovenda flower and *Euphorbia cotinifolia* leaf”, *Journal of Science: Advanced materials and devices*, vol. 1, no. 4, pp. 488-494, 2016.
<https://doi.org/10.1016/j.jsamd.2016.10.003>
- [18] Kabir F, Bhuiyan MM, Manir MS, Rahaman MS, Khan MA, Ikegami T, “Development of dye-sensitized solar cell based on a combination of natural dyes extracted from Malabar spinach and red spinach”, *Results in Physics*, vol. 14, no. 1, pp. 1-7, 2019. (Article no.102474)
<https://doi.org/10.1016/j.rinp.2019.102474>
- [19] Narayan MR, “Dye-sensitized solar cells based on natural photosensitizers”, *Renewable and Sustainable Energy Reviews*, vol. 16, no. 1, pp. 208-215, 2012.
<https://doi.org/10.1016/j.rser.2011.07.148>
-
-

-
-
- [20] Biswas R, Roy T, Chatterjee S, “Study of Electro-Optical Performance and Interfacial Charge Transfer Dynamics of Dye-Sensitized Solar Cells Based on ZnO Nanostructures and Natural Dyes”, *Journal of Nanoelectronics and Optoelectronics*, vol. 14, no. 1, pp. 99-108, 2019.
<https://doi.org/10.1166/jno.2019.2445>
- [21] Wu, J., Lan, Z., Hao, S., Li, P., Lin, J., Huang, M., et al., “Progress on the electrolytes for dye-sensitized solar cells”, *Pure and Applied Chemistry*, vol. 80, no. 11, pp. 2241-2258, 2008.
<https://doi.org/10.1351/pac200880112241>
- [22] Vasei, M, Tajabadi, F., Jabbari, A. & Taghavinia, N., "Stable dye-sensitized solar cells based on a gel electrolyte with ethyl cellulose as the gelator", *Applied Physics A* volume 120, pages869–874(2015)
<https://doi.org/10.1007/s00339-015-9332-8>
- [23] Richter, A., Hermle, M., Glunz, S. W, “Reassessment of the limiting efficiency for crystalline silicon solar cells”, *IEEE Journal of photovoltaics*, Vol. 3, no. 4, pp. 1184-1191, 2013.
<https://doi.org/10.1109/JPHOTOV.2013.2270351>
- [24] Mahmood, A., ‘Recent research progress on quasi-solid-state electrolytes for dye-sensitized solar cells’, *Journal of energy chemistry*, vol. 24, no. 6, pp. 686-692, 2015.
<https://doi.org/10.1016/j.jechem.2015.10.018>
- [25] Shi, L.-Y., Chen, T.-L., Chen, C.-H., Cho, K.-C., “Synthesis and characterization of a gel-type electrolyte with ionic liquid added for dye-sensitized solar cells. *International Journal of Photoenergy*”, vol. 2013, pp. 1–7, 2013. (special issue)
<https://doi.org/10.1155/2013/834184>
- [26] An, H., Xue, B., Li, D., Li, H., Meng, Q., Guo, L., et al., “Environmentally friendly LiI/ethanol-based gel electrolyte for dye-
-
-

-
-
- sensitized solar cells”, *Electrochemistry Communications*, vol. 8, no. 1 pp. 170-172, 2006.
<https://doi.org/10.1016/j.elecom.2005.11.012>
- [27] Pathak, C., Surana, K., Kumar Shukla, V., & Singh, P. K., “Fabrication and characterization of a dye-sensitized solar cell using natural dyes”, *Materials Today: Proceedings*, vol. 12, no. 3, pp. 665–670, 2019.
<https://doi.org/10.1016/j.matpr.2019.03.111>
- [28] Trihutomo, P., Soeparman, S., Widhiyanuriyawan, D., & Yuliati, L, “Performance Improvement of Dye-Sensitized Solar Cell- (DSSC-) Based Natural Dyes by Clathrin Protein”, *International Journal of Photoenergy*, vol. 2019, pp. 1-9, 2019. (Article ID 4384728)
- [29] Zanatta, Antonio Ricardo. "A fast-reliable methodology to estimate the concentration of rutile or anatase phases of TiO₂." *AIP Advances* 7, no. 7 (2017): 075201.
- [30] Shaikh, Shoyebmohamad F., Rajaram S. Mane, Byoung Koun Min, Yun Jeong Hwang, and Oh-shim Joo. "D-sorbitol-induced phase control of TiO₂ nanoparticles and its application for dye-sensitized solar cells." *Scientific reports* 6, no. 1 (2016): 1-10.
- [31] Zhuo, R. F., H. T. Feng, Q. Liang, J. Z. Liu, J. T. Chen, D. Yan, J. J. Feng et al. "Morphology-controlled synthesis, growth mechanism, optical and microwave absorption properties of ZnO nanocombs." *Journal of Physics D: Applied Physics* 41, no. 18 (2008): 185405.
- [32] Umale, S. V., Tambat, S. N., Sudhakar, V., Sontakke, S. M., & Krishnamoorthy, K., “Fabrication, characterization, and comparison of DSSC using anatase TiO₂ synthesized by various methods”, *Advanced Powder Technology*, vol. 28, no. 11, pp. 2859–2864, 2017.
<https://doi.org/10.1016/j.appt.2017.08.012>
-
-

-
-
- [33] Wang, Q., Moser, J.-E., Grätzel, M., “Electrochemical impedance spectroscopic analysis of dye-sensitized solar cells”, *The Journal of Physical Chemistry B*, vol. 109, no. 31, pp. 14945-14953, 2005.
<https://doi.org/10.1021/jp052768h>
- [34] Sarker, S., Ahammad, A., Seo, H. W., Kim, D. M., “Electrochemical impedance spectra of dye-sensitized solar cells: fundamentals and spreadsheet calculation”, *International Journal of Photoenergy*, Vol. 2014, pp. 1-17, 2014. (Article ID 851705)
<https://doi.org/10.1155/2014/851705>
- [35] Fabregat-Santiago F, Bisquert J, Palomares E, Otero L, Kuang D, Zakeeruddin SM, Grätzel M., “Correlation between photovoltaic performance and impedance spectroscopy of dye-sensitized solar cells based on ionic liquids”, *The Journal of Physical Chemistry C*, vol. 111, no. 17, pp. 6550-60, 2007.
<https://doi.org/10.1021/jp066178a>
- [36] Won, L.J., Kim, J.H. and Thogiti, S., 2018. A polymer electrolyte for dye-sensitized solar cells based on a poly (polyvinylidene fluoride-co-hexafluoropropylene)/hydroxypropyl methyl cellulose blend. *Electronic Materials Letters*, 14(3), pp.342-347.
<https://doi.org/10.1007/s13391-018-0031-4>
- [37] Dong, R.X., Shen, S.Y., Chen, H.W., Wang, C.C., Shih, P.T., Liu, C.T., Vittal, R., Lin, J.J. and Ho, K.C., 2013. A novel polymer gel electrolyte for highly efficient dye-sensitized solar cells. *Journal of materials chemistry A*, 1(29), pp.8471-8478.
<https://doi.org/10.1039/C3TA11331K>
- [38] Sonai, G. G., Tiihonen, A., Miettunen, K., Lund, P. D., & Nogueira, A. F., “Long-Term Stability of Dye-Sensitized Solar Cells Assembled with Cobalt Polymer Gel Electrolyte”, *The Journal of Physical Chemistry C*, vol. 121, no. 33, pp.17577–17585.
-
-

This page is intentionally left blank

Chapter 7

Summary and Conclusions

This page is intentionally left blank

It is necessary to create novel photovoltaic device designs in addition to the well-established, conventional silicon and thin-film panels if solar electricity is to reach its full potential as a clean, renewable energy source. This thesis entitled “*Investigations on Dye Sensitized Solar Cells to Optimize its Performance*” submitted for the degree of Doctor of Philosophy (Science) in Physics of the University of North Bengal, principally focuses on dye sensitized solar cells, a still-evolving type of photovoltaic converter whose advantages include, for the most part, inexpensive, safe, and readily available materials as well as easy manufacturing processes. The whole work presented in this thesis is mainly devoted to the comprehensive study and understanding of the role of different components of DSSC. It investigates their optimization conditions to enhance the device performance in terms of efficiency, stability and cost-effectiveness. This study explored several key parameters towards the performance optimization of DSSC.

The first chapter discusses the world’s current energy situation as well as the importance of renewable energy sources. This chapter provides a brief discussion of the various types of photovoltaic devices that are available. This chapter also includes a basic introduction to DSSC, its construction, working principle and the roles of its various components. To fully comprehend the DSSC’s working principles, components, and potential areas of research that could lead to commercialization, a thorough review of the relevant literature was conducted in this chapter.

Chapter 2 provides a basic theory and in-depth explanation of experimental techniques used in the study, viz. X-ray diffraction analysis (XRD), scanning electron microscopy (SEM), energy-dispersive X-ray spectroscopy (EDS) research, UV-VIS spectroscopy and Raman spectroscopy. In addition, in this chapter, the fundamentals of measuring current-voltage (I-V) characteristics and electrochemical impedance spectroscopy, as well as a

detailed explanation of the critical factors affecting device performance, are also covered.

The photovoltaic performance of a DSSC is primarily determined by the Photoanode material chosen, including surface morphology and the sensitizing dye used. Although many different DSSCs have been investigated, most of them are not commercially popular due to issues such as low conversion efficiency, higher production costs, and lower stability and durability. Among all dye sensitizers, the ruthenium complexes are the most popular. The main disadvantages of Ruthenium dyes are their rareness, high cost, and complicated synthesis process. Furthermore, ruthenium polypyridyl complexes contain heavy metals that are hazardous to the environment. In order to find out low-cost and environment-friendly alternatives to these expensive ruthenium compounds, we have used anthocyanin extracted from pomegranate (*Punica granatum*) and curcumin extracted from fresh turmeric (*Curcuma longa*) as sensitizers. Additionally, ZnO has been used as a potential alternative to TiO₂ due to its fascinating electrical and optical properties. Both ZnO nanoparticles and ZnO nanorods are used as photoanode material. ZnO nanorod based DSSC showed better performance as 1-D single-crystalline rod-like structure of ZnO nanorods provides a higher surface-to-volume ratio enabling better dye loading as well as it provides a direct path for faster charge transfer through them. Efforts are made to improve device performance using low-cost sensitizers and semiconductor materials. These research findings are put together in Chapter 3.

The Chapter 4 investigates the effect of WO₃ as a working electrode material for DSSC as an alternative to TiO₂. Despite having several advantageous properties, the performance of pure WO₃-based DSSC was found to be extremely poor. Surface modification of the WO₃ photoanode was done by spin coating ZnO nanoparticles synthesized via the sol-gel method. Device performances were recorded for different concentrations of ZnO precursor solution. The concentration of the ZnO precursor solution was found to have a

strong influence on the DSSC's photovoltaic performance. It was observed that, although the incorporation of a thin layer of ZnO onto WO₃ enhances the power conversion efficiency by creating an energy barrier and limiting the electron back-recombination, the thicker layer of ZnO degrades the cell performance by forming an aggregation of Zn⁺² ions and N₃ dye and reducing the dye adsorption quantity of WO₃ film.

Dye aggregation on the metal-oxide surface of a DSSC affects the photoelectron injection by increasing charge recombination and hence limits the overall device performance. The use of additives such as Chenodeoxycholic acid (CDCA) is a very useful and widely used strategy in lowering the self-aggregation of dye molecules by suppressing unfavourable dye-dye interactions and thereby enhancing the photoconversion efficiency. However, the strong binding of CDCA molecules to the ZnO surface partially displaces dye molecules and consequently reduces photon harvesting. Therefore, to maximize the positive effect of the co-adsorbent, it is very crucial to carefully optimize the amount of CDCA. The impact of the proper concentration of CDCA as an anti-dye-aggregation material in boosting the DSSC performance based on Rose Bengal dye is discussed in Chapter 5. Additionally, in order to minimize charge recombination, the impact of a very thin and compact ZnO blocking layer was also examined. At optimized co-adsorbent concentration, the reduced dye loading due to the presence of CDCA and consequently decreased light-harvesting was compensated by the increased electron injection efficiency leading to maximum device efficiency of 1 %. Moreover, when a compact ZnO blocking layer was applied to the FTO prior to depositing the mesoporous ZnO active layer, the performance was further improved from 1.00 percent to 1.22 percent. This resulted from the inhibition of electron back transfer from the FTO to the liquid electrolyte.

Chapter 6 focuses on the use of gel electrolytes in DSSC rather than liquid electrolytes. The leakage of liquid electrolyte, electrode corrosion, photo-

degradation of attached dyes, and solvent volatility all limit the long-term performance of liquid electrolyte-based DSSCs. Gel electrolytes were used to overcome these limitations because they reduce the volatility of organic solvents and prevent leakage. To improve the cell stability, gel electrolyte-based DSSCs were created using ethyl cellulose (EC) as the gelation material in a conventional liquid electrolyte containing LiI and I₂ as the redox couple in acetonitrile solvent. TiO₂ and ZnO were used as photoanode materials in various types of DSSCs. The effect of EC concentration on the performance of DSSCs, including stability over time, was also studied.

Although the efficiency of the gel-based DSSC is less than that of the liquid electrolyte DSSC, the cell characteristics were equivalent to those for gel electrolyte-based DSSCs by other researchers. A Comparison of these two kinds of DSSCs reveals that, despite having slightly lower photovoltaic performance than liquid electrolyte DSSC, gel-based DSSC performance is noticeably more stable than liquid electrolyte performance over time. The stability of both TiO₂ and ZnO photoanode based DSSCs can be improved by using an EC based gel electrolyte with the correct EC wt%.

Appendix

This page is intentionally left blank

Appendix A

**Dye sensitized solar cells
based on pre-dye treated ZnO
nanoparticles**

This page is intentionally left blank

1. Introduction

Recent years have seen an increase in demand for efficient solar photovoltaic (PV) cell power generation due to the world's increasing energy needs and the depletion of fossil fuels [1-3]. Effect of substantial use of fossil fuel on the environment is a matter of significant worry as well [4]. Modules made of crystalline silicon and based on bulk wafers make up the majority of the photovoltaic (PV) modules produced today. The high expense of these solar cells' fabrication as well as the use of hazardous ingredients has driven researchers to develop new, less expensive solar cells that are not silicon-based in order to capture solar energy more effectively [5-8].

Due to its high conversion efficiencies and low cost, dye-sensitized solar cells (DSSCs), a novel photovoltaic technology, have garnered much interest. Using nanoporous titanium dioxide (TiO_2) semiconductor electrodes, ruthenium (Ru) metal complex dyes, and iodine electrolyte solutions, O'Regan, B., and Grätzel reported high efficiency cells in *Nature* in 1991 [9]. Since then, many studies have been actively carried out on DSSCs and revealed their performance comparable to amorphous silicon thin films [10, 11].

Dye-sensitized solar cells (DSSCs) are a non-conventional photovoltaic technology that has attracted significant attention because of their high conversion efficiencies and low cost. O'Regan, B. & Grätzel reported high efficiency cells using nanoporous titanium dioxide (TiO_2) semiconductor electrodes, ruthenium (Ru) metal complex dyes, and iodine electrolyte solutions in the journal of *Nature* in 1991 [9]. Since then, many studies have been actively carried out on DSSCs and revealed their performance comparable to amorphous silicon thin films [10, 11]. The advantages of these DSSCs are their low cost, light weight, and ease of production; yet, problems with durability and future enhancement of their features exist. Numerous efforts have been undertaken to address these problems, including upgrading materials

and structures and solidifying electrolytes, but major advancements have not yet been accomplished [12, 13]. Two conducting glass electrodes are sandwiched together to form a dye-sensitized solar cell. Each layer plays a particular function in the cell.

The photovoltaic performance of a DSSC highly depends on all of its components and the fabrication methodology. Therefore, the optimization of every component is highly crucial to achieve the best performance. Since its introduction into the science community in 1991, the nanocrystalline photoanode in dye-sensitized solar cells has predominantly been comprised of titanium (TiO_2) nanoparticles as the semiconducting material [9, 14, 15]. Many researchers became very interested in studying the dye-sensitized solar cell performance fabricated using alternative semiconducting nanomaterials [16, 17]. Specifically, Zinc Oxide (ZnO) has been an ideal alternative to TiO_2 because of having a similar conduction band edge that is appropriate for proper electron injection from the excited dyes; moreover, ZnO provides better electron transport due to its higher electronic mobility. Moreover, ZnO is also highly transparent, allowing greater light penetration [18-22].

In this study, ZnO nanoparticles were used to fabricate the photoanode of the DSSCs and Rose Bengal dye was utilized as a sensitizer. To obtain better efficiency, the dye molecules must bind tightly to the mesoporous ZnO photoanode surface with the assistance of their anchoring group to ensure proficient electron injection from the LUMO of the dye molecule to the conduction band (CB) of ZnO . Here, we have studied the effect of the inclusion of rose bengal dye solution during the ZnO nanoparticle paste preparation. This yielded a coloured pre-dye treated paste of ZnO nanoparticles. The performance of pre-dye treated DSSC was compared with the cell prepared without pre-dye treating.

2. Materials and Method

2.1. Materials

Transparent ITO coated glass (10 Ω / square) was purchased from Techinstro, India. Commercial ZnO nanopowder, Rose Bengal dye, and Triton X-100 were bought from Sigma Aldrich, India. The liquid electrolyte used in our experiment was a Solaronix high performance electrolyte (Iodolyte AN50) with iodide/tri-iodide as redox couple, ionic liquid, and lithium salt and pyridine derivative as additives dissolved in acetonitrile solvent. The liquid platinum paint (Platisol T) purchased from Solaronix, Switzerland was used to prepare the platinum-coated transparent counter electrode. Meltonix 1170-25 (25 μ m) purchased from Solaronix was used as a spacer between the working and counter electrode to avoid short-circuiting. All the reagents utilized in the fabrication process were of analytical grades. So no further purification was required.

2.2. Preparation of pure ZnO photoanode

To prepare the thin films of the photoanode materials, the ITO coated glass substrates were first cleaned with dilute HCl in an ultrasonic bath for 15 minutes and then thoroughly rinsed with deionized water to remove the HCL residues. Then the substrates were cleaned with acetone and ethanol using an ultrasonic cleaning bath [17, 22].

The working electrode of the DSSC was prepared by following the standard doctor blade method. The paste for doctor blading was prepared by mixing ZnO nanopowder with dilute acetylacetone as a solvent and ethyl cellulose as a binder. One drop of Triton X-100 was added to the mixture to reduce the surface tension of the slurry and to enable even spreading. The mixture was stirred continuously in order to obtain a smooth lump-free slurry. The ZnO paste was then coated on the conductive side of the cleaned ITO glass substrate and subsequently annealed at 450°C on a hot plate for 30 min in order

to burn out the ethyl cellulose contents of the working electrode and strengthens the bonding between the substrate and the ZnO film. In addition to that, the annealing procedure also helps to improve the surface quality of the thin film along with increasing the crystallinity of the sample.

2.3. Preparation of pre-dye treated ZnO photoanode

To prepare the pre-dye treated ZnO photoanode, the above procedure is slightly modified by directly adding 0.3 mM ethanolic solution of Rose Bengal dye during the ZnO nanoparticle paste preparation. This yielded a coloured pre-dye treated paste of ZnO nanoparticles. This paste was also coated using the doctor blade method (Fig. 1) on a previously cleaned ITO glass substrate and annealed following the identical procedure as followed for the pure ZnO electrode to obtain the pre-dye treated ZnO working electrode.

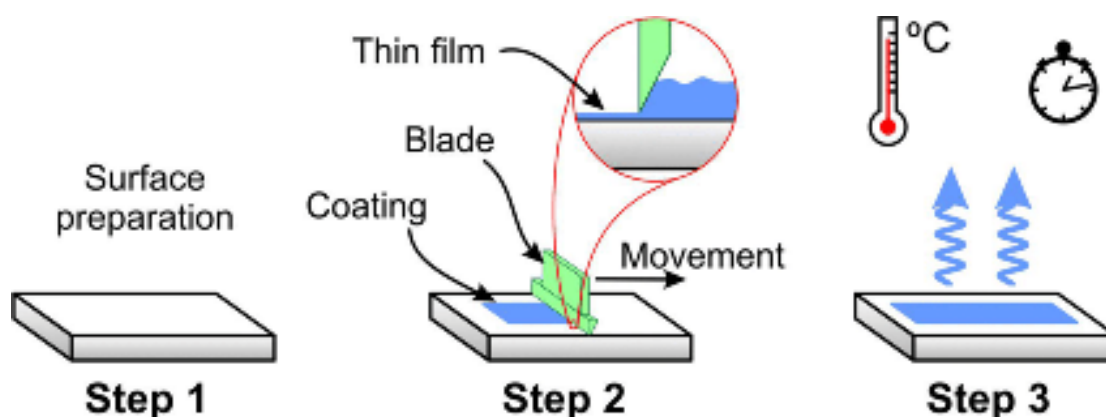


Figure 1. Schematic diagram of doctor blade method.

(<https://link.springer.com/article/10.1007/s11356-020-10022-9>)

2.4. Fabrication of the cells

Both of the pure and pre-dye treated ZnO electrodes were sensitized by immersing them in a 0.3 mM ethanolic solution of Rose Bengal dye for 12 hours. The working electrodes were then removed from the solution and thoroughly rinsed with deionized water and ethanol to remove any excess dye

from the ZnO nanoparticle film surface and left for air drying at room temperature. The platinum catalyst precursor solution Platisol-T (Solaronix) was spin-coated on the conducting side of the cleaned ITO glasses and heated at 450 ° C for 15 minutes on a hot plate to prepare the counter electrodes for the cells. The dye adsorbed working electrodes and platinum(Pt)-coated counter electrodes were assembled against the coated sides of each other in a sandwich manner using two binder clips with a Surlyn film (Meltonix 1170-25 μ m, Solaronix) gasket as a spacer in between them. The liquid electrolyte used in the fabrication process was poured inside the cell through fine holes pre-drilled on the counter electrodes. The redox concentration of the electrolyte was 50 mM. The active area of the cells for illumination was 0.16 cm².

2.5. Characterization and Measurements

PAN-analytical X'Pert PRO X-ray diffractometer (CuK α radiation, 30 mA, 40 kV, λ = 1.5406 Å) was used to study the crystalline structure of the ZnO nanoparticles. The surface morphology of the prepared ZnO thin films was studied by using scanning electron microscopy (JEOL). The Current-Voltage (I-V) characterization of the cells was done using a Keithley 2400 digital source meter under 100 mW/cm² illumination (Xenon lamp 450W).

3. Results and Discussion

3.1. UV-VIS absorption spectral analysis of the dye

UV-VIS absorption spectrum of the Rose Bengal dye is shown in Fig. 2. The Rose Bengal dye absorbs a larger fraction of the solar spectrum in the visible region of 460–600 nm and it shows the highest optical absorption at 549 nm wavelength.

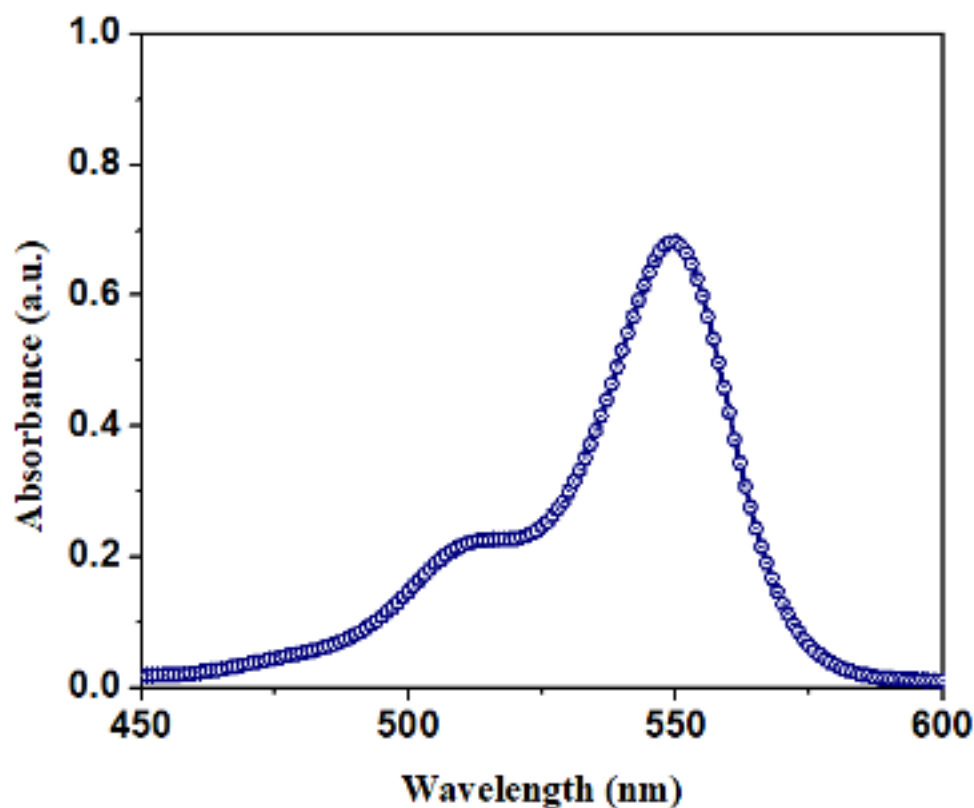


Figure 2. Absorption spectra of Rose Bengal dye.

3.2. Structural and phase characterization ZnO of the photoanode

X-ray diffraction pattern of the as-purchased ZnO nanopowder is shown in Fig. 3. The XRD pattern exhibits the hexagonal wurtzite crystal phase of ZnO and peaks well match the standard JCPDS card no. 36-1451. The diffraction peaks observed at 2θ values of 31.79° , 34.42° , 36.25° , 47.51° , 56.60° , 62.86° , 67.96° , and 69° corresponds to the reflection from the (100), (002), (101), (110), (103), (112), and (201) lattice planes respectively. Sharp and strong peaks indicate the highly crystalline nature of the material [23, 24].

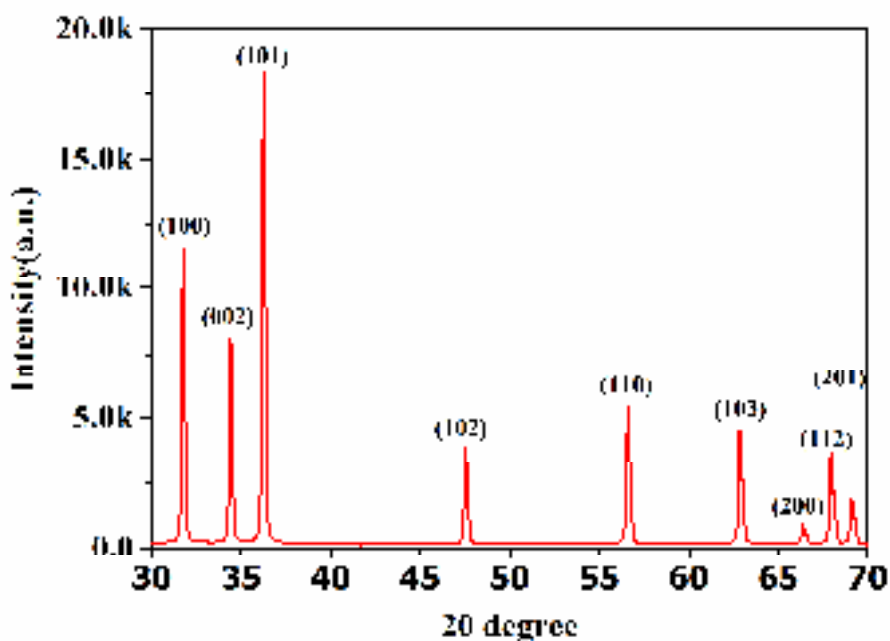


Figure 3. X-ray diffraction pattern of ZnO nanoparticles.

3.3. Surface Morphology study and energy dispersive spectroscopy of the photoanodes

Scanning electron microscopic (SEM) analysis of the ZnO nanopowder film on the ITO substrate was carried out to study the morphological properties and the particle size of the sample. The SEM image of the ZnO nanoparticles on an ITO substrate is shown in Fig.4 (a).

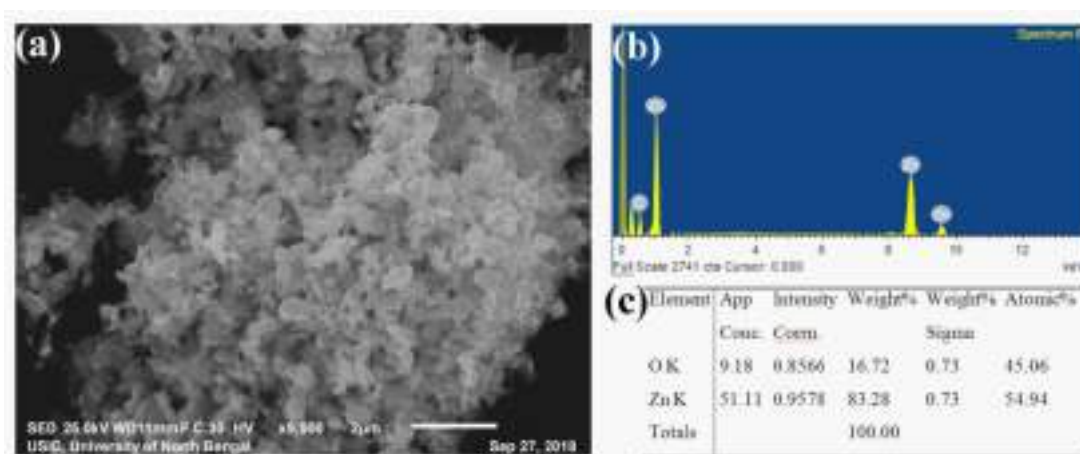


Figure 4. (a) SEM images, (b) EDS and (c) Elemental composition of ZnO Nanoparticles respectively

The SEM observation confirms that the ZnO particle size is in the nanometre range and they have a hexagonal wurtzite structure. Further, the chemical composition and elemental percentage of the film are revealed by the EDS analysis which is shown in Fig. 4 (b) and 4 (c) respectively.

3.4. Photovoltaic (Current-Voltage) characterization of the cells

The Current-Voltage characteristic is an essential measurement that reveals the values of the overall photovoltaic performance of a solar cell along with key performance parameters like open circuit voltage and short circuit current density. Fig. 5 depicts the I-V characteristics of the DSSCs based on pure and pre-dye treated ZnO as photoanodes respectively. The overall photoconversion efficiency of the solar cell is calculated by the formula

$$\eta = \frac{P_{\text{out}}}{P_{\text{in}}} = \frac{I_{\text{sc}} V_{\text{oc}} FF}{P_{\text{in}}} \quad (1)$$

Where P_{in} , V_{oc} , I_{sc} and FF denote the incident photon power, open-circuit voltage, the short circuit current density and fill factor respectively. The fill factor is calculated using the following formula:

$$FF = \frac{I_{\text{max}} V_{\text{max}}}{I_{\text{sc}} V_{\text{oc}}} \quad (2)$$

Where I_{max} and V_{max} , respectively, represent values of the current and voltage at the maximum output power point of the solar cell.

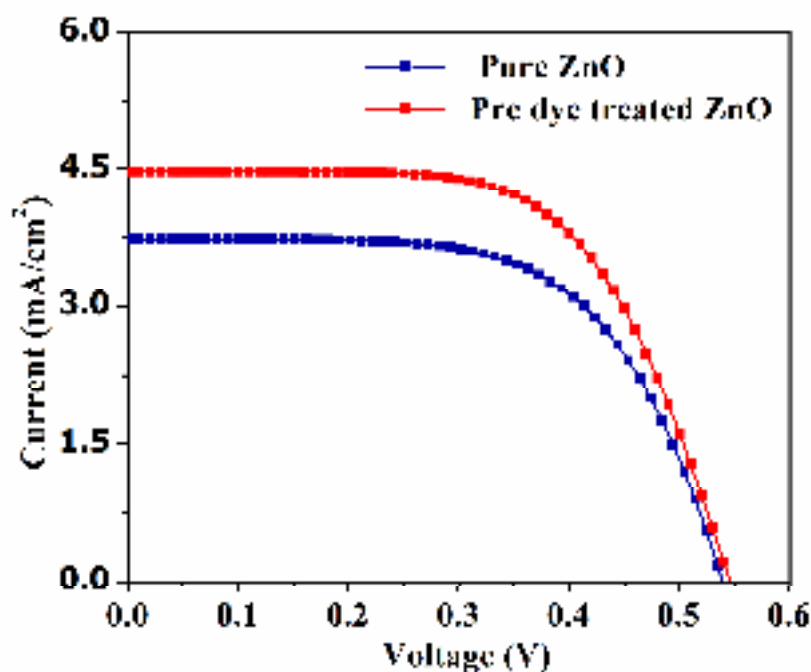


Figure 5. Current-voltage characteristics of different cells under illumination.

The photovoltaic parameters extracted from the I-V characteristics of the fabricated DSSCs are shown in table 1 below.

Table 1.

Photovoltaic performance of uncoated and ZnO coated WO_3 photoanode based DSSC

ZnO precursor concentration	J_{sc} (mA/cm ²)	V_{oc} (V)	FF	Efficiency (η %)
Pure ZnO	3.73	0.53	0.63	1.26
Pre-dye treated ZnO	4.47	0.55	0.62	1.53

A considerable improvement in the values of J_{sc} and η for the pre-dye treated DSSC can be observed compared to the conventionally prepared pure ZnO electrode from Table 1. This demonstrates the positive role of the pre-dye treating process. This may be attributed to the fact that the pre-dye loading method resulted in uniform dye adsorption, reduced agglomeration, the improved surface morphology of photoanode and less dye aggregation [25].

The V_{oc} is also improved slightly. The increased amount of dye molecule adsorption on the pre-dye treated ZnO nanoparticle surface absorbs more photons and thereby injecting more electrons to the conduction band of ZnO. This yielded increased J_{sc} and η .

4. Conclusion

DSSCs using pure and pre-dye treated ZnO nanoparticles as photoanode material were fabricated and their electro-optical performances were compared. The performance of the DSSC was remarkably improved upon pre-dye loading. The pre-dye treated ZnO DSSC showed a 19.84% improvement in Short circuit current density (J_{sc}) and 21.43 % improvement in photoconversion efficiency (η). Therefore, the method of pre-dye loading of ZnO nanoparticles may be used as an effective and novel way to improve the performance of dye sensitized solar cells.

References

- [1] Bach W. Global warming: the complete briefing (2nd ed). John Houghton. Cambridge University Press: Cambridge, 1997. Pp. xv + 251. Paperback: ISBN 0521-62932-2, ú12.95; hardback: ISBN 0-321-62089-9, ú35.00. International Journal of Climatology. 1998;18(5):579-80.
- [2] Meadows DH, Meadows DL, Randers J, Behrens WW. The limits to growth. New York. 1972;102:27.
- [3] Minger TJ, editor Greenhouse glasnost: the crisis of global warming: essays. Greenhouse/Glasnost: the Sundance Symposium on Global Climate Change,(USA), 1989; 1990: Ecco Press.

-
-
- [4] Barbir F, Veziroğlu TN, Plass Jr HJ. Environmental damage due to fossil fuels use. *International journal of hydrogen energy*. 1990 Jan 1;15(10):739-49.
- [5] Goetzberger A, Hebling C, Schock HW. Photovoltaic materials, history, status and outlook. *Materials Science and Engineering: R: Reports*. 2003 Jan 1;40(1):1-46.
- [6] Alharbi F, Bass JD, Salhi A, Alyamani A, Kim HC, Miller RD. Abundant non-toxic materials for thin film solar cells: Alternative to conventional materials. *Renewable Energy*. 2011 Oct 1;36(10):2753-8.
- [7] Lee TD, Ebong AU. A review of thin film solar cell technologies and challenges. *Renewable and Sustainable Energy Reviews*. 2017 Apr 1;70:1286-97.
- [8] Yamamoto K, Yoshimi M, Tawada Y, Okamoto Y, Nakajima A. Cost effective and high-performance thin film Si solar cell towards the 21st century. *Solar energy materials and solar cells*. 2001 Feb 1;66(1-4):117-25.
- [9] B. O'regan and M. Grätzel, A low-cost, high-efficiency solar cell based on dye-sensitized colloidal TiO₂ films, *nature* 353, 737, (1991).
- [10] Chiba Y, Islam A, Komiya R, Koide N, Han L. Conversion efficiency of 10.8% by a dye-sensitized solar cell using a Ti O₂ electrode with high haze. *Applied Physics Letters*. 2006 May 29;88(22):223505.
- [11] Grätzel M. Solar energy conversion by dye-sensitized photovoltaic cells. *Inorganic chemistry*. 2005 Oct 3;44(20):6841-51.
- [12] Chung,I., Lee,B., Jiaqing, H.,Robert, P. H. C. & Kanatzidis, M. G. (2012). All-solid-state dye-sensitized solar cells with high efficiency. *Nature*, 485,7399,415-540.
-
-

-
-
- [13] Cai, N., Moon, SJ., Cevey-Ha, L., Moehl, T., Humphry-Baker, R., Wang, P., Zakeeruddin, SM., & Grätzel, M. (2011). An organic D- π -A dye for record efficiency solid-state sensitized heterojunction solar cells. *Nano Lett.* 11, 11(4), 452–1456.
- [14] M. Grätzel, Dye-sensitized solar cells, *Journal of Photochemistry and Photobiology C: Photochemistry Reviews* 4, 145, (2003).
- [15] F. Shao, J. Sun, L. Gao, S. Yang and J. Luo, Growth of various TiO₂ nanostructures for dye-sensitized solar cells, *The Journal of Physical Chemistry C* 115, 1819, (2010).
- [16] Tiwana P, Docampo P, Johnston MB, Snaith HJ, Herz LM. Electron mobility and injection dynamics in mesoporous ZnO, SnO₂, and TiO₂ films used in dye-sensitized solar cells. *ACS nano.* 2011 Jun 28;5(6):5158-66.
- [17] Biswas R, Chatterjee S. Effect of surface modification via sol-gel spin coating of ZnO nanoparticles on the performance of WO₃ photoanode based Dye Sensitized Solar Cells. *Optik.* 2019 Dec 28:164142.
- [18] Zhang Q, Dandeneau CS, Zhou X, Cao G. ZnO nanostructures for dye-sensitized solar cells. *Advanced Materials.* 2009 Nov 6;21(41):4087-108.
- [19] Guillén E, Peter LM, Anta JA. Electron transport and recombination in ZnO-based dye-sensitized solar cells. *The Journal of Physical Chemistry C.* 2011 Nov 17;115(45):22622-32.
- [20] Quintana M, Edvinsson T, Hagfeldt A, Boschloo G. Comparison of dye-sensitized ZnO and TiO₂ solar cells: studies of charge transport and carrier lifetime. *The Journal of Physical Chemistry C.* 2007 Jan 18;111(2):1035-41.
-
-

-
-
- [21] Vittal R, Ho KC. Zinc oxide based dye-sensitized solar cells: A review. *Renewable and Sustainable energy reviews*. 2017 Apr 1;70:920-35.
- [22] Biswas R, Roy T, Chatterjee S. Study of Electro-Optical Performance and Interfacial Charge Transfer Dynamics of Dye Sensitized Solar Cells Based on ZnO Nanostructures and Natural Dyes. *Journal of Nanoelectronics and Optoelectronics*. 2019 Jan 1;14(1):99-108.
- [23] Costantino U, Marmottini F, Nocchetti M, Vivani R. New Synthetic Routes to Hydrotalcite-Like Compounds— Characterisation and Properties of the Obtained Materials. *European Journal of Inorganic Chemistry*. 1998;1998(10):1439-46.
- [24] Oh J-M, Hwang S-H, Choy J-H. The effect of synthetic conditions on tailoring the size of hydrotalcite particles. *Solid State Ionics*. 2002;151(1-4):285-91.
- [25] Ananth S, Vivek P, Arumanayagam T, Murugakoothan P. Pre dye treated titanium dioxide nanoparticles synthesized by modified sol-gel method for efficient dye-sensitized solar cells. *Applied Physics A*. 2015 Jun 1;119(3):989-95.

This page is intentionally left blank

Appendix B

List of Research Journal Publications

1. **Rajat Biswas**, Trinakhi Roy, and Suman Chatterjee, “Study of electro-optical performance and interfacial charge transfer dynamics of dye sensitized solar cells based on ZnO nanostructures and natural dyes”, *Journal of Nanoelectronics and Optoelectronics*, Vol. 14, no. 1 (2019): 99-108.
2. **Rajat Biswas** and Suman Chatterjee, “Effect of surface modification via sol-gel spin coating of ZnO nanoparticles on the performance of WO₃ photoanode based dye sensitized solar cells”, *Optik*, Vol. 212 (2020): 164142.
3. Trinakhi Roy, **Rajat Biswas**, and Suman Chatterjee, “An Investigation on the Stability Enhancement of Dye-Sensitized Solar Cells Fabricated with Ethyl Cellulose Based Gel Electrolyte”, *Applied Solar Energy*, Vol. 57, no. 1 (2021): 23-29.
4. **Rajat Biswas** and Suman Chatterjee. “Effect of chenodeoxycholic acid as dye co-adsorbent and ZnO blocking layer in improving the performance of Rose Bengal dye based dye sensitized solar cells”, *Optical and Quantum Electronics*, Vol. 54, no. 6 (2022): 1-20.
5. **Rajat Biswas**, Joy Sarkar, and Suman Chatterjee, “Improvement of Photovoltaic Performance of Dye Sensitized Solar Cells by Pre-Dye Treating of Zno Nanoparticles.” *Journal of Physics Research and Education*, Vol. 1, no. 1 (2021), pp. 17-29.

6. Joy Sarkar, **Rajat Biswas**, and Suman Chatterjee, “Electronic Band Structure and Density of States Analysis of Electron Transport Materials for Perovskite Solar Cells”, *Journal of Physics Research and Education* , Vol. 1, no. 1 (2021), pp. 46-58.
7. **Rajat Biswas** and Suman Chatterjee, “Optimizing the concentration of ethyle cellulose to improve stability and photovoltaic performance of gel electrolyte based dye-sensitized solar cells”. (Communicated)

Appendix C

List of Conference Presentations

1. **Rajat Biswas** and Suman Chatterjee, “ZnO nanorod based dye sensitized solar cells sensitized using natural dyes extracted from pomegranate and curcumin”, Modern Trends in Material Science, Dept. of Physics, University of North Bengal, Siliguri (2015).
2. **Rajat Biswas** and Suman Chatterjee, “Fabrication and characterization of ZnO nanorod based dye sensitized solar cells using some natural photosensitizers”, National Seminar on Condensed Matter, Laser and Communication, Dept. of Physics, University of Burdwan, Burdwan (2015).
3. **Rajat Biswas** and Suman Chatterjee, “Electrochemical impedance spectroscopy study of dye sensitized solar cells with gold, graphite and carbon black as counter electrode material”, Recent Innovations in Renewable Energy, Centre for renewable Energy Studies, Dept. of Physics, B.N. Mandal University, Madhepura (2018).

This Page is intentionally left blank

**Reprint of Selected
Papers**



Effect of chenodeoxycholic acid as dye co-adsorbent and ZnO blocking layer in improving the performance of Rose Bengal dye based dye sensitized solar cells

Rajat Biswas¹ · Suman Chatterjee¹

Received: 23 May 2021 / Accepted: 26 April 2022

© The Author(s), under exclusive licence to Springer Science+Business Media, LLC, part of Springer Nature 2022

Abstract

Effective suppression of dye aggregation on the photoanode surface of dye sensitized solar cells plays a key role in improving solar cell efficiency. Chenodeoxycholic acid (CDCA) is a very popular anti dye aggregation material used in dye sensitized solar cells (DSSC). However, the selection of an improper concentration of CDCA may lead to decreased solar cell efficiency by lowering the open circuit voltage and short circuit current as a consequence of reduced dye loading. The influence of CDCA as a dye co-adsorbent on the performance of DSSCs fabricated using Rose Bengal dye was studied in this paper. The concentration of the CDCA solution was varied to identify the optimum value for the best device performance. Aside from this, the effect of a very thin and compact ZnO blocking layer was also investigated to reduce the charge recombination. With photovoltaic parameters such as short circuit current density (J_{sc}) = 1.98 mA/cm², open circuit voltage (V_{oc}) = 0.58 V, and fill factor (FF) = 0.43, the traditional cell displayed an overall conversion efficiency of 0.49%, while the power conversion efficiency was found to be increased to 1.00% (J_{sc} = 2.80 mA/cm², V_{oc} = 0.64, FF = 0.58) when CDCA was added at optimised concentration of 8 mM. Reduced dye aggregation and increased electron injection in the presence of CDCA may be accounted for the DSSC's remarkable improvement in the efficiency. Moreover, the combined effect of 8 mM CDCA and the compact ZnO blocking layer dramatically enhanced the efficiency further to 1.22% (J_{sc} = 3.09 mA/cm², V_{oc} = 0.66, FF = 60). Electrochemical impedance spectroscopic (EIS) analysis revealed that the addition of CDCA as a co-adsorbent in the dye solution and addition of ZnO blocking layer resulted in significantly improved electron lifetime and reduced electron recombination yielding improved J_{sc} , V_{oc} and η .

Keywords Dye sensitized solar cell · Dye co-adsorbent · Chenodeoxycholic acid · ZnO blocking layer · Rose bengal dye · Electrochemical impedance spectroscopy

✉ Suman Chatterjee
suman@nbu.ac.in

Rajat Biswas
rajat_biswas@nbu.ac.in

¹ Department of Physics, University of North Bengal, Raja Rammohunpur, Darjeeling, Siliguri 734013, India

1 Introduction

Ever growing global energy requirement and depleting level of fossil fuels have accelerated the demand for efficient power generation from solar photovoltaic (PV) cells in recent years (Bach 1997; Meadows et al. 1972; Hosenuzzaman et al. 2015). The environmental impact of the use of fossil fuels is another major concern (Barbir et al. 1990). The current production of photovoltaic (PV) modules is dominated by crystalline silicon modules based on bulk wafers. However, the use of toxic materials and the high production cost of these solar cells have motivated the researchers to find new kinds of less expensive and non silicon-based solar cells to harvest solar energy efficiently (Goetzberger et al. 2003; Alharbi et al. 2011; Lee and Ebong 2017; Yamamoto et al. 2001).

Dye-sensitized solar cells (DSSCs) are a non-conventional photovoltaic technology that has attracted significant attention because of their high conversion efficiencies and low cost. O'Regan, B. and Grätzel reported high efficiency cells using nanoporous titanium dioxide (TiO_2) semiconductor electrodes, ruthenium (Ru) metal complex dyes, and iodine electrolyte solutions in the journal of Nature in 1991 (O'Regan and Grätzel 1991). Since then, many studies have been actively carried out on DSSCs and revealed their performance comparable to amorphous silicon thin films (Chiba et al. 2006; Grätzel 2005). These DSSCs have the advantages of low cost, lightweight and easy fabrication, but issues include durability and further improvement of their properties. To respond to these issues, many attempts have been made, such as solidifying electrolytes and improving materials and structures, but there have been no great breakthroughs yet (Chung et al. 2012; Cai et al. 2011).

A dye-sensitized solar cell consists of two conducting glass electrodes in a sandwich arrangement. Each layer has a specific role in the cell. The transparent glass electrodes allow the light to pass through the cell. The titanium dioxide serves as a holding place for the dye and participates in electron transfer. The dye molecules collect light and produce excited electrons which cause a current in the cell. The iodide electrolyte layer acts as a source for electron replacement. The bottom conductive layer is coated with platinum which plays the role of the counter electrode. A schematic structure of a liquid electrolyte DSSC and its working principle is shown in Fig. 1. When light passes through the conductive glass electrode, the dye molecules absorb the photons and the electrons in the dye go from the ground state (HOMO) to an empty excited state (LUMO). This is referred to as photoexcitation. The excited electrons jump to the conduction band of the semiconducting dioxide and diffuse across this layer reaching the conductive electrode. Then they travel through the outer circuit and reach the counter electrode. The dye molecules become oxidized after losing an electron to the semiconductor oxide material. The red-ox iodide electrolyte donates electrons to the oxidized dye molecules thereby regenerating them. When the originally lost electron reaches the counter electrode, it gives the electron back to the electrolyte (O'Regan and Grätzel 1991; Grätzel 2003).

The photovoltaic performance of a DSSC highly depends on all of its components and the fabrication methodology. Therefore, the optimization of every component is extremely crucial to achieve the best performance. Since its introduction into the science community in 1991, the nanocrystalline photoanode in dye-sensitized solar cells has predominantly been comprised of titanium (TiO_2) nanoparticles as the semiconducting material (O'Regan and Grätzel 1991; Grätzel 2003; Shao et al. 2011). Many researchers became very interested in studying the dye-sensitized solar cell performance fabricated using alternative semiconducting nanomaterials (Tiwana et al. 2011; Biswas and Chatterjee 2020).

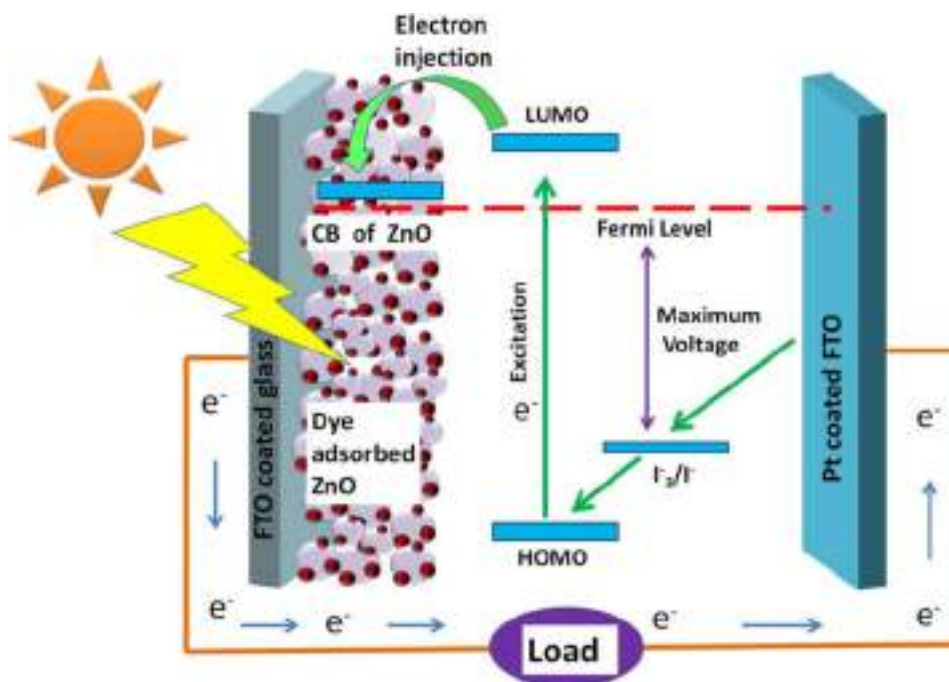


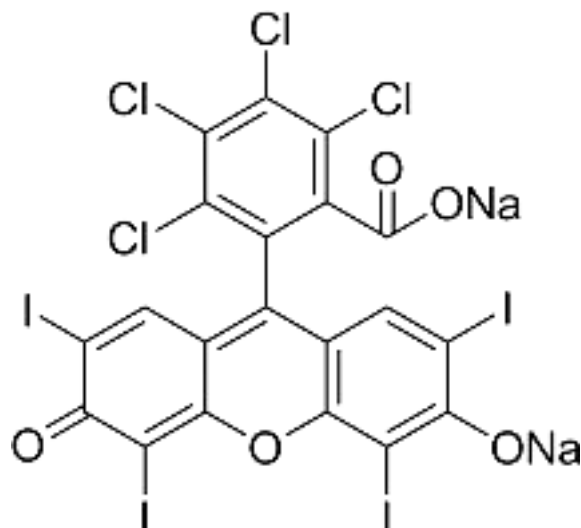
Fig. 1 Schematic diagram and working principle of a conventional DSSC

Specifically, Zinc Oxide (ZnO) has been an ideal alternative to TiO_2 because of having a similar conduction band edge that is appropriate for proper electron injection from the excited dyes; moreover, ZnO provides better electron transport due to its higher electronic mobility. Along with that, ZnO is also highly transparent, which allows greater light penetration (Zhang et al. 2009; Guillén et al. 2011; Quintana et al. 2007; Vittal and Ho 2017; Biswas et al. 2019).

In this study, ZnO nanoparticles were implemented to fabricate the photoanode of the DSSCs and rose bengal dye was utilized as a sensitizer. To obtain better efficiency, the dye molecules must bind tightly to the mesoporous ZnO photoanode surface with the assistance of their anchoring group to ensure proficient electron injection from the LUMO of the dye molecule to the conduction band (CB) of ZnO.

Ruthenium dyes have long been used as quite efficient sensitizers for the photoanodes of the DSSCs (Ito et al. 2006, Aghazada et al. 2018, Nazeeruddin et al. 2011). However, these dyes are expensive, difficult to synthesis, requires high production cost, toxic, rare and easily pollute the environment (Sayyed et al. 2016). Owing to these facts, the organic photosensitizer Rose Bengal (RB), emerges as a promising and alternative candidate. It is a xanthenes class photosensitizer having high absorption coefficient and absorbs a wide spectrum of solar radiation. It energetically matches the conduction band edge of ZnO and iodine/iodide redox couple for DSSC application (Pradhan et al. 2007, Duffy et al. 2000). Accordingly, ZnO based DSSC performs specifically well when sensitized with Rose Bengal. Although the efficiency of these type of organic sensitizer based DSSCs is less, production cost per watt will be less compared to the ruthenium based DSSCs even if we achieve moderate efficiency. As the RB dye is an organic dye and does not contain any toxic noble metal such as ruthenium, there are no environmental pollution related issues with it. It is widely used because of its high absorption coefficient in the visible region of solar spectrum and its molecular structure (Fig. 2) comprises of anchoring groups that can be adsorbed onto the semiconductor oxide surface. For the particular case of ZnO–RB combination, the interaction between the unfilled valance shell of the ZnO and the carboxyl

Fig. 2 Chemical structure of Rose Bengal dye



groups present in the dye molecules leads to easy adsorption of the dye molecules on the ZnO surface. Such kind of bonding between the dye molecule and ZnO not only increases adsorptivity of dye but also facilitates electron injection because of the substantial overlap between the electron molecular orbitals of the dye and those of the semiconductor's conduction band (Rani et al. 2010).

However, in case of ZnO photoanode based DSSCs, the dye aggregation on the ZnO surface affects the photoelectron injection by increasing charge recombination and hence limits the overall device performance (Kim et al. 2014; Patwari et al. 2017; Zhang and Cole 2017). The use of additives such as Chenodeoxycholic acid (CDCA) is a very useful and widely used strategy in lowering the self-aggregation of dye molecules by suppressing unfavourable dye-dye interactions as shown in Fig. 3 and thereby enhances the photoconversion efficiency (Buene et al. 2020; Kumar et al. 2020; Ismail et al. 2018). However, the strong binding of CDCA molecules to the ZnO surface partially displaces dye molecules and consequently reduces photon harvesting. Therefore, to maximize the positive effect of the co-adsorbent, it is very crucial to carefully optimize the amount of CDCA (Li et al. 2011). Few researchers have studied the role of CDCA as an anti-aggregation agent in ruthenium and organic dye based DSSCs and found it to be very effective in reducing the aggregation of dye molecules over the semiconductor surface (Inoue et al. 2010; Lee et al. 2007; Yum et al. 2008; Lu et al. 2009). But there is no report available related to the application of CDCA on Rose Bengal dye. Herein, we report the investigation on the effect of CDCA as co-adsorbent in the performance of Rose Bengal (RB) dye based DSSCs. Different concentrations of CDCA were studied to identify the optimum value for achieving the best device performance.

On the other hand, the mesoporous nature of the ZnO film is very essential to tender high surface area offering more dye loading and thereby generating more photoelectrons. However, small pores present in the nanocrystalline ZnO layer of the photoanode may provide a path for the direct contact between the liquid electrolyte and the FTO substrate. This may allow the electrons of FTO to recombine with the I^-_3 ion present in the electrolyte resulting in high recombination current and hence decreased cell performance (Yang et al. 2014; Yeoh and Chan 2019). Therefore, to inhibit the electron back transfer, a promising approach is to modify the FTO/electrolyte interface by adding a compact metal oxide blocking layer. A thin blocking layer (BL) of ZnO was deposited by a facile and cost-effective sol-gel spin coating process before depositing the mesoporous active ZnO layer. In this

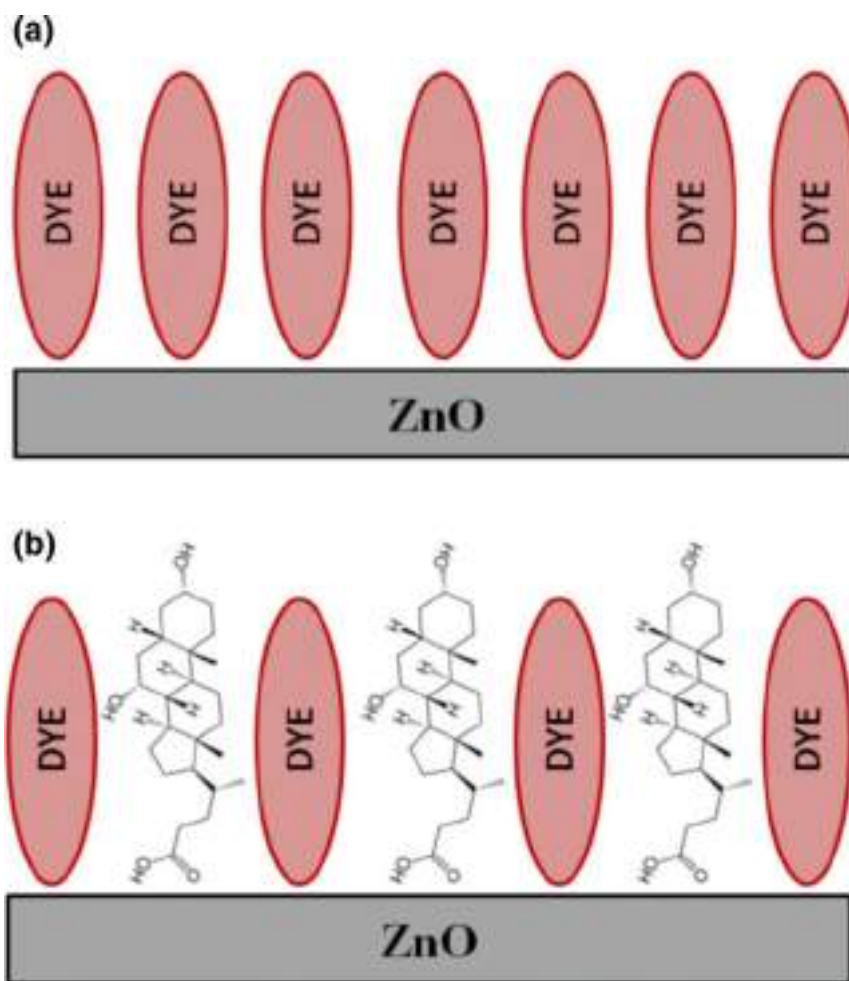


Fig. 3 **a** Unfavourable dye-dye interaction in absence of CDCA **b** reduced self-aggregation of dye molecules in presence of CDCA

work, we reported the fabrication and characterization of DSSCs based on ZnO nanoparticles and Rose Bengal dye. The effect of CDCA concentration and the compact ZnO blocking layer in boosting the photovoltaic performance of the device was investigated in terms of photocurrent–voltage (J – V) characteristics and dark current measurement. In addition to that, electrochemical impedance spectroscopy (EIS) analysis was employed to investigate the charge transfer kinetics and electron back reaction of the fabricated cells.

2 Materials and methods

2.1 Materials

ZnO nanopowder, Zinc acetate dehydrate ($(\text{CH}_3\text{COO})_2\text{Zn} \cdot 2\text{H}_2\text{O}$) and Monoethanolamine (MEA) were bought from Sigma Aldrich, India. ethylcellulose and terpeneol were bought from TCI Chemicals, India. Transparent FTO coated glass ($10 \Omega/\text{square}$), the high-performance liquid electrolyte (Iodolyte AN50), chenodeoxycholic acid (CDCA) as a dye co-adsorbent and liquid platinum paint (Platisol T) to prepare the platinum-coated counter electrode were purchased from Solaronix, Switzerland. Meltonix 1170–25 ($25 \mu\text{m}$) (Solaronix) was used as a spacer between the working and counter electrode to avoid

short-circuiting. All the reagents utilized in the fabrication process were of analytical grades. So no further purification was required.

2.2 Preparation of conventional ZnO photoanode

To prepare the thin films of the photoanode materials, the FTO coated glass substrates were first cleaned with dilute HCl in an ultrasonic bath for 15 min and then thoroughly rinsed with deionized water to remove the HCL residues. The substrates were then cleaned with acetone and ethanol using an ultrasonic cleaning bath (Biswas and Chatterjee 2020; Biswas et al. 2019). The mesoporous ZnO photoelectrode of the DSSC was prepared by following the standard doctor blade method. The paste for doctor blading was prepared by mixing 0.5 g of ZnO nanopowder with α -terpineol as a solvent and 0.45 g of ethyl cellulose as a binder (Wong et al. 2012). The mixture was stirred continuously to obtain a smooth lump-free slurry. The ZnO paste was then coated on the conductive side of the cleaned FTO glass substrate and subsequently annealed at 400 °C on a hot plate for 30 min to burn out the ethyl cellulose and other organic contents of the working electrode and to strengthening the bonding between the substrate and the ZnO film. In addition to that, the annealing procedure also helps to improve the surface quality of the thin film along with increasing the crystallinity of the sample (Elilarassi and Chandrasekaran 2010; Shivaraj et al. 2015; Al-Kahlout 2015; Pandey et al. 2017).

2.3 Preparation of photoanode with compact ZnO layer

In order to improve the photovoltaic performance of the cells further by preventing the direct contact between FTO and liquid electrolyte, a thin and compact ZnO layer was deposited on FTO coated glass substrate by employing a simple sol–gel spin coating method prior to deposition of mesoporous active ZnO nanoparticle layer. The precursor solution was prepared by mixing Zinc acetate dehydrate (CH_3COO)₂Zn, 2H₂O) in 50 ml isopropanol as solvent and monoethanolamine (MEA) was used as a stabilizer. The precursor solution concentration was maintained at 0.05 M. The mixture was vigorously stirred at 60° C by a magnetic stirrer for 1 h. MEA was added dropwise under stirring, yielding a clear homogenous solution. The solution was left for 24 h at room temperature for aging before it could be used for film deposition. The aged solution was then spin-coated on a cleaned FTO glass substrate with a programmable spin coater (Apex Instruments Co. Pvt. Ltd, Model SpinNXG-P1) at 3000 rpm for 30 s and annealed at 200 °C for 20 min to form the ZnO blocking layer. Over this compact blocking layer, the mesoporous active layer was coated using the same doctor blade method and then annealed at 400 °C as done earlier.

2.4 Assembling the devices

One set of ZnO photoanodes were sensitized by immersing them in a 0.5 mM ethanolic solution of pure Rose Bengal dye for 12 h. Another set of photoanodes (both with and without ZnO blocking layer) were sensitized with the RB dye solution containing various concentrations (0–10 mM) of CDCA at room temperature for 12 h. The working electrodes were then removed from the solution and rinsed thoroughly with deionized water and ethanol to get rid of any excess dye from the thin film surface and left for air drying at room temperature. The platinum catalyst precursor solution (Platisol-T) was spin-coated

on the conducting side of the cleaned FTO glasses and heated at 450 °C for 15 min on a hot plate to prepare the counter electrodes for the cells. The dye adsorbed working electrodes and platinum(Pt)-coated counter electrodes were assembled against the coated sides of each other in a sandwich manner using two binder clips with a Surlyn film (Meltonix 1170–25 µm, Solaronix) gasket as a spacer in between them. The liquid electrolyte used in the fabrication process was poured inside the cell through fine holes pre-drilled on the counter electrodes. The red-ox concentration of the electrolyte was 50 mM. The active area of the cells for illumination was adjusted to 0.16 cm².

2.5 Characterization and measurements

X-ray diffraction (XRD) analysis is a technique used for the determination of the crystal structure of materials in the nanomaterial, thin-film, or bulk material form. In the XRD experiment, a monochromatic X-ray beam is allowed to incident on the sample and the diffraction occurs. Constructive interference is obtained for the glancing angles (θ) corresponding to those (hkl) planes only for which the path difference is equal to integral multiple (n) of wavelength (λ) of the X-ray used. This condition is given by Bragg's equation

$$2 d \sin(\theta) = n \lambda$$

where d is the interplanar spacing. The schematic of the experimental arrangement is shown in Fig. 4. The reflected X-rays make an angle 2θ with the material surface. A typical XRD pattern consists of these reflection peaks along the y-axis with the diffraction angles 2θ along the x-axis (Epp 2016, Zhang et al. 2004). In our study, the X-ray diffraction analysis was employed using PAN-analytical X'Pert PRO X-ray diffractometer (CuK α radiation, 30 mA, 40 kV, $\lambda = 1.5406 \text{ \AA}$) to determine the crystalline structure of ZnO nanoparticles used in making the photoanode of the DSSC.

Absorbance spectrum measurement of the dye was carried out using a Perkin-Elmer Lambda-35 UV–VIS spectrophotometer. In this measurement, the sample is exposed to light within a selected range of wavelengths. Absorption occurs when the incident photon energy surpasses the energy gap between the lower energy orbital (highest occupied molecular orbital-HOMO) and the higher energy unoccupied orbital (lowest unoccupied molecular orbital-LUMO) of the materials, and then the spectrometer records the signal.

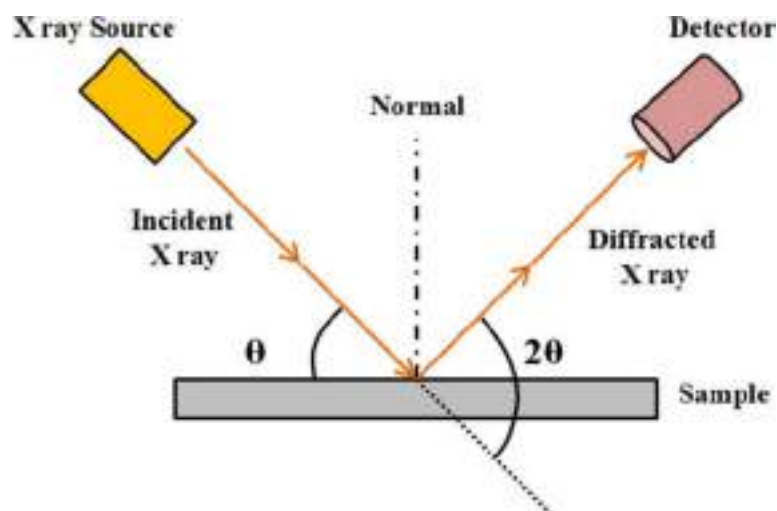


Fig. 4 X-ray diffraction at the sample film surface

The block diagram of the UV–VIS spectrophotometer is shown in Fig. 5. (Rocha et al. 2018).

Scanning electron microscopy (JEOL) was used to examine the surface morphology of the prepared ZnO thin films. The current–voltage (J–V) characterization of the cells was measured under 100 mW/cm^2 illumination using a Keithley 2400 digital source meter which was controlled by Keithley LabTracer computer software. The overall photoconversion efficiency of the solar cell was calculated using the formula

$$\eta = \frac{P_{\text{out}}}{P_{\text{in}}} = \frac{I_{\text{sc}} V_{\text{oc}} FF}{P_{\text{in}}} \quad (1)$$

where P_{in} , V_{oc} , I_{sc} and FF denote the incident photon power, open-circuit voltage, the short circuit current density and fill factor respectively. The fill factor was estimated using the following formula:

$$FF = \frac{I_{\text{max}} V_{\text{max}}}{I_{\text{sc}} V_{\text{oc}}} \quad (2)$$

where I_{max} and V_{max} , respectively, represent values of current and voltage at the maximum output power point of the solar cell. The area of the fabricated cells that was exposed to light was 1 cm^2 . The electrochemical impedance spectroscopy (EIS) of the cells was done in the frequency range of 0.1–190 kHz under open circuit conditions.

3 Results and discussion

3.1 UV–VIS absorption spectral analysis of the dye

0.5 mM ethanolic solution of Rose Bengal dye was prepared and its absorption property was studied using Perkin Elmer Lambda–35 UV–VIS spectrophotometer. UV–VIS absorption spectrum of the RB dye is shown in Fig. 7a. The value of λ_{max} obtained from the absorption spectrum is a very important parameter as it demonstrates the potential of the molecular systems for significant usage as a functional material in DSSC. It can be observed that the Rose Bengal dye absorbs a larger fraction of the solar spectrum in the visible

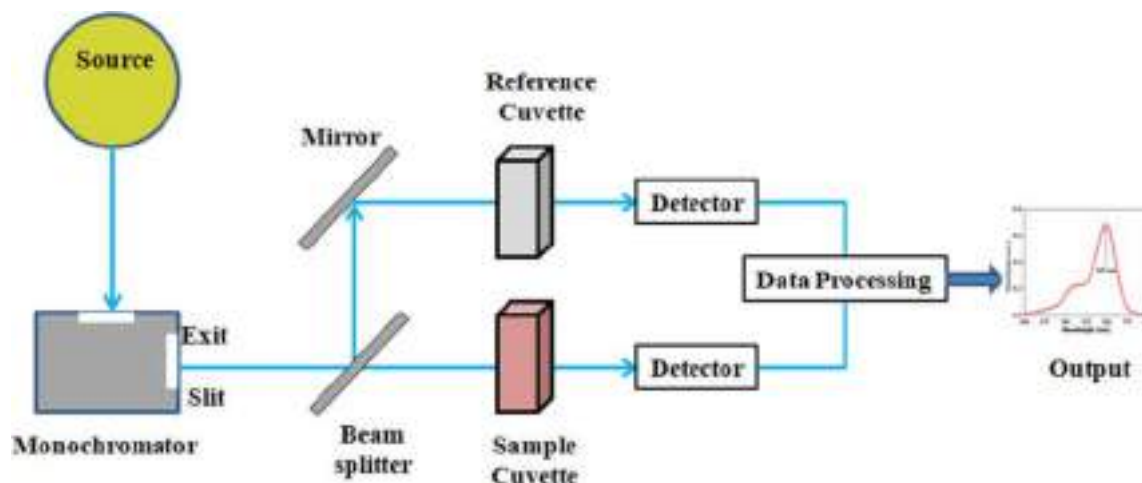
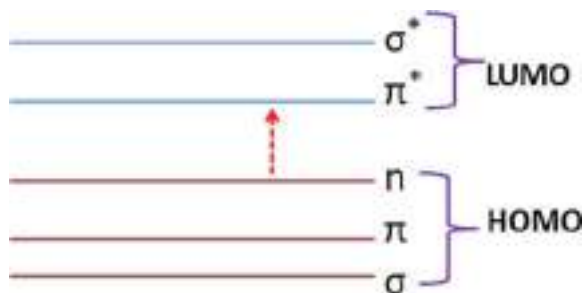


Fig. 5 Schematic of UV–VIS spectrophotometer

Fig. 6 Possible transition mechanism in the Rose Bengal molecular system



region of 460–600 nm and it shows the highest optical absorption at 549 nm wavelength. The strong absorption peak may be assigned to the intra-molecular charge transfer (ICT) transitions from the donor to acceptor level within HOMO (Highest Occupied Molecular Orbital)- (Lowest Unoccupied Molecular Orbital)LUMO energy levels as shown in Fig. 6 (Sayyed et al. 2016, Singh et al. 2012).

The optical energy gap of the dye was calculated using Tauc's relation (Eq. 3) (Shamsuddin et al. 2017, Ghobadi 2013, Uyanga et al. 2020)

$$\alpha h\nu = B(h\nu - E_g)^m \quad (3)$$

where α is the absorption coefficient, $h\nu$ is the photon energy, E_g is the optical energy gap of the material and value of m depends on type of transition. The value of m is 2 or $\frac{1}{2}$ for indirect and direct transition respectively. The direct band gap of the Rose Bengal dye was found to be 2.19 eV by extrapolating the linear part of the $(\alpha h\nu)^2$ versus $h\nu$ plot as shown in Fig. 7b. The indirect band gap of the dye was calculated through extrapolation of the linear portion of the $(\alpha h\nu)^{1/2}$ versus $h\nu$ plot as shown in Fig. 7c (Patni et al. 2020) which indicates indirect transition at $E_g = 2.13$ eV.

The HOMO–LUMO direct band gap of the dye affects the electron transfer from the LUMO of the dye molecule to the conduction band of the ZnO particles. It facilitates the vertical electron transition through the dye excitation (Henson et al. 2013). On the other hand, indirect transition is a phonon assisted transition where change in momentum must be taken into account. When the photons having energy fairly above the indirect band gap of dye molecule is absorbed by the dye electron, phonons get emitted (Seo and Hoffmann 1999). As a result the direct band gap is utilized to determine the vertical transition during the course of photosensitization (Nguyen et al. 2013, Prima et al. 2016). Hence, the lowest electronic transition, which corresponds to the onset of absorption in the UV–visible absorption spectrum, was used to calculate the optical bandgap. It is the energy difference between HOMO and LUMO which is caused by the excitation of electrons from HOMO to LUMO.

3.2 Structural and phase characterization ZnO compact layer

The X-ray diffraction pattern of the ZnO compact blocking layer, shown in Fig. 8a, exhibits the hexagonal wurtzite crystal phase of ZnO and the peaks well match with the standard JCPDS card no. 36–1451. The diffraction peaks observed at 2θ values of 31.79°, 34.42°, 36.25°, 47.51°, 56.60°, 62.86°, 67.96°, and 69° corresponds to the reflection from the (100), (002), (101), (110), (103), (112), and (201) lattice planes respectively. Sharp and strong peaks indicate the highly crystalline nature of the material

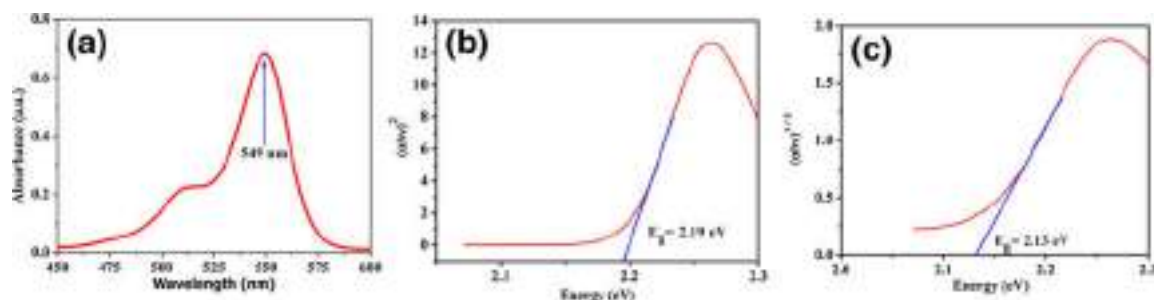


Fig. 7 **a** UV–VIS absorption spectra of Rose Bengal dye **b** Tauc's plot for direct transition and **c** Tauc's plot for indirect transition

(Costantino et al. 1998; Oh et al. 2002). The XRD pattern for the commercial ZnO nanopowder is shown in Fig. 8b. It can be clearly seen that both the commercial ZnO nanopowder and synthesized ZnO blocking layer showed similar XRD patterns. The XRD pattern of sample with both the blocking and active layer is shown in Fig. 8c. This is very similar to the XRD pattern of the blocking layer. This is because the blocking layer is more crystalline in nature, which is evident from its XRD pattern with its sharper peaks.

3.3 Surface morphology study and energy dispersive spectroscopy of the photoanodes

Scanning electron microscopic (SEM) analysis of the ZnO active layer and the compact blocking layer on the FTO substrate was carried out to study the surface morphology and the particle size of the sample. The SEM images of the ZnO active and blocking layers on the FTO substrate are depicted in Fig. 9. It can be seen from Fig. 9a that the ZnO nanoparticles have a hexagonal structure. Figure 9b and c represent the SEM images of compact blocking layer at low and high magnifications respectively. The diameter of the spin-coated nanoparticles ranges from 150 to 180 nm. Further, the chemical composition and elemental percentage of the compact ZnO film are revealed by the Energy Dispersive X-Ray Spectroscopy (EDS) analysis which is shown in Fig. 9d. Predominating peaks of Zn and O₂ unveil that the synthesized blocking layer contains pure ZnO.

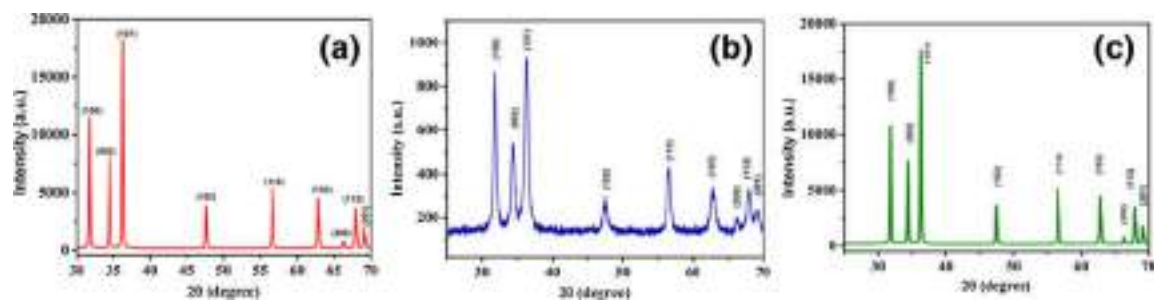


Fig. 8 X-ray diffraction pattern of **a** ZnO compact blocking layer **b** ZnO nanoparticles as active layer **c** ZnO blocking/active layer

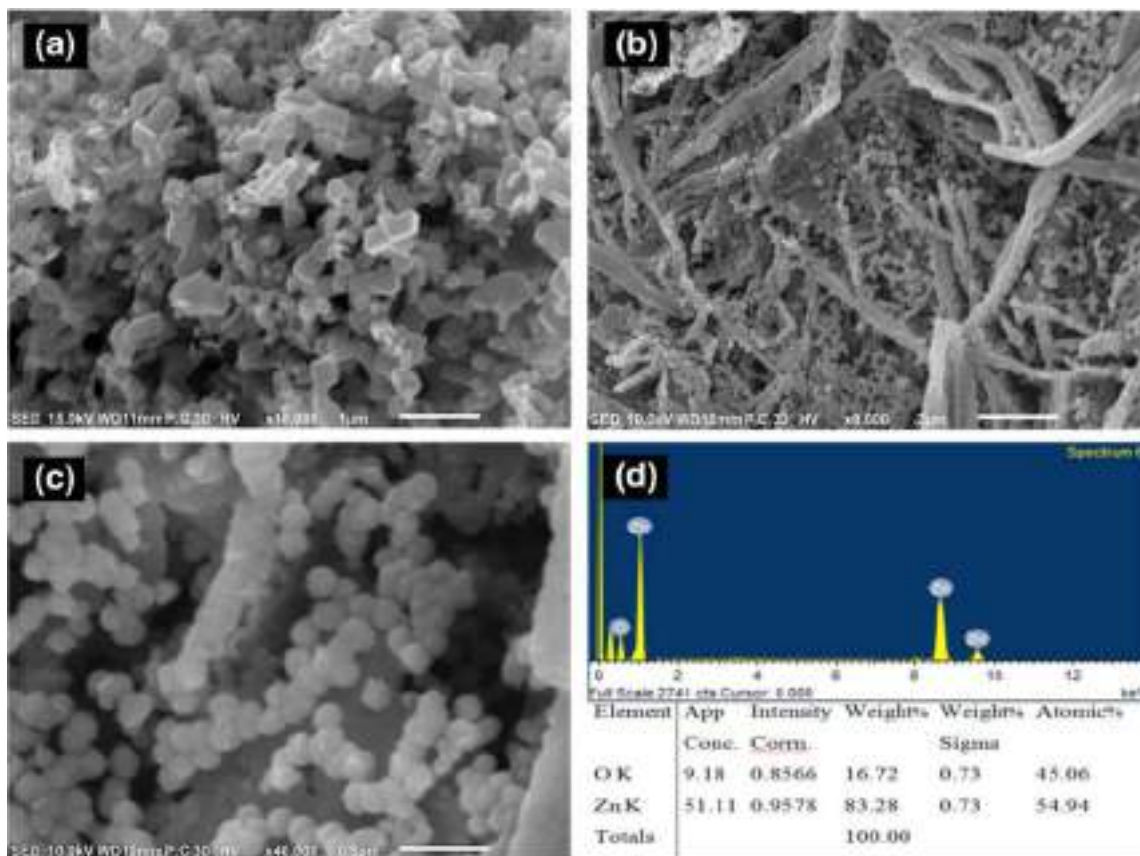


Fig. 9 SEM images of a ZnO NP active layer, b ZnO blocking layer at lower magnification, c ZnO blocking layer at higher magnification and d EDS and Elemental composition of ZnO blocking layer

3.4 Photovoltaic characterization of the cells

The Current–Voltage (J–V) characteristic is a crucial measurement that reveals the value of the overall photovoltaic performance of a solar cell along with the key performance parameters like open circuit voltage and short circuit current density. Figure 10a depicts the J–V characteristics of the DSSCs based on different types of photoanodes used in this study and the obtained photovoltaic parameters for each of the cells are summarized in Table 1.

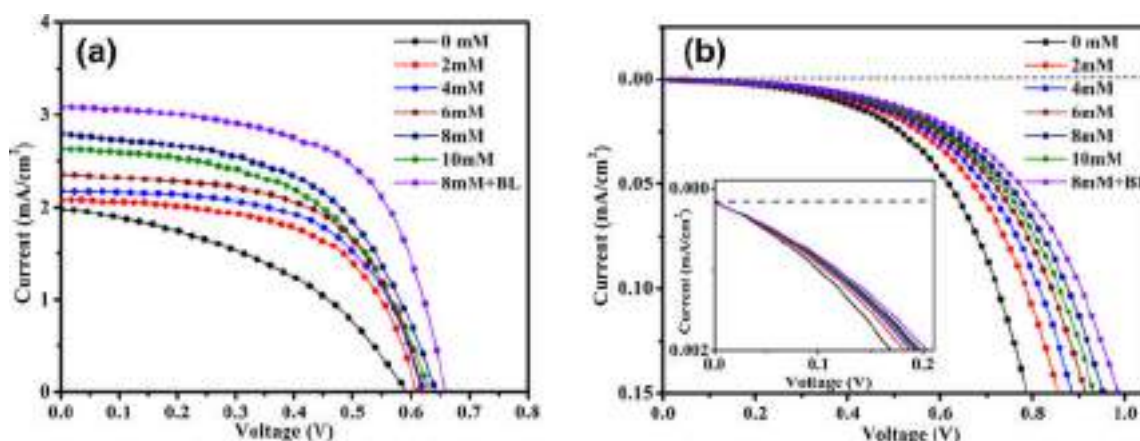


Fig. 10 Current–voltage characteristics of different cells under a illumination b dark

Table 1 Photovoltaic parameters of DSSCs fabricated with various ZnO photoanodes

Cell name	CDCA concentration	J_{sc} (mA/cm ²)	V_{oc} (V)	FF	Efficiency (η %)
DSSC1	0 mM	1.98	0.58	0.43	0.49
DSSC2	2 mM	2.08	0.61	0.58	0.74
DSSC3	4 mM	2.18	0.62	0.60	0.81
DSSC4	6 mM	2.36	0.63	0.58	0.86
DSSC5	8 mM	2.80	0.64	0.56	1.00
DSSC6	10 mM	2.63	0.64	0.54	0.91
DSSC7	8 mM + BL	3.09	0.66	0.60	1.22

3.4.1 Effect of CDCA

The conventionally prepared DSSC with ZnO nanoparticles and Rose Bengal dye displayed a short circuit current density (J_{sc}) of 1.98 mA/cm², an open circuit voltage (V_{oc}) of 0.58 V, and a fill factor (FF) of 0.43, resulting in a photoconversion efficiency(η) of 0.49%. However, under the same working conditions, the device performance was found to be highly influenced when CDCA solution was incorporated into the dye solution at various concentrations. From Table 1, it can be noted that the value of V_{oc} , as well as J_{sc} , increases with an increase in the concentration of CDCA. Optimum concentration (8 mM) provides the finest dye attachment to the ZnO surface. The best device performance was achieved for the optimized CDCA concentration of 8 mM when added with 0.5 mM RB dye solution. This improvement in the performance may be attributed to reduced dye aggregation along with uniform dye adsorption yielding better electron injection into the conduction band of ZnO.

3.4.2 Effect of compact ZnO blocking layer

To avoid the direct contact between the FTO and the liquid electrolyte through the pores present in the nanocrystalline ZnO film in a conventionally prepared DSSC, a thin and compact layer of ZnO was employed as shown in Fig. 11. From Table 1 it can be observed that the addition of a compact ZnO blocking layer in DSSC7 with 8 mM CDCA additive shows a remarkable enhancement in J_{sc} (3.09 mA/cm²) and V_{oc} (0.66 V) and consequently the highest value of photoconversion efficiency η (1.22%) was obtained among all the fabricated cells. Such type of performance enhancement may be accredited to the consolidated effect of improved dye loading due to the addition of CDCA with proper concentration and increased charge collection along with decreased electron recombination at the FTO/ZnO/electrolyte interface hindering the direct contact between FTO and electrolyte by the blocking layer.

3.4.3 Dark current measurement

To explore the effect of CDCA concentration and ZnO blocking layer in the process of electron back transfer, the J-V characteristics were also measured in the dark which is shown in Fig. 10b. It is regarded as a qualitative method to assess the degree of electron back transfer in DSSCs. The dark current generation is known to be partly due to the

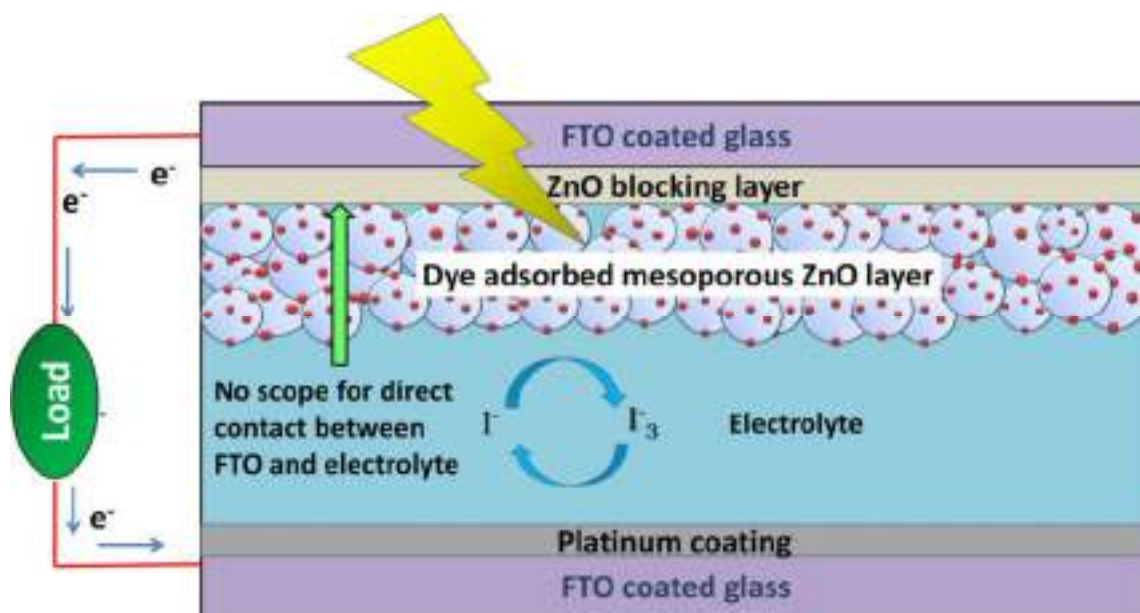


Fig. 11 Schematic diagram of a DSSC with compact ZnO blocking layer

presence of exposed FTO sites having direct contact with the liquid electrolyte and the pores left between the ZnO nanoparticles and the FTO surface (Yang et al. 2014; Yeoh and Chan 2019). These exposed FTO sites and the pores of ZnO nanoparticle film would allow the liquid electrolyte to penetrate through ZnO film and directly come in contact with bare FTO sites resulting in recombination losses as shown in the energy band diagram for conventional ZnO NP based DSSC in Fig. 12a. It can be observed from Fig. 10b that for a particular value of the voltage on the X-axis (i.e. voltage axis) of the dark current characteristics, the corresponding Y-axis value (i.e. value of dark current) is lowest for DSSC7 for that particular voltage. It can also be seen that the dark current has the highest value for conventionally prepared cell (DSSC1) with bare FTO and decreases with an increase in CDCA concentration up to 8 mM. An enlarged plot of the dark current characteristics is provided as an inset in Fig. 10b so that a clear scenario is observed. For the cell (DSSC7) with compact ZnO BL and 8 mM CDCA solution as dye co-adsorbent, the dark current is reduced significantly for the same bias potential in comparison to all other cells. This

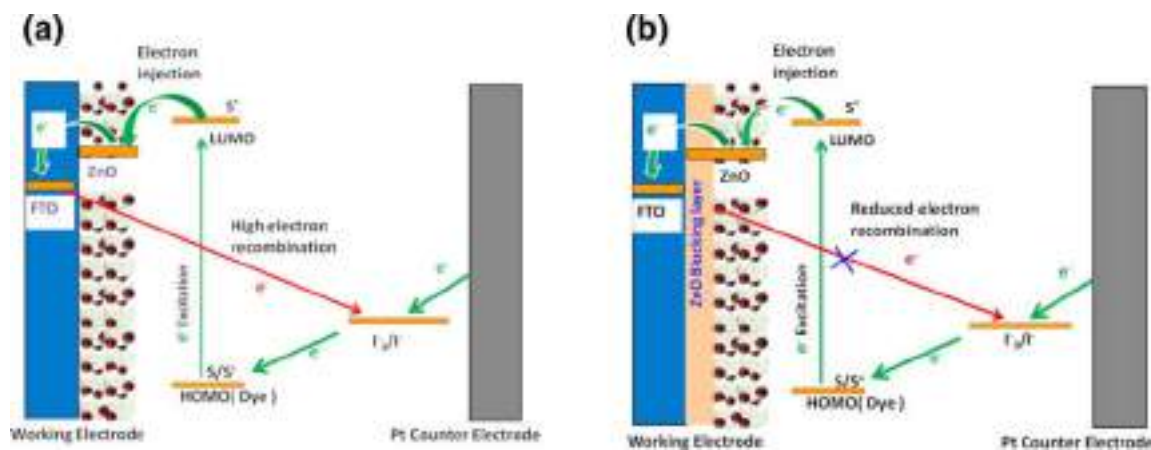


Fig. 12 Schematic diagram showing interfacial charge transfer and recombination in case of DSSCs **a** without ZnO BL **b** with compact ZnO BL

demonstrates that the compact ZnO BL reduces the bare FTO site and thereby successfully suppresses the dark current by lowering the electron back transfer. It was also observed that the DSSC7 has the slowest rate of increase of dark current with an increase in bias voltage confirming excellent suppression of electron recombination and consequently reduced current loss.

The variations of different cell parameters with the concentration of CDCA solution for the fabricated DSSCs are depicted in Fig. 13. It can be observed that CDCA concentration highly influences the value of J_{sc} . ZnO BL improves the current further. A small increase in the values of V_{oc} and FF can also be noted from Fig. 10 due to these processes. The highest values of cell parameters were obtained for the cell DSSC7.

3.5 Electrochemical impedance spectroscopy study

To further gain an insight into the influence of CDCA concentration and the coating of compact ZnO blocking layer on the charge transfer and recombination kinetics of the prepared devices, the DSSCs were further investigated by electrochemical impedance spectroscopic (EIS) measurement in dark under V_{oc} bias voltage with 10 mV AC perturbation amplitude. This gives a more precise understanding of the limiting factors for the cell performance parameters. In the EIS measurement done under the dark condition and with an applied bias voltage, electrons from FTO are injected into the conduction band of ZnO and then transported through the ZnO network. Some of the injected electrons recombine with the I_3^- ion present in the electrolyte giving rise to the recombination phenomenon (Liu et al. 2018). Figure 14a shows the Nyquist plot of all the prepared cells exhibiting two obvious semicircles. The curves are fitted using the equivalent circuit shown in the inset of Fig. 14a and the EIS measurement results obtained in terms of resistances and capacitances are summarized in Table 2. The charge transfer resistance (R_{pt}) and double layer capacitance (C_{pt}) at the Pt counter electrode/electrolyte interface is responsible for the first semicircle in the high-frequency range, while the second semicircle in the mid-frequency range may be assigned to the charge transfer and recombination resistance (R_{rec})

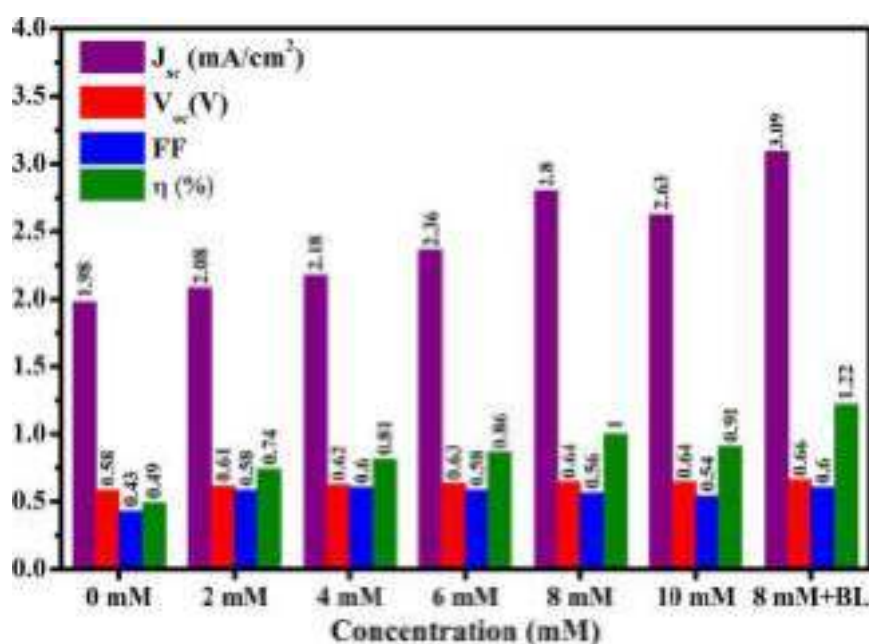


Fig. 13 Effect of CDCA concentration and ZnO blocking layer (BL) on different cell parameters

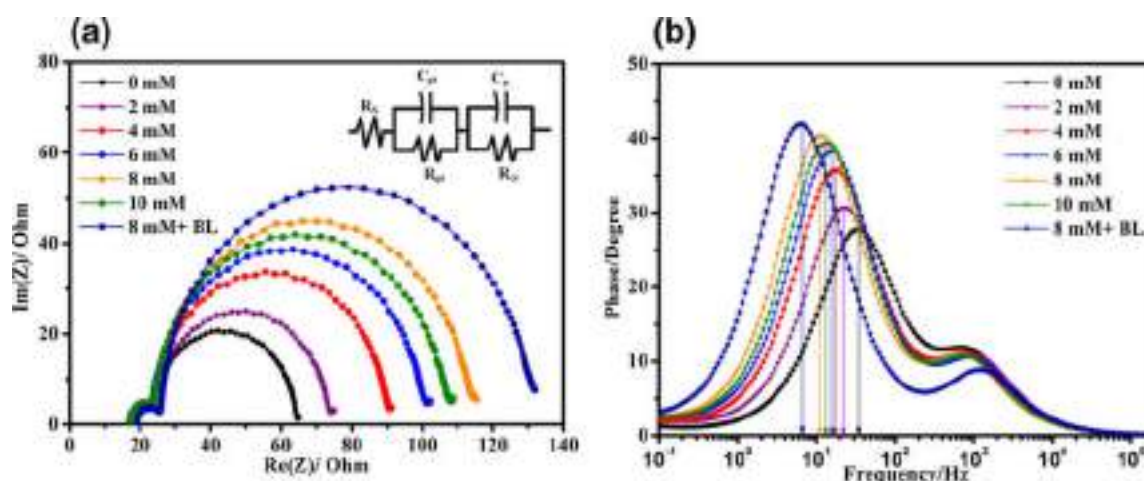


Fig. 14 EIS of the DSSCs representing **a** Nyquist plot along with equivalent circuit (inset) and **b** Bode plot

Table 2 Parameters obtained from EIS measurement

Cell name	CDCA concentration	R_s (Ω)	R_{pt} (Ω)	R_{rec} (Ω)	Peak freq. f(Hz)	Electron lifetime (τ_e) (ms)
DSSC1	0 mM	17.15	6.51	40.2	34.21	4.65
DSSC2	2 mM	17.23	6.55	48.8	22.13	7.19
DSSC3	4 mM	17.05	6.46	65.4	17.05	9.34
DSSC4	6 mM	17.12	6.23	75.2	15.62	10.94
DSSC5	8 mM	17.36	6.65	87.6	11.03	14.45
DSSC6	10 mM	17.29	6.37	81.4	13.13	12.13
DSSC7	8 mM+BL	19.23	6.39	102.7	6.54	24.35

and chemical capacitance (C) at the ZnO/dye/electrolyte interface (Li et al. 2011, Mazloum et al. 2019, Zhao et al. 2017). The intercept at the real axis of the Nyquist plot represents the series resistance (R_s) of FTO and other ohmic contacts like connecting cables, clamps and clips used to connect the cells for measurement. (Ondersma and Hamann 2010; Chou et al. 2019).

The small semicircles in the high-frequency range are almost identical indicating nearly similar values of R_{pt} for all four kinds of cells as all of them have similar Pt counter electrodes and the same electrolyte. On the contrary, a substantial dissimilarity can be observed in large semicircles in the mid-frequency range. This indicates that the charge transport and recombination behaviour at the ZnO/dye/electrolyte interface was extensively affected due to working electrode modification by the addition of CDCA and incorporation of the blocking layer. The middle arc of the Nyquist plot for the conventionally prepared DSSC has the lowest diameter indicating the lowest recombination resistance (R_{rec}) and thus representing the highest recombination process among all the cells. The diameter is evidently larger for the CDCA treated cells indicating its positive role in increasing the recombination resistance and hence lowering the recombination phenomena. It can be observed from Table 2 that the recombination resistance increases in the order of DSSC1 < DSSC2 < DSSC3 < DSSC4 < DSSC6 < DSSC5 < DSSC7 indicating that the recombination resistance increases with an increase in CDCA concentration from 0 to 8 mM and decreases at 10 mM

concentration. The larger R_{rec} value indicates it is more difficult to transfer the injected electrons from the ZnO back to the electrolyte, and thus the back recombination can be suppressed in the cell, thus giving a higher J_{sc} and V_{oc} . The highest value of recombination resistance is obtained when the optimum CDCA concentration (8 mM) is combined with the ZnO blocking layer in DSSC7 leading to the highest J_{sc} and V_{oc} of 3.09 mA/cm² and 0.66 V respectively and consequently best device performance. The highest recombination resistance is obtained for the cell with the blocking layer as the blocking layer prevents the injected electrons to come in direct contact with the electrolyte and consequently reduces the direct capture of electrons by the I_3^- ions of the electrolyte. Furthermore, the CDCA addition with optimum concentration and blocking layer increases the number of electrons accumulated in the conduction band of ZnO which led to increased electron density. This creates a small shift of Fermi level for the electrons present in the ZnO. This rise in Fermi level slightly improves V_{oc} which can also be observed from Table 1 (Li et al. 2011; Wei et al. 2015).

Apart from recombination resistance, the second semicircle also provides information about the electron lifetime in the conduction band of ZnO which gives the measure of the rate at which the recombination reaction occurs. This lifetime is inversely proportional to the oscillation frequency at which the peak on the second arc is obtained. But, since, the frequency information is missing in the Nyquist plot; the electron lifetime can be calculated from the phase bode plot using the formula

$$\tau_e = \frac{1}{2\pi f_{\text{peak}}} \quad (3)$$

where f_{peak} represents the peak frequency of phase Bode plot in the mid-frequency range as shown in Fig. 14b. A shift in the peaks may be observed in the Bode plots of the DSSCs prepared following different procedures. Shifting of peak frequency towards lower frequency represents longer electron lifetime (τ_e) and slower recombination process. The calculated electron lifetimes for all the cells are summarised in Table 2. The highest electron lifetime of 24.35 ms is obtained for the cell fabricated with 8 mM CDCA concentration along with ZnO compact blocking layer (DSSC 7). The increased electron lifetime due to CDCA and blocking layer effectively enhances the photoconversion efficiency (PCE) which is in good agreement with the results obtained from J-V measurement. The reduced dye aggregation in presence of CDCA and inhibition of electron recombination by the blocking layer may be accounted for this.

4 Conclusion

Effects of co-adsorption of CDCA and ZnO blocking layer were investigated in Rose Bengal dye based DSSCs. The surface, photovoltaic and electrochemical properties of all the cells were extensively studied. The strong binding of CDCA molecules to the ZnO surface partially displaces dye molecules and consequently reduces photon harvesting. Excessive CDCA concentration implies significantly reduced dye attachment to the ZnO surface leading to decreased amount of light energy absorption. Therefore, to maximize the positive effect of the co-adsorbent, it is very crucial to carefully optimize the amount of CDCA. The amount of CDCA has been optimized by adjusting its concentration in the dye solution and found that the best device performance was obtained for 8 mM concentration. At optimized co-adsorbent concentration, the reduced dye loading due to the presence of CDCA

and consequently decreased light-harvesting was compensated by the increased electron injection efficiency leading to maximum device efficiency of 0.97%. The performance was further increased from 1.00 to 1.22% when a compact ZnO blocking layer was added to the FTO before depositing the mesoporous ZnO active layer. This was due to the suppression of electron back transfer from the FTO to the liquid electrolyte. These results indicate that the addition of CDCA as a dye co-adsorbent and the introduction of ZnO blocking layer is an effective way to boost the performance of Rose Bengal dye based DSSCs. The efficiency of the fabricated cells is low as the dye used in this study is rose bengal. Though the efficiency is low here compared to the ruthenium based cells, it lies in the range of efficiency of rose bengal dye based DSSCs obtained by other researchers. Higher efficiencies can be obtained by using high performance ruthenium dye.

Funding The project was funded by the Department of Physics, University of North Bengal.

Data availability Datasets generated during the current study are available and shall be provided on reasonable request.

Declarations

Conflict of interest There is no financial and non-financial conflict of interest in this research work.

Consent for publication All the authors of this manuscript agree with the final version of the manuscript and give their consent for it to be published, accepting all the ethical standards of the Journal of Optical and Quantum Electronics. The authors also certify that this manuscript has not been published elsewhere and that it is not under consideration for publication in any other journal.

References

- Aghazada, S., Nazeeruddin, M.K.: Ruthenium complexes as sensitizers in dye-sensitized solar cells. *Inorganics* **6**(2), 52 (2018). <https://doi.org/10.3390/inorganics6020052>
- Alharbi, F., Bass, J.D., Salhi, A., Alyamani, A., Kim, H.C., Miller, R.D.: Abundant non-toxic materials for thin film solar cells: alternative to conventional materials. *Renew. Energy* **36**, 2753–2758 (2011). <https://doi.org/10.1016/j.renene.2011.03.010>
- Al-Kahlout, A.: Thermal treatment optimization of ZnO nanoparticles-photoelectrodes for high photovoltaic performance of dye-sensitized solar cells. *J. Assoc. Arab Univ. Basic Appl. Sci.* **17**(1), 66–72 (2015). <https://doi.org/10.1016/j.jaubas.2014.02.004>
- Bach, W.: *Global warming: the complete briefing* (2nd ed). John Houghton. Cambridge University Press: Cambridge, 1997. Pp. xv + 251. Paperback: ISBN 0521-62932-2, ??12.95; hardback: ISBN 0-321-62089-9, ??35.00. *Int. J. Climatol.* (1998). [https://doi.org/10.1002/\(sici\)1097-0088\(199804\)18:5<579::aid-joc278>3.3.co;2-0](https://doi.org/10.1002/(sici)1097-0088(199804)18:5<579::aid-joc278>3.3.co;2-0)
- Barbir, F., Veziroğlu, T.N., Plass, H.J.: Environmental damage due to fossil fuels use. *Int. J. Hydrogen Energy* **15**(10), 739–749 (1990). [https://doi.org/10.1016/0360-3199\(90\)90005-J](https://doi.org/10.1016/0360-3199(90)90005-J)
- Biswas, R., Roy, T., Chatterjee, S.: Study of electro-optical performance and interfacial charge transfer dynamics of dye sensitized solar cells based on ZnO nanostructures and natural dyes. *J. Nanoelectron. Optoelectron.* **14**(1), 99–108 (2019). <https://doi.org/10.1166/jno.2019.2445>
- Biswas, R., Chatterjee, S.: Effect of surface modification via sol-gel spin coating of ZnO nanoparticles on the performance of WO₃ photoanode based dye sensitized solar cells. *Optik* **212**, 164142 (2020). <https://doi.org/10.1016/j.ijleo.2019.164142>
- Buene, A.F., Almenningen, D.M., Hagfeldt, A., Gautun, O.R., Hoff, B.H.: First report of chenodeoxycholic acid-substituted dyes improving the dye monolayer quality in dye-sensitized solar cells. *Sol. RRL* **4**(4), 1900569 (2020). <https://doi.org/10.1002/solr.201900569>

- Cai, N., Moon, S.J., Cevey-Ha, L., Moehl, T., Humphry-Baker, R., Wang, P., Zakeeruddin, S.M., Grätzel, M.: An organic D- π -A dye for record efficiency solid-state sensitized heterojunction solar cells. *Nano Lett.* **11**(4), 1452–1456 (2011). <https://doi.org/10.1021/nl104034e>
- Chiba, Y., Islam, A., Komiya, R., Koide, N., Han, L.: Conversion efficiency of 10.8% by a dye-sensitized solar cell using a TiO₂ electrode with high haze. *Appl. Phys. Lett.* **88**(22), 223505 (2006). <https://doi.org/10.1063/1.2208920>
- Chou, J.C., Lu, C.C., Liao, Y.H., Lai, C.H., Nien, Y.H., Kuo, C.H., Ko, C.C.: Fabrication and electrochemical impedance analysis of dye-sensitized solar cells with titanium dioxide compact layer and graphene oxide dye absorption layer. *IEEE Trans. Nanotechnol.* **18**, 461–466 (2019). <https://doi.org/10.1109/TNANO.2019.2913537>
- Chung, I., Lee, B., He, J., Chang, R.P.H., Kanatzidis, M.G.: All-solid-state dye-sensitized solar cells with high efficiency. *Nature* **485**(7399), 486–489 (2012). <https://doi.org/10.1038/nature11067>
- Costantino, U., Marmottini, F., Nocchetti, M., Vivani, R.: New synthetic routes to hydroxalcalite-like compounds: characterisation and properties of the obtained materials. *Eur. J. Inorg. Chem.* **1998**(10), 1439–1446 (1998). [https://doi.org/10.1002/\(sici\)1099-0682\(199810\)1998:10%3c1439::aid-ejic1439%3e3.0.co;2-1](https://doi.org/10.1002/(sici)1099-0682(199810)1998:10%3c1439::aid-ejic1439%3e3.0.co;2-1)
- Duffy, N.W., Peter, L.M., Rajapakse, R.M.G., Wijayantha, K.G.U.: Investigation of the kinetics of the back reaction of electrons with tri-iodide in dye-sensitized nanocrystalline photovoltaic cells. *J. Phys. Chem. B* **104**(38), 8916–8919 (2000). <https://doi.org/10.1021/jp001185z>
- Elilarassi, R., Chandrasekaran, G.: Effect of annealing on structural and optical properties of zinc oxide films. *Mater. Chem. Phys.* **121**(1–2), 378–384 (2010). <https://doi.org/10.1016/j.matchemphys.2010.01.053>
- Epp, J.: X-ray diffraction (XRD) techniques for materials characterization. In: *Materials characterization using nondestructive evaluation (NDE) methods*, pp. 81–124. Elsevier (2016). <https://doi.org/10.1016/B978-0-08-100040-3.00004-3>
- Ghobadi, N.: Band gap determination using absorption spectrum fitting procedure. *Int. Nano Lett.* **3**(1), 1–4 (2013). <https://doi.org/10.1186/2228-5326-3-2>
- Goetzberger, A., Hebling, C., Schock, H.W.: Photovoltaic materials, history, status and outlook. *Mater. Sci. Eng. R. Rep.* **40**(1), 1–46 (2003). [https://doi.org/10.1016/S0927-796X\(02\)00092-X](https://doi.org/10.1016/S0927-796X(02)00092-X)
- Grätzel, M.: Dye-sensitized solar cells. *J. Photochem. Photobiol. C Photochem. Rev.* **4**(2), 145–153 (2003). [https://doi.org/10.1016/S1389-5567\(03\)00026-1](https://doi.org/10.1016/S1389-5567(03)00026-1)
- Grätzel, M.: Solar energy conversion by dye-sensitized photovoltaic cells. *Inorg. Chem.* **44**(20), 6841–6851 (2005). <https://doi.org/10.1021/ic0508371>
- Guillén, E., Peter, L.M., Anta, J.A.: Electron transport and recombination in ZnO-based dye-sensitized solar cells. *J. Phys. Chem. C* **115**(45), 22622–22632 (2011). <https://doi.org/10.1021/jp206698t>
- Henson, Z.B., Zhang, Y., Nguyen, T.Q., Seo, J.H., Bazan, G.C.: Synthesis and properties of two cationic narrow band gap conjugated polyelectrolytes. *J. Am. Chem. Soc.* **135**(11), 4163–4166 (2013). <https://doi.org/10.1021/ja400140d>
- Hosenuzzaman, M., Rahim, N.A., Selvaraj, J., Hasanuzzaman, M., Malek, A.B.M.A., Nahar, A.: Global prospects, progress, policies, and environmental impact of solar photovoltaic power generation. *Renew. Sustain. Energy Rev.* **41**, 284–297 (2015). <https://doi.org/10.1016/j.rser.2014.08.046>
- Inoue, T., Pandey, S.S., Fujikawa, N., Yamaguchi, Y., Hayase, S.: Synthesis and characterization of squaric acid based NIR dyes for their application towards dye-sensitized solar cells. *J. Photochem. Photobiol. A* **213**(1), 23–29 (2010). <https://doi.org/10.1016/j.jphotochem.2010.04.015>
- Ismail, M., Ahmad Ludin, N., Hisham Hamid, N., Adib Ibrahim, M., Sopian, K.: The Effect of Chenodeoxycholic Acid (CDCA) in Mangosteen (*Garcinia mangostana*) Pericarps Sensitizer for Dye-Sensitized Solar Cell (DSSC). In: *Journal of Physics: Conference Series*. Vol. 1083, No. 1, p. 012018 (2018). doi :<https://doi.org/10.1088/1742-6596/1083/1/012018>
- Ito, S., Nazeeruddin, M.K., Liska, P., Comte, P., Charvet, R., Péchy, P., Jirousek, M., Kay, A., Zakeeruddin, S.M., Grätzel, M.: Photovoltaic characterization of dye-sensitized solar cells: effect of device masking on conversion efficiency. *Prog. Photovolt. Res. Appl.* **14**(7), 589–601 (2006). <https://doi.org/10.1002/pip.683>
- Kim, H., Veerappan, G., Park, J.H.: Conducting polymer coated non-woven graphite fiber film for dye-sensitized solar cells: superior Pt-and FTO-free counter electrodes. *Electrochim. Acta* **137**, 164–168 (2014). <https://doi.org/10.1016/j.electacta.2014.06.012>
- Kumar, V., Gupta, R., Bansal, A.: Role of chenodeoxycholic acid as co-additive in improving the efficiency of DSSCs. *Sol. Energy* **196**, 589–596 (2020). <https://doi.org/10.1016/j.solener.2019.12.034>
- Lee, T.D., Ebong, A.U.: A review of thin film solar cell technologies and challenges. *Renew. Sustain. Energy Rev.* **70**, 1286–1297 (2017). <https://doi.org/10.1016/j.rser.2016.12.028>

- Lee, K.M., Suryanarayanan, V., Ho, K.C., Thomas, K.J., Lin, J.T.: Effects of co-adsorbate and additive on the performance of dye-sensitized solar cells: A photophysical study. *Sol. Energy Mater. Sol. Cells* **91**(15–16), 1426–1431 (2007). <https://doi.org/10.1016/j.solmat.2007.03.009>
- Li, J., Wu, W., Yang, J., Tang, J., Long, Y., Hua, J.: Effect of chenodeoxycholic acid (CDCA) additive on phenothiazine dyes sensitized photovoltaic performance. *Sci. China Chem.* **54**(4), 699–706 (2011). <https://doi.org/10.1007/s11426-011-4227-9>
- Liu, X., Zhang, Q., Li, J., Valanoor, N., Tang, X., Cao, G.: Increase of power conversion efficiency in dye-sensitized solar cells through ferroelectric substrate induced charge transport enhancement. *Sci. Rep.* **8**(1), 1–8 (2018). <https://doi.org/10.1038/s41598-018-35764-y>
- Lu, H.P., Tsai, C.Y., Yen, W.N., Hsieh, C.P., Lee, C.W., Yeh, C.Y., Diau, E.W.G.: Control of dye aggregation and electron injection for highly efficient porphyrin sensitizers adsorbed on semiconductor films with varying ratios of coadsorbate. *J. Phys. Chem. C* **113**(49), 20990–20997 (2009). <https://doi.org/10.1021/jp908100v>
- Mazloun-Ardakani, M., Arazi, R.: Improving the effective photovoltaic performance in dye-sensitized solar cells using an azobenzenecarboxylic acid-based system. *Heliyon* **5**(3), e01444 (2019). <https://doi.org/10.1016/j.heliyon.2019.e01444>
- Meadows, D.H., Meadows, D.L., Randers, J., Behrens, W.: *The Limits to Growth - Club of Rome.* (1972). <http://www.donellameadows.org/wp-content/userfiles/Limits-to-Growth-digital-scan-version.pdf>
- Nazeeruddin, M.K., Baranoff, E., Grätzel, M.: Dye-sensitized solar cells: a brief overview. *Sol. Energy* **85**(6), 1172–1178 (2011). <https://doi.org/10.1016/j.solener.2011.01.018>
- Nguyen, W.H., Bailie, C.D., Burschka, J., Moehl, T., Grätzel, M., McGehee, M.D., Sellinger, A.: Molecular engineering of organic dyes for improved recombination lifetime in solid-state dye-sensitized solar cells. *Chem. Mater.* **25**(9), 1519–1525 (2013). <https://doi.org/10.1021/cm3036357>
- O'Regan, B., Grätzel, M.: A low-cost, high-efficiency solar cell based on dye-sensitized colloidal TiO₂ films. *Nature* **353**(6346), 737–740 (1991). <https://doi.org/10.1038/353737a0>
- Oh, J.M.: The effect of synthetic conditions on tailoring the size of hydrotalcite particles. *Solid State Ionics* **151**(1–4), 285–291 (2002). [https://doi.org/10.1016/S0167-2738\(02\)00725-7](https://doi.org/10.1016/S0167-2738(02)00725-7)
- Ondersma, J.W., Hamann, T.W.: Impedance investigation of dye-sensitized solar cells employing outer-sphere redox shuttles. *J. Phys. Chem. C* **114**(1), 638–645 (2010). <https://doi.org/10.1021/jp908442p>
- Pandey, P., Parra, M.R., Haque, F.Z., Kurchania, R.: Effects of annealing temperature optimization on the efficiency of ZnO nanoparticles photoanode based dye sensitized solar cells. *J. Mater. Sci. Mater. Electron.* **28**(2), 1537–1545 (2017). <https://doi.org/10.1007/s10854-016-5693-9>
- Patni, N., Pillai, S.G., Sharma, P.: Effect of using betalain, anthocyanin and chlorophyll dyes together as a sensitizer on enhancing the efficiency of dye-sensitized solar cell. *Int. J. Energy Res.* **44**(13), 10846–10859 (2020). <https://doi.org/10.1002/er.5752>
- Patwari, J., Sardar, S., Liu, B., Lemmens, P., Pal, S.K.: Three-in-one approach towards efficient organic dye-sensitized solar cells: aggregation suppression, panchromatic absorption and resonance energy transfer. *Beilstein J. Nanotechnol.* **8**(1), 1705–1713 (2017). <https://doi.org/10.3762/bjnano.8.171>
- Pradhan, B., Batabyal, S.K., Pal, A.J.: Vertically aligned ZnO nanowire arrays in Rose Bengal-based dye-sensitized solar cells. *Sol. Energy Mater. Sol. Cells* **91**(9), 769–773 (2007). <https://doi.org/10.1016/j.solmat.2007.01.006>
- Prima, E.C., Al Qibtiya, M., Yulianto, B., Dipojono, H.K.: Influence of anthocyanin co-pigment on electron transport and performance in black rice dye-sensitized solar cell. *Ionics* **22**(9), 1687–1697 (2016). <https://doi.org/10.1007/s11581-016-1673-6>
- Quintana, M., Edvinsson, T., Hagfeldt, A., Boschloo, G.: Comparison of dye-sensitized ZnO and TiO₂ solar cells: studies of charge transport and carrier lifetime. *J. Phys. Chem. C* **111**(2), 1035–1041 (2007). <https://doi.org/10.1021/jp065948f>
- Rani, S., Shishodia, P.K., Mehra, R.M.: Enhancement of photovoltaic performance of quasi-solid state dye sensitized solar cell with dispersion of a hole conducting agent. *Mater. Sci. Pol.* **28**(1), 281 (2010)
- Rocha, F.S., Gomes, A.J., Lunardi, C.N., Kaliaguine, S., Patience, G.S.: Experimental methods in chemical engineering: ultraviolet visible spectroscopy: UV-Vis. *Can. J. Chem. Eng.* **96**(12), 2512–2517 (2018). <https://doi.org/10.1002/cjce.23344>
- Sayyed, S.A., Beedri, N.I., Kadam, V.S., Pathan, H.M.: Rose Bengal sensitized bilayered photoanode of nano-crystalline TiO₂-CeO₂ for dye-sensitized solar cell application. *Appl. Nanosci.* **6**(6), 875–881 (2016). <https://doi.org/10.1007/s13204-015-0495-6>
- Sayyed, A.R.S.A., Beedri, N.I., Kadam, V.S., Pathan, H.M.: Rose bengal-sensitized nanocrystalline ceria photoanode for dye-sensitized solar cell application. *Bull. Mater. Sci.* **39**(6), 1381–1387 (2016). <https://doi.org/10.1007/s12034-016-1279-7>
- Seo, D.K., Hoffmann, R.: Direct and indirect band gap types in one-dimensional conjugated or stacked organic materials. *Theoret. Chem. Acc.* **102**(1), 23–32 (1999). <https://doi.org/10.1007/s002140050469>

- Shamsuddin, L., Noor, I.M., Albinsson, I., Mellander, B.E., Arof, A.K.: Perovskite solar cells using polymer electrolytes. *Mol. Cryst. Liq. Cryst.* **655**(1), 181–194 (2017). <https://doi.org/10.1080/15421406.2017.1362889>
- Shao, F., Sun, J., Gao, L., Yang, S., Luo, J.: Growth of various TiO₂ nanostructures for dye-sensitized solar cells. *J. Phys. Chem. C* **115**(5), 1819–1823 (2011). <https://doi.org/10.1021/jp110743m>
- Shivaraj, B.W., Murthy, H.N.N., Krishna, M., Satyanarayana, B.S.: Effect of annealing temperature on structural and optical properties of dip and spin coated zno thin films. *Procedia Mater. Sci.* **10**, 292–300 (2015). <https://doi.org/10.1016/j.mspro.2015.06.053>
- Singh, S.P., Roy, M.S., Thomas, K.J., Balaiah, S., Bhanuprakash, K., Sharma, G.D.: New triphenylamine-based organic dyes with different numbers of anchoring groups for dye-sensitized solar cells. *J. Phys. Chem. C* **116**(9), 5941–5950 (2012). <https://doi.org/10.1021/jp210971u>
- Tiwana, P., Docampo, P., Johnston, M.B., Snaith, H.J., Herz, L.M.: Electron mobility and injection dynamics in mesoporous ZnO, SnO₂, and TiO₂ films used in dye-sensitized solar cells. *ACS Nano* **5**(6), 5158–5166 (2011). <https://doi.org/10.1021/nn201243y>
- Uyanga, K.A., Ezike, S.C., Onyedika, A.T., Kareem, A.B., Chiroma, T.M.: Effect of acetic acid concentration on optical properties of lead acetate based methylammonium lead iodide perovskite thin film. *Opt. Mater.* **109**, 110456 (2020). <https://doi.org/10.1016/j.optmat.2020.110456>
- Vittal, R., Ho, K.C.: Zinc oxide based dye-sensitized solar cells: a review. *Renew. Sustain. Energy Rev.* **70**, 920–935 (2017). <https://doi.org/10.1016/j.rser.2016.11.273>
- Wei, L., Yang, Y., Zhu, Z., Fan, R., Wang, P., Dong, Y., Chen, S.: Effect of different donor groups in bis(6-methoxypyridin-2-yl) substituted co-sensitizer on the performance of N719 sensitized solar cells. *RSC Adv.* **5**(117), 96934–96944 (2015). <https://doi.org/10.1039/c5ra19417b>
- Wong, K.K., Ng, A., Chen, X.Y., Ng, Y.H., Leung, Y.H., Ho, K.H., Djurišić, A.B., Ng, A.M.C., Chan, W.K., Yu, L., Phillips, D.L.: Effect of ZnO nanoparticle properties on dye-sensitized solar cell performance. *ACS Appl. Mater. Interfaces.* **4**(3), 1254–1261 (2012). <https://doi.org/10.1021/am201424d>
- Yamamoto, K., Yoshimi, M., Tawada, Y., Okamoto, Y., Nakajima, A.: Cost effective and high-performance thin film Si solar cell towards the 21st century. *Sol. Energy Mater. Sol. Cells.* **66**, 117–125 (2001). [https://doi.org/10.1016/S0927-0248\(00\)00164-1](https://doi.org/10.1016/S0927-0248(00)00164-1)
- Yang, Y., Peng, X., Chen, S., Lin, L., Zhang, B., Feng, Y.: Performance improvement of dye-sensitized solar cells by introducing a hierarchical compact layer involving ZnO and TiO₂ blocking films. *Ceram. Int.* **40**(9), 15199–15206 (2014). <https://doi.org/10.1016/j.ceramint.2014.07.001>
- Yeoh, M.E., Chan, K.Y.: Efficiency enhancement in dye-sensitized solar cells with ZnO and TiO₂ blocking layers. *J. Electron. Mater.* **48**(7), 4342–4350 (2019). <https://doi.org/10.1007/s11664-019-07207-5>
- Yum, J.H., Jang, S.R., Humphry-Baker, R., Grätzel, M., Cid, J.J., Torres, T., Nazeeruddin, M.K.: Effect of coadsorbent on the photovoltaic performance of zinc phthalocyanine-sensitized solar cells. *Langmuir* **24**(10), 5636–5640 (2008). <https://doi.org/10.1021/la800087q>
- Zhang, L., Cole, J.M.: Dye aggregation in dye-sensitized solar cells. *J. Mater. Chem. A.* **5**(37), 19541–19559 (2017). <https://doi.org/10.1039/c7ta05632j>
- Zhang, L.Z., Tang, G.Q.: Preparation, characterization and optical properties of nanostructured ZnO thin films. *Opt. Mater.* **27**(2), 217–220 (2004). <https://doi.org/10.1016/j.optmat.2004.03.002>
- Zhang, Q., Dandeneau, C.S., Zhou, X., Cao, C.: ZnO nanostructures for dye-sensitized solar cells. *Adv. Mater.* **21**(41), 4087–4108 (2009). <https://doi.org/10.1002/adma.200803827>
- Zhao, Y., Lu, F., Zhang, J., Dong, Y., Zhang, B., Feng, Y.: Stepwise co-sensitization of two metal-based sensitizers: probing their competitive adsorption for improving the photovoltaic performance of dye-sensitized solar cells. *RSC Adv.* **7**(17), 10494–10502 (2017). <https://doi.org/10.1039/C6RA28473F>



Contents lists available at ScienceDirect

Optik

journal homepage: www.elsevier.com/locate/ijleo

Original research article

Effect of surface modification via sol-gel spin coating of ZnO nanoparticles on the performance of WO₃ photoanode based dye sensitized solar cells



Rajat Biswas, Suman Chatterjee*

Department of Physics, University of North Bengal, Raja Rammohunpur, Darjeeling, Siliguri 734013, India

ARTICLE INFO

Keywords:

DSSC
Surface modification
WO₃ nanoparticle
Alternate photoanode
Electron back recombination

ABSTRACT

In this paper, we have reported the improvement of electro-optical performance of dye sensitized solar cells based on highly porous WO₃ nanoparticles as photoanode by an ultrathin coating of ZnO nanoparticles with varying precursor solution concentration over WO₃ surface and the results were compared with the performance of a Dye Sensitized Solar Cell (DSSC) fabricated with bare WO₃ photoanode. The semiconducting material WO₃ was chosen in search of a photoanode material for DSSC alternative to TiO₂. But the performance of pure WO₃ based DSSC was found to be extremely poor in spite of having several advantageous properties. To improve the photovoltaic performance, we have coated the WO₃ surface with varying concentrations of the ZnO precursor solution. It was observed that the concentration of the precursor solution of ZnO highly controls the performance of the DSSC. From the electrochemical measurements, it was found that the bare WO₃ cell suffers high electron recombination. But the coating of an ultrathin layer of ZnO over the WO₃ surface introduces an energy barrier and reduces the electron recombination and thereby enhances the cell performance. The solar cell energy conversion efficiency was found to be highest for 5 mM ZnO precursor solution concentration and it decreases with the increase in concentration further and becomes very low at a concentration of 25 mM. This may be attributed to the poor dye adsorption on the WO₃ surface due to complete screening by the thicker ZnO layer.

1. Introduction

Increasing energy demand and environmental contamination are the two major problems faced by the society in recent years. The major energy requirements of the world are fulfilled by fossil fuels (i.e., coal, petroleum and natural gas), which may not be sufficient to overcome the energy crisis in the future due to fast depletion, the rapid development of industrialization and environmental pollution [1–4]. To address these issues, scientists have focused on renewable and environment-friendly energy sources. As Sun represents an immense source of renewable energy, expected to provide an appreciable amount of power in the future, it is the most widespread type of alternative energy source among all the renewable energy sources [5–7]. Dye-sensitized solar cells, an unconventional photoelectrochemical device that directly converts photo-energy into electrical energy, have drawn much more attention than conventional silicon solar cells due to their easy fabrication technique, the low-level requirement of the high-temperature process, cost-effectiveness and environment-friendly nature [8,9]. But until now, DSSCs are not commercially viable as the reason for their comparatively low conversion efficiency and stability issues compared to the silicon-based solar cells [10].

* Corresponding author.

E-mail addresses: rajat_biswas@nbu.ac.in (R. Biswas), suman_chatterjee@hotmail.com (S. Chatterjee).<https://doi.org/10.1016/j.ijleo.2019.164142>

Received 27 November 2019; Accepted 27 December 2019

0030-4026/ © 2020 Elsevier GmbH. All rights reserved.

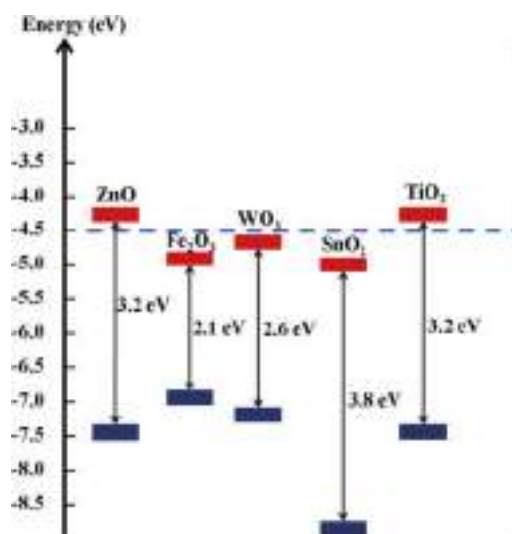


Fig. 1. Band positions of several semiconductors.

Photo anode, the heart of a DSSC system plays a key role in enhancing the overall performance of the DSSC by transferring electrons and supporting the Dye molecules [11]. It consists of a nanostructured mesoporous semiconductor film deposited on a conducting glass or a flexible substrate [12,13]. An ideal photoanode material should have some properties of high charge carrier mobility, significantly high surface areas, environmental friendliness, cost-effectiveness, and comparatively less electron-hole recombination rate. The band edge positions and corresponding band gap values of several commonly used wide bandgap metal oxide semiconductors are shown in Fig. 1 [14,15]. The semiconducting oxide material TiO₂ is mostly used as a photoanode because of its excellent optical, electrical and chemical properties [16–19]. Although appreciably high conversion efficiency is achieved with TiO₂, its low electron mobility leads many scientists to think about new alternative photoanode materials for better performance of Dye sensitized solar cells [20]. On the other hand, WO₃, a wide bandgap semiconductor having bandgap in the range of 2.6 eV–3.1 eV has been used extensively in the fabrication of gas sensors, water splitting and photocatalyst [21]. Owing to the favorable bandgap, high electron mobility and extreme stability in harsh environments, it has attracted the attention of researchers as an alternative photoanode material for DSSC fabrication. Moreover, the nonreactive nature of WO₃ in acidic environments may provide the solution of long-term stability issues in DSSCs with more acidic electrolytes. However, DSSCs based on pure WO₃ photoanode have been proven to be inefficient. On the other hand, DSSCs based on surface modified WO₃ photoanode by ultrathin layer of TiO₂ exhibited significant increase in power conversion efficiency [22]. ZnO can be used as a substitute for TiO₂ due to its agreeable properties in the view of high electron mobility and abundant nanostructure morphologies [23–25]. To the best of our knowledge, however, there are no detailed reports found in which surface modification of WO₃ is done by an ultrathin layer of ZnO in the fabrication of DSSCs. In this work, we have prepared the WO₃ photoanode and a facile sol-gel spin coating technique was utilized to alter the surface property of it by a thin layer of ZnO. Very careful control of the thickness of the ZnO layer is necessary to get the optimum performance out of the solar cell and for this purpose different concentration of ZnO precursor solution was used.

2. Materials and method

2.1. Preparation of working electrodes

All the reagents used in the fabrication process were of analytical grades. So no further purification was required. To prepare the thin films of the photoanode materials, the ITO coated glass substrates were first cleaned with dilute HCl in an ultrasonic bath for 15 min and then thoroughly rinsed with deionized water to remove the HCL residues. Then the substrates were cleaned with acetone and ethanol using an ultrasonic cleaning bath [26].

The working electrode of the DSSC was prepared by following the standard doctor blade method. The WO₃ paste for doctor blading was prepared by mixing WO₃ nanopowder with terpineol as solvent and ethyl cellulose as a binder and stirred continuously in order to obtain a smooth lump-free slurry. The WO₃ paste was then coated on the conductive side of the cleaned ITO glass substrate and subsequently annealed at 500 °C for 2 h in order to burn out the terpineol and ethyl cellulose contents of the working electrode

and strengthens the bonding between the substrate and the WO_3 film. In addition to this, the annealing procedure also helps to improve the surface quality of the thin film along with increasing the crystallinity of the sample [22].

The Sol-Gel spin-coating technique was employed to deposit thin layers of ZnO onto the surface of the as-prepared WO_3 photoanode. Zinc acetate dihydrate $(\text{CH}_3\text{COO})_2\text{Zn} \cdot 2\text{H}_2\text{O}$, (98 % Merck) was mixed with acetone at different molar ratios to obtain desired concentrations of ZnO precursor solution. The prepared solutions were then mixed extensively in an ultrasonic bath for 2 h and then spin-coated on the WO_3 coated substrate using a programmable spin coater (Apex Instruments Co. Pvt. Ltd, Model SpinNXG-P1) at 2000 rpm for 30 s. The thickness of the ZnO film can be controlled by varying the precursor solution concentration. In our experiment we have prepared 1 mM, 5 mM, 10 mM, 15 mM, 20 mM, and 25 mM solutions of ZnO precursor and spin-coated them over WO_3 film keeping the number of sol drops unchanged in order to obtain various ZnO film thickness and study the effect on the solar cell performance. The ZnO coated WO_3 electrode was annealed at 450 °C for 1 h. All the electrodes were sensitized by immersing them in a 0.3 mM ethanolic solution of Ruthenium based dye ($\text{C}_{26}\text{H}_{20}\text{O}_{10}\text{N}_6\text{S}_2\text{Ru}$) known as N_3 (Solaronix) for 48 h. The working electrodes were then removed from the solution and thoroughly rinsed with deionized water and ethanol to remove any excess dye from the semiconductor film surface and air-dried at room temperature.

The counter electrodes of the cells were prepared by spin coating the platinum catalyst precursor solution Platisol-T (Solaronix) on the conducting side of the cleaned ITO coated glasses and heating on a hot plate at 450 °C for 15 min.

The dye adsorbed working electrode and Pt-coated counter electrode was assembled against the coated sides of each other in a sandwich manner using two binder clips with a Surlyn film (Meltonix 1170 – 25 μm , Solaronix) gasket as a spacer in between them. The liquid electrolyte used in our experiment was a Solaronix high-performance electrolyte (Iodolyte AN50) with iodide/tri-iodide as redox couple, ionic liquid, lithium salt and pyridine derivative as additives dissolved in acetonitrile solvent. The redox concentration of the electrolyte was 50 mM. The active area of the cells for illumination was determined by employing a black mask of aperture size 0.25 cm^2 .

2.2. Characterization and measurements

The crystalline structure of the WO_3 and ZnO were analyzed with the help of X-ray diffraction analysis using the PAN-analytical X'Pert PRO X-ray diffractometer (CuK α radiation, 30 mA, 40 kV, $\lambda = 1.5406 \text{ \AA}$). Scanning electron microscopy (JEOL) was done to reveal the surface morphology of the prepared thin films. More detailed structural information of the samples was obtained from Raman Spectroscopy. The Photocurrent-Voltage (I-V) characteristics data of the cells were recorded using Keithley 2400 digital source meter with the help of a computer under 100 mW/cm^2 illumination (Xenon lamp 450 W). HIOKI Impedance Analyzer in the frequency range of 0.1 Hz to 190 kHz was used to study the electrochemical impedance spectra of the cells.

3. Results and discussion

3.1. Structural and phase characterization WO_3 of the photoanode

Fig. 2 shows the X-ray diffraction pattern of the as-purchased WO_3 nanopowder. The XRD pattern exhibits the coexistence of both the monoclinic and orthorhombic crystal phases. The peaks corresponding to the monoclinic phase well matches with the standard JCPDS card no. 43-1035 and the orthorhombic phase matches with JCPDS card no. 20-1324. Sharp and strong peaks signify the high crystalline nature of the sample [27,28].

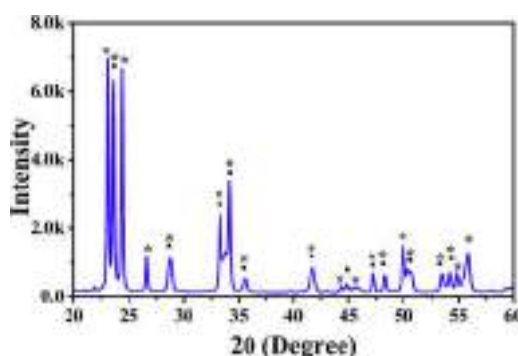


Fig. 2. X-ray diffraction pattern of WO_3 nanoparticles. The peaks correspond to Monoclinic (*) and orthorhombic (●) phases of WO_3 respectively.

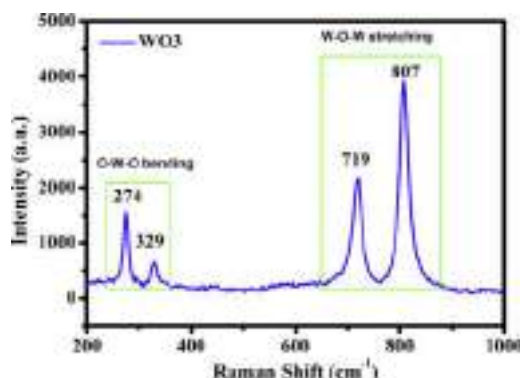


Fig. 3. Raman spectra of WO₃ nanoparticle.

The crystal phases are further confirmed by Raman spectra of the pure WO₃ powder, which is shown in Fig. 3 and it consists of well-resolved four sharp Raman peaks at 274, 329, 719 and 807 cm⁻¹. The lower peaks centered at 274 cm⁻¹ and 329 cm⁻¹ attributed to OWO— bending vibrations and the higher peaks at 719 cm⁻¹ and 807 cm⁻¹ are due to WOW— stretching mode vibration [29]. Sharp peaks suggest profoundly crystalline nature of the sample. All four Raman peaks attribute to the monoclinic phase [30]. However, the Raman peaks corresponding to the orthorhombic phase lie neighboring to the peaks mentioned above. Consequently, both phases are believed to be present in the sample. No impurity was found in the Raman spectra of the pure WO₃ sample.

3.2. Surface Morphology study and energy dispersive spectroscopy of the photoanodes

Scanning Electron Microscopy was employed to investigate the surface morphology of the pure and ZnO coated WO₃ photoanodes. Fig. 4(a) shows the SEM image of pure WO₃ photoanode on the FTO substrate whereas Fig. 4(b–g) show the SEM images of WO₃ photoanodes coated with 1 mM, 5 mM, 10 mM, 15 mM, 20 mM and 25 mM concentrations of ZnO precursor solution concentrations respectively. Highly porous films with nearly spherical shape WO₃ nanoparticle having a diameter in the range of 140 nm–150 nm can be clearly seen from the SEM images. High porosity the film enhances the surface to volume ratio, consequently increasing the dye loading amount resulting in high photocurrent [31–34]. It can also be observed from the SEM images that the surface morphology of uncoated and ZnO coated WO₃ substrate are not so visually different for low ZnO precursor concentrations, but for higher concentrations like 20 mM and 25 mM, the screening of WO₃ surface by ZnO nanoparticles may be evidently observed in Fig. 4(f) and 4 (g).

The EDS spectrum, which reveals the elementary analysis are shown in Fig. 4(h) and (i) for bare WO₃ and the WO₃ surface coated with 5 mM ZnO precursor solution concentration respectively. Predominating peaks of W and O₂ in Fig. 4(h) unveil that the sample contains only WO₃ whereas in Fig. 4(i) additional strong peak of Zn confirms the presence of ZnO coating over WO₃.

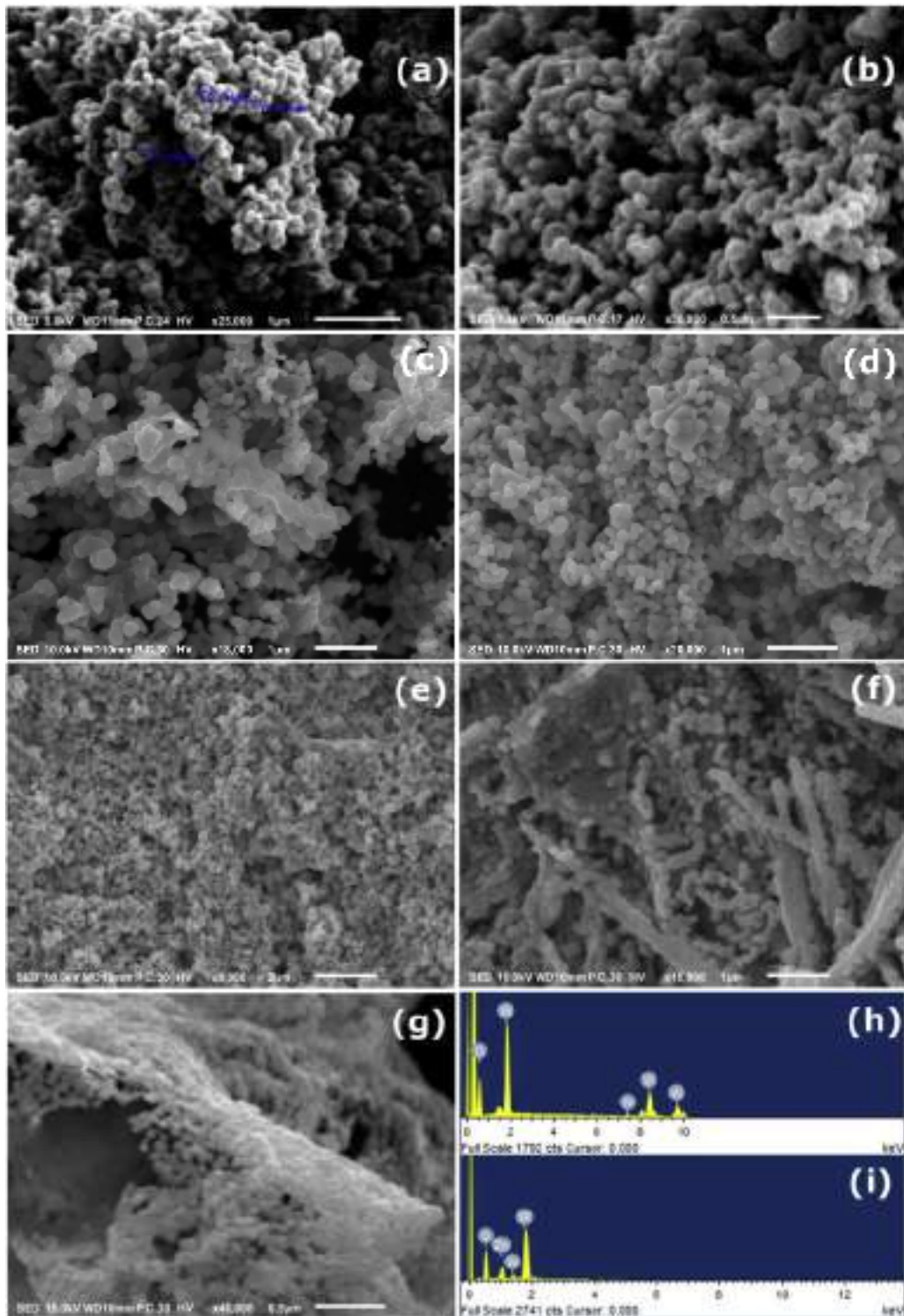


Fig. 4. SEM images of (a) Bare WO_3 photoelectrode; photoelectrodes having WO_3 coated with (b) 1 mM (c) 5 mM (d) 10 mM (e) 15 mM (f) 20 mM and (g) 25 mM ZnO precursor solution respectively. (h) EDS of Bare WO_3 and (i) EDS of WO_3 coated with 5 mM ZnO.

3.3. Photovoltaic (Current-Voltage) characterization of the cells

The Current-Voltage characteristic is a crucial characterization to investigate the overall photovoltaic performance of a solar cell. Fig. 5(a) illustrates the I–V characteristics of the seven DSSCs based on pure and coated WO₃ as photoanodes with different precursor solution concentrations. The overall photoconversion efficiency of the solar cell is given by

$$\eta = \frac{P_{\text{out}}}{P_{\text{in}}} = \frac{I_{\text{sc}} V_{\text{oc}} FF}{P_{\text{in}}} \quad (1)$$

Where V_{oc} , I_{sc} , P_{in} , and FF represent open-circuit voltage, the short circuit current density, Fill factor and incident light power respectively. The fill factor is calculated by the formula

$$FF = \frac{I_{\text{max}} V_{\text{max}}}{I_{\text{sc}} V_{\text{oc}}} \quad (2)$$

Where V_{max} and I_{max} are the voltage and current corresponding to the maximum output power point of the solar cell respectively. The photovoltaic parameters like Short circuit current density, Open circuit voltage, Fill factor and the efficiency obtained from the I–V curve are summarized in Table 1.

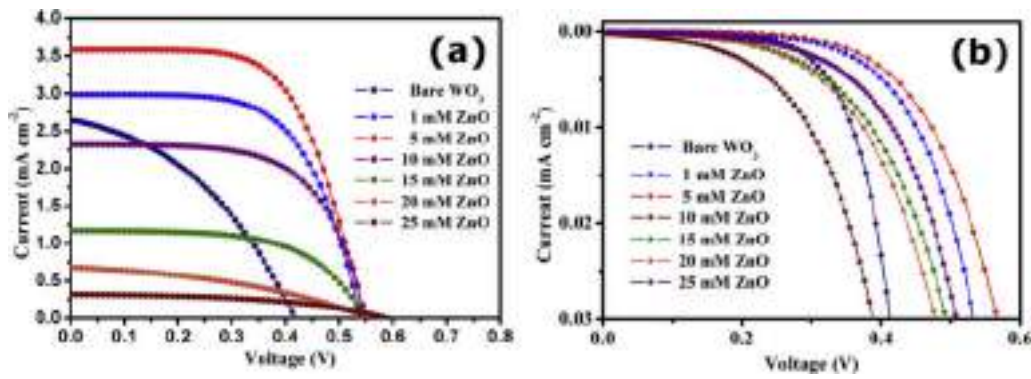


Fig. 5. Current-voltage characteristics of different cells under (a) Illumination and (b) Dark.

A clear enhancement in the efficiency and fill factor due to the presence of ZnO on the WO₃ surface compared to the bare WO₃ electrode can be observed from Table 1. The fill factor, which represents the squareness of the I–V curve [35], is very low for bare WO₃ which in turn decreases cell efficiency. The low fill factor may be attributed to the high recombination rate of electrons for bare WO₃ photoelectrode DSSC. However, a significant improvement in the value of J_{sc} can be noted from Table 1 upon ZnO coating over the WO₃ surface which demonstrates the positive role of the ZnO layer in reducing the recombination process. The DSSC with 5 mM ZnO precursor solution concentration yielded the highest short circuit photocurrent J_{sc} and efficiency η . But the photocurrent and the efficiency start falling sharply with a further increase in the precursor solution concentration.

The maximum value of open-circuit voltage is determined by the difference between the Fermi level of the photoanode (metal oxide) material and the red-ox potential of the liquid electrolyte [36]. WO₃ is known to possess a lower conduction band edge (E_{cb}) i.e. more positive E_{cb} thereby reducing the open-circuit voltage (V_{oc}). However, employing an ultrathin layer of more E_{cb} negative metal oxides like ZnO onto WO₃ surface may increase the value of V_{oc} as the photogenerated electrons from LUMO of dye molecules are now injected to the more negative conduction band of ZnO and then step down to the conduction band of WO₃ which is illustrated in Fig. 6(b).

Table 1
Photovoltaic performance of uncoated and ZnO coated WO₃ photoanode based DSSC.

ZnO precursor solution concentration	J_{sc} (mA/cm ²)	V_{oc} (V)	FF	Efficiency (η %)
Pure WO ₃	2.65	0.42	0.39	0.44
1 mM ZnO	2.98	0.53	0.63	1.07
5 mM ZnO	3.58	0.55	0.62	1.21
10 mM ZnO	2.32	0.56	0.62	0.80
15 mM ZnO	1.15	0.56	0.60	0.38
20 mM ZnO	0.68	0.57	0.38	0.15
25 mM ZnO	0.32	0.58	0.47	0.09

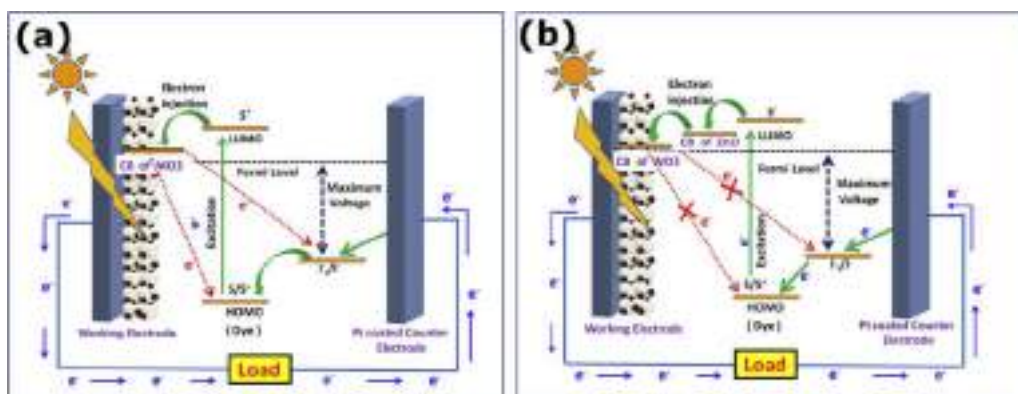


Fig. 6. Schematic energy level diagram and mechanism of the (a) Conventional DSSC and (b) DSSC with the ZnO barrier.

Furthermore, the energy barrier created due to the incorporation of ZnO onto the WO₃ film surface may prevent the charge carrier recombination and as well as decreasing back transfer of electrons to the HOMO of the dye molecule. Aside from this, the ultrathin layer of ZnO incorporation on the WO₃ surface facilitates the amount of dye adsorption and hence increasing the amount of photon absorption resulting in higher J_{sc} .

The dark current measurement was done in order to interpret the variation of charge recombination reaction of the photo-generated electrons with I₃⁻ ions at the Pt coated counter electrode/red-ox electrolyte interface. Fig. 5(b) shows the dark J–V characteristics of the DSSCs fabricated with uncoated and coated with different concentrations of the ZnO precursor solution. The photoelectron injection from LUMO of dye to the CB of the working electrode is completely absent in the dark condition and hence the dark current is mainly due to the diffusion of electrons from semiconductor to the redox electrolyte [37]. Ultrathin coating of ZnO layer on the WO₃ surface decreases the dark current which can be observed in dark current characteristics in Fig. 5(b). On the other hand, the uncoated WO₃ possesses a higher dark current for a particular bias voltage. This may be due to the fact that poor dye

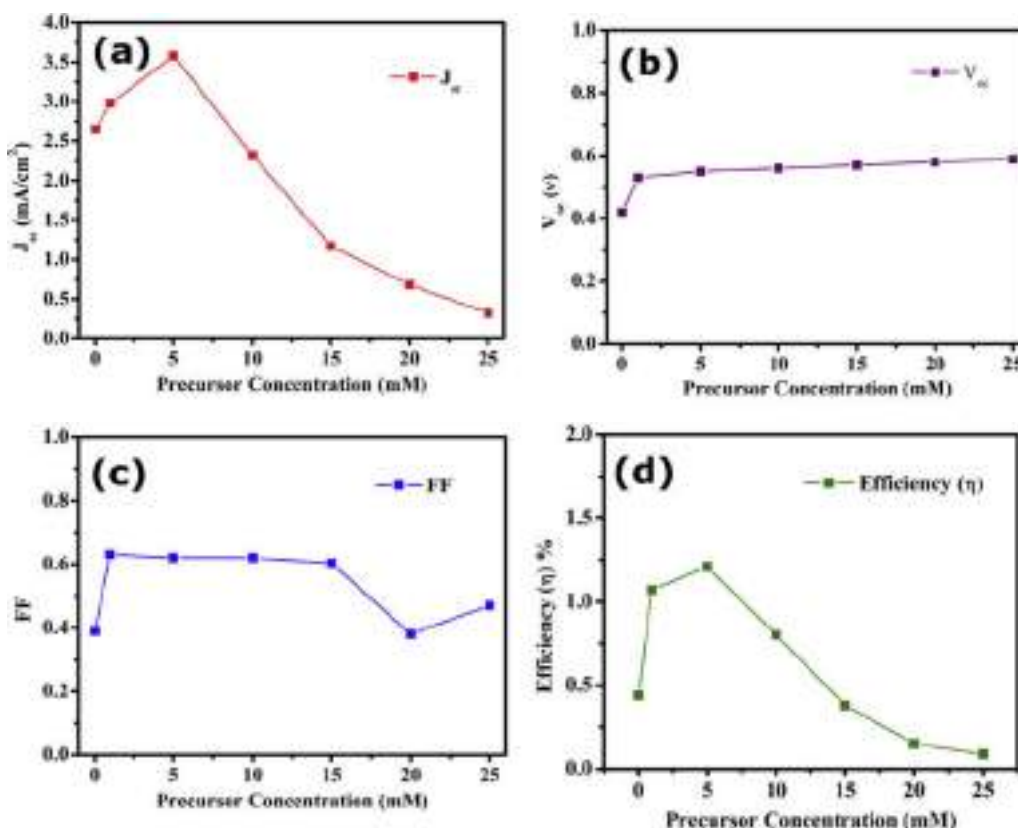


Fig. 7. Effect of ZnO precursor solution concentration on the values of photovoltaic parameters (a) J_{sc} (b) FF (c) V_{oc} and (d) η .

loading capacity of WO_3 allows more direct contact between WO_3 surface and liquid electrolyte. This facilitates the back transfer of electrons from WO_3 to electrolyte via reduction of I_3^- into I^- which led to increased dark current [22]. But the coating of ZnO creates an energy barrier that effectively reduces the rate of electron recombination thereby decreasing the dark current, consequently suppressed recombination of charge carriers due to ZnO coating increases cell FF. In addition to that, a very thin coating of ZnO also improves the dye loading which enables the ZnO treated WO_3 DSSC to harvest more light energy compared to ordinary WO_3 DSSC and significantly enhances current density. However, with the increase in the ZnO precursor concentration of more than 5 mM, the values of FF and J_{sc} start decreasing. This decrease in J_{sc} and FF might be due to the fact that thicker ZnO layer completely screens WO_3 from dye molecules. Moreover, a higher amount of ZnO content act as recombination sites [38]. Apart from this, an increased amount of ZnO deposition via increasing the ZnO precursor solution concentration promotes aggregation of Zn^{+2} ions and N3 dye which may decrease the photocurrent due to light loss due to absorption and scattering of light by these aggregates [39–41].

Fig. 7 shows the variation of DSSC performance parameters as a function of ZnO precursor solution concentration. The values of J_{sc} , FF, and η enhanced significantly for the cells with ultrathin ZnO nanoparticles coating as compared to the cell with bare WO_3 nanoparticle thin film. The best performance was obtained with 5 mM ZnO solution concentration with values of cell parameters like J_{sc} , V_{oc} , FF, and η as 3.56 mA/cm^2 , 0.55 V, 0.62 and 1.21 % respectively.

3.4. Electrochemical impedance spectroscopy

Electrochemical impedance spectroscopy was performed to further explore the interfacial charge transport properties and recombination resistances for a better understanding of the cell parameters. The EIS measurement was carried out at V_{oc} bias voltage and applying an AC voltage of 10 mV amplitude to the DSSC under 1 sun illumination in the frequency range 0.1 Hz to 190 kHz. The Nyquist plot of the different DSSCs fabricated using bare WO_3 and with a coating of different concentrations of ZnO onto it are depicted in Fig. 8(a). Usually, a typical Nyquist plot consists of three semi-circles. The first semicircle in the high-frequency range is attributed to the charge transport resistance at the Pt counter electrode/ electrolyte interface, while the second semicircle in the mid-frequency range represents the recombination resistance at the semiconductor/dye/electrolyte interface. The third semicircle is associated with Nernst diffusion (Warburg diffusion impedance Z_w) which is the impedance faced by the electrons during diffusion through the electrolyte [39]. However, in our case only two semicircles are present as the third semicircle is usually observed at frequencies below 0.1 Hz [42]. The intercept of the 1st semicircle on the real axis of the Nyquist plot in the high-frequency range represents the sheet resistance of FTO and other ohmic contact resistances (R_s) of the assembled cells. The capacitive components C_1 & C_2 in the equivalent circuit are due to the formation of charge double layer between the counter electrode/electrolyte and semiconductor/dye/electrolyte interfaces respectively [43]. The equivalent circuit, shown in the inset of Fig. 8(a) is used to fit the experimental Nyquist plot and the obtained EIS parameters are represented in Table 2. The value of contact resistance (R_s) is almost the same for all the coated cells except the bare WO_3 cell. The increase in the value of R_s in ZnO coated cells may be due to the increase in the number of layers. The value of recombination resistance (R_2) is very low for bare WO_3 . But a gradual increase in R_2 with an increase in ZnO precursor concentration may be observed in Fig. 8(a) and Table 2. The highest value of R_2 is observed for 5 mM ZnO concentration as this much concentration provided the highest amount of dye adsorption without affecting the carrier transport through WO_3 thereby generating the highest number of charge carriers and also reducing the charge carrier recombination at the semiconductor/dye/electrolyte interface.

Further increase in ZnO concentration starts decreasing R_2 due to poor dye loading on the WO_3 surface. Along with that presence of recombination sites for the free charge carriers in the thick layer of ZnO (38). Thick ZnO layer also makes the thickness of the film such a high that it becomes greater than the diffusion length of the electrons. This decreases the net photocurrent reaching the FTO and lowers the cell performance. The highest value of chemical capacitance C_2 also reflects the transformation of a higher amount of photon energy into chemical energy [44,45]. To estimate the charge carrier lifetime, the Bode plot representing variation in phase angle (θ) with frequency (f) for varying amounts of ZnO concentration is depicted in Fig. 8(b). The electron lifetime is calculated

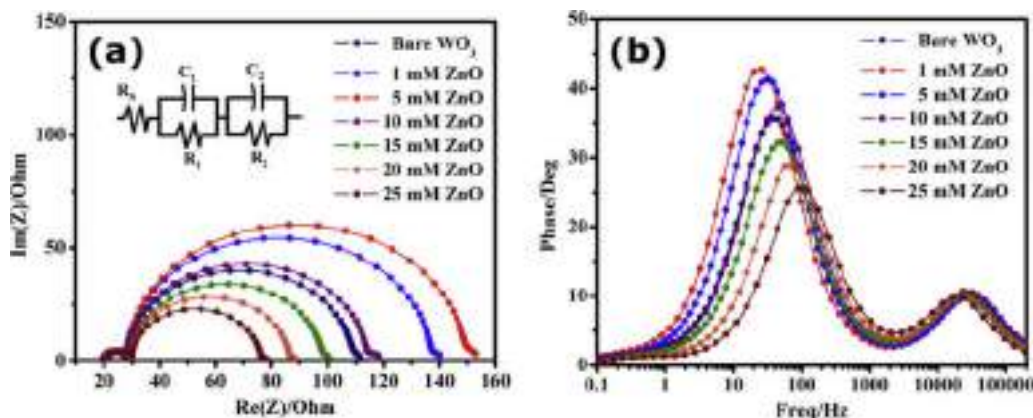


Fig. 8. Electrochemical Impedance Spectra of the DSSCs (a) Nyquist plot along with equivalent circuit (inset) (b) Bode plot.

Table 2
Summary of EIS measurements of DSSCs.

ZnO precursor solution concentration	R_s (Ω)	R_2 (Ω)	R_1 (Ω)	C_2 (μF)	Peak freq. f (Hz)	Electron lifetime (τ_e) (ms)
Pure WO ₃	19.3	85.2	8.67	84.3	37.18	4.28
1 mM ZnO	19.5	108.3	8.4	103.7	31.36	5.08
5 mM ZnO	19.6	119.7	8.62	125.4	24.15	6.59
10 mM ZnO	20.1	79.57	8.36	98.35	40.72	3.91
15 mM ZnO	20.8	67.57	8.79	87.35	48.47	3.29
20 mM ZnO	21.1	56.23	8.41	68.3	68.67	2.32
25 mM ZnO	21.3	45.76	8.52	55.57	97.29	1.64

using formula [46–49],

$$\tau_n = \frac{1}{2\pi f_{\max}} \quad (3)$$

Where f_{\max} represents the characteristic peak frequency of the Bode plot in the mid-frequency range. The lower value of f_{\max} is associated with a higher electron lifetime. The DSSC with 5 mM ZnO coating has the lowest value of f_{\max} leading to the highest lifetime of photogenerated electrons. This enhancement in electron lifetime reduces the recombination process leading to the highest photocurrent among the seven fabricated cells in our study. These results are in accordance with the results obtained from J–V characteristics under illumination and dark.

4. Conclusion

In this study, we have fabricated DSSCs based on WO₃ as an alternative photoanode material. The DSSC showed an efficiency of 0.44 % with a low FF of 0.39. This was due to very high recombination rates of photoexcited electrons along with poor dye loading due to the highly acidic surface of WO₃. Apart from that, the lower conduction band edge position of WO₃ limits the open-circuit voltage of the DSSC. In order to improve the performance of WO₃ based DSSC, the effect of inclusion of the ZnO thin layer on the surface of WO₃ was studied. The current density (J) – voltage (V) characteristics of the prepared cells were compared and a clear enhancement of cell efficiency was recorded upon ZnO coating and the highest efficiency was achieved for 5 mM concentration. Although the incorporation of a thin layer of ZnO onto WO₃ enhances the power conversion efficiency by creating an energy barrier and limiting the electron back-recombination, the thicker layer of ZnO degrades the cell performance by forming an aggregation of Zn²⁺ ions and N3 dye and reducing the dye adsorption quantity of WO₃ film. This suggests an optimum concentration for ZnO to be deposited over WO₃ film to achieve the highest efficiency. The improvement of the value of V_{oc} due to ZnO coating was attributed to the upward shift in CB of WO₃. Apart from J–V characteristics study under illumination and dark, EIS measurement was also performed. It was found that the cell with 5 mM of ZnO over WO₃ film has the highest recombination resistance which efficiently suppresses the electron recombination rate and as result, the lifetime of photogenerated electrons is also highest. The decrease in the photoconversion efficiency with further increase in ZnO concentration above optimum value is due to the complete screening of WO₃ film by a thicker layer of ZnO. Therefore, the novel method used here to modify the surface property of the WO₃ photoelectrode of DSSC is found to be promising to enhance the cell performance and thereby develop an efficient WO₃ based Dye sensitized Solar cell.

Declaration of Competing Interest

The authors declare that they have no known competing financial interests or personal relationships that could have appeared to influence the work reported in this paper.

Acknowledgment

Authors gratefully acknowledge the Dept. of Physics, the University of North Bengal for providing financial support and laboratory facilities for carrying out the research work.

References

- [1] W. Bach, *Global warming: the complete briefing* (2nd ed). John Houghton. Cambridge University Press: Cambridge, 1997. Pp. xv + 251. Paperback: ISBN 0521-62932-2, ú12.95; hardback: ISBN 0-321-62089-9, ú35.00. Int. J. Climatol. 18 (5) (1998) 579–580.
- [2] D.H. Meadows, D.L. Meadows, J. Randers, W.W. Behrens, *The Limits to Growth* 102 (1972), p. 27 New York.
- [3] *Greenhouse glasnost: the crisis of global warming: essays*, in: T.J. Minger (Ed.), *Greenhouse/Glasnost: The Sundance Symposium on Global Climate Change* (USA), 1989, Ecco Press, 1990.
- [4] J. Peet, *Energy and the Ecological Economics of Sustainability*, Island Press, 1992.
- [5] A. Rose, A global view of solar energy in rational units, *Physica Status Solidi A* 56 (1) (1979) 11–26.
- [6] A. Shah, P. Torres, R. Tscharnner, N. Wyrtsch, H. Keppner, *Photovoltaic technology: the case for thin-film solar cells*, *Science* 285 (5428) (1999) 692–698.
- [7] J.A. Turner, A realizable renewable energy future, *Science* 285 (5428) (1999) 687–689.
- [8] J. Gong, J. Liang, K. Sumathy, Review on dye-sensitized solar cells (DSSCs): fundamental concepts and novel materials, *Renew. Sustain. Energy Rev.* 16 (8)

- (2012) 5848–5860.
- [9] H.M. Upadhyaya, S. Senthilarasu, M.-H. Hsu, D.K. Kumar, Recent progress and the status of dye-sensitized solar cell (DSSC) technology with state-of-the-art conversion efficiencies, *Sol. Energy Mater. Sol. Cells* 119 (2013) 291–295.
- [10] K. Sharma, V. Sharma, S. Sharma, Dye-sensitized solar cells: fundamentals and current status, *Nanoscale Res. Lett.* 13 (1) (2018) 381.
- [11] B. O'regan, M. Grätzel, A low-cost, high-efficiency solar cell based on dye-sensitized colloidal TiO₂ films, *Nature* 353 (6346) (1991) 737.
- [12] S. Ito, G. Rothenberger, P. Liska, P. Comte, S.M. Zakeeruddin, P. Péchy, et al., High-efficiency (7.2%) flexible dye-sensitized solar cells with Ti-metal substrate for nanocrystalline-TiO₂ photoanode, *Chem. Commun.* (38) (2006) 4004–4006.
- [13] T. Yamaguchi, N. Tobe, D. Matsumoto, T. Nagai, H. Arakawa, Highly efficient plastic-substrate dye-sensitized solar cells with validated conversion efficiency of 7.6%, *Sol. Energy Mater. Sol. Cells* 94 (5) (2010) 812–816.
- [14] C. Cavallo, F. Di Pascasio, A. Latini, M. Bonomo, D. Dini, Nanostructured semiconductor materials for dye-sensitized solar cells, *J. Nanomater.* 2017 (2017).
- [15] M. Grätzel, Photoelectrochemical cells, *Nature* 414 (6861) (2001) 338.
- [16] D.Y. Leung, X. Fu, C. Wang, M. Ni, M.K. Leung, X. Wang, et al., Hydrogen production over titania-based photocatalysts, *ChemSusChem* 3 (6) (2010) 681–694.
- [17] G. Liu, J. Gong, L. Kong, R.D. Schaller, Q. Hu, Z. Liu, et al., Isothermal pressure-derived metastable states in 2D hybrid perovskites showing enduring bandgap narrowing, *Proc. Natl. Acad. Sci.* 115 (32) (2018) 8076–8081.
- [18] G. Liu, L. Kong, P. Guo, C.C. Stoumpos, Q. Hu, Z. Liu, et al., Two regimes of bandgap red shift and partial ambient retention in pressure-treated two-dimensional perovskites, *ACS Energy Lett.* 2 (11) (2017) 2518–2524.
- [19] X. Wang, Z. Li, J. Shi, Y. Yu, One-dimensional titanium dioxide nanomaterials: nanowires, nanorods, and nanobelts, *Chem. Rev.* 114 (19) (2014) 9346–9384.
- [20] A.K. Chandiran, M. Abdi-Jalebi, M.K. Nazeeruddin, M. Grätzel, Analysis of electron transfer properties of ZnO and TiO₂ photoanodes for dye-sensitized solar cells, *ACS Nano* 8 (3) (2014) 2261–2268.
- [21] M. Gillet, K. Aguir, C. Lemire, E. Gillet, K. Schierbaum, The structure and electrical conductivity of vacuum-annealed WO₃ thin films, *Thin Solid Films* 467 (1–2) (2004) 239–246.
- [22] H. Zheng, Y. Tachibana, K. Kalantar-zadeh, Dye-sensitized solar cells based on WO₃, *Langmuir* 26 (24) (2010) 19148–19152.
- [23] H. Bae, M. Yoon, J. Kim, S. Im, Photodetecting properties of ZnO-based thin-film transistors, *Appl. Phys. Lett.* 83 (25) (2003) 5313–5315.
- [24] Ü. Özgür, Y.I. Alivov, C. Liu, A. Teke, M. Reshchikov, S. Doğan, et al., A comprehensive review of ZnO materials and devices, *J. Appl. Phys.* 98 (4) (2005) 11.
- [25] Q. Zhang, C.S. Dandaneau, X. Zhou, G. Cao, ZnO nanostructures for dye-sensitized solar cells, *Adv. Mater.* 21 (41) (2009) 4087–4108.
- [26] R. Biswas, T. Roy, S. Chatterjee, Study of electro-optical performance and interfacial charge transfer dynamics of dye sensitized solar cells based on ZnO nanostructures and natural dyes, *J. Nanoelectron. Optoelectron.* 14 (1) (2019) 99–108.
- [27] U. Costantino, F. Marmottini, M. Nocchetti, R. Vivani, New synthetic routes to hydroxalcite-like compounds – characterisation and properties of the obtained materials, *Eur. J. Inorg. Chem.* 1998 (10) (1998) 1439–1446.
- [28] J.-M. Oh, S.-H. Hwang, J.-H. Choy, The effect of synthetic conditions on tailoring the size of hydroxalcite particles, *Solid State Ion.* 151 (1–4) (2002) 285–291.
- [29] M. Daniel, B. Desbat, J. Lassegues, B. Gerand, M. Figlarz, Infrared and Raman study of WO₃ tungsten trioxides and WO₃·xH₂O tungsten trioxide hydrates, *J. Solid State Chem.* 67 (2) (1987) 235–247.
- [30] A.Z. Sadek, H. Zheng, M. Breedon, V. Bansal, S.K. Bhargava, K. Latham, et al., High-temperature anodized WO₃ nanoplatelet films for photosensitive devices, *Langmuir* 25 (16) (2009) 9545–9551.
- [31] S. Hore, C. Vetter, R. Kern, H. Smit, A. Hinsch, Influence of scattering layers on efficiency of dye-sensitized solar cells, *Sol. Energy Mater. Sol. Cells* 90 (9) (2006) 1176–1188.
- [32] E.M. Jin, K.-H. Park, J.-J. Yun, C.K. Hong, M.-J. Hwang, B.-K. Park, et al., Photovoltaic properties of TiO₂ photoelectrode prepared by using liquid PEG-EEM binder, *Surf. Rev. Lett.* 17 (1) (2010) 15–20.
- [33] K.H. Ko, Y.C. Lee, Y.J. Jung, Enhanced efficiency of dye-sensitized TiO₂ solar cells (DSSC) by doping of metal ions, *J. Colloid Interface Sci.* 283 (2) (2005) 482–487.
- [34] K.-H. Park, E.M. Jin, H.B. Gu, S.E. Shim, C.K. Hong, Effects of HNO₃ treatment of TiO₂ nanoparticles on the photovoltaic properties of dye-sensitized solar cells, *Mater. Lett.* 63 (26) (2009) 2208–2211.
- [35] B. Qi, J. Wang, Fill factor in organic solar cells, *J. Chem. Soc. Faraday Trans.* 15 (23) (2013) 8972–8982.
- [36] M. Grätzel, Dye-sensitized solar cells, *J. Photochem. Photobiol. C Photochem. Rev.* 4 (2) (2003) 145–153.
- [37] S. Ito, P. Liska, P. Comte, R. Charvet, P. Péchy, U. Bach, et al., Control of dark current in photoelectrochemical (TiO₂/I⁻/I³⁻) and dye-sensitized solar cells, *Chem. Commun.* (34) (2005) 4351–4353.
- [38] S. Noor, S. Sajjad, S.A.K. Leghari, S. Shaheen, A. Iqbal, ZnO/TiO₂ nanocomposite photoanode as an effective UV-vis responsive dye sensitized solar cell, *Mater. Res. Express* 5 (9) (2018) 095905.
- [39] M. Adachi, M. Sakamoto, J. Jiu, Y. Ogata, S. Isoda, Determination of parameters of electron transport in dye-sensitized solar cells using electrochemical impedance spectroscopy, *J. Phys. Chem. B* 110 (28) (2006) 13872–13880.
- [40] F. Al-juaid, A. Merazga, A. Al-Baradi, F. Abdel-wahab, Effect of sol-gel ZnO spin-coating on the performance of TiO₂-based dye-sensitized solar cell, *Solid-State Electronics* 87 (2013) 98–103.
- [41] I. Bedja, P.V. Kamat, X. Hua, A. Lappin, S. Hotchandani, Photosensitization of Nanocrystalline ZnO Films by Bis (2, 2'-bipyridine)(2, 2'-bipyridine-4, 4'-dicarboxylic acid) ruthenium (II), *Langmuir* 13 (8) (1997) 2398–2403.
- [42] S. Sarker, A. Ahammad, H.W. Seo, D.M. Kim, Electrochemical impedance spectra of dye-sensitized solar cells: fundamentals and spreadsheet calculation, *Int. J. Photoenergy* 2014 (2014).
- [43] M. Younas, M. Gondal, M. Dastageer, U. Baig, Fabrication of cost effective and efficient dye sensitized solar cells with WO₃-TiO₂ nanocomposites as photoanode and MWCNT as Pt-free counter electrode, *Ceram. Int.* 45 (1) (2019) 936–947.
- [44] Q. Wang, J.-E. Moser, M. Grätzel, Electrochemical impedance spectroscopic analysis of dye-sensitized solar cells, *J. Phys. Chem. B* 109 (31) (2005) 14945–14953.
- [45] J. Bisquert, Chemical capacitance of nanostructured semiconductors: its origin and significance for nanocomposite solar cells, *J. Chem. Soc. Faraday Trans.* 5 (24) (2003) 5360–5364.
- [46] S.P. Lim, A. Pandikumar, N.M. Huang, H.N. Lim, Silver/titania nanocomposite-modified photoelectrodes for photoelectrocatalytic methanol oxidation, *Int. J. Hydrogen Energy* 39 (27) (2014) 14720–14729.
- [47] S. Buda, S. Shafie, S.A. Rashid, H. Jaafar, N. Sharif, Enhanced visible light absorption and reduced charge recombination in AgNP plasmonic photoelectrochemical cell, *Results Phys.* 7 (2017) 2311–2316.
- [48] S.G. Kim, M.J. Ju, I.T. Choi, W.S. Choi, H.-J. Choi, J.-B. Baek, et al., Nb-doped TiO₂ nanoparticles for organic dye-sensitized solar cells, *RSC Adv.* 3 (37) (2013) 16380–16386.
- [49] P. Archana, A. Gupta, M.M. Yusoff, R. Jose, Tungsten doped titanium dioxide nanowires for high efficiency dye-sensitized solar cells, *J. Chem. Soc. Faraday Trans.* 16 (16) (2014) 7448–7454.

An Investigation on the Stability Enhancement of Dye-Sensitized Solar Cells Fabricated with Ethyl Cellulose Based Gel Electrolyte

Trinakhi Roy^a, Rajat Biswas^a, and Suman Chatterjee^{a, *}

^a Department of Physics, University of North Bengal, Raja Rammohunpur, Darjeeling, Siliguri-734013 India

*e-mail: suman_chatterjee@hotmail.com

Received December 11, 2019; revised January 10, 2020; accepted June 17, 2020

Abstract—Liquid electrolyte based Dye-Sensitized Solar Cells (DSSC) often suffers stability problems which limit its durability. The stability of the dye-sensitized solar cell is enhanced with the use of gel electrolyte instead of liquid electrolyte in this paper. A detailed effective fabrication method of the DSSC based on gel electrolyte has been presented here. In this approach, the gel-state electrolyte solution was prepared by mixing the traditional liquid-state electrolyte with ethyl cellulose as a gelator and was placed into the DSSC in its quasi-solid state. The prepared gel state electrolyte showed appreciable conductivity, which is comparable to those of traditional liquid electrolytes by Electrochemical impedance analysis. The gel electrolyte based DSSCs exhibited a considerable power-conversion efficiency of 1.29% and enhanced stability compared to the traditional liquid electrolyte based DSSC.

Keywords: dye-sensitized solar cells, electrochemical impedance spectroscopy, gel electrolyte, I–V characteristics, liquid electrolyte, stability

DOI: 10.3103/S0003701X21010084

INTRODUCTION

Due to increasing energy demand, polluting environment, and the rising price of non-renewable fuel sources, scientists are constantly thinking of new ways to find pollution-free renewable energy [1]. The natural resources that can renew itself over time are called renewable energy sources [2]. It is believed that solar energy would be the main source of alternative energy [3]. Conventional Crystalline and polycrystalline silicon solar cells have attained energy conversion efficiency of over 20%, but due to their complicated and difficult fabrication process and high cost [4], people have started to think about its alternative. Grätzel and co-workers first reported Dye-Sensitized Solar Cells (DSSC)s as a useful substitute for conventional solar cells [1], and subsequently, a huge interest has been developed for DSSCs because of its easy fabrication technique and low cost [5].

The various components of a DSSC are fluorine-doped tin oxide (FTO) electrode coated with porous TiO₂ nanoparticles, dye sensitizer, a platinum-coated counter electrode, and an electrolyte containing redox mediator [6]. A schematic diagram of the construction and operating principle of a dye-sensitized solar cell is shown in Fig. 1a,b, respectively. The photons are absorbed by the dye sensitizer molecules and the electrons are excited from the HOMO to LUMO state. Then photogenerated electrons from the sensitizer are injected into the TiO₂ nanostructures and transported

through the external circuit. Subsequently, electrons from the electrolyte are transferred to the dye sensitizer and the oxidized dye is restored. The transported electrons are accepted by the electrolyte through the platinum-coated counter electrode, and the electrolyte gets regenerated [7].

Photo anode of a DSSC performs a vital role in determining the overall performance of the DSSC by transporting electrons and supporting the Dye molecules [8]. The semiconducting oxide material TiO₂ is mostly used as a photoanode because of its excellent optical, electrical, and chemical properties [9–12]. Although appreciably high conversion efficiency is achieved with TiO₂, its low electron mobility results in low electron mobility has led renewed investigations in new alternative about new alternative wide-bandgap photoanode materials like ZnO, WO₃, SnO₂ for better performance of Dye-sensitized solar cells [13–15]. Researchers are also using natural dyes extracted from different fruits, vegetables, and flowers in search of low-cost DSSC fabricated with environment-friendly and non-toxic material [16–20].

But the electrolyte has a close interaction with all the components of DSSC and it determines the time stability of the cell. Due to this, scientists have been paying more attention to electrolytes these days [21, 22]. Though the theoretically estimated maximum photoelectric conversion efficiency of a DSSC is 29% [23] has been recorded with liquid electrolytes, the

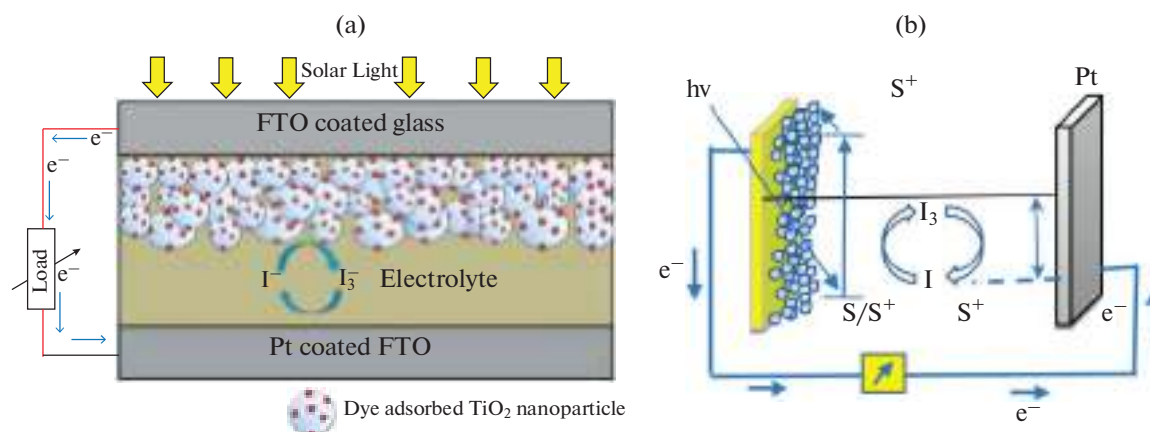


Fig. 1. Schematic diagram of (a) construction and (b) working principle of dye-sensitized solar cell.

actual efficiency of 14.3% could be achieved. This is due to leakage problems, photodegradation of attached dyes, and solvents volatility restrict the long-term performance of DSSCs [24]. To overcome these limitations gel electrolytes have been used instead of liquid electrolytes as the please provide the atmosphere for the sintering process (inert, activated, etc?) [25]. Gel electrolytes are usually prepared by adding materials of high molecular weights with organic solvents and iodides. Polyvinyl carbonate (PC), Acetonitrile (ACN), ethylene carbonate (EC) are an example of some of the popularly used solvents and Lithium iodide (LiI), potassium iodide (KI), Sodium iodide are some of the commonly utilized iodides with iodine (I₂). For gelation of liquid electrolyte, many materials are used namely polyethylene glycol, polyvinylidene fluoride-co-hexafluoropropylene (PVDF-HFP), polyethylene oxide, etc. [26].

In this study, we prepared gel electrolytes using ethyl cellulose (EC) as gelator in the liquid electrolyte, and fabricated DSSCs with both liquid and gel electrolytes to study were fabricated with both liquid and gel electrolytes to study their overall photovoltaic performance including their performance stability over a certain period. Gel electrolyte was also studied in earlier investigation [22], reporting higher stability. A detailed comparison of Photoelectric properties is presented in the investigation.

MATERIALS AND METHODS

All the chemicals used in this study were purchased from commercial sources and used as received. Fluorine-doped tin oxide (FTO) glass slides (10 Ω/square; thickness 2.2 mm), ruthenium dye (N719), Surlyn spacer, and Platinum Precursors solution (Plastisol T) for counter electrode preparation, all were purchased from Solaronix, Switzerland. Titanium dioxide nanopowder (TiO₂), Lithium Iodide (LiI), and Iodine (I₂) were purchased from Sigma-Aldrich, India. The

chemicals, used in gel preparation are Acetonitrile (Merck, India), 4-tert-butylpyridine (TCI CHEMICALS, Japan), Tetrabutylammonium iodide (Merck), Ethyl Cellulose (Sigma-Aldrich, India), acetone (C₃H₆O), ethanol (C₂H₅OH), and acetic acid (CH₃CO₂H) (Sigma-Aldrich). All the reagents purchased were used without further purification.

The working electrode of the DSSC was prepared by following the standard available procedure [27]. At first, 10 gm of the TiO₂ nanopowder was mixed with diluted acetic (1 in 50 ml deionized water) acid in a mortar and pastel and adding few drops of Triton X100 (Merck) as surfactant and ground continuously until a homogenous smooth suspension was obtained. The lump-free slurry was then applied on the conductive side of an FTO coated glass using the doctor blade method to make a homogeneous layer. To strengthen the bonding between the FTO glass and the semiconductor paste, the TiO₂ coated glass plate was sintered in normal atmospheric condition at 450°C for 45 min. In the sintering process, at first, after introducing the sample in furnace, the temperature was raised with a rate of 10°C/5 min until the temperature had reached 350°C and after that, it was increased with a rate of 10°C/10 min until 450°C. When it cooled down to room temperature, the sintered glass substrate was immersed in the ruthenium dye (N719) solution for dye adsorption on the surface of the TiO₂ nanoparticles for 24 hours. FTO glass coated with a platinum catalyst (Plastisol-T) and heated at 400°C was used as a counter electrode and a sealed sandwich-type cell was fabricated by assembling dye adsorbed TiO₂ electrode and the platinum (Pt) coated counter electrode with Surlyn film as a spacer between them. Then electrolyte was introduced into the assembled cell through the drilled hole of the counter with a syringe. Glass glue was used to seal the hole and finally the cell was connected to the external circuit with the help of crocodile clips.

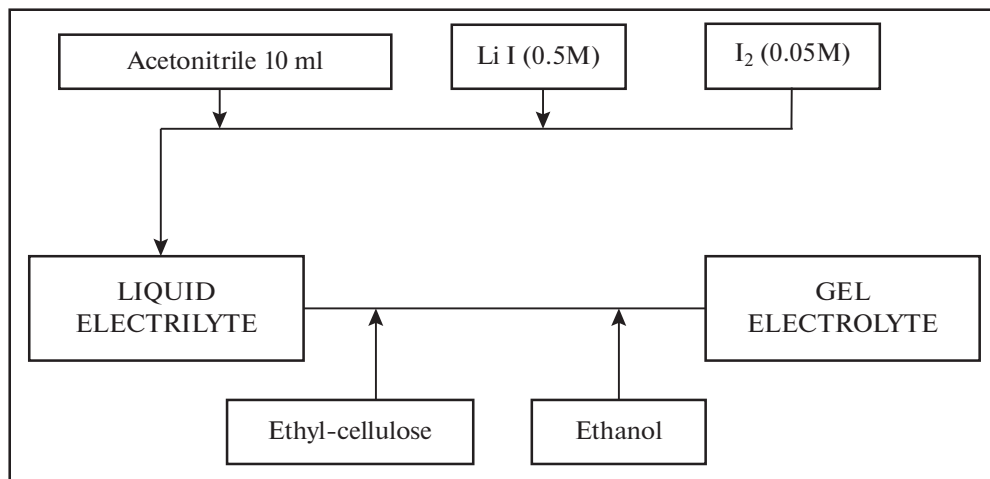


Fig. 2. The fabrication procedure of DSSC's with Liquid and Gel electrolytes.

The liquid electrolyte, which we used here, was prepared by mixing LiI (0.5M) and I₂ (0.05M) in 10 ml acetonitrile. To prepare gel electrolyte, ethyl-cellulose powder mixed with ethanol was added to the prepared liquid electrolyte. For our investigation, two cells were fabricated; one was filled with liquid type electrolyte and another one with gel-type electrolyte (Fig. 2).

After completion of the fabrication of two different cells with liquid and gel type electrolytes, the cells were placed under artificial solar illumination of 100 mW/cm² and connected with the J-V measurement system to calculate the photoelectric conversion efficiencies [28]. The photo-current voltage (I-V) characteristics were recorded using a Keithley 2400 source meter. Simulated sunlight was supplied using a xenon lamp (450W). This process had been repeated every alternate day and accordingly, the photovoltaic performances were recorded to investigate the long-term stability of the DSSCs. The ethyl cellulose gelator was selected for its easy availability and low cost.

RESULTS AND DISCUSSIONS

Scanning Electron Microscope (SEM) Analysis

The scanning electron microscope (SEM) was used to examine the surface morphology of TiO₂ film over the FTO glass substrate [29]. The highly porous morphology of the TiO₂ nanostructure deposited on a glass substrate can be observed from the SEM image shown in Fig. 3.

The particle size of the TiO₂ nanoparticles was about 60 nm. The higher porous structure resulted in greater dye molecules adsorption on the surface of the TiO₂ nanoparticles. Also, smaller the particle size of the TiO₂ particles, the higher the overall surface area for dye molecules attachment for a particular volume of the photoanode. More dye adsorption causes a

greater number of electron excitation from HOMO to LUMO of dye molecules after photon absorption [29].

Photovoltaic Performance of the DSSCs

The I-V characteristics of the fabricated DSSCs based on liquid and gel electrolyte and pure TiO₂ photoanode is shown in Fig. 3. The energy conversion efficiency of each DSSC was calculated using the formula:

$$\eta = \frac{P_{\text{out}}}{P_{\text{in}}} = \frac{I_{\text{sc}}V_{\text{oc}}FF}{P_{\text{in}}}, \quad (1)$$

where, I_{sc} is the short circuit current density, V_{oc} the open-circuit voltage, P_{in} is the total incident power density, and is FF the fill factor. The fill factor (FF) determines the quality of the solar cell, and it was calculated by

$$FF = \frac{I_{\text{max}}V_{\text{max}}}{I_{\text{sc}}V_{\text{oc}}}, \quad (2)$$

where I_{max} and V_{max} represent the current density and the voltage at maximum power output.

The Current-Voltage (I-V) characteristics of the DSSCs fabricated using liquid and gel-based electrolytes are shown in Fig. 4. The different electrical parameters of the cells obtained from the I-V characteristics are listed in Table 1 below.

The energy conversion efficiency of gel electrolyte based DSSC was lower than liquid electrolyte based DSSC. The photovoltaic efficiency of DSSCs using liquid and gel type electrolytes is 1.90 and 1.29% respectively. Tab. 1 represents the various photovoltaic parameters extracted from the I-V curves of the cells with liquid and gel electrolytes. The solar cell fabricated using liquid electrolyte exhibits higher short-circuit photocurrent density (J_{SC}), open-circuit voltage (V_{OC}), and fill factor (FF) compared to the DSSC fab-

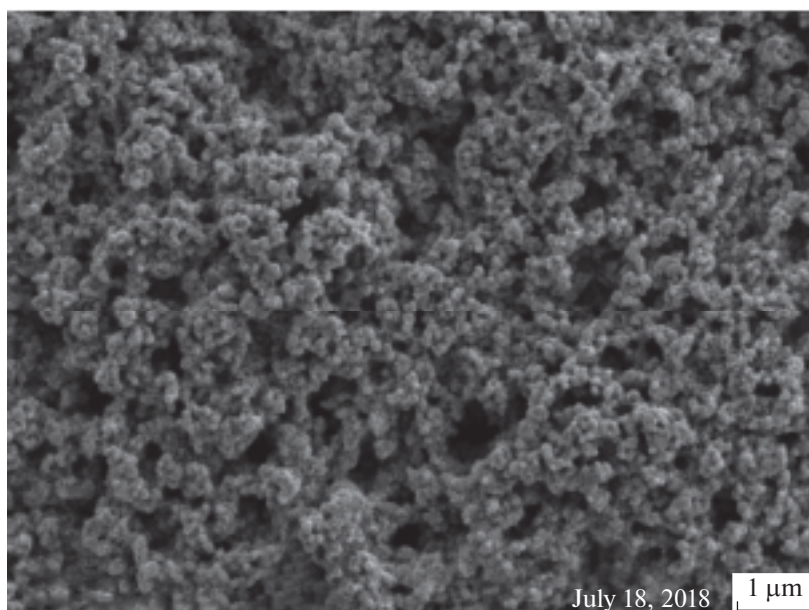


Fig. 3. Scanning electron microscope (SEM) image of TiO_2 nanoparticles on FTO substrate.

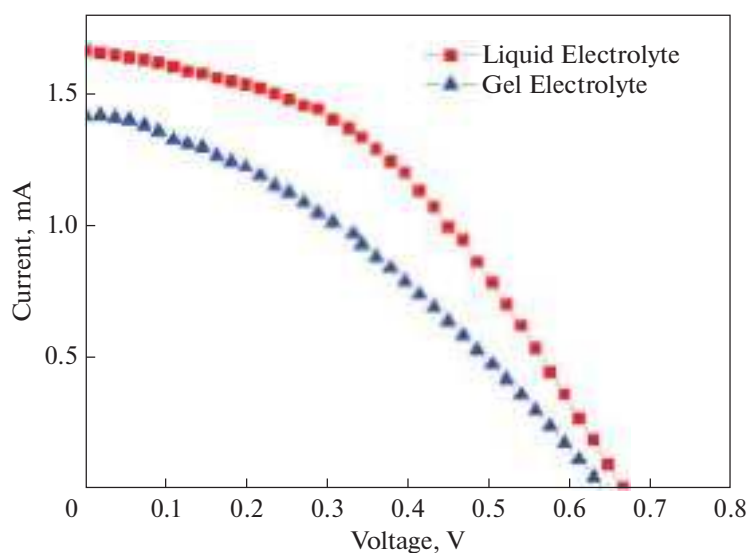


Fig. 4. Current-Voltage characteristics of the cells under illumination.

ricated using gel electrolyte as a dye. The efficiency of the gel-based DSSC may be low compared to the liquid electrolyte based DSSC, but the values of cell parameters obtained are found to be comparable to the efficiencies obtained for gel electrolyte based DSSCs [29].

Electrochemical behavior Analysis of the DSSCs

Electrochemical Impedance Spectroscopy (EIS) is a very useful technique for the interpretation of the kinetics of charge transport processes in different lay-

Table 1. Photovoltaic parameters of the fabricated cells

Cell	Electrolyte used	J_{sc} (mA/cm ²)	V_{oc} (V)	R_s (Ω cm ²)	R_{sh} (Ω cm ²)	FF	Efficiency (η %)
Cell-1	Liquid	1.67	0.662	309.5	1793	0.43	1.90
Cell-2	Gel	1.42	0.646	253.7	1547	0.35	1.29

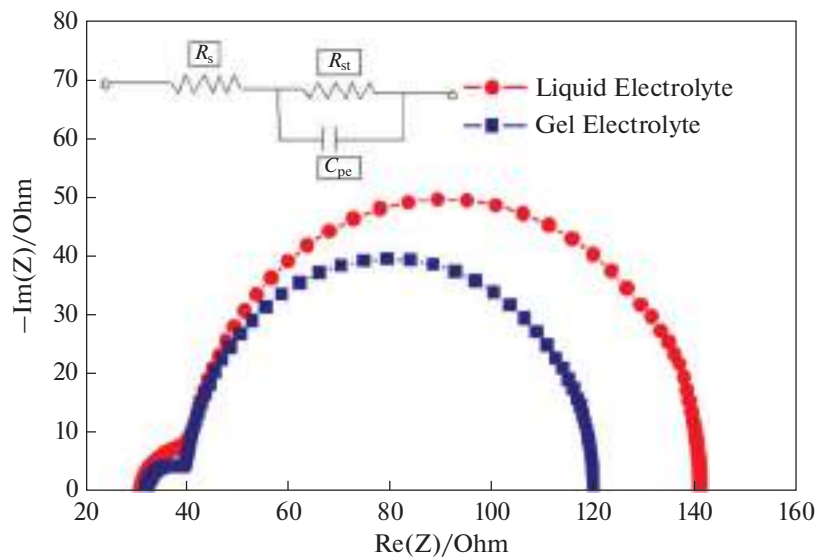


Fig. 5. Nyquist plot of DSSCs.

ers of DSSCs [30]. Generally, EIS data are represented by Nyquist and Bode plots. In the Nyquist plot, the imaginary part of impedance $\text{Im}(Z)$ is plotted against the real part of impedance $\text{Re}(Z)$ by varying frequencies of the applied signal [31].

An equivalent circuit is incorporated to analyze the EIS data, shown in the inset of Fig. 5. In the Nyquist plot, two semicircles are exhibited. The first semicircle in the low-frequency region represents the electron transfer resistance (R_{ct}) in the electrolyte and the second semicircle in the mid-frequency region indicates the charge transfer resistance (R_s) at photoanode/dye/electrolyte interface [32] and C_{PE} is the equivalent parallel capacitance. In the Nyquist plot, it is obvious that the second semicircle is more prominent than the other one. From the Fig. 4, it was seen that the diameter of the second semicircle for liquid electrolyte (cell 1) is less than the diameter of the semicircle for gel electrolyte (cell-2). This indicates that the charge transfer resistance at the TiO_2 /electrolyte interface for liquid electrolyte is lower than the same for gel electrolyte which justifies the slightly greater open circuit voltage, short circuit current, and overall cell efficiency of liquid electrolyte based DSSCs (Table 1). It is also suggested that the more viscous gel electrolyte does not affect the charge transfer process very much in the photoanode/electrolyte interface of the cell, but it affects the charge transfer resistance at the TiO_2 /electrolyte interface.

Stability Study of the Cells

The effect of electrolyte on the durability of DSSCs was characterized by calculating the photoelectric conversion efficiency over time [33], as shown in Fig. 6. The photoelectric conversion efficiency of DSSC

based on liquid electrolyte was recorded 1.90% immediately after fabrication and was changed to 0.89% after 120 hours. The photoelectric conversion efficiency of DSSC developed with gel electrolyte was recorded at 1.29% immediately after fabrication and 1.13% after some time. From here it is clear that however there is a small decrease in the efficiency for the gel electrolytes, the cell developed with gel electrolyte shows better stability than that with liquid electrolyte. The improvement in long term stability is probably due to the higher viscosity of gel inhibits the ionic migration to stabilize the system over a longer time and also by control of evaporation of liquid electrolyte. Also, higher stability of gel electrolyte gives it a better cost effectiveness than that of liquid electrolyte.

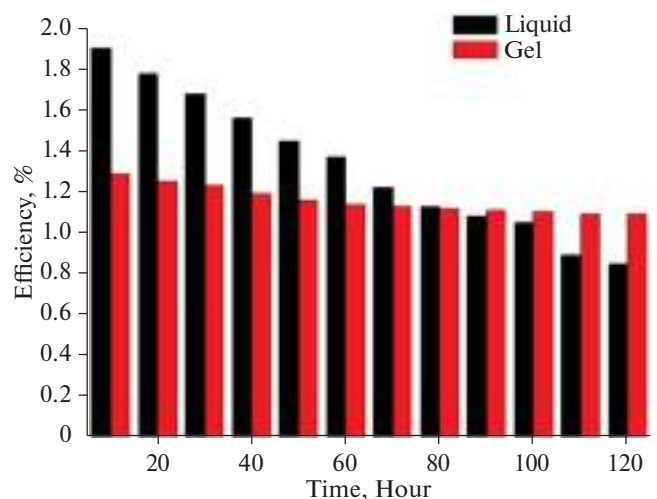


Fig. 6. Stability behavior of the fabricated DSSCs over time.

CONCLUSIONS

DSSCs were fabricated with pure TiO₂ photoanode with liquid and gel-type electrolyte, and cell performances were recorded. The liquid electrolyte cells exhibited higher short-circuit photocurrent density, open-circuit voltage, fill factor, and efficiency compared to the gel electrolyte DSSC. Though the efficiency of the gel-based DSSC is lower than the liquid electrolyte DSSC, the cell parameters obtained were comparable to the parameters obtained for gel electrolyte DSSC. Comparing these two types of DSSCs, it is clear that though the photovoltaic performance of gel electrolyte DSSC is slightly lower than liquid electrolyte DSSC, the performance of gel-based DSSC remains noticeably stable while for the liquid electrolyte the stability decreases remarkably over time.

FUNDING

The financial support to carry out this research was provided by the University of North Bengal. One of the authors' availed Ph.D. Inspire fellowship from the Department of Science and Technology (DST), Govt. of India.

ACKNOWLEDGMENTS

Authors gratefully acknowledge the Dept. of Physics, the University of North Bengal, for providing financial support and laboratory facilities for carrying out the research work. We also acknowledge the financial support from DST for providing a DST Inspire fellowship to one of our co-workers for carrying out the research work.

REFERENCES

- Grätzel, M., Dye-sensitized solar cells, *J. Photochem. Photobiol. C: Photochem. Rev.*, 2003, vol. 4, no. 2, pp. 145–153.
[https://doi.org/10.1016/S1389-5567\(03\)00026-1](https://doi.org/10.1016/S1389-5567(03)00026-1)
- Elliott, D., Renewable energy and sustainable futures, *Futures*, 2000, vol. 32, nos. 3–4, pp. 261–274.
[https://doi.org/10.1016/S0016-3287\(99\)00096-8](https://doi.org/10.1016/S0016-3287(99)00096-8)
- Gong, J., Liang, J., Sumathy, K., Review on dye-sensitized solar cells (DSSCs): fundamental concepts and novel materials, *Renewable Sustainable Energy Rev.*, 2012, vol. 16, no. 8, pp. 5848–5860.
<https://doi.org/10.1016/j.rser.2012.04.044>
- Blakers, A., Zin, N., McIntosh, K.R., and Fong, K., High-efficiency silicon solar cells, *Energy Procedia*, 2013, vol. 33, pp. 1–10.
<https://doi.org/10.1016/j.egypro.2013.05.033>
- McConnell, R.D., Assessment of the dye-sensitized solar cell, *Renewable Sustainable Energy Rev.*, 2002, vol. 6, no. 3, pp. 271–293.
[https://doi.org/10.1016/S1364-0321\(01\)00012-0](https://doi.org/10.1016/S1364-0321(01)00012-0)
- Sharma, K., Sharma, V., and Sharma, S.S., Dye-sensitized solar cells: fundamentals and current status, *Nanoscale Res. Lett.*, 2018, vol. 13, no. 1, art. no. 381.
<https://doi.org/10.1186/s11671-018-2760>
- Al-Alwani, M.A., Mohamad, A.B., Ludin, N.A., et al., Dye-sensitized solar cells: development, structure, operation principles, electron kinetics, characterization, synthesis materials & natural photosensitizers, *Renewable Sustainable Energy Rev.*, 2016, vol. 65, no. 1, pp. 183–213.
<https://doi.org/10.1016/j.rser.2016.06.045>
- O'Regan, B. and Grätzel, M.A., Low-cost, high-efficiency solar cell based on dye-sensitized colloidal TiO₂ films, *Nature*, 1991, vol. 353, no. 6346, pp. 737–740.
<https://doi.org/10.1038/353737a0>
- Leung, D.Y., Fu, X., Wang, C., et al., Hydrogen production over titania-based photocatalysts, *ChemSusChem*, 2010, vol. 3, no. 6, pp. 681–694.
<https://doi.org/10.1002/cssc.201000014>
- Liu, G., Gong, J., Kong, L., et al., Isothermal pressure-derived metastable states in 2D hybrid perovskites showing enduring bandgap narrowing, *Proc. National Academy of Sciences*, 2018, vol. 115, no. 32, pp. 8076–8081.
<https://doi.org/10.1073/pnas.1809167115>
- Liu, G., Kong, L., Guo, P., et al., Two regimes of band-gap redshift and partial ambient retention in pressure-treated two-dimensional perovskites, *ACS Energy Lett.*, 2017, vol. 2, no. 11, pp. 2518–2524.
<https://doi.org/10.1021/acsenergylett.7b00807>
- Wang, X., Li, Z., Shi, J., and Yu, Y., One-dimensional titanium dioxide nanomaterials: nanowires, nanorods, and nanobelts, *Chem. Rev.*, 2014, vol. 114, no. 19, pp. 9346–9384.
<https://doi.org/10.1021/cr400633s>
- Biswas, R. and Chatterjee, S., Effect of surface modification via sol-gel spin coating of ZnO nanoparticles on the performance of WO₃ photoanode-based dye-sensitized solar cells, *Optik*, 2020, vol. 212, art. id. 164142.
<https://doi.org/10.1016/j.ijleo.2019.164142>
- Lee, J.H., Park, N.G., and Shin, Y.J., Nano-grain SnO₂ electrodes for high conversion efficiency SnO₂-DSSC, *Sol. Energy Mater. Sol. Cells*, 2011, vol. 95, no. 1, pp. 179–183.
<https://doi.org/10.1016/j.solmat.2010.04.027>
- Zheng, H., Tachibana, Y., and Kalantar-Zadeh, K., Dye-sensitized solar cells based on WO₃, *Langmuir*, 2010, vol. 26, no. 24, pp. 19148–19152.
<https://doi.org/10.1021/la103692y>
- Karki, I.B., Nakarmi, J.J., Mandal, P.K., and Chatterjee, S., Effect of organic dyes on the performance of ZnO based dye-sensitized solar cells, *Appl. Sol. Energy*, 2013, vol. 49, no. 1, pp. 40–45.
<https://doi.org/10.3103/S0003701X13010052>
- Ayalew, W.A. and Ayele, D.W., Dye-sensitized solar cells using natural dye as light-harvesting materials extracted from *Acanthus sennii chiovenda* flower and *Euphorbia cotinifolia* leaf, *J. Sci.: Adv. Mater. Devices*, 2016, vol. 1, no. 4, pp. 488–494.
<https://doi.org/10.1016/j.jsamd.2016.10.003>
- Kabir, F., Bhuiyan, M.M., Manir, M.S., et al., Development of dye-sensitized solar cell based on a combination of natural dyes extracted from Malabar spinach and red spinach, *Results Phys.*, 2019, vol. 14, no. 1, art. id. 102474.
<https://doi.org/10.1016/j.rinp.2019.102474>

19. Narayan, M.R., Dye-sensitized solar cells based on natural photosensitizers, *Renewable Sustainable Energy Rev.*, 2012, vol. 16, no. 1, pp. 208–215. <https://doi.org/10.1016/j.rser.2011.07.148>
20. Biswas, R., Roy, T., and Chatterjee, S., Study of electro-optical performance and interfacial charge transfer dynamics of dye-sensitized solar cells based on ZnO nanostructures and natural dyes, *J. Nanoelectron. Optoelectron.*, 2019, vol. 14, no. 1, pp. 99–108. <https://doi.org/10.1166/jno.2019.2445>
21. Wu, J., Lan, Z., Hao, S., et al., Progress on the electrolytes for dye-sensitized solar cells, *Pure Appl. Chem.*, 2008, vol. 80, no. 11, pp. 2241–2258. <https://doi.org/10.1351/pac200880112241>
22. Vasei, M., Tajabadi, F., Jabbari, A., and Taghavinia, N., Stable dye-sensitized solar cells based on a gel electrolyte with ethyl cellulose as the gelator, *Appl. Phys. A*, 2015, vol. 120, pp. 869–874. <https://doi.org/10.1007/s00339-015-9332-8>
23. Richter, A., Hermle, M., and Glunz, S.W., Reassessment of the limiting efficiency for crystalline silicon solar cells, *IEEE J. Photovoltaics*, 2013, vol. 3, no. 4, pp. 1184–1191. <https://doi.org/10.1109/JPHOTOV.2013.2270351>
24. Mahmood, A., Recent research progress on quasi-solid-state electrolytes for dye-sensitized solar cells, *J. Energy Chem.*, 2015, vol. 24, no. 6, pp. 686–692. <https://doi.org/10.1016/j.jechem.2015.10.018>
25. Shi, L.Y., Chen, T.L., Chen, C.H., and Cho, K.C., Synthesis and characterization of a gel-type electrolyte with ionic liquid added for dye-sensitized solar cells, *Int. J. Photoenergy*, 2013, vol. 2013, art. id. 834184. <https://doi.org/10.1155/2013/834184>
26. An, H., Xue, B., Li, D., et al., Environmentally friendly LiI/ethanol-based gel electrolyte for dye-sensitized solar cells, *Electrochem. Commun.*, 2006, vol. 8, no. 1, pp. 170–172. <https://doi.org/10.1016/j.elecom.2005.11.012>
27. Pathak, C., Surana, K., Kumar Shukla, V., and Singh, P.K., Fabrication and characterization of a dye-sensitized solar cell using natural dyes, *Mater. Today: Proc.*, 2019, vol. 12, no. 3, pp. 665–670. <https://doi.org/10.1016/j.matpr.2019.03.111>
28. Trihutomo, P., Soeparman, S., Widhiyanuriyawan, D., and Yuliati, L., Performance improvement of dye-sensitized solar cell- (DSSC-) based natural dyes by clathrin protein, *Int. J. Photoenergy*, 2019, vol. 2019, art. id. 4384728. <https://doi.org/10.1155/2019/4384728>
29. Umale, S.V., Tambat, S.N., Sudhakar, V., et al., Fabrication, characterization, and comparison of DSSC using anatase TiO₂ synthesized by various methods, *Adv. Powder Technol.*, 2017, vol. 28, no. 11, pp. 2859–2864. <https://doi.org/10.1016/j.apt.2017.08.012>
30. Wang, Q., Moser, J.E., and Grätzel, M., Electrochemical impedance spectroscopic analysis of dye-sensitized solar cells, *J. Phys. Chem. B*, 2005, vol. 109, no. 31, pp. 14945–14953. <https://doi.org/10.1021/jp052768h>
31. Sarker, S., Ahammad, A., Seo, H.W., and Kim, D.M., Electrochemical impedance spectra of dye-sensitized solar cells: fundamentals and spreadsheet calculation, *Int. J. Photoenergy*, 2014, vol. 2014, art. id. 851705. <https://doi.org/10.1155/2014/851705>
32. Fabregat-Santiago, F., Bisquert, J., Palomares, E., et al., Correlation between photovoltaic performance and impedance spectroscopy of dye-sensitized solar cells based on ionic liquids, *J. Phys. Chem. C*, 2007, vol. 111, no. 17, pp. 6550–6560. <https://doi.org/10.1021/jp066178a>
33. Sonai, G.G., Tiihonen, A., Miettunen, K., et al., Long-term stability of dye-sensitized solar cells assembled with cobalt polymer gel electrolyte, *J. Phys. Chem. C*, 2017, vol. 121, no. 33, pp. 17577–17585. <https://doi.org/10.1021/acs.jpcc.7b03865>

SPELL: 1. OK

ARTICLE

Study of Electro-Optical Performance and Interfacial Charge Transfer Dynamics of Dye Sensitized Solar Cells Based on ZnO Nanostructures and Natural Dyes

Rajat Biswas, Trinakhi Roy, and Suman Chatterjee*

The present work reports comparative assessment of optical and electrical properties of DSSCs fabricated using vertically aligned ZnO nanorods synthesized using low cost Sol–Gel spin coating technique on ITO coated glass substrate and ZnO nanopowder and their application in the fabrication of natural dye based Dye Sensitized Solar Cells. Natural dyes extracted from pomegranate and turmeric are used sensitizers. The surface morphology and crystal structure have been investigated by scanning electron microscopy and X-ray diffraction techniques. Optical absorption properties of the dyes were studied using UV-VIS spectroscopy. Photovoltaic parameters like Open Circuit voltage (V_{OC}), Short Circuit current (I_{SC}), fill factor (FF), Energy Conversion efficiency (η) were calculated to study the performances of the cells. Cell parameters like series resistance (R_s) and shunt Resistance (R_{sh}) were calculated from the I – V curve. Electrochemical impedance spectroscopy (EIS) was employed for detail investigation of the charge carrier recombination properties and the charge transfer mechanism at different interfaces of the DSSC devices. Various cell parameters were determined by fitting the experimental EIS curves with the appropriate equivalent circuit. The electron lifetimes were determined using bode plot of EIS measurement for the ZnO nanorod and ZnO nanoparticle photo electrodes sensitized using curcumin dye from turmeric and anthocyanin dye from pomegranate juice. The ZnO nanorod sensitized with curcumin cell emerged out as the best performing cell among the four cells which can be attributed to the highest electron lifetime, higher recombination resistance resulting in lower charge carrier recombination in the ZnO/Dye/Electrolyte interface. Many researchers have studied sensitizing effect of curcumin dye with different nanostructures of ZnO but we are the first to study the sensitizing effect of curcumin dye on ZnO nanorod like structure.

Keywords: Dye-Sensitized Solar Cells, Zinc Oxide Nanorod, Sol–Gel Hydrothermal Growth, Natural Dyes, Electrochemical Impedance Spectroscopy, Carrier Lifetime.

1. INTRODUCTION

With the increasing world population, spreading urbanization and technological advancement, matching the energy supply with the energy demand is the major challenging issue world is facing these days. The environmental consequences related to extensive use of fossil fuels, safety related issues of nuclear power, ever-growing energy

demand and depleting the stock of fossil fuels have motivated the researchers to search for alternative economically and environmentally sustainable renewable energy sources.¹ In such a context of global energy requirement, among all the non-polluting and renewable energy sources, the photovoltaic technology utilizing solar energy has emerged as the most assuring candidate.² Though conventional photovoltaic devices (silicon-based solar cells) are promising for the direct conversion of photons into electrons, the prohibitive cost of these cells is noncompetitive with conventional power generating methods.^{3,4} On the contrary, dye-sensitized solar cells (DSSCs), invented by O'Regan and Grätzel in 1991, are non-conventional

Department of Physics, University of North Bengal, Raja Rammohunpur, Siliguri 734013, India

*Author to whom correspondence should be addressed.

Email: suman_chatterjee@hotmail.com

Received: 14 June 2018

Accepted: 3 September 2018

photovoltaic technology based solar cells that have attracted significant attention because of its novel fabrication concept derived from nature's principle (photosynthesis), easy fabrication procedure using abundant materials, cost-effectiveness, suitability for wide variety of end-user products and can be made flexible. DSSC is a device which converts the solar energy into electrical energy, based on the principle of sensitization of wide bandgap semiconductors.⁵ The photoelectrochemical performance of a DSSC mainly depends on the selected Photoanode material including its surface morphology and the sensitizing dye used.⁶⁻⁹ Although a large number of different DSSCs have been investigated, most of them are not commercially popular until now because of its issues with low conversion efficiency, higher production cost, lower stability and durability.^{10, 11}

Different inorganic, organic and hybrid dyes were employed as sensitizers in DSSCs. But among all of them, the ruthenium complexes are the most popular sensitizers because of their intense charge transfer absorption across the complete visible range and immensely efficient metal-to-ligand charge transfer mechanism.¹² But the major downsides of Ruthenium dyes are its rareness, high cost and complicated synthesis process.¹³ Also, ruthenium polypyridyl complexes contain heavy metal, which is harmful to the environment.¹⁴ In order to find out low cost and environment-friendly alternative to these expensive ruthenium compounds, researchers are focusing on easily available natural dyes extracted from various natural resources. Many researchers have studied sensitizing effects of several natural dyes derived from various fruits, flowers and leaves.¹⁵ Most of them are used with TiO₂ nanostructures as photoanode.¹⁶⁻²⁰ However, recently ZnO has been emerging out as a great potential alternative to TiO₂ due to some its fascinating electrical and optical properties. ZnO is a wide band gap semiconductor having a direct band gap of 3.37 eV making it suitable as a photoanode material for DSSC.^{21, 22} Apart from this, ZnO is very easy to synthesis, abundant, inexpensive and poses higher electron mobility (200–300 cm²V⁻¹S⁻¹ for bulk material and 1000 cm²V⁻¹S⁻¹ for nanowire) than that of TiO₂ nanoparticles (0.1–4 cm²V⁻¹S⁻¹).²³⁻²⁵ Moreover, the 1-D single crystalline rod-like structure of ZnO nanorods provide a higher surface to volume ratio enabling better dye loading.²⁶ These qualities of ZnO make it a potential alternative to TiO₂ for fabrication of DSSCs.

In this study, we aimed to combine natural sensitizers with two types of nanostructured ZnO to get both the advantages of ZnO and also the benefits of natural organic dyes targeting lower fabrication cost, eco friendly devices along with good cell performance and wanted to find out the best suitable ZnO nanostructure-Natural dye combination. In this regard, we fabricated four DSSCs using two types of natural dyes, anthocyanin extracted from pomegranate (*Punica granatum*) and curcumin extracted

from fresh turmeric (*Curcuma longa*) and studied their electro-optical responses to investigate their usefulness as natural sensitizers when adsorbed onto ZnO nanorod (NR) and ZnO nanoparticle (NP) films in DSSCs. Hydroxyl and Carbonyl groups existing the natural sensitizers bound them easily to the surface of the ZnO nanorods which facilitates very easy electron injection from LUMO of dye molecule to the conduction band of ZnO.²⁷

2. EXPERIMENTAL DETAILS

2.1. Structure and Working Principle of DSSC

A typical DSSC consists of four elements: a photoanode with a thin layer of mesoporous wide band gap semiconductor oxide layer (usually TiO₂, ZnO, SnO₂ or Nb₂O₅) over a transparent conducting substrate (ITO or FTO), a monolayer of the sensitizing dye adsorbed on the semiconductor oxide surface to facilitate light absorption, an redox mediator electrolyte solution (typically I⁻/I³⁻) in an organic solvent and a counter electrode made up of a catalyst (platinized ITO or FTO) to facilitate charge collection. The schematic of device architecture and working principle of a typical DSSC is shown in Figures 1(a) and (b).

Upon exposure to the sunlight, dye molecule absorbs photon energy and goes through an electronic state change, the electron jumps from ground state (HOMO) to the excited state (LUMO). As a result, electron injection into the conduction band of the semiconductor oxide (ZnO) film takes place whereby the dye molecule gets oxidized. This oxidized dye molecule is regenerated by taking an electron from the redox species of the electrolyte (I⁻). Subsequently, I⁻ is regenerated by reduction of I³⁻ with electrons migrated from photo anode via external load and collected at the counter electrode, completing the cycle.^{5, 6}

2.2. Materials

Transparent ITO coated glass (10 Ω/square) was purchased from Techinstro, India. The liquid platinum paint (Platisol T) purchased from Solaronix, Switzerland was used to prepare the platinum coated transparent counter electrode. Commercial ZnO nanopowder (<50 nm.), Zinc acetate dehydrate and Hexamethylenetetramine all were purchased from Sigma Aldrich. Ethylene Glycol (Sigma Aldrich) was used as a solvent for the electrolyte preparation using KI (S D Fine-Chemical Ltd., India) and I₂ (RANKEM, India). Meltonix 1170-60 (60 μm) purchased from Solaronix was used as a spacer between the electrodes to avoid short-circuiting between them.

2.3. Extraction and Preparation of Natural Dye Sensitizers

In the fabrication of Dye Sensitized solar cells, selection of the dyes is one the crucial task as it significantly affects the performance and production cost the cells. By choosing abundant natural dyes instead of expensive synthetic

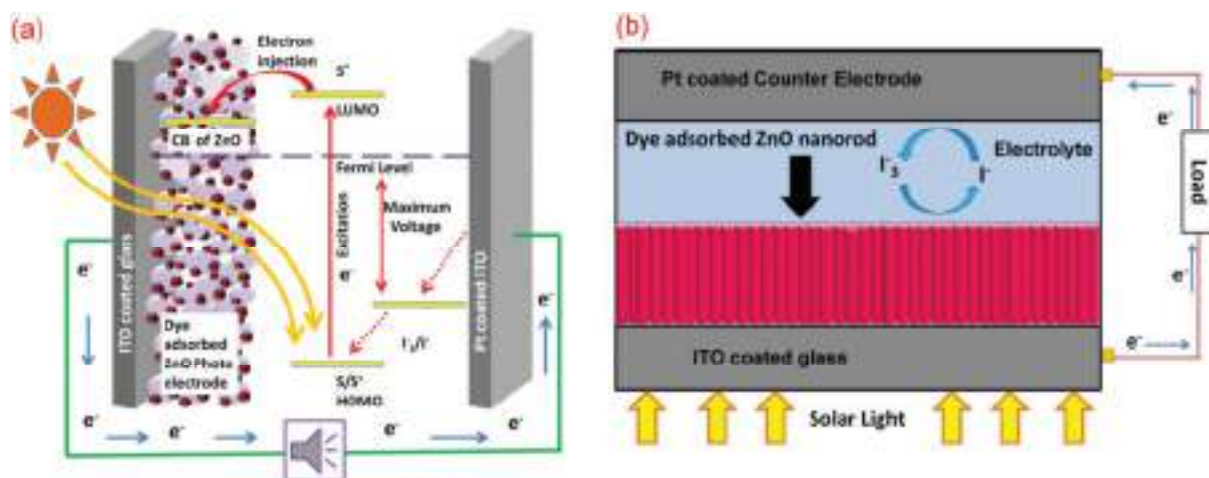


Fig. 1. Schematic diagram and basic working mechanism of DSSCs based on (a) ZnO nanoparticle (b) ZnO nanorod.

ruthenium dyes we can reduce the production cost by a large amount. In this work, we have chosen extracts of Curcumin and pomegranate juice as sensitizers. Curcumin was extracted by grinding turmeric root in an iron mortar and then mixing in 100 ml ethanol. After extraction, solid residues were filtered out to obtain a clear natural dye solution.

For pomegranate extraction of pomegranate juice, a fresh pomegranate was squeezed and then mixed with 100 ml deionized water. This solution is also filtered to obtain pure dye. The dye solutions were properly stored protecting from direct sunlight for further use. Studies have shown that Curcumin dyes have two forms and they are identified as Keto and Enol.²⁸ On the other hand, it was found that pomegranate juice mostly contains six type anthocyanins. These are cyanidin 3-glucoside, cyanidin 3,5-diglucoside, delphinidin 3-glucoside, delphinidin 3,5-diglucoside, pelargonidin 3-glucoside and pelargonidin 3,5-diglucoside.²⁹ The chemical structures of these dyes are shown in Figure 2.

2.4. Sol–Gel Synthesis of ZnO Nanorods: Preparation of Working Electrodes

To prepare the working electrode, first, the ITO coated glass was cut into 2×2 cm square shaped pieces. Cleaning of this substrate is very important as it removes any organic or inorganic contaminant present on its surface which can significantly affect the performances of the cells. Furthermore, cleaning enhances the adhesion of the subsequent layers to be deposited over it. The ITO substrates were cleaned using dilute HCl for 15 minutes in an ultrasonic cleaner to remove oxide impurities. Then they were rinsed extensively with deionized water to remove the HCl residues. The substrates were then subjected to cleaning in acetone, ethanol and deionized water for 15 minutes each using an ultrasonic bath. Finally, the substrates were dried using a hairdryer. The cleaned substrates

were masked using scotch tape on four sides leaving the central area empty for semiconductor material deposition.

ZnO nanorods were grown on the ITO coated glass substrate by following a simple two-step Sol–Gel spin coating protocol followed by hydrothermal growth.³⁰ In the first step, a thin ZnO seed layer was formed on the ITO glass substrates using 5 mM Zinc acetate dehydrate $(\text{CH}_3\text{COO})_2\text{Zn} \cdot 2\text{H}_2\text{O}$, (98% Merck) in acetone as precursor solution. The solution was well mixed using an ultrasonic bath for 2 hours at room temperature and then spun onto cleaned and masked ITO coated glass substrates using a programmable spin coater (Apex Technologies, Model SCU-2008C) at 1000 rpm for 30 seconds. The coated substrates were then annealed at 350 °C temperature for 30 minutes. After evaporation of the solvent, a thin ZnO film was formed whose thickness can be controlled by repeating the above process. In this way, the seed layer is formed. The thickness of the film can also be controlled by varying solution concentration and the spinning speed of the spin coater.³¹ In the second step, vertically aligned ZnO nanorods were grown over the seed layer-coated ITO glass substrate by hydrothermal method. In this method, the seed layer coated substrate was immersed in a solution containing an equal proportion of 5 mM Zinc acetate dehydrate, $(\text{CH}_3\text{COO})_2\text{Zn} \cdot 2\text{H}_2\text{O}$ and 5 mM Hexamethylenetetramine, $(\text{C}_6\text{H}_{12}\text{N}_4)$ at 90 °C temperature in a Pyrex vessel for 2 hours. This creates an array of vertically aligned ZnO nanorods on the substrate. It was then taken out from the solution and rinsed immediately with ethanol and deionized water in order to remove any left-over residues from the film surface and allowed to air dry at room temperature. Finally, the ZnO nanorod formation was completed by annealing the film at 450 °C for 30 min. This ZnO nanorod array coated substrates were then immersed in the dye solutions to allow adsorption of the dye molecules onto the semiconductor nanorod surface for 24 hours. Then the electrodes were taken out from the

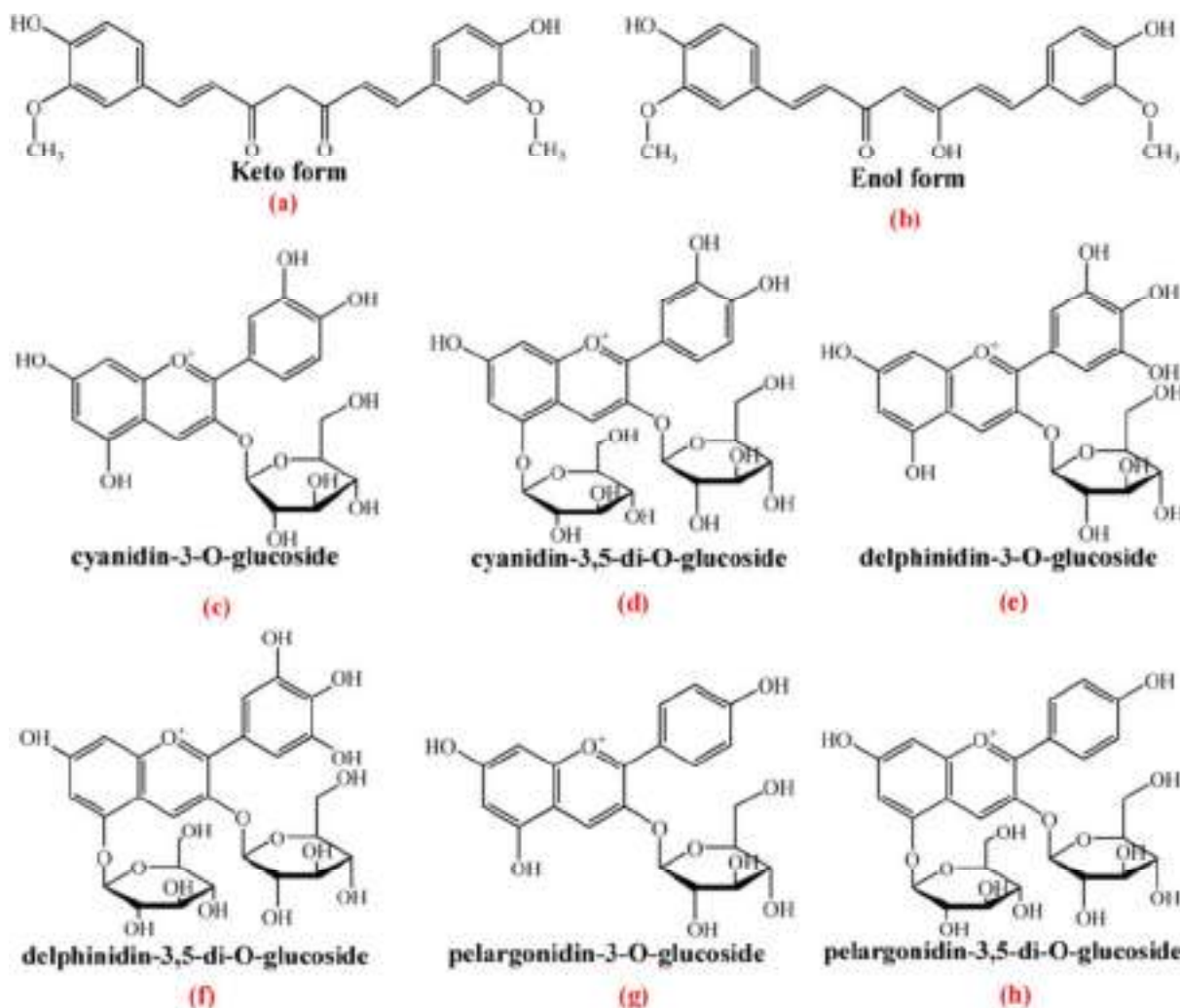


Fig. 2. Chemical structures of curcumin (a and b) present in turmeric and six major anthocyanins (c–h) present in pomegranate fruit extracts.

solutions and rinsed with ethanol and deionized water to remove the excess dye from the surface of the films and air dried at room temperature. The platinum counter electrode was prepared by spin coating the platinum precursor solution (platisol T-solaronix) at 1000 rpm for 30 seconds onto a drilled ITO substrate and giving heat treatment at 450 °C for 15 minutes.

2.5. DSSC Assembling

To assemble the solar cell, the conductive side of the platinum coated counter electrode was placed over the dye adsorbed ZnO nanorod photoanode so that the platinumized side of the counter electrode faces the ZnO film. Surlyn spacer (Meltonix 1170-25 μm) was placed in between them to prevent the uncoated areas of the electrodes from short-circuiting. Two binder clips were used to firmly clamp the two electrodes together in a sandwich manner. The redox electrolyte was prepared by mixing 0.5 M KI and 0.05 M I_2 in Ethylene Glycol solvent

in a proportionate amount. This electrolyte solution was injected into the cell through the drilled hole on the counter electrode. The hole was then sealed using a hot melt sealant. The effective cell area was 1 cm^2 .

2.6. Device Characterization and Measurements

The absorption spectra of the dyes were studied using a Perkin Elmer Lambda-35 UV-VIS spectrophotometer in the wavelength range of 200–600 nm range. The crystalline structure of the ZnO films was studied using PANalytical X'Pert PRO X-ray diffractometer with $\text{CuK}\alpha$ (30 mA, 40 kV, $\lambda = 1.5406 \text{ \AA}$). The surface morphologies of the ZnO films were characterized by using scanning electron microscopy (JEOL). The current–voltage (I – V) characteristics of the fabricated cells under illumination of 100 mW/cm^2 (Oriel Xenon lamp 450 W) were recorded by employing a Keithley 2400 source meter connected to a PC. The desired intensity of incident light was obtained

with the help of a reference cell by adjusting the distance between the light source and the cell.

The performance of the solar cell is determined by the overall photoconversion efficiency of the cell which is defined as the ratio of maximum electrical output power of the cell to the incident optical power and is given by the equation

$$\eta = \frac{P_{out}}{P_{in}} = \frac{I_{sc} V_{oc} FF}{P_{in}} \quad (1)$$

where P_{in} is the power of the incident light, I_{max} and V_{max} are the current and voltage corresponding to the maximum output power from the solar cell and I_{sc} and V_{oc} represents the short circuit current and open circuit voltage respectively. The term FF is known as Fill factor of the cell. It is determined from the $I-V$ characteristics and calculated as

$$FF = \frac{I_{max} V_{max}}{I_{sc} V_{oc}} \quad (2)$$

The efficiency is generally expressed in percentage.

3. RESULTS AND DISCUSSION

3.1. UV-VIS Absorption Spectral Analysis of the Dyes

UV-VIS absorption spectra of the Curcumin and pomegranate dye in are shown in Figure 3. A clear difference the absorption peaks of the two dyes can be seen. Curcumin exhibits absorption peak at 422 nm whereas pomegranate fruit extract solution at 517 nm. The difference in the absorption peaks is due to the different types of colors and chromophores present in Curcumin and pomegranate extracts.

3.2. X-ray Diffraction Analysis of the ZnO Film

The structural and crystalline quality information of the synthesized ZnO nanorods and purchased ZnO nanopowder were studied using X-ray diffraction pattern of the samples which is shown in Figure 4. The consistency of the obtained diffraction peak was confirmed by comparing them with the standard JCPDS card no. 36-1451. A remarkably enhanced diffraction peak for (002) plane at 34.4595°

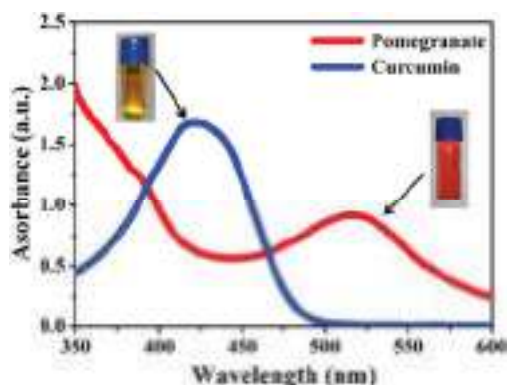


Fig. 3. Absorption spectra of the natural sensitizers.

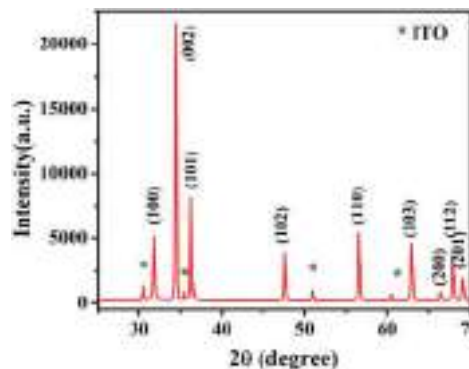


Fig. 4. XRD pattern of ZnO nanorods.

can be clearly observed for the ZnO nanorods. It indicates strong preferential growth of ZnO nanorods along c -axis and vertical alignment on the ITO substrate and also the hexagonal wurtzite structure. XRD of ZnO nanoparticles was not performed since the powder was commercially purchased.

The average crystalline size of the ZnO films were estimated from the width of the (002) peak for ZnO nanorod and (101) peak for ZnO nanoparticle using Debye-Scherrer formula for X-ray diffraction,

$$\text{Crystalline Size } (D) = \frac{0.9\lambda}{\beta \cos \theta} \text{ \AA} \quad (3)$$

where β , θ and λ are FWHM of the peak, Bragg angle and wavelength of X-ray used. The dislocation density (δ), representing the amount of defects in the crystal and the strain (ϵ) of the film were determined using following formulae respectively:³²

$$\delta = \frac{1}{D^2} \quad (4)$$

$$\epsilon = \frac{\beta \cos \theta}{4} \quad (5)$$

The values of different parameters calculated from the structural analysis of the XRD pattern are given in Table I.

Crystalline size estimated from X-ray analysis is generally found to be less than the particle size found from SEM images. The reason behind this is that generally a particle may be formed by combination of several crystallites or just one crystallite.

3.3. Scanning Electron Microscope Studies

Scanning electron microscopy (SEM) was carried out to study the morphological properties of the sample film.

Table I. Structure parameters of the ZnO nanorod thin film.

ZnO particle type	Plane	FWHM (β) $^\circ$	2θ $^\circ$	D (nm)	δ nm $^{-2}$	ϵ
Nanorod	002	0.20567	34.4595	40.43	6.11×10^{-4}	4.91×10^{-2}

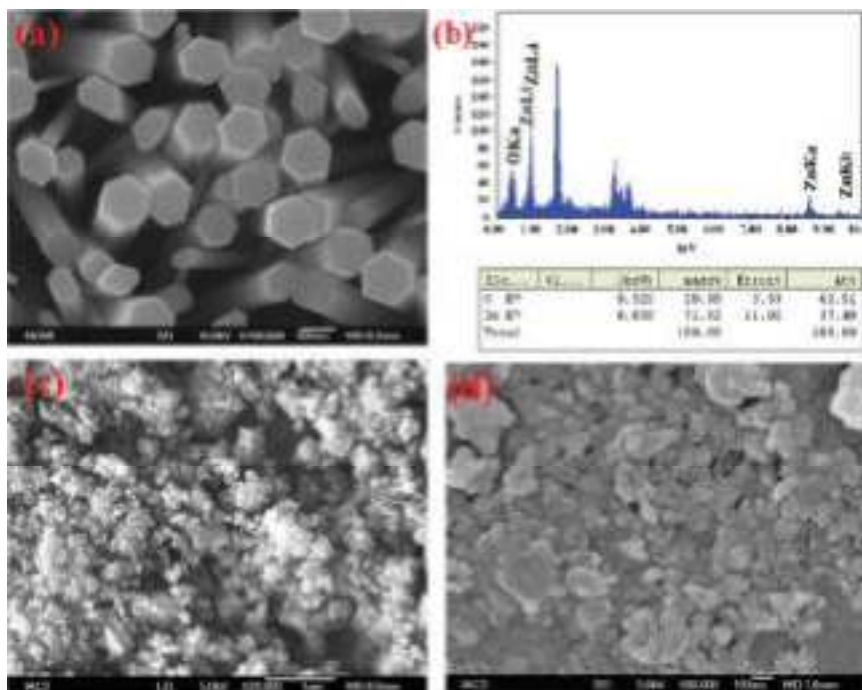


Fig. 5. SEM image of (a) ZnO nanorods grown on ITO substrate (b) EDX spectra of the nanorod sample showing elemental composition (c and d) ZnO nanoparticle deposited sample at lower and higher magnification respectively.

Figure 5(a) is the SEM image of the ZnO nanorod arrays on ITO substrate. The SEM observation reveals that most of the nanorods have grown vertical to the seed layer on the ITO substrate and have hexagonal wurtzite.

The nanorods have diameters ranging from 100–200 nm with an average length of 300 to 400 nm and in case of nanoparticles; the average particle size was around 50 nm. To investigate the chemical composition of the nanorods, EDX analysis was performed which is shown in Figure 5(b), which confirms the presence of Zn and O. The unidentified peaks are due to the presence of indium (In) and tin (Sn) in ITO substrate.

3.4. Current–Voltage Characteristics Study of Cells/Solar Cell Efficiency Measurements

The current–voltage characteristic of a Solar cell allows us to determine the photovoltaic performance of the cell. The $J-V$ curves of the fabricated cells under illumination of 100 mW/cm^2 are shown in Figure 6(a). The Power–Voltage plot to calculate the maximum power point (P_{max}), I_{max} and V_{max} are represented in Figure 6(b). Table II shows various parameters extracted from the $I-V$ curves of the ZnO nanorod based DSSCs fabricated using natural dyes Curcumin and Pomegranate. The solar cell fabricated using Curcumin extract exhibits higher shortcircuit photocurrent density (J_{SC}), open-circuit voltage (V_{OC}) and

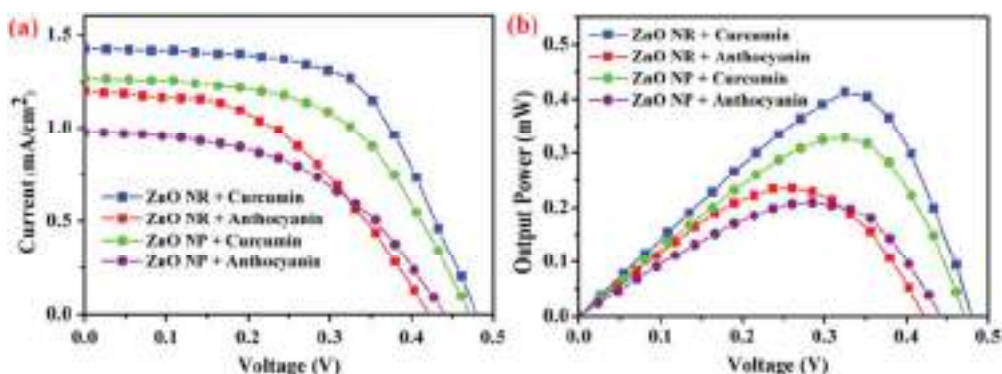


Fig. 6. (a) Current density–voltage characteristics of the cells under illumination (b) power–voltage curve to obtain maximum power point.

Table II. Solar cell parameters of fabricated DSSC's.

Cell No.	Dye used and ZnO microstructure	J_{sc} (mA/cm ²)	V_{oc} (V)	R_s (Ω cm ²)	R_{sh} (Ω cm ²)	FF	Efficiency (η %)
1	Curcumin and ZnO NR	1.43	0.49	86.28	7866.28	0.59	0.41
2	Anthocyanin and ZnO NR	1.20	0.43	116.67	2722.90	0.46	0.24
3	Curcumin and ZnO NP	1.27	0.46	101.19	6629.31	0.56	0.33
4	Anthocyanin and ZnO NP	0.98	0.45	146.87	4659.92	0.48	0.21

fill factor (FF) compared to the DSSC fabricated using pomegranate extract as a dye. The Curcumin dye cell shows an improved overall photoelectric conversion efficiency (η) over the anthocyanin dye cell. The efficiency of these natural dye based cells may be low compared to the synthetic dye based DSSCs but these values are comparable to the efficiencies obtained for natural dye based DSSCs reported by other researchers.³³

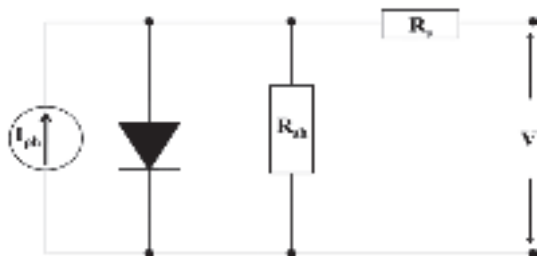
Equivalent circuit modeling is a very important tool required for better understanding and explanation of the solar cell performance and analysis of the electrical processes occurring inside the cell. The functioning of a solar cell generally modeled by a single diode with a constant photo-generated current source, a series (R_s) and shunt resistance (R_{sh}) as shown in Figure 7. The current-voltage relation is given by the equation

$$I = I_{ph} - I_0 \left[\exp \left\{ \frac{q(V + IR_s)}{Ak_B T} \right\} - 1 \right] - \frac{V + IR_s}{R_{sh}} \quad (6)$$

where I_{ph} , I_0 , R_s , R_{sh} , q , A , k_B and T are the photocurrent, the saturation current of the diode, the series resistance, the shunt resistance, the electron charge, the ideality factor, the Boltzmann constant, and absolute temperature, respectively.³⁴

The circuit parameters like R_s and R_{sh} are not directly measurable. They are calculated by fitting the experimental J - V curve with the Eq. (6). Values of these parameters obtained for the fabricated cells are also represented in Table II.

Cell-1 shows lowest series resistance (R_s) compared to other cells. This indicates improved electrical contacts,

**Fig. 7.** The equivalent circuit (single diode model) of a solar cell.

lower junction resistances and better ZnO nanorod morphology in case of cell-1. Higher series resistance means greater voltage drop inside the cell resulting in lower terminal voltage and sagging of current controlled part of the J - V curve towards the origin which can be correlated with Table II and Figure 6(a). In addition, from single diode equivalent circuit of the solar cell (Fig. 7), it can be clearly seen that R_{sh} provides an alternative path to the photocurrent which causes power losses in the solar cell. Lower R_{sh} results in partial shorting between the two electrodes of the solar cell giving rise to leakage current. So, the highest value of R_{sh} of cell-1 attributes to lowest leakage current which results in improved cell performance. Also, from Table II it can be confirmed that higher shunt resistance results in higher fill factor and consequently better photoconversion efficiency.

3.5. Electrochemical Impedance Spectroscopy Study of the Cells

The electrochemical impedance spectroscopy is a very useful diagnostic technique which has often been performed to investigate the interfacial charge transfer dynamics and recombination mechanisms occurring inside a DSSC.³⁵ These are generally modelled using appropriate equivalent circuit in terms of resistors and capacitors. The EIS measurements were performed using HIOKI Impedance Analyser in the frequency range 0.1 Hz to 190 kHz under dark condition with employing an AC sinusoidal signal having amplitude of 10 mV under influence of V_{oc} bias voltage. EIS findings as Nyquist plot of the DSSCs are shown in Figure 8(a). Physical interpretation of the different electrochemical operations across the interfacial regions of the DSSCs can be done by fitting the EIS spectra with the equivalent circuit shown in Figure 8(b). Generally a typical Nyquist plot exhibits three semicircles. However, only two semicircles are present in our study due to low frequency limitation of our instrument. The first smaller semicircle (in the high frequency range) attributes to the charge transfer resistance at the Pt counter electrode/Electrolyte interface (R_{CE}) and the second semicircle (mid frequency range) having higher diameter corresponds to the resistance of charge transfer and recombination process at the ZnO photoelectrode/dye/electrolyte interface (R_{ct}). The intercept of the first semicircle in the high frequency range on real axis of the Nyquist plot is associated with the contact resistances and external ohmic series resistance (R_{SER}) of the assembled cell.³⁶ The experimental Nyquist plot is fitted with the equivalent circuit shown in inset of Figure 8(a) using MEISP software by Kumho Chemical Laboratories, on the basis of algorithm developed by Professor J. R. Macdonald (LEVME v7.0) for non-linear complex least square fitting, and the obtained parameters are represented in Table III. The chemical capacitance (C_{μ}) is very useful in illustrating the underlying mechanism through which photoelectrons store free energy and generates current and voltage in the outer circuit.³⁷ Also, the

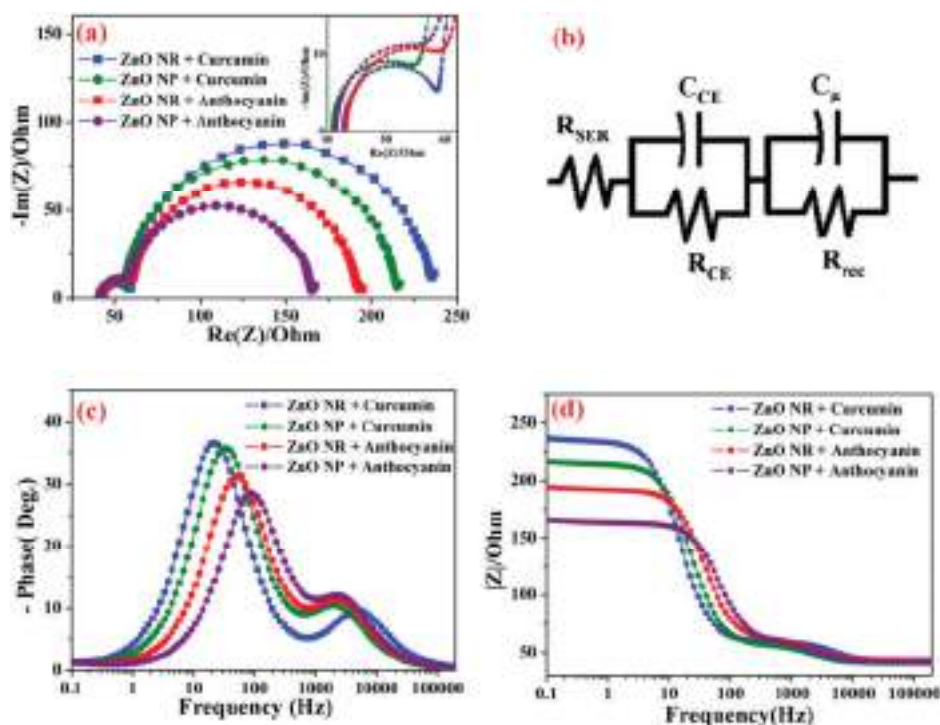


Fig. 8. EIS spectra of DSSCs (a) nyquist plot (b) equivalent circuit for fitting (c) bode phase plot and (d) bode magnitude plot for impedance.

chemical capacitance (C_μ) reflects charge carrier accumulation on the ZnO film and the density of states in the band-gap region.³⁸ From Table III, it can be seen that Cell-1 exhibits much higher C_μ value than the other cells, which indicates conversion of higher amount of photon energy into chemical energy resulting in higher amount of energy storage by virtue of carrier injection into the conduction band of ZnO. Reduced C_μ values for cell-2, 3 and 4 also suggest poor dye loading.^{39,40} It can also be clearly observed from the Nyquist plot that the recombination resistance (R_{rec}) at the ZnO NR-Dye/Electrolyte interface is highest for cell-1 compared to the other three cells. This shows that cell-1 has better resistance to the charge recombination between the photo-generated electrons and

the electron acceptors in the red-ox electrolyte attributing lower recombination current.⁴¹

Since counter electrodes of all the cells were prepared using same procedure, the values of R_{CE} are almost same for all the four cells. Another important representation of the EIS data is Phase and Magnitude bode plots representing Phase ($-\theta$) versus Frequency (f) and Magnitude of Impedance ($|Z|$) versus Frequency (f) curve. Unlike Nyquist plot, the very important aspect of this plot is that frequency information is not lost. The average carrier lifetime can be estimated from phase bode plots (shown in EIS Fig. 8(b)) using the formula

$$\tau_e = \frac{1}{2\pi f_{\max}}$$

where f_{\max} represents peak frequency in the mid-frequency range.⁴² ZnO NR loaded with Curcumin dye shows lowest characteristic peak frequency attributing to highest electron lifetime in the LUMO of the Curcumin dye molecule. It shifts towards higher frequency values for the other cells which results in decreased electron lifetime (refer to Table III). The lowest value of τ_e in ZnO NP cell loaded with anthocyanin (cell-4) extracted from pomegranate juice attributes to fastest electron recombination leading to degraded overall cell performance.

On the other hand, bode magnitude plots depicted in Figure 8(d) represents the variation of magnitude of impedance with frequency. It may be noted from bode magnitude plot shown in Figure 8(d) that at low frequencies the magnitude of impedance is high, which indicates

Table III. EIS parameters of the DSSCs determined by fitting experimental data.

Cell No.	Dye used and ZnO microstructure	R_{SER} (Ω)	R_{rec} (Ω)	R_{CE} (Ω)	C_μ (μF)	Peak freq. (Hz)	Electron lifetime (τ_e) (ms)
1	Curcumin and ZnO NR	42.85	173.21	16.28	83.16	22	7.24
2	Anthocyanin and ZnO NR	40.93	156.37	15.17	59.41	33.29	4.78
3	Curcumin and ZnO NP	43.25	129.74	17.56	42.52	51	3.12
4	Anthocyanin and ZnO NP	41.63	103.56	16.85	29.40	88.48	1.80

higher recombination resistance. But with increase in frequency the impedance starts falling which is due to the faster electron recombination at higher frequencies. In the lower frequency region, the ZnO NR cell sensitized with Curcumin is showing highest magnitude of impedance implying slowest recombination rate, giving rise to highest short circuit current (I_{SC}). In contrary, ZnO NP cell sensitized with anthocyanin extracted from pomegranate fruit shows the lowest impedance in the low frequency region implying fastest recombination process which is reflected in Table III. The possible reason behind these behaviours may be the better adsorption of Curcumin dye molecules over the hexagonal rod shaped ZnO nanostructures in comparison to the other cells. It also can be seen that the value of characteristic frequency shifts towards lower side for increasing value of either R_{rec} or C_{μ} . One more thing can be noted from the impedance plots that the maximum value of phase angle is also decreases with the decrease in value of R_{rec} .

4. CONCLUSIONS

In this study, hexagonal shaped ZnO nanorods with preferential growth along (002) plane were successfully grown on ITO substrates using low cost sol-gel hydrothermal technique. The nanorods have diameters ranging from 100–200 nm. XRD study revealed remarkably high crystalline quality of the nanorods. These ZnO nanorod based substrates were used as photoanodes to prepare DSSCs using natural dyes extracted from pomegranate and turmeric. On the other hand, commercial ZnO nano powder is also used to fabricate DSSCs using the same natural dyes. Photo electrochemical performances of all the four cells were recorded. From the $J-V$ measurements, a clear enhanced overall cell performance was noticed for the cell constructed using ZnO nanorods and sensitized using Curcumin dye compared to the other three cells. One of the reasons for this could be the higher amount of Curcumin dye molecule adsorption by the ZnO film due to the better interaction between the carbonyl and hydroxyl groups of Curcumin molecule and the ZnO nanorod film than that of Pomegranate extract. For deeper understanding of the performances obtained from the cells, the different interfacial mechanisms of the cells were investigated using EIS technique. It is found that the shape of ZnO nanostructures and different dye molecules present in the extracts affected the electrochemical parameters of the cells. Best performance of the cell prepared with ZnO nanorod with Curcumin dye is found to be due to highest chemical capacitance (C_{μ}) along with lowest electron recombination rate and fast charge transport along the ZnO nanorod. Therefore, the Curcumin dye should be an alternative to anthocyanin source for natural dye sensitized solar cells. These results also show that the performances of the natural extract based DSSCs can be enhanced significantly by combining

proper natural dye with appropriate shape of semiconductor nanostructures and they can become potential alternative to the synthetic sensitizers based DSSCs. In fact, such combination may result in environment friendly, remarkably low cost and easily manufacturable dye sensitized solar cells.

Acknowledgment: Authors gratefully acknowledge the Dept. of Physics, University of North Bengal for providing financial support and laboratory facilities for carrying out the research work.

References and Notes

1. A. Horvath and E. Rachlew, Nuclear power in the 21st century: Challenges and possibilities. *Ambio* 45(Suppl. 1), S38 (2016).
2. S. Chu and A. Majumdar, Opportunities and challenges for a sustainable energy future. *Nature* 488, 294 (2012).
3. N. L. Chang, Y. Ho-Baillie, A. Wing, P. A. Basore, T. L. Young, R. Evans, and R. J. Egan, A manufacturing cost estimation method with uncertainty analysis and its application to perovskite on glass photovoltaic modules. *Progress in Photovoltaics: Research and Applications* 25, 390 (2017).
4. A. Kumar, M. Bieri, T. Reindl, and A. G. Aberle, Economic viability analysis of silicon solar cell manufacturing: Al-BSF versus PERC. *Energy Procedia* 130, 43 (2017).
5. M. Grätzel, Dye-sensitized solar cells. *Journal of Photochemistry and Photobiology C: Photochemistry Reviews* 4, 145 (2003).
6. B. O'regan and M. Grätzel, A low-cost, high-efficiency solar cell based on dye-sensitized colloidal TiO₂ films. *Nature* 353, 737 (1991).
7. Y.-T. Kim, J. Park, S. Kim, D. W. Park, and J. Choi, Fabrication of hierarchical ZnO nanostructures for dye-sensitized solar cells. *Electrochim. Acta* 78, 417 (2012).
8. C. Jiang, X. Sun, G. Lo, D. Kwong, and J. Wang, Improved dye-sensitized solar cells with a ZnO-nanoflower photoanode. *Appl. Phys. Lett.* 90, 263501 (2007).
9. J. B. Baxter and E. S. Aydil, Nanowire-based dye-sensitized solar cells. *Appl. Phys. Lett.* 86, 053114 (2005).
10. A. Jena, S. P. Mohanty, P. Kumar, J. Naduvath, V. Gondane, P. Lekha, J. Das, H. K. Narula, S. Mallick, and P. Bhargava, Dye sensitized solar cells: A review. *Transactions of the Indian Ceramic Society* 71, 1 (2012).
11. J. Gong, J. Liang, and K. Sumathy, Review on dye-sensitized solar cells (DSSCs): Fundamental concepts and novel materials. *Renewable and Sustainable Energy Reviews* 16, 5848 (2012).
12. S. Hao, J. Wu, Y. Huang, and J. Lin, Natural dyes as photosensitizers for dye-sensitized solar cell. *Solar Energy* 80, 209 (2006).
13. H. Zhu, H. Zeng, V. Subramanian, C. Masarapu, K.-H. Hung, and B. Wei, Anthocyanin-sensitized solar cells using carbon nanotube films as counter electrodes. *Nanotechnology* 19, 465204 (2008).
14. Y. Amao and T. Komori, Bio-photovoltaic conversion device using chlorine-e6 derived from chlorophyll from spirulina adsorbed on a nanocrystalline TiO₂ film electrode. *Biosens. Bioelectron.* 19, 843 (2004).
15. K.-H. Park, T.-Y. Kim, S. Han, H.-S. Ko, S.-H. Lee, Y.-M. Song, J.-H. Kim, and J.-W. Lee, Light harvesting over a wide range of wavelength using natural dyes of gardenia and cochineal for dye-sensitized solar cells. *Spectrochimica Acta Part A: Molecular and Biomolecular Spectroscopy* 128, 868 (2014).

16. F. Shao, J. Sun, L. Gao, S. Yang, and J. Luo, Growth of various TiO₂ nanostructures for dye-sensitized solar cells. *The Journal of Physical Chemistry C* 115, 1819 (2010).
17. X. Mao, R. Zhou, S. Zhang, L. Ding, L. Wan, S. Qin, Z. Chen, J. Xu, and S. Miao, High efficiency dye-sensitized solar cells constructed with composites of TiO₂ and the hot-bubbling synthesized ultra-small SnO₂ nanocrystals. *Scientific Reports* 6, 19390 (2016).
18. D. Maheswari and D. Sreenivasan, Review of TiO₂ nanowires in dye sensitized solar cell. *Applied Solar Energy* 51, 112 (2015).
19. B. Roose, S. Pathak, and U. Steiner, Doping of TiO₂ for sensitized solar cells. *Chem. Soc. Rev.* 44, 8326 (2015).
20. M. S. Ahmad, A. Pandey, and N. A. Rahim, Advancements in the development of TiO₂ photoanodes and its fabrication methods for dye sensitized solar cell (DSSC) applications. A review. *Renewable and Sustainable Energy Reviews* 77, 89 (2017).
21. K. Tennakone, G. Kumara, A. Kumarasinghe, P. Sirimanne, and K. Wijayantha, Efficient photosensitization of nanocrystalline TiO₂ films by tannins and related phenolic substances. *Journal of Photochemistry and Photobiology A: Chemistry* 94, 217 (1996).
22. J. A. Anta, E. Guillen, and R. Tena-Zaera, ZnO-based dye-sensitized solar cells. *The Journal of Physical Chemistry C* 116, 11413 (2012).
23. Ü. Özgür, Y. I. Alivov, C. Liu, A. Teke, M. Reshchikov, S. Doğan, V. Avrutin, S.-J. Cho, and H. Morkoc, A comprehensive review of ZnO materials and devices. *J. Appl. Phys.* 98, 11 (2005).
24. H. Bae, M. Yoon, J. Kim, and S. Im, Photodetecting properties of ZnO-based thin-film transistors. *Appl. Phys. Lett.* 83, 5313 (2003).
25. Q. Zhang, C. S. Dandeneau, X. Zhou, and G. Cao, ZnO nanostructures for dye-sensitized solar cells. *Adv. Mater.* 21, 4087 (2009).
26. Y. Zhang, M. K. Ram, E. K. Stefanakos, and D. Y. Goswami, Synthesis, characterization, and applications of ZnO nanowires. *Journal of Nanomaterials* 2012, 20 (2012).
27. T. Senthil, N. Muthukumarasamy, and M. Kang, ZnO nanorods based dye sensitized solar cells sensitized using natural dyes extracted from beetroot, rose and strawberry. *Bull. Korean Chem. Soc.* 35, 1050 (2014).
28. S.-I. Kawano, Y. Inohana, Y. Hashi, and J.-M. Lin, Analysis of keto-enol tautomers of curcumin by liquid chromatography/mass spectrometry. *Chin. Chem. Lett.* 24, 685 (2013).
29. M. Viuda-Martos, J. Fernández-López, and J. Pérez-Álvarez, Pomegranate and its many functional components as related to human health: A review. *Comprehensive Reviews in Food Science and Food Safety* 9, 635 (2010).
30. B. Pradhan, S. K. Batabyal, and A. J. Pal, Vertically aligned ZnO nanowire arrays in Rose Bengal-based dye-sensitized solar cells. *Sol. Energy Mater. Sol. Cells* 91, 769 (2007).
31. F. Zhang, C. A. Di, N. Berdunov, Y. Hu, Y. Hu, X. Gao, Q. Meng, H. Sirringhaus, and D. Zhu, Ultrathin film organic transistors: Precise control of semiconductor thickness via spin-coating. *Adv. Mater.* 25, 1401 (2013).
32. A. H. Kurda, Y. M. Hassan, and N. M. Ahmed, Controlling diameter, length and characterization of ZnO nanorods by simple hydrothermal method for solar cells. *World Journal of Nano Science and Engineering* 5, 34 (2015).
33. H. Zhou, L. Wu, Y. Gao, and T. Ma, Dye-sensitized solar cells using 20 natural dyes as sensitizers. *Journal of Photochemistry and Photobiology A: Chemistry* 219, 188 (2011).
34. M. Murayama and T. Mori, Equivalent circuit analysis of dye-sensitized solar cell by using one-diode model: Effect of carboxylic acid treatment of TiO₂ electrode. *Japanese Journal of Applied Physics* 45, 542 (2006).
35. M. Wang, A. M. Anghel, B. Marsan, N.-L. C. Ha, N. Pootrakulchote, S. M. Zakeeruddin, and M. Grätzel, CoS supersedes Pt as efficient electrocatalyst for triiodide reduction in dye-sensitized solar cells. *J. Am. Chem. Soc.* 131, 15976 (2009).
36. L. Tao, Z. Huo, Y. Ding, Y. Li, S. Dai, L. Wang, J. Zhu, X. Pan, B. Zhang, and J. Yao, High-efficiency and stable quasi-solid-state dye-sensitized solar cell based on low molecular mass organogelator electrolyte. *Journal of Materials Chemistry A* 3, 2344 (2015).
37. S. S. Negi, Integrated electronic, optical, and structural features in pseudo-3D mesoporous TiO₂-X delivering enhanced dye-sensitized solar cell performance. *ACS Omega* 3, 1645 (2018).
38. G. Di Carlo, A. O. Biroli, M. Pizzotti, F. Tessore, V. Trifiletti, R. Ruffo, A. Abbotto, A. Amat, F. De Angelis, and P. R. Mussini, Tetraaryl ZnII porphyrinates substituted at β-pyrrolic positions as sensitizers in dye-sensitized solar cells: A comparison with meso-disubstituted push-pull znii porphyrinates. *Chem. Eur. J.* 19, 10723 (2013).
39. J. Bisquert, Chemical capacitance of nanostructured semiconductors: Its origin and significance for nanocomposite solar cells. *PCCP* 5, 5360 (2003).
40. F. Fabregat-Santiago, E. M. Barea, J. Bisquert, G. K. Mor, K. Shankar, and C. A. Grimes, High carrier density and capacitance in TiO₂ nanotube arrays induced by electrochemical doping. *J. Am. Chem. Soc.* 130, 11312 (2008).
41. J. Akilavasan, K. Wijeratne, H. Moutinho, M. Al-Jassim, A. Alamoud, R. Rajapakse, and J. Bandara, Hydrothermally synthesized titania nanotubes as a promising electron transport medium in dye sensitized solar cells exhibiting a record efficiency of 7.6% for 1-D based devices. *Journal of Materials Chemistry A* 1, 5377 (2013).
42. P. Bhatt, K. Pandey, P. Yadav, B. Tripathi, and M. Kumar, Impedance spectroscopic investigation of the degraded dye-sensitized solar cell due to ageing. *International Journal of Photoenergy* Article ID 8523150 (2016), DOI: [10.1155/2016/8523150](https://doi.org/10.1155/2016/8523150).

National Conference
on
Modern Trends in Materials Science - 2015
(MTMS – 2015)

Organized by
Department of Physics, University of North Bengal, West Bengal, India



Paper Presentation Certificate

This is to certify that Prof./Dr./Mr./Mrs./Ms. *Rajat Biswas*.....
of ... *Dept. of Physics, N. B. U., Siliguri - 734013*.....
has presented a paper (~~Oral~~/Poster) entitled ... *ZnO Nanorod Based*
Dye Sensitized Solar cells Sensitized Using Natural
Dyes Extracted from Pomegranate and Curcumin
in the National Conference On-Modern Trends in Materials Science – 2015 (MTMS –
2015) held at Department of Physics, University of North Bengal, West Bengal, India
during 5 – 6 February, 2015.

M. K. Das
Dr. M. K. Das
Chairman

S. Chatterjee
Dr. S. Chatterjee
Organizing Secretary

S. Halder
Dr. S. Halder
Convener



UGC SPONSORED
NATIONAL SEMINAR ON
CONDENSED MATTER, LASER AND COMMUNICATION (NSCMLC 2015)
February 27-28, 2015

Organized by
Department of Physics
(UGC-Centre of Advanced Study)
The University of Burdwan, Golapbag, Burdwan

Certificate of Participation

This is to certify that Prof./Dr./Mr./Mrs. *Rajat Biswas*
of *University of North Bengal*
has participated and delivered an invited talk/presented a paper (~~or~~ poster) in National Seminar on
Condensed Matter, Laser and Communication (NSCMLC 2015).

A. Bose
A. Bose & A. Dutta
Secretaries

S. Mukhopadhyay
S. Mukhopadhyay & P. Mitra
Conveners